Université Fédérale

Toulouse Midi-Pyrénées

THÈSE

En vue de l'obtention du

DOCTORAT DE L'UNIVERSITÉ DE TOULOUSE

Délivré par : *l'Université Toulouse 3 Paul Sabatier (UT3 Paul Sabatier)*

Présentée et soutenue par : *Malika Denis*

Date de soutenance : *3 février 2017*

Probing Physics Beyond the Standard Model in Diatomic Molecules.

JURY

Ephraim ELIAV	Professeur	Rapporteur
Robert BERGER	Professeur	Rapporteur
Phuong Mai DINH	Professeure	Examinatrice
Timo FLEIG	Professeur	Directeur

École doctorale et spécialité :

SDM : Physique

Unité de Recherche :

Laboratoire de Chimie et Physique Quantiques (UMR5626)

Directeur de Thèse :

Timo FLEIG

Rapporteurs :

Ephraim ELIAV et *Robert BERGER.*

Je suis de ceux qui pensent que la science a une grande beauté. [...] Sans la curiosité de l'esprit, que serions-nous ? Telle est bien la beauté et la noblesse de la science : désir sans fin de repousser les frontières du savoir, de traquer les secrets de la matière et de la vie sans idée préconçue des conséquences éventuelles.

Marie Curie

Acknowledgements.

Mon œuvre achevée, je reprends la plume pour remercier les personnes qui ont contribué à sa réalisation que ce soit par le soutien qu'ils m'ont apporté pendant les années de thèse ou de façon plus générale, en m'inspirant et/ou en me procurant un environnement propice à l'épanouissement personnel et intellectuel au cours de ces vingt-sept (*erratum* : vingt-huit) dernières années.

Alors que ma longue (trop longue ?) scolarité touche officiellement à sa fin, je commencerai par remercier les enseignants qui l'ont particulièrement marquée. J'ai eu la chance, au cours de toutes ces années, de rencontrer des professeurs exceptionnels qui ont fait bien plus que m'enseigner leur matière. Ils ont su, chacun à leur façon, éveiller, encourager ma curiosité intellectuelle et m'ont inspirée tout au long de mon cursus. Je citerai **M. Ouala** qui a su me transmettre sa passion pour les mathématiques par son enthousiasme et ses exercices stimulants ; et surtout, **Mme Duhamel**, dont chaque cours était une invitation à la réflexion et son exigeance, une incitation à se dépasser. J'ajouterai à cette liste mon directeur de thèse **Timo Fleig** qui m'a permis de travailler sur un sujet aussi passionnant et enthousiasmant.

Je garderai de mes quatre années passées au laboratoire, le souvenir d'un quotidien agréable et joyeux et cela, je le dois aux sympatiques personnes que j'y ai cotoyées. La plupart faisaient partie de ce que j'appellerai "le groupe du midi" dont les membres les plus éminents sont la bienveillante **Nadia** toujours prête à apporter son aide ou des cannelés, le loufoque **Nicolas** qui nous a souvent offert des conversations absurdes et surréalistes, l'excentrique **Sophie** toujours prête à mener un combat pour révolutionner l'enseignement, l'imposant **Arjan** venu du nord, mes interlocuteurs de ces derniers mois qui m'ont écouté leur confier mes doutes **Bastien** et **Ruben**. Mais aussi tous les membres honoraires parmi lesquels se trouvent le sage **Daniel**, une source inépuisable d'anecdotes et d'histoires ; et le deuxième meilleur joueur de Pylos du laboratoire, avec qui je partage une passion pour le thé et le chocolat et l'exil en Allemagne, j'ai nommé **Vijay**. Merci aussi aux convives occasionnels que sont la **petite Bessac**, **Cyril**, **Jean-Paul**, **Aude**, **Jérome**, **Matthias**... à mes autres collègues doctorants **Kseniia**, **Florian**... et plus généralement, à toutes

les personnes bienveillantes du laboratoire.

Si j'ai résisté au stress et aux épreuves qui ont jalonné mon parcours de thèse, c'est avant tout grâce à la fine équipe, ma petite bulle de bonheur avec qui j'ai partagé l'indispensable pause goûter au laboratoire pendant toutes ces années de thèse et avec qui j'ai hanté tous les restaurants et salons de thés de Toulouse. Le premier membre est la meilleure rencontre que j'ai faite pendant ces quatre années à Toulouse, mon meilleur ami, le fameux **Thomas Applencourt**. Grâce à toi, j'ai pu "catharsiser" mon ennui, mes découragements, mes frustrations en donnant libre cours à nos valeurs communes, le cynisme, la mysanthropie mais aussi un refus obstiné de prendre la vie et les gens au sérieux. Sache que même si tu t'es envolé loin, très loin (comme un bohémien :)), je ne t'oublie pas et *"Si le destin le veut, la postérité, sois-en sûr/Portera nos deux noms sur la liste des amis célèbres"* [1].

Et, je ne pouvais omettre de remercier l'autre membre de la fine équipe, mon amoureux **Nathou** qui a dû user de tout son calme, sa nonchalance et son flegme tourangeaux pour m'aider à surmonter mes crises d'angoisse et de son humour caustique si particulier, que l'on voit poindre dans ses yeux quand s'y allume une lueur espiègle, pour dédramatiser la situation quand elle me semblait insurmontable. Merci de ton soutien et d'avoir été si confiant en la réussite de cette thèse, sans doute plus que moi-même et d'avoir su me communiquer ne serait-ce qu'une infime partie de cette sérénité.

Autres sources de réconfort, les séances de yoga de **Cécile** qui m'ont beaucoup apporté et permis de gagner en sérénité  . Et, mon compagnon mangeur de carottes, mon cher lapin **Cookie** qui m'a soutenue par ses câlins et a été le témoin privilégié des premières répétitions de la soutenance, merci petite boule de poils.

Je suis aussi reconnaissante à ces personnes qui m'ont soutenue de loin en se désespérant parfois de ne pas comprendre le sujet de cette mystérieuse thèse (Ne vous inquiétez pas, vous n'êtes pas les seuls !) ; ma grand-mère, tu vois **Mamie** ? je m'en suis sortie sans avoir recours à la sophrologie ; mes parents **Papa** et **Maman**[2] qui, naïvement, ont cru à une blague quand, à cinq ans, je leur ai annoncé que je voulais rester à l'école toute ma vie ; mon petit frère **Alexis** pour son soutien indéfectible et ses nombreuses visites (l'ironie de cette description n'échappera à personne) et mon amie de toujours **Manon** qui a été le témoin lointain mais non moins solidaire et compatissant de ces années de thèse, elle, mieux que personne, peut comprendre l'épreuve qu'a été la soutenance. Merci à vous d'avoir cru aveuglément en moi et en

[1] Etienne de la Boétie à Michel de Montaigne.

[2] Maman me fait remarquer que pour que je naisse, condition indispensable à l'obtention de ce doctorat, elle a quand même beaucoup souffert ce matin de février 1989, donc doublement merci !

ma capacité à réussir. Si j'en suis là, peut-être est-ce au fond parce que j'ai fini par me laisser convaincre par vos encouragements et votre soutien ou parce que je n'ai pu me résoudre à vous décevoir ... *Trop têtue pour être faible !*[3].

Il est maintenant temps de faire place à la science. Entre ici atome de Thorium avec ton terrible cortège, tous les électrons, les protons et les neutrons [4].

[3]Thomas Applencourt, 3 février 2017.

[4]Les plus érudits auront reconnu une piètre tentative d'imitation de la prose d'André Malraux rendant hommage à Jean Moulin.

Abstract.

Nowadays, the incompleteness of the Standard Model of particles is largely acknowledged. One of its most obvious shortcomings is the lack of explanation for the huge surplus of matter over antimatter in the universe, the so-called Baryon Asymmetry of the Universe. New $\mathcal{CP}$ (Charge conjugation and spatial Parity) violations absent in the SM are assumed to be responsible for this asymmetry. Such a violation could be observed, in ordinary matter through a set of interactions violating both parity and time-reversal symmetries ($\mathcal{P},\mathcal{T}$-odd) among which the preponderant ones are the electron Electric Dipole Moment (eEDM), the electron-nucleon scalar-pseudoscalar (enSPS) and the nuclear magnetic quadrupole moment (nMQM) interactions. Hence, an experimental evidence of a non-zero $\mathcal{P},\mathcal{T}$-odd interaction constant would be a probe of this New Physics beyond the Standard Model.

The calculation of the corresponding molecular parameters is performed by making use of an elaborate four-component relativistic configuration interaction approach in polar diatomic molecules containing an actinide, that are particularly adequate systems for eEDM experiments, such as ThO that allowed for assigning the most constraining upper bound on the eEDM and ThF^+ that will be used in a forthcoming experiment. Those results will be of crucial importance in the interpretation of the measurements since the fundamental constants can only be evaluated if one combines both experimental energy shift measurements and theoretical molecular parameters.

Layout of the manuscript.

This manuscript proceeds as follows, after an introduction to the general background of the search of $\mathcal{CP}$-violations and its consequences for the understanding of the Universe (Chapter 1), a presentation of the underlying theory of the evidence of such violation in ordinary matter, namely the $\mathcal{P},\mathcal{T}$-odd sources of the Electric Dipole Moment of a many-electron system, as well as the relevant molecular parameters is given in Chapter 2. A similar introduction to the hyperfine interaction and in particular of the parallel magnetic hyperfine interaction constant can be found in Chapter 3. This first quite bibliographic and theoretical part ends up with a review of the methodological tools employed in this work (Chapter 4). Next is the application part that consists of two theoretical studies for the search of $\mathcal{CP}$-violation in ThF^+ (Chapter 5) and ThO (Chapter 6), respectively, and of an explorative study of the hyperfine interaction constant of the fluorine atom in diatomic molecules (Chapter 7). Finally, Chapter 8 summarises the works conducted during this thesis and some conclusions on the applications and the following studies are drawn.

Contents

1 General background.

1.1 EDM as probe of new physics.

1.1.1 Is the electron a sphere?

The search of an Electric Dipole Moment (EDM) of the electron is often referred to as investigating the shape of the electron. Indeed, for easier understanding, the arduous and quite abstract issue of the possible existence of an electron EDM is reduced to the simpler question of the sphericity of the electron. So, mainstream media relayed the recent results of EDM experiments as the measurement of the roundness of the electron. However, this description has to be clarified since the electron is assumed to be a point-like object even if this statement is only true to some extent. Actually, a limit on the radius of the electron was set based on the deviation of a measured electron magnetic moment from the theoretical value obtained by Quantum Electrodynamics theory within a size-less electron framework, the upper bound obtained is $R_e < 10^{-18}$ m [HFG08].

As a matter of fact, what is at stake in the electron EDM experiments is not the shape of the electron itself but the asphericity of its charge distribution. The detection of the distortion, deviation from a spherical distribution, is a very challenging task for the experimentalists because what they expect to measure is outstandingly tiny. As a picture, if the distribution was scaled up to the size of the solar system, the deviation would be of the width of a hair [Hin14]. This deviation makes the electron charge distribution raindrop-shaped or egg-like and gives birth to a difference of charge between the two "poles" that entails the existence of an electric dipole moment going from one side of the distorted distribution to the other.

1.1.2 $\mathcal{CP}$ violation and BAU.

Then, it is not unreasonable to wonder why one would struggle to measure such a tiny quantity. Despite its modest size, the asymmetry of the charge distribution is far from insignificant for the understanding of particle physics and the nature

of the Universe. An electric dipole moment of an electron, and more generally of a fundamental particle, has to align either parallely or anti-parallely to the spin, under the projection theorem for a vector operator $\hat{\mathbf{V}}$,

$$\langle \alpha', JM_J|\hat{V}_q|\alpha', JM_J\rangle = \frac{\langle \alpha', JM_J|\hat{\mathbf{J}}\cdot\hat{\mathbf{V}}|\alpha', JM_J\rangle}{\hbar^2 J^2(J+1)}\langle JM_J|\hat{J}_q|JM_J\rangle^1 \tag{1.1}$$

where α and α' denote the rotationally-invariant quantum numbers, $\hat{\mathbf{J}}$ is the angular momentum vector operator, J is the angular momentum quantum number and M_J its projection along the z-axis.

Yet, under a time reversal transformation, the spin direction is reversed while the permanent electric dipole moment, which is a static property, remains unchanged (see Fig. 1.1), thus the resulting particle has an opposite direction of the EDM in relation to the spin. A conserved $\mathcal{T}$-symmetry would imply the double degeneracy of particles with both spin and EDM, according to their relative direction, which is inconsistent with the observations, therefore the time-reversal symmetry is necessarily violated. The $\mathcal{CPT}$ theorem that states the conservation of combined charge conjugation, parity inversion and time-reversal symmetries is supposed valid and leads to the following conclusion; the existence of a non-zero EDM of an elementary particle would violate the combined symmetry of charge conjugation ($\mathcal{C}$) which transforms a particle into its anti-particle and parity inversion ($\mathcal{P}$) that changes the sign of spatial coordinates. This contradicts Landau statement [Lan57] that $\mathcal{CP}$ could not be violated because such a violation "would seem to be extremely strange" [Hin97].

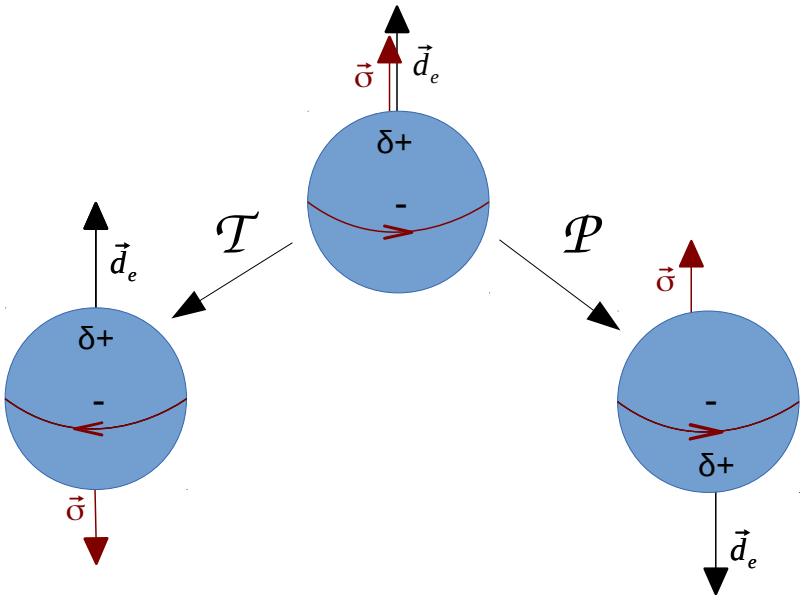

Figure 1.1 – Violation of $\mathcal{P}$- and $\mathcal{T}$-symmetry.

[1]Here and in the whole manuscript, bolded symbols denote vectorised quantities.

Now, Sakharov [Sak67] considered the $\mathcal{CP}$ violation as an explanation of the predominance of matter over antimatter, also known as the baryon asymmetry of the Universe (BAU). This is one of the biggest mysteries in physics since there is still no theory that explains why antimatter is found in so tiny quantities although it is assumed to have been created right after the Big Bang in the same amount as matter and to be ruled by the same laws.

The Standard Model (SM), the most successful theory of particle physics, does include $\mathcal{CP}$ violating phenomena that can be observed, such as the decays of neutral K [Ala99, eaNC99] and B [eaBC01a, eaBC01b] mesons. This is the consequence of the flavour mixing in the quark sector contained in the Cabibbo–Kobayashi–Maskawa (CKM) matrix [KM73]. However, in the standard model, the interaction of the electron with the quarks gives rise to an extremely tiny permanent electric dipole moment ($10^{-38} e.cm$), expected to be unobservable in experiments and that does not provide sufficient level of $\mathcal{CP}$ violation to explain the baryon asymmetry of the Universe. Thus, theories beyond the standard model have been developed, the Standard Model failures and these theories will be introduced in more details in section 1.1.3. They introduce new sources of $\mathcal{CP}$ violation and new particles the interaction of which with the electron could induce a bigger asymmetry of the charge distribution and consequently a much greater EDM than expected in the standard model. Typically there would be a gain of ten orders of magnitude and the interaction would reach the range of what current experiments are capable of measuring. Moreover, each extension to the standard model predicts different ranges for the EDMs. So the measurement of the permanent EDM of a fundamental particle could be a means of testing these theories. No EDM has been detected yet but by increasing the sensitivity of the measurement, experimentalists could invalidate some models which predicted greater values of the permanent electric dipole moment of the electron, *i.e.* greater than the current precision $9.6 \times 10^{-29} e.cm$ [CBC+14]. The EDM experiments are noteworthy because they make it possible to probe new physics, as it is done in super colliders such as the LHC where physicists try to create the presumptive new particles by colliding protons, however at a very low energy in an ordinary laboratory.

1.1.3 Beyond the standard model.

Despite its many successes in the prediction of phenomena and particles, such as the existence of the W and Z bosons or the decay of the Z boson, both experimentally confirmed at the CERN [Rub85, CKS+12], the very elegant description of the world given by the Standard Model is not complete. In addition to the baryonic asymmetry of the Universe, the most striking flaw of the Standard Model is the impossibility to include gravity and its framework, the *General Relativity*, preventing physicists to

accomplish the so-called *Grand Unification*. Attempts were done to explain gravity within the Standard Model, namely by adding a particle, the *graviton*; yet, it still fails to recreate experimental observations and explain the weakness of the magnitude of the gravitational force in comparison with the three other forces (electromagnetic, weak and strong forces). This is part of what is called the *hierarchy problem* with the large spectrum of masses among the elementary particles that also raises the issue of the mass of the Higgs boson smaller than expected. Another failure of the Standard Model is that it only accounts for the visible matter, estimated to make up only 5% of the Universe. So, the major constituents remain undescribed by the Standard Model that does not provide suitable candidate particles to constitute the dark matter and the dark energy expected to form 26% and 69% of the Universe, respectively. Even if dark matter is not observable, probes of its existence can be found in its gravitational effects on ordinary matter. In an attempt to address the Standard Model issues, a large number of extensions have been developed, amongst which are the Left-Right Symmetric models [PS73], the Multi-Higgs models [Wei76] or the well-known Supersymmetric models [HK85]. The proposed values for the electron electric dipole moment by these models [Liu86, BZ90, BHS95] and the Standard Model are compiled in Table 1.1, along with the current upper bound provided by the experiment [CBC$^+$14] combined to the theory [SPT13] which reached the decisive range that allows one to constrain new physics and disqualify some of these new particle physics theories as likely explanations of the Universe.

Table 1.1 – Predicted values of the electron Electric Dipole Moment [Com99]

Model	$d_e[e.cm]$
Standard model	$< 10^{-38}$
Left-Right Symmetry	$10^{-28} - 10^{-26}$
Multi-Higgs	$10^{-28} - 10^{-27}$
Supersymmetry	$\leq 10^{-25}$
Experimental upper limit	9.6×10^{-29}

The most popular and promising extensions to the Standard Model are the Supersymmetry including ones. They do not aim to invalidate or replace the Standard Model but to complete it by fixing its shortcomings. The basic idea is the prediction of one or more superpartners for each ordinary particle (*i.e.* included in the Standard Model) that would share identical properties, with the major exception of the spin; if the particle is a boson (integer spin) then the associated superparticle will be a fermion (half-integer spin) and conversely, a fermionic particle will have a bosonic superpartner. The new particles would solve the Higgs boson mass issue by cancelling

out the contributions from the SM that would make the Higgs boson heavy.
Though, this very harmonious picture of the world is obviously false, since superpartners are assumed to share the same mass as their associate particle as well as their interactions with other known and unknown particles and hence they should have been detected already. Thus, theoreticians thought of processes that may have broken the Supersymmetry; it is actually what makes the many Supersymmetric models distinct from each other[2]. Whatever the mechanism, it would have made superpartners very massive to such an extent that no experiments have yet reached a sufficient scale of energy to detect them. There is still hope to see them at the LHC thanks to the $\mathcal{R}$-parity[3] conservation that states that a superparticle can only decay into another lighter supersymmetric particle, so that the lightest supersymmetric particle (LSP) is extremely stable and thus rather easy to find, provided that one searches in the right range of masses, which turns out to be an arduous task since there is no accurate prediction of the superpartners masses available. Besides, the so-called LSP totally matches the profile of dark matter - stable, electrically neutral, interacting weakly with ordinary matter - which would solve another problem of the Standard Model.

1.2 Measuring an EDM.

1.2.1 Choice of a system.

As previously said, the electric dipole moments are extremely tiny quantities, which raises some problems when it comes to building an experiment to measure them. One is the so-called magnetic moment problem. As a matter of fact, experimentalists measure an energy shift due to both Stark and Zeeman effects that reads: $hw = 2(\mu B + d_e E)$, where μ is the magnetic dipole moment. In order to reduce uncertainty, they aim to get the same magnitude for both interactions. For instance, let us consider the EDM of the electron and a value consistent with most of the theories beyond the Standard Model: $d_e = 5 \times 10^{-28}$ e.cm and a 10 kV/cm electric field, the typical operating electric field magnitude in atomic experiments [KSH+12]. Thus, the EDM interaction is in the order of $d_e \boldsymbol{\sigma} \times \mathbf{E} \approx 1$ nHz and the magnetic interaction would be of the same magnitude for a 10^{-19} T magnetic field, which is far too small to keep under control. It becomes even more obvious if we compare this figure with the magnitude of the magnetic field of the Earth which is $\approx 5.10^{-5}$ T. Moreover,

[2]Details on the various Supersymmetric models can be found in [Lyk10].

[3]$\mathcal{R}$-parity is a symmetry introduced in Supersymmetric models that prevents undesirable couplings that do not conserve lepton and baryon numbers. It assigns +1 $\mathcal{R}$-parity to particles and −1 to superparticles.

when applied to the bare electron, such an enormous electric field would cause the acceleration of the charged particle, making the measurement impossible. As a consequence, the first EDM experiments were made on the neutron [SPR57].

In 1965, Sandars [San65] reported the suitability of atoms in the search for the EDM of the electron by pointing out that Schiff's theorem [Sch63] - which states that an atom has no permanent EDM even if the electron does - failed when relativity is taken into account. He demonstrated that, not merely could an atom with a single electron have an electric dipole moment but the EDM of an unpaired electron in an atom or a molecule would be enhanced and be a few orders of magnitude larger than in the case of a free electron. The enhancement factor defined as the ratio of the atomic EDM to the electron EDM reads [PR05]:

$$R \propto \frac{Z^3\alpha^2}{J(J+\frac{1}{2})(J+1)} \tag{1.2}$$

with J, the angular momentum, Z, the atomic number and α, the fine structure constant. It results in a few hundreds enhancement for an electron in an heavy electronically paramagnetic atom such as Cesium, Thallium the respective factors of which are +114 [HLMP] and −585 [LK92]. The most accurate result obtained by an atomic experiment was given by the Berkeley experiment on the Thallium atom that manages to produce a 100 kV/cm electric field. The interpretation of their measurement of the atomic dipole moment combined with the calculated enhancement factor [LK92] yields an upper limit on the electron EDM $|d_e| \leq 1.6 \times 10^{-27}$e.cm [RCSD02]. Nevertheless, atomic experiments face difficulties that prevent physicists to further improve the sensitivity. Among other challenges, as previously explained, is the control of the stray magnetic fields that mimic the effect of an EDM. One of the most important is the motional magnetic field experienced by the electron in the applied electric field :

$$\mathbf{B}_m = \frac{\mathbf{v}}{c^2} \times \mathbf{E} \tag{1.3}$$

and it is much larger than the femtoTesla (fT) necessary to have magnetic and electric interactions of the same magnitude. Even though experimentalists developed strategies to address these issues, it emerged that a new generation of experiments was needed, this is where diatomic molecules came into play. Such molecules are more sensitive to the effect of the existence of an EDM of the electron, the enhancement factor can reach 10^6, many orders of magnitude larger than in atoms. One has to note that in the molecular framework, the enhancement factor R is no longer relevant, one needs to define the effective electric field $\mathcal{E}_{\text{eff}}$ related to the internal electric field of the molecules $\boldsymbol{\mathcal{E}}_{int}$ through $\langle \mathbf{d_e} \cdot \boldsymbol{\mathcal{E}}_{int} \rangle = d_e \mathcal{E}_{\text{eff}}$ and to R through $R = \frac{\mathcal{E}_{\text{eff}}}{\mathcal{E}_{\text{lab}}}$ because the effective electric field depends on the polarisation and is no longer proportional

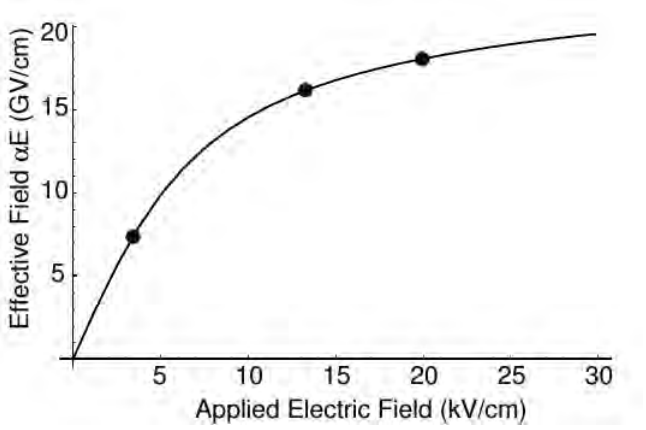

Figure 1.2 – Enhancement factor for YbF [SAHH06].

to the applied electric field $\mathcal{E}_{\text{lab}}$. In Figure 1.2, the effective electric field $\mathcal{E}_{\text{eff}}$ is plotted against the applied electric field $\mathcal{E}_{\text{lab}}$. The non-linear shape due to the polarisation factor is the one of a rigid rotor and the asymptotic value of the effective electric field $\mathcal{E}_{\text{eff,max}}$ has to be theoretically determined, which is one of the purposes of this thesis.

In diatomic molecules, the magnitude of the interaction to detect is in the range of the mHz and the magnetic field only needs to be controlled at the pT level which is still tiny but yet manageable, all the more so many features of the chosen molecules tend to suppress or at least strongly reduce the effects of the stray magnetic fields. First, this kind of molecules has a huge electric polarisability which not only ensures a large enhancement and a complete polarisation at a modest laboratory electric field $\mathcal{E}_{\text{lab}}$ (in the range of 10 V/cm for ThO [VSG+11]), minimising the magnetic field due to current leakage and making the shift to be measured independent of the laboratory electric field, but also a large tensor Stark shift that cancels the effect of the motional magnetic field (1.3). The large polarisability is ensured by the Ω-doublet structure that brings more assets for the detection of an electron EDM. One is the possibility for experimentalists to perform the spectroscopy reversal. Each of the two states of the Ω-doublet owns a dipole and thus an effective electric field respectively parallely and anti-parallely aligned with the laboratory electric field. Hence, it gives access to the reversed electron EDM interaction without reversing the applied electric field. In a following section, it will be explained how this constitutes an advantage for the experiment.

Finally, many experiments are carried out on molecules that exhibit a low-lying $^3\Delta_1$ state, like ThO, HfF^+ or ThF^+, which derives from a $s^1 d^1_\delta$ occupation. This configuration is really adequate since it ensures the main features required to both have a non-zero EDM and a very polar diatomic molecule, they were first exposed in [MBD06]. Indeed, the "science" electron occupying the s orbital undergoes the

relativistic electron EDM enhancement, due to the good overlap with the nucleus while the "spectroscopy" d_δ electron permits the large polarisability of the molecule. Besides, the total magnetic moment that reads $m_\Omega = -g_s\mu_B(\Sigma + \frac{\Lambda}{2})$ with g_s is the spin g-factor, μ_B the Bohr magneton, Σ the total spin quantum number and Λ the total orbital quantum number, vanishes since in the state of interest, either $\Sigma = -1$ and $\Lambda = 2$ or $\Sigma = 1$ and $\Lambda = -2$ [4]. This characteristic further reduces the effects of residual $\mathcal{B}$-fields.

Current EDM experiments, as well as the previous ones, are not measuring but rather improving the sensitivity to set an upper bound for the EDM. Nevertheless, the ultimate purpose is obviously to actually measure an electron EDM (eEDM). The figure-of-merit for the experimental uncertainty that accounts for the statistical noise, i.e the best sensitivity reachable, is:

$$\delta d_e = \frac{\hbar}{2\mathcal{E}_{\text{eff}}\tau\sqrt{N}} \tag{1.4}$$

where τ is the coherence time, N the number of measurements or N=$\dot{\text{N}}$T with $\dot{\text{N}}$ the detection rate and T the integration time of the experiment. In Table 1.2, we compiled for comparison these parameters in the most recent eEDM experiments.

Table 1.2 – Comparison of parameters of interest for the figure-of-merit in most recent eEDM experiments [LBL+11, Stu10].

Group	Molecule	$\mathcal{E}_{\text{lab}}$(V/cm)	$\mathcal{E}_{\text{eff}}$(V/cm)	τ(s)	$\dot{\text{N}}$(s^{-1})
Imperial College	YbF	8.3×10^3	1.3×10^{10}	10^{-3}	
ACME	ThO	10^2	10^{11}	2×10^{-3}	10^5
JILA	HfF^+	5	2×10^{10}	0.3	10

1.2.2 Experimental design.

Figure 1.3 displays the measurement scheme of the ThO experiment carried out by the ACME collaboration that provided the most restrictive limit on the electron EDM. The determination of the molecular electric dipole moment that allows for the evaluation of the electron electric dipole moment is made through a series of measurements of the energy shifts between the different $^3\Delta_1$ sublevels.

Let us describe the structure of the manifold of states. In such states the relevant quantum numbers are J, M_J, Ω where Ω is the absolute value of the projection of the total electronic angular momentum J_e along the molecular axis, J is the total

[4] This statement is valid because in this specific state, Hund's case (a) approximation remains appropriate. For more details on Hund's cases, see Appendix A.

Figure 1.3 – Energy level structure of ThO in the $^3\Delta_1(J=1)$ state in applied electric and magnetic fields [VCG+].

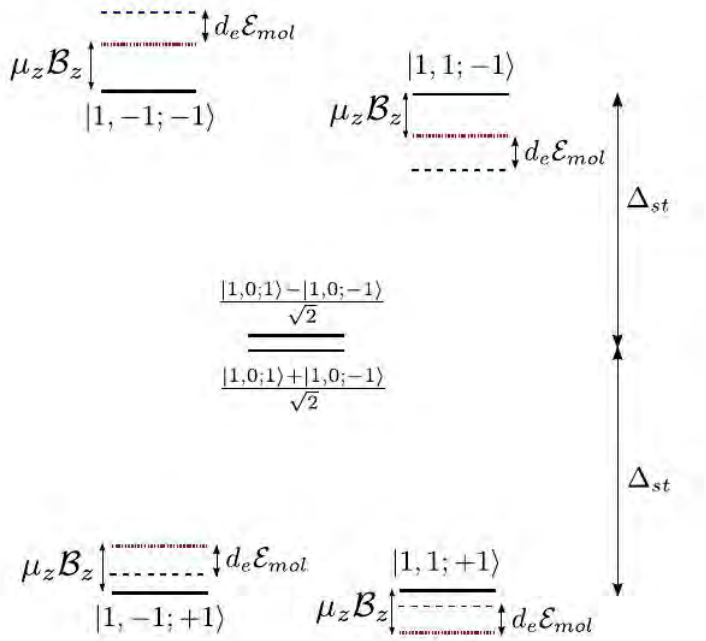

angular momentum of the molecule, sum of J_e and the nuclear rotation R, and M_J is its projection along the molecular axis.

In the absence of any external electric field, the eigenstates of the system are the parity states $|\pm\rangle = (|\Omega=+1\rangle \pm |\Omega=-1\rangle)$ following the symmetric or antisymmetric superposition of the two $|\Omega|=1$ states shifted by the Ω-doubling energy.

When an external electric field, large enough to fully polarise the molecule, is applied, the parity eigenstates are mixed, yielding $M_J = \pm 1$ states well described by Hund's case (c) for which the good quantum number is Ω. They split into pairs of levels that corresponds to $\mathcal{N} = \pm 1$ where $\mathcal{N}$ reflects the alignement or anti-alignement of the molecular dipole (hence the $\mathcal{E}_{eff}$) with the external electric field $\mathcal{E}_{lab}$. (One will note that the $M_J = 0$ states are not perturbed by the electric field.)

Lastly, the application of an external magnetic field ($\mathcal{B}$) and the existence of a permanent electron EDM (d_e) combined with an internal electric field induce Zeeman and EDM shifts that add up to the Stark effect to give the following energy splitting:

$$\Delta E_H = -\tilde{\mathcal{N}} d(J)|\mathcal{E}| - M_J g(J)\mu_B \tilde{\mathcal{B}}|\mathcal{B}| - M_J \tilde{\mathcal{N}}\eta\mu_B|\mathcal{E}|\tilde{\mathcal{B}}|\mathcal{B}| - M_J\tilde{\mathcal{N}}\tilde{\mathcal{E}} d_e \mathcal{E}_{eff} \quad (1.5)$$

where $d(J)$ and $g(J)$ are the electric dipole moment and the g-factors respectively of the J state, η reflects the difference of $g(J)$ between the $\mathcal{N}$ pairs and a quantity marked with a "~" denotes the sign of this same quantity that will be reversed during the experiment, $\tilde{\mathcal{N}} = sign(\mathcal{N})$, $\tilde{\mathcal{B}} = sign(\mathbf{B}\cdot\mathbf{e_z})$ and $\tilde{\mathcal{E}} = sign(\mathbf{E}\cdot\mathbf{e_z})$ where $\mathbf{e_z}$ is

Figure 1.4 – Energy level structure of HfF^+ in the $^3\Delta_1(J = 1)$ state including the hyperfine shifting respectively in the absence of electric field (a), in the presence of an external electric field (b) and under the application of a magnetic field in addition to the electric field and the existence of a permanent eEDM (c) [LBL+11].

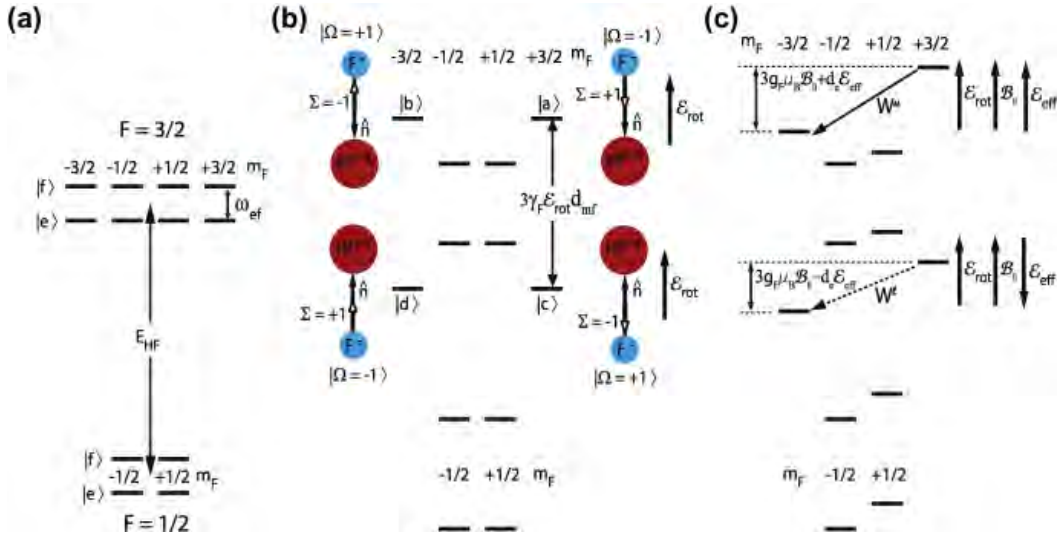

the unitary vector along the molecular axis. Note that the different $\mathcal{N}$ levels exhibit opposite Stark shifts while the Zeeman shift has opposite sign for two M_J levels and the direction of the electron EDM is determined by M_J. These features allow one to isolate one effect from the others by playing with the set of parameters $\{\tilde{\mathcal{B}}, \tilde{\mathcal{E}}, \tilde{\mathcal{N}}\}$. Thus, by measuring the energy difference between the $M_J = \pm 1$ states through spin precession measurement:

$$\Delta E(\mathcal{N}) = 2(\mathcal{N} d_e \mathcal{E}_{eff} + g_{\mathcal{N}} \mu_B \mathcal{B}), \tag{1.6}$$

and switching between the $\mathcal{N} = \pm 1$ pairs, one can determine the eEDM interaction independently of the magnetic field:

$$\Delta E(1) - \Delta E(-1) = 4 d_e \mathcal{E}_{eff}. \tag{1.7}$$

However, the measurement is not totally immune to the effect of magnetic fields because of the non-zero difference of $g(J)$ between the two $\mathcal{N}$ levels.

The JILA experiment scheme (Figure 1.4) is very similar to the one used by ACME. The specificity of the experiments led in JILA is the use of this scheme on molecular ions that provide further assets for the measurement, in particular long coherence times due to the easiness to trap them.

2 $\mathcal{P},\mathcal{T}$-ODD INTERACTIONS.

In order to complete and refine the assertions in Chapter 1, it is necessary to outline that the Electric Dipole Moment of a given system comprises a number of possible contributions, not only stemming from the assumed electron EDM. Thus, the EDM of a system can be written as a summation over the various sources,

$$d_i = \sum_j \alpha_{ij} C_j \tag{2.1}$$

where the C_j are the $\mathcal{P}$- and $\mathcal{T}$-violating fundamental parameters accounting for the strength of the corresponding $\mathcal{CP}$-violating interactions and α_{ij}, the system-dependent enhancement factors for which theoretical calculations are required. By taking into account the seven leading contributors, Eq. (2.1) can be expanded [CRM15]:

$$d = \alpha_{d_e} d_e + \alpha_{C_S} C_S + \alpha_{C_T} C_T + \alpha_{\bar{d}_n} \bar{d}_n + \alpha_{\bar{d}_p} \bar{d}_p + \alpha_{g_\pi^0} \bar{g}_\pi^0 + \alpha_{g_\pi^1} \bar{g}_\pi^1 \tag{2.2}$$

where d_e is the electron EDM (see Section 2.1), C_S and C_T are respectively the scalar-pseudoscalar and tensor constant of the electron-nucleon interaction (see Section 2.2), $\bar{d}_n$ and $\bar{d}_p$ are the short-range contributions to the neutron and proton EDMs and $\bar{g}_\pi^0$ and $\bar{g}_\pi^1$ are the isoscalar and the isovector pion-nucleon coupling constants.

In the paramagnetic sector under the scope of this thesis, the dominant contributing parameters are d_e and C_S. More robust, model-independent, constraint limits may be set on these interaction constants [Jun13]. First, one should take into account the scalar-pseudoscalar electron-nucleon parameter that may be naively set to zero. Likewise, to refine the upper bounds, one has to consider both experimental uncertainties and numerical uncertainty on the theoretical $\frac{\alpha_{C_S}}{\alpha_{d_e}}$ ratio. Finally, improved constraints on d_e and C_S are established through a fit of the results obtained by the recent measurements on the paramagnetic systems Tl, YbF and ThO that exhibit similar combination of the two terms. In this way, as displayed in Figure 2.1, error ellipses are obtained and allow for setting more robust upper bounds on the parameters.

In the following, the expressions for the enhancement factors of the relevant $\mathcal{P},\mathcal{T}$-odd interactions will be derived.

Figure 2.1 – Fit in the $d_e - C_S$ plane of the recent experimental and theoretical results in paramagnetic systems [Jun15].

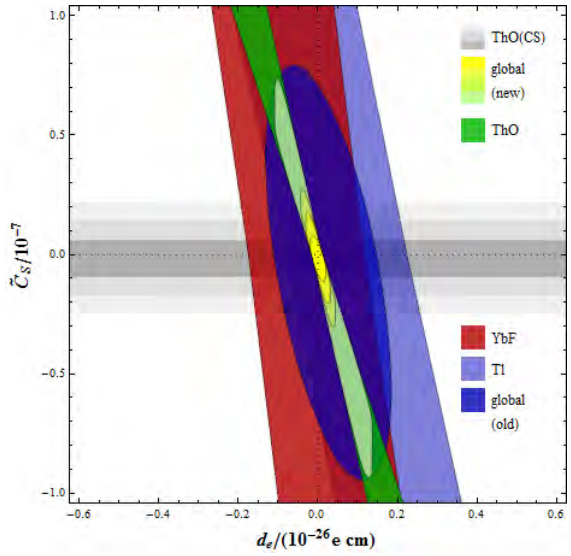

2.1 Electron EDM.

In this section, the theory of the dominant contribution to the EDM of a paramagnetic system, *i.e.* the electron EDM interaction is tackled in a detailed review of the eEDM interaction.

2.1.1 Electron EDM interaction Hamiltonian.

First, the Lorentz- and gauge invariant, $\mathcal{P},\mathcal{T}$-odd Lagrangian that accounts for the electron EDM interaction is derived. For that purpose, one has to modify the Dirac equation[1]:

$$\left\{\left[\pi^\mu\pi_\mu + m_0^2c^2\right] + \frac{\hbar e}{2ic}\gamma^\mu\gamma^\nu F_{\mu\nu}\right\}\hat{\psi} = 0 \tag{2.3}$$

where m_0 is the mass of the electron in its rest frame, c is the speed of light in vacuum and π^μ satisfies the minimal coupling[2], *i.e.*, $\pi^\mu = p^\mu + \frac{e}{c}A^\mu$ with $p^\mu = \left(\frac{E}{c},\ \boldsymbol{p}\right)$, the 4-momentum and $A^\mu = (\phi,\ \boldsymbol{A})$, the 4-potential. Besides $F_{\mu\nu}$ is the electromagnetic field tensor, $\hat{\psi}$ is a fermion Dirac field and γ^μ, γ^ν are 4×4 Dirac matrices

$$\gamma^k = \begin{pmatrix} 0 & \sigma^k \\ -\sigma^k & 0 \end{pmatrix}, \quad \gamma^0 = \begin{pmatrix} \mathbb{1}_2 & 0 \\ 0 & -\mathbb{1}_2 \end{pmatrix} \tag{2.4}$$

[1]The following forms of the Dirac and Salpeter-modified Dirac equation differ from [BS12]'s Eq.(10.14) and [Sal58]'s Eq.(1) by the use of Einstein summation convention.

[2]The derivation of this substitution is given in Appendix B, moreover in this Section 2.1.1, the Gaussian unit system is employed.

build from the Pauli matrices. The first term of Eq. (2.3) corresponds to the Klein-Gordon equation, relativistic version of the Schrödinger equation for spin-less particles while the second term, characteristic of the Dirac theory, represents the interaction of an electromagnetic field with electric and magnetic dipole moments, it is the so-called Dirac moment. To make the equation Lorentz- and gauge invariant, some combinations of the Dirac matrices γ^μ and derivatives of the electromagnetic potentials are added, yielding to the modified Dirac equation[BS12]:

$$\left(\pi^\mu\gamma_\mu - \imath m_0 c\right)\hat{\psi} = \left[g_1\frac{\hbar e}{4m_0c^2}\gamma^\mu\gamma^\nu F_{\mu\nu} - g_2\frac{e}{c}\left(\frac{\hbar}{m_0 c}\right)^2\gamma^\mu\partial^\mu\partial_\mu A_\mu\right]\hat{\psi} \tag{2.5}$$

The term of interest in this equation is the one involving g_1, it is akin to the Dirac moment defined above and is refered to as the Pauli moment term.
In order to include the electric dipole moment interaction in the Dirac equation, one will proceed by introducing a term similar to the Pauli moment term [Sal58] and will get the following modified equation:

$$\left(\pi^\mu\gamma_\mu - \imath m_0 c\right)\hat{\psi} = -\zeta\left(\frac{e\hbar}{4m_0c^2}\right)\gamma^5\gamma^\mu\gamma^\nu F_{\mu\nu}\hat{\psi} \tag{2.6}$$

and the apropriate Lagrangian density to account for the EDM interaction:

$$\hat{L}_{EDM} = -\imath\frac{d_e}{2}\hat{\psi}^\dagger\gamma^0\gamma^5\frac{\imath}{2}\left(\gamma^\mu\gamma^\nu - \gamma^\nu\gamma^\mu\right)\hat{\psi}F_{\mu\nu}[\text{Com99}]. \tag{2.7}$$

The $\mathcal{P},\mathcal{T}$-odd character of the Lagrangian is assured by the γ^5 factor. Indeed, the γ^5 matrix is off diagonal: $\gamma^5 = \imath\gamma^0\gamma^1\gamma^2\gamma^3 = \begin{pmatrix}\mathbf{0} & \mathbb{1}_2\\ \mathbb{1}_2 & \mathbf{0}\end{pmatrix}$, and thus entails the coupling of Large and Small components of the 4-component wavefunction and as a consequence, the non conservation of the parity. And, the $\imath$ prefactor guarantees the hermiticity of the corresponding Hamiltonian that reads as follows:

$$\hat{H}_{EDM} = -\frac{d_e}{4}\gamma^0\gamma^5\left(\gamma^\mu\gamma^\nu - \gamma^\nu\gamma^\mu\right)\hat{F}_{\mu\nu}. \tag{2.8}$$

2.1.2 Electromagnetic contributions to $\hat{H}_{EDM}$.

For the sake of clarity, one may rewrite the Hamiltonian to explicitly exhibit the respective contributions of the magnetic and electric fields. They are contained in the electromagnetic field tensor $F_{\mu\nu}$:

$$F^{\mu\nu} = \begin{pmatrix} 0 & E_1 & E_2 & E_3\\ -E_1 & 0 & B_3 & -B_2\\ -E_2 & -B_3 & 0 & B_1\\ -E_3 & B_2 & -B_1 & 0\end{pmatrix}. \tag{2.9}$$

defined with the same convention employed by J.D. Jackson in [Jac99]. Here, the chosen unit system sets the same unit for both fields.
First, we divide the $(\gamma^\mu\gamma^\nu - \gamma^\nu\gamma^\mu)\,\hat{F}_{\mu\nu}$ term into two parts that will bring respectively electric F_{0i} and magnetic contributions F_{ij} where i, j take the values $\{1, 2, 3\}$,

$$(\gamma^\mu\gamma^\nu - \gamma^\nu\gamma^\mu)\,\hat{F}_{\mu\nu} = \left(\gamma^0\gamma^i - \gamma^i\gamma^0\right) F_{0i} + \left(\gamma^i\gamma^0 - \gamma^0\gamma^i\right) F_{i0} + \left(\gamma^i\gamma^j - \gamma^j\gamma^i\right) F_{ij}. \tag{2.10}$$

Since the electromagnetic tensor is anti-symmetric, $F_{\mu\nu} = -F_{\nu\mu}$ and in particular: $F_{i0} = -F_{0i}$, $F_{ij} = -F_{ji}$, yielding:

$$(\gamma^\mu\gamma^\nu - \gamma^\nu\gamma^\mu)\,\hat{F}_{\mu\nu} = 2\left(\gamma^0\gamma^i - \gamma^i\gamma^0\right) F_{0i} + 2\left(\gamma^i\gamma^j - \gamma^j\gamma^i\right) F_{ij>i}. \tag{2.11}$$

Let us calculate the required commutators $[\gamma^0, \gamma^i]$, $[\gamma^i, \gamma^j]$. One will get $[\gamma^0, \gamma^i] = 2\gamma^0\gamma^i$ and $[\gamma^i, \gamma^j] = 2\gamma^i\gamma^j$ since

$$\gamma^0\gamma^i = \begin{pmatrix} \mathbb{1}_2 & 0 \\ 0 & -\mathbb{1}_2 \end{pmatrix} \begin{pmatrix} 0 & \sigma^i \\ -\sigma^i & 0 \end{pmatrix} = \begin{pmatrix} 0 & \sigma^i \\ \sigma^i & 0 \end{pmatrix} \tag{2.12}$$

and

$$\gamma^i\gamma^0 = \begin{pmatrix} 0 & \sigma^i \\ -\sigma^i & 0 \end{pmatrix} \begin{pmatrix} \mathbb{1}_2 & 0 \\ 0 & -\mathbb{1}_2 \end{pmatrix} = -\begin{pmatrix} 0 & \sigma^i \\ \sigma^i & 0 \end{pmatrix}. \tag{2.13}$$

Likewise, one could demonstrate:

$$\gamma^i\gamma^j = -\gamma^j\gamma^i = -\imath\varepsilon^{ijk} \begin{pmatrix} \sigma^k & 0 \\ 0 & \sigma^k \end{pmatrix} \tag{2.14}$$

where ε^{ijk} is the three-dimensional Levi-Civita permutation symbol that gives $+1$ for any even (cyclic) permutation of $(1, 2, 3)$, -1 for an odd (anticyclic) permutation and zero if an index is repeated. Explicitly, it gives:

$$\varepsilon^{ijk} = \begin{cases} +1 & \text{for } (i,j,k) = (1,2,3), (2,3,1), \text{ or } (3,1,2), \\ -1 & \text{for } (i,j,k) = (3,2,1), (1,3,2), \text{ or } (2,1,3), \\ 0 & \text{for } i = j, \text{ or } j = k, \text{ or } k = i. \end{cases} \tag{2.15}$$

Thus Eq. (2.11) becomes

$$(\gamma^\mu\gamma^\nu - \gamma^\nu\gamma^\mu)\,\hat{F}_{\mu\nu} = 4\gamma^0\gamma^i F_{0i} + 4\gamma^i\gamma^j F_{ij>i}. \tag{2.16}$$

In order to insert the latter equalities in the EDM Hamiltonian, one needs to calculate the following products:

$$\gamma^5\gamma^0\gamma^i = \begin{pmatrix} \mathbf{0} & \mathbb{1}_2 \\ \mathbb{1}_2 & \mathbf{0} \end{pmatrix} \begin{pmatrix} 0 & \sigma^i \\ \sigma^i & 0 \end{pmatrix} = \begin{pmatrix} \sigma^i & 0 \\ 0 & \sigma^i \end{pmatrix} = \Sigma^i \tag{2.17}$$

and

$$\gamma^5\gamma^i\gamma^j = -\imath \begin{pmatrix} \mathbf{0} & \mathbb{1}_2 \\ \mathbb{1}_2 & \mathbf{0} \end{pmatrix} \begin{pmatrix} \sigma^k & 0 \\ 0 & \sigma^k \end{pmatrix} = -\imath\varepsilon^{ijk} \begin{pmatrix} \mathbf{0} & \sigma^k \\ \sigma^k & \mathbf{0} \end{pmatrix} = -\imath\varepsilon^{ijk}\alpha^k. \tag{2.18}$$

Then, by making use of $F_{\mu\nu} = g_{\mu\alpha}g_{\nu\beta}F^{\alpha\beta}$ where $g_{\mu\nu}$ is the metric tensor and is conventionally defined as:

$$g_{\mu\nu} = \begin{pmatrix} 1 & 0 & 0 & 0 \\ 0 & -1 & 0 & 0 \\ 0 & 0 & -1 & 0 \\ 0 & 0 & 0 & -1 \end{pmatrix}, \tag{2.19}$$

we have $F_{0i} = g_{00}g_{ii}F^{0i} = -E_i$ and $F_{ij} = g_{ii}g_{jj}F^{ij} = \varepsilon^{ijk}B_k$ that leads to

$$\hat{H}_{EDM} = -d_e \left[\gamma^0\Sigma^i E_i + i\gamma^k B_k\right] = -d_e \left[\gamma^0\boldsymbol{\Sigma}\cdot\mathbf{E} + i\boldsymbol{\gamma}\cdot\mathbf{B}\right]. \tag{2.20}$$

In the following, that will focus on the paramagnetic sector, the magnetic contributions will be assumed to be negligible. The first term and in particular its symmetry properties will be examined carefully. But first, let us consider the physical meaning of this operator. This can be done by analogy with the electrostatic energy of a dipole

$$\epsilon_{dip} = -\mathbf{D}\cdot\mathbf{E} \tag{2.21}$$

where $d_e\gamma^0\boldsymbol{\Sigma}\cdot\mathbf{E}(i)$ would be the dipole moment operator and $\mathbf{E}(i)$, the electric field at the position of the considered particle i. The latter includes both external and internal electric fields $\mathbf{E}(i) = \mathbf{E}_{int}(i) + \mathbf{E}_{ext}(i)$. $\mathbf{E}_{ext}(i)$ is an external field such as an applied laboratory field and $\mathbf{E}_{int}(i)$ is the resulting electric field applied by other particles in the molecule or the atom. It can be decomposed into a nuclear and an electronic part.

$$\mathbf{E}_{int}(i) = -\sum_{A=1}^{N} \vec{\nabla}_{iA}\phi_{iA} - \sum_{j=1}^{n} \vec{\nabla}_{ij}\phi_{ij} = \sum_{A=1}^{N} \frac{Ze(\mathbf{r}_i - \mathbf{r}_A)}{||\mathbf{r}_i - \mathbf{r}_A||^3} - \sum_{j=1}^{n} \frac{e(\mathbf{r}_i - \mathbf{r}_j)}{||\mathbf{r}_i - \mathbf{r}_j||^3} \tag{2.22}$$

with N is the number of nuclei and n the number of electrons within the Born-Oppenheimer approximation where the nuclei are assumed to be at rest. Due to the dramatic decrease of $\mathbf{E}_{int}(i)$ while the distance between the considered electron and the other particles -particularly the nuclei- increases, the electron will undergo a large electric field in the vicinity of a heavy nucleus.

2.1.3 Symmetry properties of $\hat{H}_{EDM}$.

As we argued that the existence of a permanent Electric Dipole Moment could entail a $\mathcal{P},\mathcal{T}$-odd interaction, let us consider the behaviour of the electric part of the corresponding EDM interaction Hamiltonian under the relevant symmetry transformations, which are the Parity and Time-reversal operations.

2.1.3.1 Parity transformation.

First, let us derive the parity inversion $\hat{\mathcal{P}}$ operator that would act in spinor space. In the Minkowski space-time, this operator reads:

$$\Lambda(\hat{\mathcal{P}}) = \begin{pmatrix} 1 & 0 & 0 & 0 \\ 0 & -1 & 0 & 0 \\ 0 & 0 & -1 & 0 \\ 0 & 0 & 0 & -1 \end{pmatrix} = g, \tag{2.23}$$

its representation coincides with the metric tensor. However, we aim to represent the $\hat{\mathcal{P}}$ operator in the spinor space. For this purpose, since we know that spins are well described in Dirac theory and that the Dirac equation verifies the Lorentz-invariance, we seek for a Lorentz-transformation:

$$S^{-1}(\Lambda)\gamma^{\mu}S(\Lambda) = \Lambda^{\mu}{}_{\nu}\gamma^{\nu} \tag{2.24}$$

corresponding to the improper orthochronous ($\hat{\mathcal{P}}$) transformation. The relation to satisfy is:

$$\hat{\mathcal{P}}^{-1}(\Lambda)\gamma^{\mu}\hat{\mathcal{P}}(\Lambda) = g^{\mu}{}_{\nu}\gamma^{\nu}. \tag{2.25}$$

A possible solution is

$$\hat{\mathcal{P}} = e^{i\varphi}\gamma^0 \tag{2.26}$$

where $e^{i\varphi}$ is an irrelevant phase. Hence, the parity inversion operator in the spinor space reads:

$$\hat{\mathcal{P}} = \gamma^0. \tag{2.27}$$

This can be easily checked by applying it on the Dirac matrices:

$$\begin{aligned} \gamma^0\gamma^0\gamma^0 &= \mathbb{1}_4\gamma^0 = \gamma^0 \\ \gamma^0\gamma^k\gamma^0 &= -\gamma^k\gamma^0\gamma^0 = -\gamma^k. \end{aligned} \tag{2.28}$$

Then, one can apply the $\hat{\mathcal{P}}$ operator on the EDM Hamiltonian:

$$\begin{aligned} \hat{\mathcal{P}}^{\dagger}\hat{H}_{EDM}\hat{\mathcal{P}} &= -d_e\hat{\mathcal{P}}^{\dagger}\gamma^0\boldsymbol{\Sigma}\cdot\mathbf{E}\hat{\mathcal{P}} \\ &= -d_e\gamma^0\hat{\mathcal{P}}^{\dagger}\boldsymbol{\Sigma}\hat{\mathcal{P}}\cdot\hat{\mathcal{P}}^{\dagger}\mathbf{E}\hat{\mathcal{P}}. \end{aligned} \tag{2.29}$$

Considering that $\boldsymbol{\Sigma}$ which accounts for the angular momentum is a pseudo-vector and $\mathbf{E}$ is a contravariant vector, we have:

$$\begin{aligned} \hat{\mathcal{P}}^{\dagger}\boldsymbol{\Sigma}\hat{\mathcal{P}} &= \boldsymbol{\Sigma} \\ \hat{\mathcal{P}}^{\dagger}\mathbf{E}\hat{\mathcal{P}} &= -\mathbf{E} \end{aligned} \tag{2.30}$$

yielding:

$$\hat{\mathcal{P}}^{\dagger}\hat{H}_{EDM}\hat{\mathcal{P}} = -d_e\gamma^0\boldsymbol{\Sigma}\cdot(-\mathbf{E}) = -\hat{H}_{EDM}. \tag{2.31}$$

This proves that $\hat{H}_{EDM}$ is purely $\mathcal{P}$-odd (parity-odd).

2.1.3.2 Time-reversal transformation.

In a very similar way, we focus on the time-reversal transformation, starting by defining the anti-chronous operator $\hat{\mathcal{K}}$. In the Minkowski space, it reads:

$$\Lambda(\hat{\mathcal{K}}) = \begin{pmatrix} -1 & 0 & 0 & 0 \\ 0 & 1 & 0 & 0 \\ 0 & 0 & 1 & 0 \\ 0 & 0 & 0 & 1 \end{pmatrix} = \tilde{g}, \tag{2.32}$$

yielding the equation for the improper anti-chronous Lorentz-transformation:

$$\hat{\mathcal{K}}^{-1}(\Lambda)\gamma^{\mu}\hat{\mathcal{K}}(\Lambda) = \tilde{g^{\mu}}_{\mu}\gamma^{\mu}. \tag{2.33}$$

The solution is expected to be anti-unitary and therefore to take the form:

$$\hat{\mathcal{K}} = U\hat{\mathcal{K}}_0 \tag{2.34}$$

where U is a unitary operator to determine and $\hat{\mathcal{K}}_0$ is the complex conjugation. Let us make the $\hat{\mathcal{K}}$ operator act on the Dirac matrices and deduce the arising constraints on U for a fermion,

$$\begin{aligned} \hat{\mathcal{K}}^{-1}\gamma^0\hat{\mathcal{K}} &= U^{-1}\gamma^0 U = -\gamma^0, \\ \hat{\mathcal{K}}^{-1}\gamma^1\hat{\mathcal{K}} &= U^{-1}\gamma^1 U = \gamma^1, \\ \hat{\mathcal{K}}^{-1}\gamma^2\hat{\mathcal{K}} &= -U^{-1}\gamma^2 U = \gamma^2, \\ \hat{\mathcal{K}}^{-1}\gamma^3\hat{\mathcal{K}} &= U^{-1}\gamma^3 U = \gamma^3. \end{aligned} \tag{2.35}$$

Thus, U has to commute with γ^0 and γ^2 and anticommute with γ^1 and γ^3. We seek the 4×4 U matrix as a combination of the 4×4 Σ^k matrices equivalent to Pauli matrices:

$$\Sigma^k = \begin{pmatrix} \sigma^k & 0 \\ 0 & \sigma^k \end{pmatrix}. \tag{2.36}$$

The latter are related to γ matrices through:

$$\Sigma^k = \gamma^5\gamma^0\gamma^k \tag{2.37}$$

demonstrated in Eq. (2.17). Therefore, we seek for k such as

$$\left[\gamma^5\gamma^0\gamma^k, \gamma^0\right] = \left[\gamma^5\gamma^0\gamma^k, \gamma^2\right] = 0 \tag{2.38}$$

and

$$\left\{\gamma^5\gamma^0\gamma^k, \gamma^1\right\} = \left\{\gamma^5\gamma^0\gamma^k, \gamma^3\right\} = 0. \tag{2.39}$$

By making use of the following equalities:

$$\{\gamma^\mu, \gamma^\nu\} = 2g^{\mu\nu}\mathbb{1}_4, \quad \left(\gamma^0\right)^2 = \mathbb{1}_4, \quad \left(\gamma^k\right)^2 = -\mathbb{1}_4, \tag{2.40}$$

one deduce that k necessarily equals 2 and for the sake of the unitarity of U, the prefactor must be $\imath$. Finally, the time-reversal operator in the spinor space is:

$$\hat{\mathcal{K}} = -\imath\Sigma^y\hat{\mathcal{K}}_0. \tag{2.41}$$

Now, we analyse the property of the Hamiltonian under the application of the $\mathcal{K}$ operator,

$$\begin{aligned}\hat{\mathcal{K}}^\dagger\hat{H}_{EDM}\hat{\mathcal{K}} &= -d_e\hat{\mathcal{K}}^\dagger\gamma^0\boldsymbol{\Sigma}\cdot\mathbf{E}\hat{\mathcal{K}} \\ &= -d_e\gamma^0\hat{\mathcal{K}}^\dagger\boldsymbol{\Sigma}\hat{\mathcal{K}}\cdot\hat{\mathcal{K}}^\dagger\mathbf{E}\hat{\mathcal{K}}.\end{aligned} \tag{2.42}$$

$\mathbf{E}$ deriving from charges does not change sign under time-reversal transformation while the angular momentum $\boldsymbol{\Sigma}$ does which entails the $\mathcal{T}$-oddness of the Hamiltonian

$$\hat{\mathcal{K}}^\dagger\hat{H}_{EDM}\hat{\mathcal{K}} = -\hat{H}_{EDM}. \tag{2.43}$$

These two symmetry properties of the EDM Hamiltonian, in particular the $\mathcal{P}$-oddness, have consequences of importance when one aims to calculate the expectation value of $\hat{H}_{EDM}$. The method employed to determine this latter will be expounded below.

2.1.3.3 Expectation value.

A consequence of the $\mathcal{P}$-odd characteristic of the $\hat{H}_{EDM}$ Hamiltonian is its vanishing expectation value over atomic electronic wavefunctions. Indeed, unperturbed states of an atom are parity eigenstates, i.e., their wavefunction is either even or odd under parity transformation. Thus, the expectation value of $\hat{H}_{EDM}$ over such a state is written as

$$\begin{aligned}\left\langle\psi_p\left|\hat{H}_{EDM}\right|\psi_p\right\rangle &= \left\langle\psi_p\left|\hat{\mathcal{P}}^\dagger\hat{\mathcal{P}}\hat{H}_{EDM}\hat{\mathcal{P}}^\dagger\hat{\mathcal{P}}\right|\psi_p\right\rangle \\ &= \left\langle\psi_p\left|p(-\hat{H}_{EDM})p\right|\psi_p\right\rangle\end{aligned} \tag{2.44}$$

where $p = \pm 1$ is the parity eigenvalue of the considered state. It follows:

$$\begin{aligned}\left\langle\psi_p\left|\hat{H}_{EDM}\right|\psi_p\right\rangle &= -p^2\left\langle\psi_p\left|\hat{H}_{EDM}\right|\psi_p\right\rangle \\ &= -\left\langle\psi_p\left|\hat{H}_{EDM}\right|\psi_p\right\rangle \\ &= 0.\end{aligned} \tag{2.45}$$

If we assume that the expectation value of the electron EDM Hamiltonian is non-zero, the states are necessarily no longer parity eigenstates. Hence, the eEDM can be

sought in an atom placed in a perturbing external electric field that would mix states of different parity such as s- and p- orbitals. Therefore, it would result in a non-zero expectation value of the EDM Hamiltonian. The same reasoning can be applied to heteronuclear diatomic molecules made up of a heavy nucleus atom and another lighter atom. Then, the light atom acts as a perturbing field and mixes the states of the heavy atom, in particular, the science state in which we aim to determine the eEDM.

Besides, the energy shifts induced by a $\mathcal{P},\mathcal{T}$-violating interaction[3] are expected to be very small and the energy differences between electronic states (characterised by the Ω quantum number following the Hund's case C Appendix A) are in the range of eV. Thus, the corrections to $E^{(0)}_{\Omega_j}$ of higher order than the first order such as[4]

$$E^{(2)}_{\mathcal{P},\mathcal{T}}(\Omega_j) = \sum_{k\neq j} \frac{\left|\left\langle \Omega_j \left| \hat{H}_{\mathcal{P},\mathcal{T}} \right| \Omega_k \right\rangle\right|^2}{E^{(0)}_{\Omega_j} - E^{(0)}_{\Omega_k}} \tag{2.46}$$

will be extremely small and may be neglected.
Let us focus on the calculation of the integrals in a $\{|\Omega_j\rangle, |-\Omega_j\rangle\}$ subspace made up of the Ω-doublet ($\Omega \neq 0$) whose eigenstates undergo a small splitting in the presence of an external electric field and assuming a perfect polarization (as it is the case in the $^3\Delta_1$ molecular states). By making use of symmetry arguments, it can be shown that the off-diagonal matrix elements vanish:

$$\left\langle -\Omega_j \left| \hat{H}_{\mathcal{P},\mathcal{T}} \right| \Omega_j \right\rangle = \left\langle \Omega_j \left| \hat{H}_{\mathcal{P},\mathcal{T}} \right| -\Omega_j \right\rangle = 0. \tag{2.47}$$

Indeed, irreducible representation of the integrand does not contain the totally symmetric representation, therefore the integral over symmetric ranges will give zero. Furthermore,

$$\left\langle -\Omega_j \left| \hat{H}_{\mathcal{P},\mathcal{T}} \right| -\Omega_j \right\rangle = \left\langle \Omega_j \left| \hat{\mathcal{P}}^\dagger \hat{H}_{\mathcal{P},\mathcal{T}} \hat{\mathcal{P}} \right| \Omega_j \right\rangle = -\left\langle \Omega_j \left| \hat{H}_{\mathcal{P},\mathcal{T}} \right| \Omega_j \right\rangle \tag{2.48}$$

and

$$\left\langle -\Omega_j \left| \hat{H}_{\mathcal{P},\mathcal{T}} \right| -\Omega_j \right\rangle = \left\langle \Omega_j \left| \hat{\mathcal{K}}^\dagger \hat{H}_{\mathcal{P},\mathcal{T}} \hat{\mathcal{K}} \right| \Omega_j \right\rangle = -\left\langle \Omega_j \left| \hat{H}_{\mathcal{P},\mathcal{T}} \right| \Omega_j \right\rangle \tag{2.49}$$

where $\hat{\mathcal{P}}$ and $\hat{\mathcal{K}}$ the parity and time-reversal operator respectively. Hence, in the $\{|\Omega_j\rangle, |-\Omega_j\rangle\}$ subspace, only one matrix element needs to be calculated.

2.1.4 Alternative form.

In an attempt to solve the two problems that one has to cope with when calculating the EDM, one could use an alternative form. These two problems and

[3] Here, we consider the electron EDM interaction but it is valid for all $\mathcal{P},\mathcal{T}$-odd interactions.
[4] $\hat{H}_{\mathcal{P},\mathcal{T}}$ denotes any $\mathcal{P},\mathcal{T}$-odd Hamiltonian.

the respective advantages of each formulation will be expounded in the following subsection.

2.1.4.1 Hydrogen-like case.

First, let us derive the alternative form in the case of a hydrogen-like system before generalising to many-electron systems.
We want to obtain another way to write the expectation value of $\hat{H}_{EDM}$

$$E^{(1)}_{EDM} = \left\langle -d_e\gamma^0\boldsymbol{\Sigma}\cdot\mathbf{E}\right\rangle_{\psi^{(0)}} \tag{2.50}$$

over the wavefunction $\psi^{(0)}$ obtained as an eigenfunction

$$\hat{H}^{(0)}\left|\psi^{(0)}\right\rangle = E^{(0)}\left|\psi^{(0)}\right\rangle \tag{2.51}$$

of the zeroth-order Hamiltonian

$$\hat{H}^{(0)} = c\boldsymbol{\alpha}\cdot\mathbf{p} + \gamma^0 m_0c^2 - e\phi\mathbb{1}_4. \tag{2.52}$$

For this purpose, we write the electric field $\mathbf{E}$ as a gradient of the scalar potential $-e\phi$

$$\left\langle -d_e\gamma^0\boldsymbol{\Sigma}\cdot\mathbf{E}\right\rangle_{\psi^{(0)}} = \frac{d_e}{e}\left\langle -d_e\gamma^0\boldsymbol{\Sigma}\cdot(\nabla_{\mathbf{r}}\mathbf{e}\phi)\right\rangle_{\psi^{(0)}} \tag{2.53}$$

and we absorb it in a commutator with the momentum $\mathbf{p}$ with respect to the following equality:

$$\begin{aligned}[\boldsymbol{\Sigma}\cdot\mathbf{p}, e\phi\mathbb{1}_4] &= (\boldsymbol{\Sigma}\cdot\mathbf{p})e\phi - e\phi\boldsymbol{\Sigma}\cdot\mathbf{p}\\ &= \boldsymbol{\Sigma}\cdot e(\mathbf{p}\phi) + \boldsymbol{\Sigma}\cdot e\phi\mathbf{p} - e\phi\boldsymbol{\Sigma}\cdot\mathbf{p}\\ &= \boldsymbol{\Sigma}\cdot e(\mathbf{p}\phi)\end{aligned} \tag{2.54}$$

leading to:

$$\left\langle -d_e\gamma^0\boldsymbol{\Sigma}\cdot\mathbf{E}\right\rangle_{\psi^{(0)}} = \frac{\imath d_e}{e\hbar}\left\langle\gamma^0\left[\boldsymbol{\Sigma}\cdot\mathbf{p}, e\phi\mathbb{1}_4\right]\right\rangle_{\psi^{(0)}}. \tag{2.55}$$

Then, we insert the γ^0 matrix in the commutator by using the rule: $\hat{A}[\hat{B},\hat{C}] = [\hat{A}\hat{B},\hat{C}] - [\hat{A},\hat{C}]\hat{B}$,

$$\begin{aligned}\left\langle -d_e\gamma^0\boldsymbol{\Sigma}\cdot\mathbf{E}\right\rangle_{\psi^{(0)}} &= \frac{\imath d_e}{e\hbar}\left\langle\left[\gamma^0\boldsymbol{\Sigma}\cdot\mathbf{p}, e\phi\mathbb{1}_4\right] - \left[\gamma^0, e\phi\mathbb{1}_4\right]\boldsymbol{\Sigma}\cdot\mathbf{p}\right\rangle_{\psi^{(0)}}\\ &= \frac{\imath d_e}{e\hbar}\left\langle\left[\gamma^0\boldsymbol{\Sigma}\cdot\mathbf{p}, e\phi\mathbb{1}_4\right]\right\rangle_{\psi^{(0)}}.\end{aligned} \tag{2.56}$$

Then, Eq. (2.52) is used to replace the electric potential,

$$\left\langle -d_e\gamma^0\boldsymbol{\Sigma}\cdot\mathbf{E}\right\rangle_{\psi^{(0)}} = \frac{\imath d_e}{e\hbar}\left\langle\left[\gamma^0\boldsymbol{\Sigma}\cdot\mathbf{p}, c\boldsymbol{\alpha}\cdot\boldsymbol{p} + \gamma^0 m_0c^2 - \hat{H}^{(0)}\right]\right\rangle_{\psi^{(0)}}. \tag{2.57}$$

We are left with three commutators, one can prove that two of them vanish.
The commutator with the zeroth-order Hamiltonian cancels out because $\psi^{(0)}$ is an eigenstate of this Hamiltonian:

$$\begin{aligned}\left\langle\left[\gamma^0\boldsymbol{\Sigma}\cdot\mathbf{p},\hat{H}^{(0)}\right]\right\rangle_{\psi^{(0)}} &= \left\langle\psi^{(0)}\left|\gamma^0\boldsymbol{\Sigma}\cdot\mathbf{p}\hat{H}^{(0)}\right|\psi^{(0)}\right\rangle - \left\langle\psi^{(0)}\left|\hat{H}^{(0)}\gamma^0\boldsymbol{\Sigma}\cdot\mathbf{p}\right|\psi^{(0)}\right\rangle \\ &= E\left\langle\psi^{(0)}\left|\gamma^0\boldsymbol{\Sigma}\cdot\mathbf{p}\right|\psi^{(0)}\right\rangle - E^*\left\langle\psi^{(0)}\left|\gamma^0\boldsymbol{\Sigma}\cdot\mathbf{p}\right|\psi^{(0)}\right\rangle \\ &= 0. \end{aligned} \tag{2.58}$$

One has to keep in mind that this result is exact for a hydrogen-like system . The second commutator to vanish is

$$\left[\gamma^0\boldsymbol{\Sigma}\cdot\mathbf{p}, m_0c^2\gamma^0\right] = 0 \tag{2.59}$$

since diagonal matrices always commute. We are left with

$$\left\langle -d_e\gamma^0\boldsymbol{\Sigma}\cdot\mathbf{E}\right\rangle_{\psi^{(0)}} = \frac{\imath d_e c}{e\hbar}\left\langle\left[\gamma^0\boldsymbol{\Sigma}\cdot\mathbf{p},\boldsymbol{\alpha}\cdot\mathbf{p}\right]\right\rangle_{\psi^{(0)}} \tag{2.60}$$

that we want to simplify further on. First, the $\boldsymbol{\alpha}$ matrix is replaced, following the equality:

$$\boldsymbol{\alpha} = \begin{pmatrix}\mathbf{0} & \boldsymbol{\sigma}\\ \boldsymbol{\sigma} & \mathbf{0}\end{pmatrix} = \begin{pmatrix}\mathbf{0} & \mathbb{1}_2\\ \mathbb{1}_2 & \mathbf{0}\end{pmatrix}\begin{pmatrix}\boldsymbol{\sigma} & \mathbf{0}\\ \mathbf{0} & \boldsymbol{\sigma}\end{pmatrix} = \gamma^5\boldsymbol{\Sigma}, \tag{2.61}$$

$$\left[\gamma^0\boldsymbol{\Sigma}\cdot\mathbf{p},\boldsymbol{\alpha}\cdot\mathbf{p}\right] = \left[\gamma^0\boldsymbol{\Sigma}\cdot\mathbf{p},\gamma^5\boldsymbol{\Sigma}\cdot\mathbf{p}\right]. \tag{2.62}$$

We obtain a commutator of two products that we expand into four commutators,

$$\begin{aligned}\left[\gamma^0\boldsymbol{\Sigma}\cdot\mathbf{p},\boldsymbol{\alpha}\cdot\mathbf{p}\right] =& \gamma^0\left(\gamma^5\left[\boldsymbol{\Sigma}\cdot\mathbf{p},\boldsymbol{\Sigma}\cdot\mathbf{p}\right] + \left[\boldsymbol{\Sigma}\cdot\mathbf{p},\gamma^5\right]\boldsymbol{\Sigma}\cdot\mathbf{p}\right) \\ &+ \left(\gamma^5\left[\gamma^0,\boldsymbol{\Sigma}\cdot\mathbf{p}\right] + \left[\gamma^0,\gamma^5\right]\boldsymbol{\Sigma}\cdot\mathbf{p}\right)\boldsymbol{\Sigma}\cdot\mathbf{p}. \end{aligned} \tag{2.63}$$

We have to evaluate them, the first one is straightforward:

$$\left[\boldsymbol{\Sigma}\cdot\mathbf{p},\boldsymbol{\Sigma}\cdot\mathbf{p}\right] = 0\ . \tag{2.64}$$

Besides, based on the rule that states that diagonal square matrices with identical elements (such as $\boldsymbol{\Sigma}\cdot\mathbf{p}$) commute with anti-diagonal square matrices with identical elements (such as γ^0 and γ^5), we have:

$$\left[\boldsymbol{\Sigma}\cdot\mathbf{p},\gamma^5\right] = 0 \text{ and } \left[\gamma^0,\boldsymbol{\Sigma}\cdot\mathbf{p}\right] = 0\ . \tag{2.65}$$

Finally, as previously shown,

$$\left[\gamma^0,\gamma^5\right] = 2\gamma^0\gamma^5 \tag{2.66}$$

and by using the Dirac relation:

$$(\boldsymbol{\Sigma}\cdot\mathbf{p})\,(\boldsymbol{\Sigma}\cdot\mathbf{p}) = \mathbf{p}^2\mathbb{1}_4, \tag{2.67}$$

it yields:

$$\left[\gamma^0\boldsymbol{\Sigma}\cdot\mathbf{p}, \boldsymbol{\alpha}\cdot\mathbf{p}\right] = 2\gamma^0\gamma^5\mathbf{p}^2. \tag{2.68}$$

Thus, we obtained an exact alternative form of the electron EDM energy shift E_{EDM}

$$\left\langle -d_e\gamma^0\boldsymbol{\Sigma}\cdot\mathbf{E}\right\rangle_{\psi^{(0)}} = \frac{2\imath c d_e}{e\hbar}\left\langle\gamma^0\gamma^5\mathbf{p}^2\right\rangle_{\psi^{(0)}}, \tag{2.69}$$

allowing us to calculate it by evaluating the expectation value of either electric field or kinetic energy, two stratagems that both have advantages and disadvantages. They will be detailed in the following, but first, we need to generalise this derivation of an alternative form to the many-body case that applies to atomic and molecular eEDM experiments.

2.1.4.2 Many-electron case.

In that case, the starting point of our derivation is:

$$E^{(1)}_{EDM} = -d_e\left\langle\sum_{i=1}^{n}\gamma^0(i)\boldsymbol{\Sigma}(i)\cdot\mathbf{E}_{int}(i)\right\rangle_{\psi^{(0)}} = -d_e\sum_{i=1}^{n}\left\langle\gamma^0(i)\boldsymbol{\Sigma}(i)\cdot\mathbf{E}_{int}(i)\right\rangle_{\psi^{(0)}} \tag{2.70}$$

where $\mathbf{E}_{int}(i)$, defined in Eq. (2.22), is rewritten as a gradient of a scalar potential:

$$\mathbf{E}_{int}(i) = -\vec{\nabla}_i\phi(i) \tag{2.71}$$

that contains a nuclear and an electronic part:

$$\phi(i) = \sum_{A=1}^{N}\phi_{iA} + \sum_{j=1}^{n}\phi_{ij}. \tag{2.72}$$

We substitute $\mathbf{E}_{int}(i)$ with the gradient in the expression of the energy shift and introduce the momentum operator $\mathbf{p}(i)$ that acts on both nuclear and electronic part of the scalar potential and determines the momentum of the particle (i)

$$\begin{aligned} E^{(1)}_{EDM} &= -d_e\sum_{i=1}^{n}\left\langle\gamma^0(i)\boldsymbol{\Sigma}(i)\cdot\left(-\vec{\nabla}_i\phi(i)\right)\right\rangle_{\psi^{(0)}} \\ &= \frac{\imath d_e}{e\hbar}\sum_{i=1}^{n}\left\langle\gamma^0(i)\boldsymbol{\Sigma}(i)\cdot(\mathbf{p}(i)\cdot e\phi(i))\right\rangle_{\psi^{(0)}}. \end{aligned} \tag{2.73}$$

By applying the same procedure as for the hydrogen-like system, we insert $\phi(i)$ in a commutator with $\mathbf{p}(i)$

$$E^{(1)}_{EDM} = \frac{\imath d_e}{e\hbar}\sum_{i=1}^{n}\left\langle\gamma^0(i)\left[\boldsymbol{\Sigma}(i)\cdot\mathbf{p}(i), e\phi(i)\mathbb{1}_4\right]\right\rangle_{\psi^{(0)}} \tag{2.74}$$

and by using the expression of the many-body electron EDM Hamiltonian,

$$\hat{H}^{(0)}(i) = c\boldsymbol{\alpha}(i)\cdot\mathbf{p}(i) + \gamma^0(i)m_0c^2 - e\phi(i)\mathbb{1}_4 \tag{2.75}$$

we get without any approximation so far:

$$E^{(1)}_{EDM} = \frac{\imath d_e}{e\hbar}\sum_{i=1}^{n}\left\langle\left[\gamma^0(i)\boldsymbol{\Sigma}(i)\cdot\mathbf{p}(i), c\boldsymbol{\alpha}(i)\cdot\mathbf{p}(i) + \gamma^0(i)m_0c^2 - \hat{H}^{(0)}(i)\right]\right\rangle_{\psi^{(0)}}. \tag{2.76}$$

Then, it is convenient to decompose the latter equation into two commutators in order to relate to the discussion of E. Lindroth [LLS89].

$$\begin{aligned} E^{(1)}_{EDM} =& \frac{\imath d_e}{e\hbar}\sum_{i=1}^{n}\Big\{\left\langle\left[\gamma^0(i)\boldsymbol{\Sigma}(i)\cdot\mathbf{p}(i), c\boldsymbol{\alpha}(i)\cdot\mathbf{p}(i) + \gamma^0(i)m_0c^2\right]\right\rangle_{\psi^{(0)}} \\ &- \left\langle\left[\gamma^0(i)\boldsymbol{\Sigma}(i)\cdot\mathbf{p}(i), \hat{H}^{(0)}(i)\right]\right\rangle_{\psi^{(0)}}\Big\} \end{aligned} \tag{2.77}$$

Relations (2.68) and (2.59) established in the hydrogen-like case still hold here and allow us to write:

$$E^{(1)}_{EDM} = \frac{\imath d_e}{e\hbar}\sum_{i=1}^{n}\Big\{\left\langle 2c\gamma^0(i)\gamma^5(i)\mathbf{p}^2(i)\right\rangle_{\psi^{(0)}} - \left\langle\left[\gamma^0(i)\boldsymbol{\Sigma}(i)\cdot\mathbf{p}(i), \hat{H}^{(0)}(i)\right]\right\rangle_{\psi^{(0)}}\Big\}. \tag{2.78}$$

This expression differs from Eq. (2.69) by the second term that vanished in the hydrogen-like case. This term cannot be cancelled, without any approximation, in the case of a many-body problem because the numerical methods employed to determine the wavefunction only permit to access an approximation and not the exact wavefunction, eigenfunction of the unperturbed Hamiltonian $\hat{H}^{(0)}(i)$.
We reached the Lindroth decomposition as it appears in stratagem II.

2.1.4.3 Lindroth stratagems.

In [LLS89], Lindroth *et al.* pointed out the various problems suffered by the calculation of the electron EDM energy shift $E^{(1)}_{EDM}$ that are the necessarily vanishing of the expectation value of $\hat{H}_{EDM}$ in the non-relativistic limit (problem a) and the presence in this Hamiltonian of a two-particle term accounting for the interaction of the EDM with others particles field (problem b). Two stratagems are expounded, each of them addresses one of the problems.
In both stratagems, the Hamiltonian is written as a commutator of an operator $\hat{P}$ with the zeroth-order Hamiltonian $\hat{H}^{(0)}(i)$ and an effective Hamiltonian $\hat{H}^{\text{eff}}$

$$\hat{H}_{EDM} = \left[\hat{P}, \hat{H}^{(0)}\right] + \hat{H}^{\text{eff}}. \tag{2.79}$$

The stratagem I, where

$$\hat{P}_I = -\frac{\imath d_e}{e\hbar}\sum_{i=1}^{n}\boldsymbol{\Sigma}(i)\cdot\mathbf{p}(i) \quad\text{and}\quad \hat{H}^{\text{eff}}_I = -d_e\sum_{i=1}^{n}(\gamma_0 - 1)\boldsymbol{\Sigma}(i)\cdot\mathbf{E}(i), \tag{2.80}$$

solves the problem a) since $\hat{H}_I^{\text{eff}}$ cancels out in the non-relativistic limit; however it is still a two-particle operator. Conversely, in stratagem II where

$$\hat{P}_{II} = -\frac{\imath d_e}{e\hbar}\sum_{i=1}^{n}\gamma^0(i)\mathbf{\Sigma}(i)\cdot\mathbf{p}(i) \quad \text{and} \quad \hat{H}_{II}^{\text{eff}} = \frac{2\imath d_e c}{e\hbar}\sum_{i=1}^{n}\gamma^0(i)\gamma^5(i)\mathbf{p}^2(i), \tag{2.81}$$

the problem b) is solved but the vanishing in the non-relativistic limit has to be achieved numerically. This is the latter stratagem that is implemented and used in most numerical calculations with the assumption that the expectation value of the commutator vanishes. It is an approximation since, as explained below, it is only true if the wavefunction over which is evaluated the expectation value is an eigenstate of the zeroth-order Hamiltonian, which is not achievable by numerical means in a many-body system. Then, the EDM energy shift reads

$$\Delta E_{EDM} = \frac{2\imath d_e c}{e\hbar}\left\langle\sum_{i=1}^{n}\gamma^0(i)\gamma^5(i)\mathbf{p}^2(i)\right\rangle_{\psi^{(0)}} \tag{2.82}$$

and we define and computed the effective electric field as

$$\mathcal{E}_{eff} = \frac{2\imath c}{e\hbar}\left\langle\sum_{i=1}^{n}\gamma^0(i)\gamma^5(i)\mathbf{p}^2(i)\right\rangle_{\psi^{(0)}}. \tag{2.83}$$

2.1.5 Schiff's theorem and its failure.

At first sight, one may be discouraged to measure an electron electric dipole moment in an atom or a molecule because of the so-called Schiff's theorem that suggested that such systems could not exhibit an electric dipole moment even though it contains a single electron with an EDM.
We now aim to derive analytically the Schiff's theorem [Sch63] for a paramagnetic atom in an external electric field and show how it fails in the relativistic framework and what it means for the calculation of the EDM of an unpaired electron. For that purpose, we go back to the first formulation of the EDM Hamiltonian (where the magnetic contributions are neglected)

$$\hat{H}_{EDM} = -d_e\gamma^0\mathbf{\Sigma}\cdot\mathbf{E} \tag{2.84}$$

that we divide into a relativistic and a non-relativistic part [CJD07]:

$$\hat{H}_{EDM} = -d_e\mathbf{\Sigma}\cdot\mathbf{E} - d_e(\gamma^0 - 1)\mathbf{\Sigma}\cdot\mathbf{E}. \tag{2.85}$$

Let us analyse the expectation value of the non-relativistic term $\langle -d_e\mathbf{\Sigma}\cdot\mathbf{E}\rangle_{\psi^{(0)}}$ where $\psi^{(0)}$ is the unperturbed wavefunction.As it is done in Eqs. (2.53) and (2.55), we rewrite the non-relativistic term

$$-d_e\mathbf{\Sigma}\cdot\mathbf{E} = \frac{\imath d_e}{e\hbar}\left[\mathbf{\Sigma}\cdot\mathbf{p}, e\phi\right] \tag{2.86}$$

and using the unperturbed Hamiltonian:

$$-d_e\boldsymbol{\Sigma}\cdot\mathbf{E} = \frac{\imath d_e}{e\hbar}\left[\boldsymbol{\Sigma}\cdot\mathbf{p}, c\boldsymbol{\alpha}\cdot\boldsymbol{p} + \gamma^0 m_0 c^2 - \hat{H}^{(0)}\right] \tag{2.87}$$

Among the three commutators, one already proved to be zero $[\boldsymbol{\Sigma}\cdot\mathbf{p}, \gamma^0] = 0$, another can be evaluated easily by making use of Eq. (2.65),

$$\left[\boldsymbol{\Sigma}\cdot\mathbf{p}, \gamma^5\boldsymbol{\Sigma}\cdot\mathbf{p}\right] = \gamma^5\left[\boldsymbol{\Sigma}\cdot\mathbf{p}, \boldsymbol{\Sigma}\cdot\mathbf{p}\right] + \left[\boldsymbol{\Sigma}\cdot\mathbf{p}, \gamma^5\right]\boldsymbol{\Sigma}\cdot\mathbf{p} = 0. \tag{2.88}$$

Finally, the expectation value of the only non-zero commutator, as expounded in Eq. (2.58), gives zero provided that $\psi^{(0)}$ is an eigenstate of the zeroth-order Hamiltonian

$$\left\langle\psi^{(0)}\right| - d_e\boldsymbol{\Sigma}\cdot\mathbf{E}\left|\psi^{(0)}\right\rangle = \left\langle\psi^{(0)}\right| - \frac{\imath d_e}{e\hbar}\left[\boldsymbol{\Sigma}\cdot\mathbf{p}, \hat{H}^{(0)}\right]\left|\psi^{(0)}\right\rangle = 0. \tag{2.89}$$

This proves the Schiff's theorem in the non-relativistic limit. However, the relativistic part, the second term on the right-hand side of Eq. (2.85), gives a non-zero contribution to the first-order energy shift

$$E^{(1)}_{EDM} = \left\langle\psi^{(0)}\right| - d_e(\gamma^0 - 1)\boldsymbol{\Sigma}\cdot\mathbf{E}\left|\psi^{(0)}\right\rangle \neq 0 \tag{2.90}$$

Herewith, the failure of the Schiff's theorem applied to the electron is due to the appearance of the γ^0 matrix in the Hamiltonian. It is of importance since it allows us to detect the existence of the electric dipole moment of an electron by measuring the enhanced energy shift due to the EDM of an unpaired electron in a many-electron system (atom, molecule) without a cancellation of the electric field on the average. An intuitive explanation for the evasion of the Schiff's theorem has been proposed by Commins *et al.* in [CJD07]. They pointed out that it was due to the Lorentz contraction of the electric dipole moment while transforming from the electron rest frame to the atomic center-of-mass frame following:

$$d_e^L = d_e - \frac{\gamma}{1+\gamma}\gamma^0 d_e\cdot\gamma^0 \tag{2.91}$$

with $\gamma = (1-\beta^2)^{-\frac{1}{2}}$ and $\beta = \frac{v}{c}$.

2.2 Scalar-pseudoscalar electron-nucleon coupling.

As previously stated, the electron electric dipole moment (d_e) is directly linked to the atomic electric dipole moment (d_a) through $d_a = Rd_e$ where R, the enhancement factor is the ratio between the effective electric field $\mathcal{E}_{eff}$ and the applied external electric field $\mathcal{E}_{lab}$. However, the atomic EDM of a paramagnetic atom can originate from various sources, among which is the so-called $\mathcal{P},\mathcal{T}$-odd electron-nucleon interaction.

To describe such an interaction, four-fermion operators are required. Three $\mathcal{P},\mathcal{T}$-odd four-fermion operators can be built

$$\text{SP} = \bar{\psi}_1\psi_1\bar{\psi}_2 i\gamma^5\psi_2 \tag{2.92}$$

$$\text{PS} = \bar{\psi}_1 i\gamma^5\psi_1\bar{\psi}_2\psi_2 \tag{2.93}$$

$$\text{T-PT} = \frac{1}{2}\epsilon^{\mu\nu\kappa\lambda}\bar{\psi}_1\sigma_{\mu\nu}\psi_1\bar{\psi}_2\sigma_{\kappa\lambda}\psi_2 \tag{2.94}$$

from the basic operators $\text{S} = \bar{\psi}\psi$, $\text{P} = \bar{\psi}i\gamma^5\psi$ and $\text{T}^{\mu\nu} = i\bar{\psi}\sigma^{\mu\nu}\psi$ which are scalar, pseudoscalar and tensor respectively [KL12]. Here, we denote in terms of field operators where $\bar{\psi}$ and ψ are creation and annihilation operators, respectively. One can easily demonstrate the assigned character of the S, P and T operators in the non-relativistic limit where $S = \bar{\phi}\phi$ with ϕ, the non-relativistic wavefunction corresponds to the number density that is even under both $\mathcal{P}$ and $\mathcal{T}$ operations. Likewise, the pseudoscalar nature, *i. e.* changing sign under inversion and time-reversal transformations, of P straightforwardly arises from the non-relativistic form where it is written as the divergence of the spin density $\text{P} = -\frac{1}{2m}\nabla(\phi^\dagger\sigma\phi)$. Finally, the total T operator transforms as $F^{\mu\nu}\tilde{F}_{\mu\nu}$ with $\tilde{F}_{\mu\nu} = \frac{1}{2}\epsilon^{\mu\nu\kappa\lambda}F_{\kappa\lambda}$ and $F^{\mu\nu}\tilde{F}_{\mu\nu} = 2\mathbf{EB}$. Since the electric field $\mathbf{E}$ is a $\mathcal{T}$-even polar vector and the magnetic field is an axial vector that changes sign under time-reversal operation, the $\mathcal{P},\mathcal{T}$-odd nature of T is confirmed.

Herewith, the electron-nucleon couplings that violate both $\mathcal{P}$ and $\mathcal{T}$ symmetries [Com99] are:

S-P	(scalar-pseudoscalar)	$\imath\bar{N}N\bar{e}\gamma^5 e$	(2.95)
P-S	(pseudoscalar-scalar)	$\imath\bar{N}\gamma^5 N\bar{e}e$	(2.96)
T	(tensor)	$\imath\bar{N}\sigma^{\mu\nu}N\bar{e}\sigma_{\mu\nu}\gamma^5 e$ [5]	(2.97)

where N and e are the respective nucleon and electron field operators. The $\mathcal{P},\mathcal{T}$-odd Hamiltonian density that describes these interactions reads:

$$\hat{h}_{e-N}^{\mathcal{P},\mathcal{T}} = \imath\frac{G_\text{F}}{\sqrt{2}}\left[C_\text{S}\sum_{i=1}^{A}\bar{N}_i N_i\bar{e}\gamma^5 e + C_\text{T}\sum_{i=1}^{A}\bar{N}_i\sigma^{\mu\nu}N_i\bar{e}\sigma_{\mu\nu}\gamma^5 e + C_\text{P}\sum_{i=1}^{A}\bar{N}_i\gamma^5 N_i\bar{e}e\right] \tag{2.98}$$

where G_F is the Fermi constant, $\sigma^{\mu\nu} = \frac{\imath}{2}[\gamma^\mu,\gamma^\nu]$, C_S, C_T, C_P are coupling constants that characterise the strength of the scalar-pseudoscalar, tensor and pseudoscalar-scalar interactions respectively.

In the following, we will focus on the dominant $\mathcal{P},\mathcal{T}$-odd coupling in the paramagnetic sector, the scalar-pseudoscalar term. In a many-electron system, the corresponding Hamiltonian is written as [MPL91]:

$$\hat{H}_S = \sum_{j=1}^{n}\hat{h}_S = \imath\frac{G_\text{F}}{\sqrt{2}}Zk_S\sum_{j=1}^{n}\gamma_j^0\gamma_j^5\rho_N(r_j) \tag{2.99}$$

[5] One may go from Eq. (2.94) to Eq. (2.97) by making use of $\frac{1}{2}\epsilon^{\mu\nu\kappa\lambda} = i\gamma^5\sigma_{\mu\nu}$.

and the corresponding energy shift calculated over the wavefunction characterised by the Ω quantum number reads:

$$\Delta E_S = \imath \frac{G_\mathrm{F}}{\sqrt{2}} Z k_S \left\langle \sum_{j=1}^{n} \gamma_j^0 \gamma_j^5 \rho_N(r_j) \right\rangle_{\psi_\Omega} \tag{2.100}$$

where k_S is the dimensionless scalar-pseudoscalar interaction constant. The presence of the nuclear charge density $\rho_N(r_j)$ entails the short-range character of the interaction, a specificity shared with the eEDM interaction, as well as the dependency of their matrix elements in the electric charge as Z^3.

2.3 Nuclear magnetic quadrupole moment.

Moreover, some nuclear $\mathcal{P},\mathcal{T}$-odd interactions can contribute to the measurable atomic or molecular EDM. In paramagnetic systems of interest for the search of the electron EDM, the dominant nuclear $\mathcal{P},\mathcal{T}$-odd effect is induced by the nuclear Magnetic Quadrupole Moment (MQM). This latter originates from the orbital motion of a nucleon with an EDM [KL12]. Note that, like the eEDM, the nuclear MQM benefits from an enhancement of its energy shift due to the assets of the $^3\Delta_1$ molecular state in which the measurements of the EDM are performed.

A detailed review of the nMQM theory has been published in [FNK16].

2.3.1 Nuclear MQM interaction Hamiltonian.

In our work we studied the interaction of a nuclear magnetic quadrupole moment with an electronic magnetic field which is described by [FDK14]:

$$\hat{H}_{MQM} = -\frac{W_M M}{2I(2I-1)} \mathbf{J_e} \hat{\mathbf{T}} \mathbf{n} \tag{2.101}$$

where $\mathbf{n}$ is the molecular axis unit vector, $\mathbf{J_e}$ is the total electronic angular momentum and, M and $\hat{\mathbf{T}}$ arise from the expression of the components of the second-rank nuclear magnetic quadrupole moment tensor $\hat{\mathbf{M}}$:

$$M_{mk} = \frac{3M}{2I(2I-1)} T_{mk}. \tag{2.102}$$

$\hat{\mathbf{T}}$ is the unique second-rank irreducible tensor one can build from the components of the total spin of the system $\mathbf{I}$ [KL95],

$$T_{mk} = I_m I_k + I_k I_m - \frac{2}{3} I(I+1)\delta_{mk}. \tag{2.103}$$

Hence, we have:

$$M_{mk} = \frac{3M}{2I(2I-1)} \left[I_m I_k + I_k I_m - \frac{2}{3} I(I+1)\delta_{mk} \right] \tag{2.104}$$

where $\mathbf{I}$ the nuclear angular momentum and M, the nuclear MQM magnitude which corresponds to the value of M_{zz} for the maximal nuclear spin projection along the molecular axis $I_z = I$.

2.3.2 Alternative form.

As it was done for the electron EDM interaction Hamiltonian, it may be convenient to rewrite nuclear MQM interaction Hamiltonian in a more explicit way, more suitable for the implementation.
First, let us write the i^{th} component of the quadrupole term of the associated classical vector potential:

$$A_{\mathcal{Q}}(\mathbf{r})_i = -\frac{1}{6}\sum_{k,l,n}\varepsilon_{iln}M_{nk}\frac{\partial}{\partial r_l}\frac{\partial}{\partial r_k}\frac{1}{r} = \frac{1}{6}\sum_{k,l,n}\varepsilon_{iln}M_{nk}\left(\frac{\delta_{kl}}{r^3} - \frac{3r_k r_l}{r^5}\right). \tag{2.105}$$

The symmetric character of the magnetic quadrupole tensor $\hat{\mathbf{M}}$ entails the vanishing of the first term since by summing the tensor components and the Kronecker delta, one gets

$$\sum_{k,l,n}\varepsilon_{iln}M_{nk}\delta_{kl} = \sum_{ln}\varepsilon_{iln}M_{nl} \tag{2.106}$$

and, by exchanging the dummy indexes and using the symmetry of $\hat{\mathbf{M}}$ and anti-symmetry of $\varepsilon_{ikj} = -\varepsilon_{ijk}$ one obtains zero:

$$\sum_{ln}\varepsilon_{iln}M_{nl} = |l \leftrightarrow n| = \sum_{ln}\varepsilon_{inl}M_{ln} = |\text{symmetry}| = -\sum_{ln}\varepsilon_{iln}M_{nl} = 0. \tag{2.107}$$

Then, the quadrupole vector potential reads:

$$\mathbf{A}_{\mathcal{Q}}(\mathbf{r}) = -\sum_{k,n}M_{nk}\frac{1}{2r^5}\sum_{i,l}\varepsilon_{iln}r_l r_k \mathbf{e}_i. \tag{2.108}$$

The corresponding Hamiltonian is obtained by writing the potential energy of an electron with velocity $\mathbf{v}$ with respect to the origin of $\mathbf{A}_{\mathcal{Q}}$, $V_{\mathcal{Q}e} = -\frac{e}{c}\mathbf{v}\cdot\mathbf{A}_{\mathcal{Q}}(\mathbf{r})$ and quantising it for a Dirac particle $\mathbf{v} \to c\boldsymbol{\alpha}$:

$$\hat{H}_{\mathcal{Q}e} = -\sum_{k,n}M_{nk}\frac{1}{2r^5}\sum_{i,l}\varepsilon_{iln}r_l r_k \mathbf{e}_i\cdot\mathbf{e}_j\alpha_j \tag{2.109}$$

with $\mathbf{e}_i\cdot\mathbf{e}_j = \delta_{ij}$, the Hamiltonian is

$$\hat{H}_{\mathcal{Q}e} = -\sum_{j,k,l,n}\frac{1}{2r^5}\varepsilon_{jln}\alpha_j r_l r_k M_{kn}. \tag{2.110}$$

For the sake of compactness, we introduce the contracted tensor $(\mathbf{rM}) = \sum_i (rM)_i \mathbf{e}_i$ that yields

$$\hat{H}_{\mathcal{Q}e} = -\sum_{j,k,l,n}\frac{1}{2r^5}\varepsilon_{jln}\alpha_j r_l \mathbf{e}_n\cdot(\mathbf{rM}) \tag{2.111}$$

and the final expression for the nuclear MQM interaction Hamiltonian as it would be implemented

$$\hat{H}_{\mathcal{Q}e} = \frac{\boldsymbol{\alpha} \times \mathbf{r}}{2r^5} \cdot (\mathbf{r}\mathbf{M}) \,. \tag{2.112}$$

We are interested in the expectation value of the z-component of $\hat{H}_{\mathcal{Q}e}$ that brings the energy shift ΔE_{MQM}. For a many-electron system with axial symmetry, it reads:

$$\Delta E_{\mathrm{MQM}} = M \left\langle \sum_{j=1}^{n} \left(\frac{\boldsymbol{\alpha}_j \times \mathbf{r}_{jA}}{2r_{jA}^5} \right)_k (r_{jA})_k \right\rangle_{\psi_\Omega} \tag{2.113}$$

where ψ_Ω is the wavefunction of the electronic state defined by the Ω quantum number. The latter equation relates to the nuclear-MQM electronic magnetic field interaction constant through $\Delta E_{\mathrm{MQM}} = -\frac{1}{3} W_M M \Omega$.

2.4 $\mathcal{P},\mathcal{T}$-odd interaction constants

In order to extract from experiments the fundamental constants d_e, $k_{\mathcal{P},\mathcal{T}}$ and M, respectively the electron electric dipole moment, the dimensionless scalar-pseudoscalar constant and the nuclear magnetic quadrupole moment, the determination of molecular parameters is required. These parameters are evaluated as expectation values over the wavefunction of the considered state characterised by the Ω quantum number, projection of the total electronic momentum along the molecular axis. The electron EDM interaction factor is given by

$$W_d := \frac{2\imath c}{\Omega e \hbar} \left\langle \sum_{j=1}^{n} \gamma_j^0 \gamma_j^5 \mathbf{p}^2 \right\rangle_{\psi_\Omega} , \tag{2.114}$$

the $\mathcal{P},\mathcal{T}$-odd scalar-pseudoscalar electron-nucleus interaction is characterised by

$$W_{\mathcal{S}} := \frac{\imath G_F}{\Omega\sqrt{2}} Z \left\langle \sum_{j=1}^{n} \gamma_j^0 \gamma_j^5 \rho_N(\mathbf{r}) \right\rangle_{\psi_\Omega} \tag{2.115}$$

and, the interaction of a nuclear MQM with electrons is described by

$$W_M := \frac{3}{2\Omega} \left\langle \sum_{j=1}^{n} \left(\frac{\boldsymbol{\alpha}_j \times \mathbf{r}_{jA}}{r_{jA}^5} \right)_k (r_{jA})_k \right\rangle_{\psi_\Omega} . \tag{2.116}$$

They are related to the corresponding energy shift, Eqs. (2.82), (2.100) and (2.113) respectively, through $\Delta E = C\Omega W$ where C is a fundamental constant (d_e, k_s, M), ΔE and W are the relevant energy shift and molecular parameter, respectively.

The values of the interaction parameters can only be obtained by a theoretical calculation that requires an accurate determination of the electronic structure of the

system. One way of testing the accuracy is to calculate a parameter with features similar to the $\mathcal{P},\mathcal{T}$ -odd interaction constants characteristics, *inter alia*, the sensitivity to the spin electronic density in the vicinity of the nucleus. Although, contrary to the constants, the parameter probe of the wavefunction quality has to be measurable. The parallel magnetic hyperfine interaction constant $A_{||}$ meets those conditions. In the following, (Chapter 3), the hyperfine theory will be developped and the parallel magnetic hyperfine interaction constant will be derived.

3 Hyperfine interaction.

In the context of search of new physics beyond the Standard Model through the determination of value or upper-bound of $\mathcal{P},\mathcal{T}$-odd constants, it is instructive and necessary, in more than one respect to examine the hyperfine interaction. Amongst other things, as exposed below, the so-called magnetic hyperfine interaction constant exhibits characteristics akin to those of the $\mathcal{P},\mathcal{T}$-odd constants we are looking for. One of them is the strong dependency on the electron density around the nucleus. This feature allows us to get valuable informations regarding the electronic wavefunction and in particular, the spin density in the vicinity of the nucleus. Besides, on the experimental point of view, it is crucial to know with high accuracy the energy of the various electronic states. The latter entails the need to identify the hyperfine levels. The good knowledge of the states is useful both for elaborating a states preparation process and identifying and limiting the uncertainties of the measurements.

3.1 Foldy-Wouthuysen Transformation.

So as to get more insight on the physical meaning of the four-component relativistic Dirac equation, it is convenient to seek a two-component Hamiltonian that would contain the electromagnetic fields and would still be relativistic. Such a method was developped by Foldy and Wouthuysen [FW50] and will be used in the following.

The Dirac Hamiltonian $\mathcal{H} = c\boldsymbol{\alpha}\cdot\boldsymbol{p} + \beta m_0 c^2$ for a free particle or $\mathcal{H} = c\boldsymbol{\alpha}\cdot(\boldsymbol{p} + e\boldsymbol{A}) + \beta m_0 c^2 - e\phi$ in an electromagnetic field connects states of positive and negative energy. The aim of this work is to derive a relativistically correct Hamiltonian in a two-component Pauli-form that only acts on the positive energy state. We can separate terms coupling electron and positron wavefunctions from non-coupling terms in the Hamiltonian. They will be respectively called odd ($\mathcal{O}$) and even ($\mathcal{E}$) operators. Then, we write:

$$\mathcal{H} = \beta m_0 c^2 + \mathcal{E} + \mathcal{O} \tag{3.1}$$

where $\mathcal{E} = -e\phi$ and $\mathcal{O} = c\,\boldsymbol{\alpha}\cdot[\boldsymbol{p} + e\boldsymbol{A}]$. Even though $\beta m_0 c^2$ has vanishing matrix

elements between electron and positron wavefunctions, we do not include it in the $\mathcal{E}$-operator because its order of magnitude is much greater. We will strive, by the means of successive unitary transformations, to decrease the order of magnitude of the odd operator until it vanishes in an Hamiltonian correct to order $\frac{1}{c^2}$ [BC03, Str98].

Let us define the Foldy-Wouthuysen transformation [FW50]. In the stationary case[1], the new Hamiltonian $\mathcal{H}'$ after a Foldy-Wouthuysen transformation will be given by:

$$\mathcal{H}' = e^{i\bar{S}}\mathcal{H}e^{-i\bar{S}}. \tag{3.2}$$

with the $\bar{S}$ operator defined as:

$$\bar{S} = -\frac{i\beta\mathcal{O}}{2m_0c^2} \tag{3.3}$$

where $\mathcal{H}$ is the current Hamiltonian and $\mathcal{O}$, its odd part.
By expanding the exponentials,

$$e^{i\bar{S}} = 1+i\bar{S}+\frac{i^2}{2!}\bar{S}^2+\frac{i^3}{3!}\bar{S}^3+\frac{i^4}{4!}\bar{S}^4+\dots \text{ and } e^{-i\bar{S}} = 1-i\bar{S}+\frac{i^2}{2!}\bar{S}^2-\frac{i^3}{3!}\bar{S}^3+\frac{i^4}{4!}\bar{S}^4+\dots \tag{3.4}$$

and replacing them in (3.2) up to order $\bar{S}^4$, we get:

$$\begin{aligned}
&e^{i\bar{S}_i}\mathcal{H}e^{-i\bar{S}_i}\\
=&\mathcal{H} - \mathcal{H}i\bar{S} + \mathcal{H}\frac{i^2}{2!}\bar{S}^2 - \mathcal{H}\frac{i^3}{3!}\bar{S}^3 + \mathcal{H}\frac{i^4}{4!}\bar{S}^4 + i\bar{S}\mathcal{H} - i\bar{S}\mathcal{H}i\bar{S} + i\bar{S}\mathcal{H}\frac{i^2}{2!}\bar{S}^2 + i\bar{S}\mathcal{H}\frac{i^3}{3!}\bar{S}^3\\
&+\frac{i^2}{2!}\bar{S}^2\mathcal{H} - \frac{i^2}{2!}\bar{S}^2\mathcal{H}i\bar{S} + \frac{i^2}{2!}\bar{S}^2\mathcal{H}\frac{i^2}{2!}\bar{S}^2 + \frac{i^3}{3!}\bar{S}^3\mathcal{H} - \frac{i^3}{3!}\bar{S}^3\mathcal{H}i\bar{S} + \frac{i^4}{4!}\bar{S}^4\mathcal{H} + O(\bar{S}^5)\\
=&\mathcal{H} + i[\bar{S},\mathcal{H}] + \frac{i^2}{2!}[\bar{S},[\bar{S},\mathcal{H}]] + \frac{i^3}{3!}[\bar{S}[\bar{S},[\bar{S},\mathcal{H}]]] + \frac{i^4}{4!}[\bar{S}[\bar{S}[\bar{S},[\bar{S},\mathcal{H}]]]] + O(\bar{S}^5)
\end{aligned} \tag{3.5}$$

Thus, the Hamiltonian after the transformation will be given by:

$$\mathcal{H}' = \mathcal{H}[\bar{S},\mathcal{H}] + \frac{i^2}{2!}[\bar{S},[\bar{S},\mathcal{H}]] + \frac{i^3}{3!}[\bar{S}[\bar{S},[\bar{S},\mathcal{H}]]] + \frac{i^4}{4!}[\bar{S}[\bar{S}[\bar{S},[\bar{S},\mathcal{H}]]]] \tag{3.6}$$

In the first transformation $\mathcal{H} = \beta mc^2+\mathcal{E}+\mathcal{O}$ as defined in (3.1) and $\bar{S} = -\frac{i\beta\mathcal{O}}{2m_0c^2}$. We can calculate commutators that will come out of those in (3.6). In this purpose, we will apply some properties of the β-matrix; the even or odd nature of the operators $\mathcal{O}$ and $\mathcal{E}$ can be linked to the commutativity or anticommutativity of these operators with the β-matrix. Thus, $[\mathcal{E},\beta] = 0$ and $[\mathcal{O},\beta] = 2\mathcal{O}\beta$. In the case of $\mathcal{O}$, we used the anticommutativity of the Dirac's α matrices: $\{\beta,\alpha_i\} = 0$, besides $\beta^2 = \mathbf{1}$. Then, the following equalities can be stated:

$$\begin{aligned}
&[\beta\mathcal{O},\beta] = -2\mathcal{O} && [\beta,\mathcal{O}^3] = 2\beta\mathcal{O}^3\\
&[\beta\mathcal{O},\mathcal{E}] = \beta[\mathcal{O},\mathcal{E}] && [\beta\mathcal{O},\mathcal{O}^3] = 2\beta\mathcal{O}^4\\
&[\beta\mathcal{O},\mathcal{O}] = 2\beta\mathcal{O}^2 && [\beta\mathcal{O},\beta\mathcal{O}^2] = -2\mathcal{O}^3.
\end{aligned} \tag{3.7}$$

[1] A similar derivation for the non-stationary case can be found in Appendix C.

Let us evaluate the commutators of (3.6).

$$[\bar{S},\mathcal{H}] = i\left\{\mathcal{O} - \frac{\beta}{2m_0c^2}[\mathcal{O},\mathcal{E}] - \frac{\beta\mathcal{O}^2}{m_0c^2}\right\} \tag{3.8}$$

$$[\bar{S},[\bar{S},\mathcal{H}]] = \frac{\beta\mathcal{O}^2}{m_0c^2} + \frac{1}{4m_0^2c^4}[\mathcal{O},[\mathcal{O},\mathcal{E}]] + \frac{\mathcal{O}^3}{m_0^2c^4} \tag{3.9}$$

$$[\bar{S},[\bar{S},[\bar{S},\mathcal{H}]]] = \frac{i\mathcal{O}^3}{m_0^2c^4} - \frac{i\beta}{8m_0^3c^6}[\mathcal{O},[\mathcal{O},[\mathcal{O},\mathcal{E}]]] - \frac{i\beta\mathcal{O}^4}{m_0^3c^6} \tag{3.10}$$

$$[\bar{S},[\bar{S},[\bar{S},[\bar{S},\mathcal{H}]]]] = \frac{\beta\mathcal{O}^4}{m_0^3c^6} + O\left(\frac{1}{m_0^4c^8}\right) \tag{3.11}$$

Now, we can collect terms of order up to $\frac{1}{c^2}$ by taking into account that $\mathcal{O}$ is proportional to c and sort them into even and odd terms. Then, we get:

$$\mathcal{H}' = \beta m_0c^2 + \mathcal{E}' + \mathcal{O}' \tag{3.12}$$

with

$$\mathcal{E}' = \mathcal{E} + \frac{\beta\mathcal{O}^2}{2m_0c^2} - \frac{1}{8m_0^2c^4}[\mathcal{O},[\mathcal{O},\mathcal{E}]] - \frac{\beta\mathcal{O}^4}{8m_0^3c^6} \tag{3.13}$$

and

$$\mathcal{O}' = \frac{\beta}{2m_0c^2}[\mathcal{O},\mathcal{E}] - \frac{\mathcal{O}^3}{3m_0^2c^4} \quad . \tag{3.14}$$

This first transformation brings an improvement since the odd terms are now of order c^{-1} when they were of order c^1 in the initial Hamiltonian $\mathcal{H}$ (3.1). Nevertheless, we aim to have an even Hamiltonian up to order c^{-2} so we perform another transformation described by:

$$\bar{S}' = -\frac{i\beta\mathcal{O}'}{2m_0c^2} \tag{3.15}$$

Once again, we need to evaluate the commutators but this time, only $[\bar{S}',\mathcal{H}']$ will give terms of order higher than c^{-3}. Indeed, $\bar{S}'$ will be of order c^{-3} and $\mathcal{H}'$ of order c^2 so $[\bar{S}',[\bar{S}',\mathcal{H}']]$ upper order will be c^{-4}. As a consequence, $\mathcal{H}''$ will be given by:

$$\mathcal{H}'' = \mathcal{H}' + i[\bar{S}',\mathcal{H}'] \tag{3.16}$$

$$[\bar{S}',\mathcal{H}'] = -\frac{i}{2}[\beta\mathcal{O}',\beta] - \frac{i}{2m_0c^2}[\beta\mathcal{O}',\mathcal{E}'] - \frac{i}{2m_0c^2}[\beta\mathcal{O}',\mathcal{O}'] = i\mathcal{O}' + O(c^{-3}) \tag{3.17}$$

Then,

$$\mathcal{H}'' = \beta m_0c^2 + \mathcal{E}' + \mathcal{O}' - \mathcal{O}' = \beta m_0c^2 + \mathcal{E}'. \tag{3.18}$$

The Hamiltonian obtained is then purely even up to order c^{-2}, what we aimed for.

$$\mathcal{H}'' = \beta m_0 c^2 + \mathcal{E} + \frac{\beta \mathcal{O}^2}{2m_0 c^2} - \frac{1}{8m_0^2 c^4}[\mathcal{O}, [\mathcal{O}, \mathcal{E}]] - \frac{\beta \mathcal{O}^4}{8m_0^3 c^6} \tag{3.19}$$

We will now expand the various terms and analyse them.
By substituting $\mathcal{E}$ and $\mathcal{O}$ by their expression, we get:

$$\mathcal{H}'' = \beta m_0 c^2 - e\phi + \frac{\beta (c\boldsymbol{\alpha} \cdot \boldsymbol{\pi})^2}{2m_0 c^2} - \frac{1}{8m_0^2 c^4}[c\boldsymbol{\alpha} \cdot \boldsymbol{\pi}, [c\boldsymbol{\alpha} \cdot \boldsymbol{\pi}, -e\phi]] - \frac{\beta (c\boldsymbol{\alpha} \cdot \boldsymbol{\pi})^4}{8m_0^3 c^6} \tag{3.20}$$

where $\boldsymbol{\pi} = \boldsymbol{p} + e\boldsymbol{A}$ and the last three terms have to be evaluated. In this purpose, we will use the following properties of the α and σ Dirac matrices:

$$\boldsymbol{\alpha} = \rho\boldsymbol{\sigma}; \qquad \rho^2 = 1; \qquad (\boldsymbol{\sigma} \cdot \boldsymbol{u})(\boldsymbol{\sigma} \cdot \boldsymbol{v}) = (\boldsymbol{u} \cdot \boldsymbol{v}) + i\boldsymbol{\sigma} \cdot (\boldsymbol{u} \times \boldsymbol{v}). \tag{3.21}$$

It leads to:

$$(\boldsymbol{\alpha} \cdot \boldsymbol{\pi})^2 = \rho(\boldsymbol{\sigma} \cdot \boldsymbol{\pi})^2 = \boldsymbol{\pi}^2 + i\boldsymbol{\sigma} \cdot (\boldsymbol{\pi} \times \boldsymbol{\pi}). \tag{3.22}$$

If we expand $\boldsymbol{\pi} = \boldsymbol{p} + e\boldsymbol{A}$, $\boldsymbol{p} = -i\hbar\nabla$ and make use of Maxwell equations in the second term of (3.22), the magnetic field $\boldsymbol{B}$ arises:

$$\boldsymbol{\pi} \times \boldsymbol{\pi} = e(\boldsymbol{A} \times \boldsymbol{p} + \boldsymbol{p} \times \boldsymbol{A}) = e\boldsymbol{p} \times \boldsymbol{A} = -i\hbar\nabla \times \boldsymbol{A} = -i\hbar\boldsymbol{B} \tag{3.23}$$

To understand this calculation, one has to keep in mind that the $(\boldsymbol{A} \times \boldsymbol{p} + \boldsymbol{p} \times \boldsymbol{A})$ term is an operator acting on a spinor. Let us consider the x-component,

$$\begin{aligned}(\boldsymbol{A} \times \boldsymbol{p} + \boldsymbol{p} \times \boldsymbol{A})_x\psi &= A_y(p_z\psi) - A_z(p_y\psi) + p_y(A_z\psi) - p_z(A_y\psi) \\ &= A_y(p_z\psi) - A_z(p_y\psi) + (p_yA_z)\psi + A_z(p_y\psi) - (p_zA_y)\psi - A_y(p_z\psi) \\ &= (\boldsymbol{p} \times \boldsymbol{A})_x\psi. \end{aligned} \tag{3.24}$$

Then, Equation (3.22) becomes:

$$(\boldsymbol{\alpha} \cdot \boldsymbol{\pi})^2 = \boldsymbol{\pi}^2 + e\hbar\boldsymbol{\sigma} \cdot \boldsymbol{B} = \boldsymbol{\pi}^2 + 2mg_s\mu_B\boldsymbol{S} \cdot \boldsymbol{B}. \tag{3.25}$$

In the last step, we exhibit the spin magnetic moment, given by $\boldsymbol{\mu}_S = -g_s\mu_B\boldsymbol{S} = +\frac{e\hbar}{m}\boldsymbol{S}$ with $\boldsymbol{S} = \frac{\boldsymbol{\sigma}}{2}$. Now, let us evaluate $[\mathcal{O}, \mathcal{E}]$.

$$\begin{aligned}[\mathcal{O}, \mathcal{E}] = [c\boldsymbol{\alpha} \cdot \boldsymbol{\pi}, -e\phi] &= -ec\boldsymbol{\alpha} \cdot ((p + e\boldsymbol{A})\phi - \phi(p + e\boldsymbol{A})) \\ &= -ec\boldsymbol{\alpha} \cdot ((\boldsymbol{p}\phi) + e[\boldsymbol{A}, \phi]) \\ &= i\hbar ec\boldsymbol{\alpha} \cdot \nabla\phi \end{aligned} \tag{3.26}$$

Since we are in the stationary case, the electric field springs up in this term: $\nabla\phi = -\boldsymbol{E}$ and we get $[\mathcal{O}, \mathcal{E}] = -i\hbar e\boldsymbol{\alpha}\cdot\boldsymbol{E}$ that allows us to evaluate $[\mathcal{O}, [\mathcal{O}, \mathcal{E}]]$.

$$\begin{aligned}[\mathcal{O}, [\mathcal{O}, \mathcal{E}]] &= -i\hbar ec^2[\boldsymbol{\alpha}\cdot\boldsymbol{\pi}, \boldsymbol{\alpha}\cdot\boldsymbol{E}] \\ &= -i\hbar ec^2((\boldsymbol{\sigma}\cdot\boldsymbol{\pi})(\boldsymbol{\sigma}\cdot\boldsymbol{E}) - (\boldsymbol{\sigma}\cdot\boldsymbol{E})(\boldsymbol{\sigma}\cdot\boldsymbol{\pi})) \\ &= -i\hbar ec^2([\boldsymbol{\pi}, \boldsymbol{E}] + i\boldsymbol{\sigma}(\boldsymbol{\pi}\times\boldsymbol{E} - \boldsymbol{E}\times\boldsymbol{\pi})) \end{aligned} \tag{3.27}$$

As we showed that $[\boldsymbol{\pi}, \phi] = -i\hbar\nabla\phi$ in (3.26), it can be shown that $[\boldsymbol{\pi}, \boldsymbol{E}] = -i\hbar\nabla\cdot\boldsymbol{E}$. Moreover we substitute μ_S for σ and we obtain:

$$[\mathcal{O}, [\mathcal{O}, \mathcal{E}]] = -ec^2\hbar^2\nabla\boldsymbol{E} + 2ec\hbar\boldsymbol{S}\cdot(\boldsymbol{\pi}\times\boldsymbol{E} - \boldsymbol{E}\times\boldsymbol{\pi}) \tag{3.28}$$

At this point, $(\boldsymbol{\alpha}\cdot\boldsymbol{\pi})^4$ remains to be examined.

$$(\boldsymbol{\alpha}\cdot\boldsymbol{\pi})^4 = ((\boldsymbol{\alpha}\cdot\boldsymbol{\pi})^2)^2 = (\boldsymbol{\pi}^2 + e\hbar\boldsymbol{\sigma}\cdot\boldsymbol{B})^2 = \boldsymbol{\pi}^4 + 2e\hbar(\boldsymbol{\sigma}\cdot\boldsymbol{B})\boldsymbol{\pi}^2 + e^2\hbar^2(\boldsymbol{\sigma}\cdot\boldsymbol{B})^2 \tag{3.29}$$

We will only retain the first term of the developpement in $-\frac{\beta(c\boldsymbol{\alpha}\cdot\boldsymbol{\pi})^4}{8m_0^3c^6}$ because terms in $\boldsymbol{B}$ will be of higher order in $\frac{1}{c^2}$ (see Maxwell's equations). Let us substitute in (3.20).

$$\begin{aligned}\mathcal{H}'' =& \beta m_0c^2 - e\phi + \frac{\beta\boldsymbol{\pi}^2}{2m_0} + \beta g_S\mu_B\boldsymbol{S}\cdot\boldsymbol{B} + \frac{e\hbar^2}{8m_0^2c^2}\nabla\cdot\boldsymbol{E} \\ &- \frac{e\hbar}{4m_0^2c^2}\boldsymbol{S}\cdot(\boldsymbol{\pi}\times\boldsymbol{E} - \boldsymbol{E}\times\boldsymbol{\pi}) - \frac{\beta\boldsymbol{\pi}^4}{8m_0^3c^2}. \end{aligned} \tag{3.30}$$

In an effort to analyse the Hamiltonian that only acts on positive energy states, we set $\beta = 1$ and replace the 4×4 σ-matrices with the 2×2 σ-matrices since $\mathcal{H}$" is now exclusively even. Then, we are left with seven terms to which we give a physical meaning. The first three terms are easily interpreted, they are the rest mass energy, the electric potential energy and the kinetic energy of the electron. Besides, the seventh term $-\frac{\beta\boldsymbol{\pi}^4}{8m_0^3c^2}$ is a relativistic correction to this kinetic energy. The fourth term $g_S\mu_B\boldsymbol{S}\cdot\boldsymbol{B}$ is the interaction of the spin magnetic moment with the magnetic field that leads to the spin-orbit coupling. Finally, the fifth term which has no equivalence in non-relativistic quantum mechanics is called the Darwin term and the sixth shows the interaction of a perpendicular electric moment created by a moving magnetic moment with the electric field.

3.2 Magnetic hyperfine interaction constant.

The parameter that characterises the hyperfine interaction and that can be a test of accuracy of the determination of the $\mathcal{P},\mathcal{T}$-odd constants is the parallel magnetic

hyperfine interaction constant $A_{||}$. It accounts for the interaction of two magnetic dipole moments, respectively those of the nucleus and the electron, that leads to the coupling of the nuclear spin $\mathbf{I}$ with the electron total momentum $\mathbf{J} = \mathbf{S} + \mathbf{L}$ where $\mathbf{S}$ is the spin of the electron and $\mathbf{L}$ is its angular momentum. To derive the expression of the $A_{||}$ constant, one needs to start with the kinetic term $\boldsymbol{\alpha} \cdot \mathbf{p}$ of the Dirac equation [Dir58]

$$\left(\beta mc^2 + c\boldsymbol{\alpha} \cdot \mathbf{p}\right) \psi = i\hbar \frac{\partial \psi}{\partial t} \tag{3.31}$$

in which the minimal substitution $\mathbf{p} \rightarrow \mathbf{p} + e\mathbf{A}$ has to be applied to include the effect of the presence of an electromagnetic field[2].
On the other hand, the dipole term of the vector potential arising from the nuclear current distribution reads:

$$\mathbf{A}_D(\mathbf{r}) = \frac{\mathbf{m} \times \mathbf{r}}{r^3} \tag{3.32}$$

with $\mathbf{m}$, the magnetic dipole moment

$$\mathbf{m} := \frac{1}{2} \int_{\mathcal{V}'} \mathbf{r}' \times \mathbf{J}(\mathbf{r}') d\mathcal{V}'. \tag{3.33}$$

Then, the vector potential $\mathbf{A}_D(\mathbf{r})$ is substituted in the kinetic term and we restrict our development to the potential term:

$$\boldsymbol{\alpha} \cdot e\mathbf{A}_D = \boldsymbol{\alpha} \cdot \left(e \frac{\mathbf{m} \times \mathbf{r}}{r^3}\right) = \frac{e}{r^3} \boldsymbol{\alpha} \cdot (\mathbf{r} \times \mathbf{m}) \tag{3.34}$$

and, since $\mathbf{m}$ is purely nuclear and thus commutes with the purely electronic $\boldsymbol{\alpha}$ and $\mathbf{r}$, we have:

$$\boldsymbol{\alpha} \cdot e\mathbf{A}_D = \frac{e}{r^3} \mathbf{m} \cdot (\boldsymbol{\alpha} \times \mathbf{r}). \tag{3.35}$$

We now aim to make appear the nuclear magnetic dipole moment, to this end, we use the following expression:

$$e\mathbf{m} = g_A \mu_N \mathbf{I} \tag{3.36}$$

where g_A is the g-factor for the nucleus A, $\mathbf{I}$ is the nuclear spin vector and μ_N is the nuclear magneton.
The parallel magnetic hyperfine interaction constant $A_{||}$ that we seek is, per definition, the expectation value of the projection of the coupling term along the molecular axis divided by the spin quantum number I which is:

$$\frac{\mu_z}{I} \left(\frac{\alpha \times \mathbf{r}}{r^3}\right)_z. \tag{3.37}$$

[2]If the physical content of the Dirac equation was explained within the two-component formalism above, our work is carried out in the four-component framework.

So, the expectation over an electronic state of a linear molecule where Hund's case (c) (see Appendix A) applies is:

$$A_{\parallel} := \frac{\mu_z}{I\Omega} \left\langle \left(\frac{\alpha \times \mathbf{r}}{r^3} \right)_z \right\rangle_{\psi} \tag{3.38}$$

where ψ is the wavefunction of the considered state. In the works that will be presented in this thesis, the hyperfine constant is evaluated in diatomic molecules that constitute many-electron systems. Then, the relevant expression for a nucleus A is:

$$A_{\parallel} = \frac{\mu_z(A)}{I\Omega} \left\langle \sum_{i=1}^{n} \left(\frac{\alpha_i \times \mathbf{r_{iA}}}{r_{iA}^3} \right)_z \right\rangle_{\psi} . \tag{3.39}$$

where the operator is summed over the n electrons i of the molecule.
This constant is calculated numerically on an equal footing with the $\mathcal{P},\mathcal{T}$-odd parameters introduced in Section 2.4 as an expectation value over the molecular wavefunction of the electronic state of interest. Details of the implementation are given in Chapter 4.

4 Methodology.

For purposes of evaluating the parameters introduced in the previous chapters (*cf.* Chapters 2 and 3), an accurate and reliable determination of the electronic structure of the system is required. This is far from being trivial since the systems of interest in our study are many-electron systems and besides, contain heavy elements. In the present work, the electronic structure is accurately described by a four-component method in which the electron correlation and the magnetic couplings are treated on equal footing.

4.1 Four-component relativistic theory.

4.1.1 Hamiltonian operator.

Most relativistic electronic structure theory apply within the Born-Oppenheimer framework that allows the separated treatement of electrons and nuclei motion. It is justified by the tiny ratio of the respective velocities of nuclei and electrons. In this approximation, a general many-body Hamiltonian reads:

$$\hat{H} = \sum_{A}^{N} \sum_{i}^{n} \hat{h}_i + \sum_{i,j>i} \hat{g}_{ij} + \sum_{A,B>A} V_{AB} \tag{4.1}$$

where n is the number of electrons, N is the number of atomic nuclei and V_{AB} is the potential energy due to the internuclear electrostatic repulsion of the clamped nuclei. As to $\hat{h}_i$ and $\hat{g}_{ij}$, they are the one- and two-electron operators respectively that should be wisely chosen to fit in our relativistic four-component framework. The appropriate choice for $\hat{h}_i$ is the Dirac Hamiltonian[Dir58] for a particle in a static potential:

$$\hat{h} = c\,\boldsymbol{\alpha}\cdot(\boldsymbol{p} + e\boldsymbol{A}) + \beta m_0 c^2 + V_{iA}\mathbb{1}_4 \tag{4.2}$$

To account for the electron-electron interaction in a relativistic framework, *i.e.*, including the non-classical effects such as magnetic interactions and retardations

effects, one may use the Breit operator [Bre29]:

$$\hat{g}_{ij} = \frac{1}{r_{ij}}\mathbb{1}_4 - \frac{1}{2}\left(\frac{\boldsymbol{\alpha}_i \cdot \boldsymbol{\alpha}_j}{r_{ij}} + \frac{(\mathbf{r}_{ij} \cdot \boldsymbol{\alpha}_i)(\mathbf{r}_{ij} \cdot \boldsymbol{\alpha}_j)}{r_{ij}^3}\right). \tag{4.3}$$

The following alternative form of the Breit operator allows the identification of the physical content of the terms [Vis02]:

$$\begin{aligned}\hat{g}_{ij} &= \frac{1}{r_{ij}}\mathbb{1}_4 - \frac{c\boldsymbol{\alpha}_i \cdot c\boldsymbol{\alpha}_j}{c^2 r_{ij}} - \frac{1}{2c^2}\left(c\boldsymbol{\alpha}_i \cdot \boldsymbol{\nabla}_i\right)\left(c\boldsymbol{\alpha}_j \cdot \boldsymbol{\nabla}_j\right) r_{ij} \\ &= \hat{g}_{ij}^{Coulomb} + \hat{g}_{ij}^{Gaunt} + \hat{g}_{ij}^{gauge},\end{aligned} \tag{4.4}$$

the first term is the well-known Coulomb operator that includes the Spin-Same-Orbit interaction, the second is the Gaunt term [Gau29] that describes the Spin-Other-Orbit interaction and the last one is a gauge term. However, in our work we restrict the two-electron operator to the zeroth order in $\frac{1}{c^2}$ keeping only the Coulomb term, which is empirically a reasonable approximation. Then, by combining $\hat{h}_i$ and $\hat{g}_{ij}$, we obtain the all-electron Dirac-Coulomb Hamiltonian operator in the Born-Oppenheimer approximation which is at the heart of most relativistic quantum chemistry methods:

$$\hat{H}^{DC} = \sum_{A}^{N}\sum_{i}^{n}\left[c\left(\boldsymbol{\alpha}\cdot\mathbf{p}\right)_i + \beta_i m_0 c^2 + V_{iA}\mathbb{1}_4\right] + \sum_{i,j>i}\frac{1}{r_{ij}}\mathbb{1}_4 + \sum_{A,B>A} V_{AB}\mathbb{1}_4 \tag{4.5}$$

where V_{iA} accounts for the potential energy experienced by the electron i in the electric field of the nucleus A.

Owing to its 4×4 matrix form, the solution to the stationary equation obtained from the Dirac-Coulomb Hamiltonian through $\hat{H}^{DC}\Psi = E^{DC}\Psi$ is necessarily a four-component vector whose components can be split into two two-component vectors Ψ^L and Ψ^S whose components are respectively called *large* and *small* components

$$\Psi = \begin{pmatrix}\Psi^L \\ \Psi^S\end{pmatrix} = \begin{pmatrix}\Psi^{L_1} \\ \Psi^{L_2} \\ \Psi^{S_1} \\ \Psi^{S_2}\end{pmatrix}. \tag{4.6}$$

4.1.2 Brown-Ravenhall disease.

The presence of both one-particle Dirac operator and two-particle Coulomb operator in Eq. (4.5) has consequences. The solution of the one-particle Dirac equation is a continuum of negative and positive energy solutions that can be respectively identified as positronic and electronic solutions. However, the situation is not that trivial as far as a two-particle operator is concerned. A bound state with positive

energy, solution of a Dirac two-electron operator, does not necessarily refers to a two-electron state, it is also possible to construct an infinite number of degenerate states with one particle excited to the positive energy continuum and the other one de-excited to the negative energy continuum. Herewith, a bound state of two mc^2 electrons will be degenerate with, *e.g*, a state made up of a particle with energy near $3mc^2$ and the other one close to $-mc^2$. This kind of state is unphysical since a proper electron-positron with the same energies would have an energy near $4mc^2$, a zero charge and would not interact with the $2mc^2$ two-electron state with charge $-2e$. This issue was first exposed by Brown and Ravenhall in [BR51] and redefined by Sucher as the "continuum dissolution" in [Suc80] where he pointed out that Hamiltonians such as Eq. (4.1) would bring no bound states.

A remedy to this so-called "Brown-Ravenhall" disease that is employed in the `DIRAC` program [DIRa] is the "empty Dirac" picture [DF07]. The purpose is to get rid of the unphysical solutions by treating the negative-energy state as virtual orbitals in the Hartree-Fock optimization [SJ99] and applying a *minimax principle* [Tal86]. It involves a minimised energy for spinor transformations within the positive branch and a maximised energy for spinor transformations involving positive- and negative energy spinors. In this way, the coupling between negative- and positive-energy states is ruled out and thus, the negative-energy states may be discarded. This method is refered as a *no-pair approximation a posteriori* [Vis02]. Hereafter, one can focus on the positive-energy spinors that are stil decribed by four-component spinors with a non-vanishing *small* component

$$\Psi^+ = \begin{pmatrix} \Psi^L \\ \Psi^S \end{pmatrix}. \tag{4.7}$$

4.1.3 Symmetries.

Symmetry is a central point in physics and chemistry and it becomes crucial when it comes to computational methods. One would seek to minimise the amount of operations to be performed. For that purpose, it is advantageous to block-diagonalising the operators in a symmetry-adapted basis so that the dimension is reduced and identifying the vanishing expectation values. In the following, we will demonstrate how one may take advantage of both fermion wavefunctions and molecular symmetries to reduce the computational cost of a relativistic many-body method[1].

4.1.3.1 Kramers' Time Reversal Symmetry.

The entanglement of spin and spatial symmetries through the spin-orbit coupling in four-component electronic structure theory disqualifies the spin symmetry as a

[1] An extensive treatement is available in [RW07].

proper symmetry of the relativistic four-component wavefunctions. There is a need for a replacement symmetry such as the *jj*-coupling for spherically symmetric atoms but in a more general framework. This concept was brought forward by Hendrik Kramers [Kra30] in where he stated that the *time-reversal* symmetry [LL81] could be appropriate. In the absence of an external magnetic field, the energy levels of a fermion is doubly degenerate. The wavefunctions of such degenerate states are called *Kramers pair*. Each fermion function φ_p is related to its Kramers partner $\varphi_{\bar{p}}$ through time-reversal transformation:

$$\hat{\mathcal{K}}\varphi_p = \varphi_{\bar{p}} \tag{4.8}$$

where $\hat{\mathcal{K}}$ is the antiunitary time-reversal operator defined in Section 2.1.3.2 as:

$$\hat{\mathcal{K}} = -\imath \begin{pmatrix} \sigma_y & 0 \\ 0 & \sigma_y \end{pmatrix} \hat{\mathcal{K}}_0 \tag{4.9}$$

with σ_y a spin Pauli matrix and $\hat{\mathcal{K}}_0$, the complex conjugation operator, that implies:

$$\hat{\mathcal{K}}\left(a\varphi_p\right) = a^*\varphi_p \tag{4.10}$$

where a is a complex factor. It can be shown [FOM01] that Hamiltonians such as the free-particle Dirac operator, the one-particle Dirac operator including external electric potential or the Dirac-Coulomb operator are invariant under time-reversal unitary transformation, giving for this latter:

$$\hat{\mathcal{K}}^\dagger \hat{H}^{DC} \hat{\mathcal{K}} = \hat{H}^{DC}. \tag{4.11}$$

It implies the commutation of these Hamiltonian operator with the Kramers operator and makes time-reversal a fundamental symmetry.

The simplest Kramers pair one can think about is the hydrogenic $\{1s\alpha, 1s\beta\}$ functions where α et β are the spins functions, respectively $\begin{pmatrix} 1 \\ 0 \end{pmatrix}$ and $\begin{pmatrix} 0 \\ 1 \end{pmatrix}$. Likewise, the hydrogenic $2p_1\alpha$ forms a Kramers pair along with $2p_{-1}\beta$, note that its Kramers partner is not $2p_1\beta$ because of the complex conjugation operator. In relativistic theory, where the spin-orbit coupling discredit spin and angular momentum as good quantum numbers, the relevant quantum number is the total electronic angular momentum J_e. Thus, $\hat{\mathcal{K}}$ relates functions of equal J_e and n but flips the sign of Ω (projection of J_e along the z-axis) and in this way, a one-particle basis of Kramers-paired spinors is set for the relativistic description of many-electron atoms. In the case of molecules, we can keep this Kramers formalism even if J_e is no longer an appropriate quantum number by resorting to a Kramers-restricted formalism [SJ99]. Likewise, even if $\mathcal{T}$-symmetry is broken by the presence of $\mathcal{P},\mathcal{T}$-odd effects in our systems, their smallness allows us to neglect them and employ $\mathcal{T}$-symmetric functions.

4.1.3.2 Integrals over Kramers-paired Spinors.

The use of the Kramers-restricted formalism allows one to take advantage of the time-reversal symmetry in order to reduce the computational demand of relativistic electronic structure methods. Let us consider a hermitian one-particle operator and analyse how the number of integrals reduce in a Kramers-paired basis. The lower

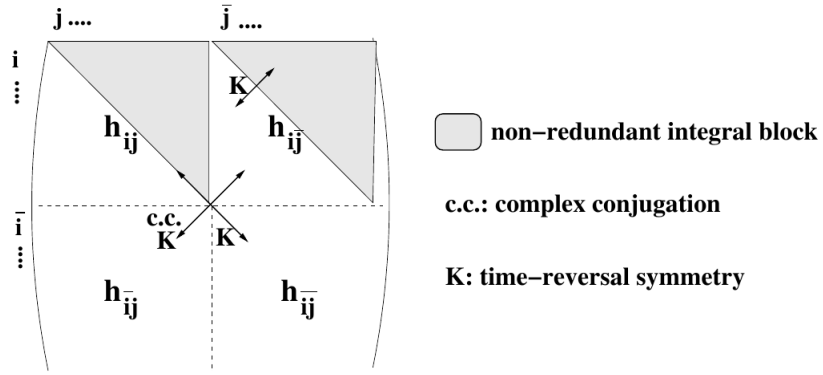

Figure 4.1 – Reduction to non-redundant set of one-particle integrals in a Kramers restricted formalism [Fle10].

left block in Fig. 4.1 corresponding to the integral over two unbarred functions is rewritten:

$$h_{\bar{i}\bar{j}} = \left\langle \varphi_{\bar{i}} | \hat{h} | \varphi_{\bar{j}} \right\rangle = \left\langle \hat{\mathcal{K}}\varphi_i | \hat{h} | \hat{\mathcal{K}}\varphi_j \right\rangle = \left\langle \varphi_i | \hat{\mathcal{K}}^\dagger \hat{h} \hat{\mathcal{K}} | \varphi_j \right\rangle^* . \tag{4.12}$$

In the latter step, the complex conjugation property (Eq. (4.10)) is used and in the next step, we make use of Eq. (4.11), the following stems from the hermicity of the Hamiltonian:

$$h_{\bar{i}\bar{j}} = \left\langle \varphi_i | \hat{h} | \varphi_j \right\rangle^* = \left\langle \hat{h}\varphi_j | \varphi_i \right\rangle = \left\langle \varphi_j | \hat{h}^\dagger | \varphi_i \right\rangle = \left\langle \varphi_j | \hat{h} | \varphi_i \right\rangle = h_{ji}. \tag{4.13}$$

Likewise, it can be shown that the lower left and upper right blocks are related via $h_{\bar{i}j} = -h^*_{i\bar{j}}$. Therefore, the calculation of the integrals of only two of the four blocks is required. Furthermore, the $i\bar{j}$ block undergoes a further reduction:

$$\begin{aligned} h_{i\bar{j}} &= \left\langle \varphi_i | \hat{h} \hat{\mathcal{K}} | \varphi_j \right\rangle = \left\langle \varphi_i | \hat{\mathcal{K}}^\dagger \hat{h} \hat{\mathcal{K}} \hat{\mathcal{K}} | \varphi_j \right\rangle = - \left\langle \varphi_i | \hat{\mathcal{K}}^\dagger \hat{h} | \varphi_j \right\rangle = - \left\langle \hat{\mathcal{K}}\varphi_i | \hat{h} | \varphi_j \right\rangle^* \\ &= - \left\langle \varphi_{\bar{i}} | \hat{h} | \varphi_j \right\rangle^* = - \left\langle \varphi_{\bar{j}} | \hat{h} | \varphi_i \right\rangle = -h_{j\bar{i}} \end{aligned} \tag{4.14}$$

that makes it triangular. Hence, the only one-particle integrals to calculate are h_{ij} and $h_{i\bar{j}}$. In the case of two-particle operators, an alike reduction of the integrals occurs and the unique set of two-particle integrals is

$$(ij|kl) \quad (\bar{i}j|kl) \quad (\bar{i}j|\bar{k}l) \quad (\bar{i}j|k\bar{l}). \tag{4.15}$$

4.1.3.3 Double groups.

In relativistic theories, spin and orbital angular momentum are combined into a total angular momentum J_e and hence, point-group symmetries are no longer relevant to describe atomic and molecular half-integer-spin (fermionic) systems within the relativistic framework. As to the integer-spin (bosonic) systems, point-group symmetries remain appropriate. A proper approach was proposed by Bethe [Bet29] who added the 2π rotation ($\bar{E}$) to the symmetries operations that constituted the finite point groups. This is necessary to account for the change of sign of half-integer spin functions under rotation by angle 2π. In this way, the *double groups* are introduced through the direct product of a given non-relativistic point group and the group $\{E, \bar{E}\}$ where the identity operation E corresponds to a 4π rotation. Hence, the new expanded group is of order $2n$ if the order of the point group is n, which translates into a doubling of the number of fermion irreducible representations (irreps). The character tables of the double groups can be found in dedicated textbooks [Bal97, Kos63]. The symmetry operations that one may encounter in those tables are rotations, reflections, inversion. The time reversal is not an element of double groups, however, a link can be made [Wig32].

This introduction to double groups allows us to discuss the implications of those molecular symmetries for the integrals over Kramers-paired spinors expounded in the previous paragraph (Section 4.1.3.2). We will base our discussion on the exemplifying complex-valued double group C_{2h}^* whose character table is displayed in Section 4.1.3.3.

Table 4.1 – Character table of the double point group C_{2h}^*.

	E	C_2	σ_h	I	$\bar{E}$	$\bar{C_2}$	$\bar{\sigma_h}$	$\bar{I}$
A_g	1	1	1	1	1	1	1	1
B_g	1	-1	-1	1	1	-1	-1	1
A_u	1	1	-1	-1	1	1	-1	-1
B_u	1	-1	1	-1	1	-1	1	-1
${}^1E_g$	1	i	i	1	-1	-i	-i	-1
${}^2E_g$	1	-i	-i	1	-1	i	i	-1
${}^1E_u$	1	i	-i	-1	-1	-i	i	1
${}^2E_u$	1	-i	i	-1	-1	-i	i	1

Any spinor transforms as to one of the fermion irreducible representations E and the functions of a given pair are ${}^1E$ and ${}^2E$ respectively. Besides, the relativistic Hamiltonian operators transform as to the totally symmetric representation of a

double group, *i.e.*, A_g for the C_{2h}^* group. Then, one may make use of the powerful theorem of group theory that states that an integral over a symmetric range does not vanish if and only if the integrand transforms as to the totally symmetric irreducible representation. Hence, it can be shown that the $h_{i\bar{j}}$ one-particle integrals vanish since the irreducible representation of the product $\varphi_i \hat{h} \varphi_{\bar{j}}$ can not be the totally symmetric A_g, *e. g.*,

$$^1E_g \otimes A_g \otimes^1 E_g = B_g. \tag{4.16}$$

Likewise, the two-particle integrals of the type $(\bar{i}j|kl)$ give zero. Those considerations are valid for any complex-valued (C_2^*, C_s^*) and real-valued $(D_{2h}^*, D_2^*, C_{2v}^*)$ double groups. Nevertheless, they do not hold for the quaternionic groups C_i^* and C_1^* where the functions of a Kramers pair belong to the same irreducible representation.

It is obviously possible to take advantage of the double-group symmetries and many relativistic electronic structure methods include them to increase the computational efficiency [Vis96, Aer84, YHN+07].

4.1.4 Basis sets.

Most of electronic structure calculations based on expansions in finite atomic basis sets are carried out with basis sets of Gaussian-type orbitals

$$\chi_\mu(r) = f(r)e^{-\zeta_\mu r^2}. \tag{4.17}$$

They are seen as the most efficient and convenient type of basis in particular in relativistic four-component calculations where they are often employed in their uncontracted form [DF07]. This is the case in the present work where we use Dyall uncontracted Gaussian-type basis sets [Dya] whose exponents are optimized for the relativistic case.

This choice of uncontracted basis sets is, amongst other things, motivated by the need to fulfill the *kinetic balance* condition [SH84]

$$\chi_\mu^S \propto (\boldsymbol{\sigma} \cdot \mathbf{p})\chi_\mu^L \tag{4.18}$$

that guarentees the exact non-relativistic limit for the kinetic energy by connecting the large χ_μ^L and small χ_μ^S components. This condition is satisfied in calculations carried out in the `DIRAC` program [DIRa] where the set of small components is determined by applying the restricted kinetic balance condition to an uncontracted basis set that consitutes the large component basis. [DF90]

4.2 Correlated Relativistic Wavefunction Theory.

4.2.1 Correlation Methods.

In both relativistic and non-relativistic quantum chemistry, the simplest starting points to describe the electronic structure of many-electron systems are the so-called mean-field methods among which is the Hartree-Fock (HF) model. However, these methods in which the motion of each electron is described by a mean-field repulsion of all other electrons of the system only provide qualitative insights into the electronic structure. Indeed, even though the Hartree-Fock total energy can reach up to 95% of the exact electronic energy, the missing 5%, due to the electron correlation, turn out to be decisive to molecular relative energies and the effect of the correlation of electrons equally decisive for chemical properties. Thus, to get more reliable results, one needs to take into account the electron correlation defined as the difference between a mean-field approach and the exact description of the system, *i. e.,*

$$E_{corr} = E_{exact} - E_{Hartree-Fock} \tag{4.19}$$

within a given basis set. The post-Hartree-Fock methods that go beyond the mean-field approach are referred to as correlation methods. In the following, we will introduce the correlation method employed in the present work that is the *Kramers-restricted Configuration Interaction* model.

It is one version of the Configuration Interaction approach that includes dynamical correlation in a post-Hartree-Fock treatement by expanding the wavefunction Ψ in a linear combination of M N-particle functions ϕ_i,

$$\Psi = \sum_{i}^{M} C_i \phi_i. \tag{4.20}$$

The parametrisation is performed by solving the matrix eigenvalue equation,

$$\mathbf{HC} = E\mathbf{C} \tag{4.21}$$

with $\mathbf{C}$, the CI coefficient vector and E, the corresponding eigenvalue.

4.2.2 String-based Methods.

The Kramers-restricted Configuration Interaction algorithm implemented in the `DIRAC` program [DIRa] as the `LUCIAREL` module by Fleig and co-workers [FOM01, FOV03, FJOV06, TFJ08] is a string-based method. In such a method, the many-body wavefunctions are defined within the second-quantisation framework by the means of strings of creation and annihilation operators that allows for an efficient

determination of coupling coefficients and inclusion of higher-order excitations (such as triple or quadruple excitations). In non- or scalar-relativistic Configuration Interaction approaches, a Slater determinant is represented as a product of $\alpha-$ and $\beta-$strings [ORJJ88] with a well-defined M_S value, projection of the spin operator along the z-axis. In the relativistic Kramers formalism, one substitute the latter strings with $\mathcal{S}$- and $\overline{\mathcal{T}}$-strings of n Kramers spinors $\{\varphi_p\}$ and $\bar{n}$ Kramers partners $\{\varphi_{\bar{p}}\}$ respectively[KJF10, Fle10],

$$\hat{\mathcal{S}}^\dagger|vac\rangle = \hat{a}^\dagger_{S_1}\hat{a}^\dagger_{S_2}\cdots\hat{a}^\dagger_{S_n}|vac\rangle \tag{4.22}$$

$$\hat{\overline{\mathcal{T}}}^\dagger|vac\rangle = \hat{a}^\dagger_{\bar{T}_1}\hat{a}^\dagger_{\bar{T}_2}\cdots\hat{a}^\dagger_{\bar{T}_{\bar{n}}}|vac\rangle \tag{4.23}$$

where $N = n + \bar{n}$ is the number of electrons in the system to study. A Slater determinant can be written through a combination of a Kramers-unbarred and a Kramers-barred string :

$$\left|\mathcal{S}\overline{\mathcal{T}}\right\rangle = \hat{\mathcal{S}}^\dagger\hat{\overline{\mathcal{T}}}^\dagger|vac\rangle. \tag{4.24}$$

Similarly, the spin projection is replaced by the Kramers projection

$$M_K = \frac{N_p - N_{\bar{p}}}{2} \tag{4.25}$$

with N_p and $N_{\bar{p}}$, the number of creation operators of electrons in Kramers unbarred and barred spinors respectively. All determinants can be ordered in subsets according to their M_K value. Thus, the CI expansion of the wavefunctions over Slater determinants in the Kramers formalism reads:

$$|\psi_k\rangle = \sum_{I=1}^{dim\mathcal{F}^t(M,N)} c_{kI}|(\mathcal{S}\overline{\mathcal{T}})_I\rangle \tag{4.26}$$

where $dim\mathcal{F}^t(M,N)$ is the dimension of the truncated N-particle Fock space sector over M one-particle basis functions and c_{kI} are the expansion coefficients derived by diagonalising the Dirac-Coulomb Hamiltonian $\hat{H}^{DC}$ Eq. (4.5) in the Slater determinant basis.

4.2.3 Operators Expansion in Second Quantisation.

The same Kramers formalism is employed to expand operators in second quantisation. In this way, the Dirac-Coulomb Hamiltonian can be written as [JDSF96,

FOM01]:

$$\begin{aligned}\hat{\mathcal{H}}_{DC} = &\sum_{pq}\left[h_{pq}\hat{X}^{+}_{pq} + \frac{1}{2}\left(h_{\bar{p}q}\hat{X}^{+}_{\bar{p}q} + h_{p\bar{q}}\hat{X}^{+}_{p\bar{q}}\right)\right] \\ &+ \frac{1}{2}\sum_{pqrs}\left[(pq|rs)\hat{x}^{++}_{pq,rs} + (\bar{p}q|rs)\hat{x}^{++}_{\bar{p}q,rs} + (p\bar{q}|rs)\hat{x}^{++}_{p\bar{q},rs}\right] \\ &+ \frac{1}{4}\sum_{pqrs}(\bar{p}q|r\bar{s})\hat{x}^{++}_{\bar{p}q,r\bar{s}} \\ &+ \frac{1}{8}\sum_{pqrs}\left[(\bar{p}q|\bar{r}s)\hat{x}^{++}_{\bar{p}q,\bar{r}s} + (p\bar{q}|r\bar{s})\hat{x}^{++}_{p\bar{q},r\bar{s}}\right] \end{aligned} \tag{4.27}$$

where $\hat{X}^{S}_{pq}$ and $\hat{x}^{S_1,S_2}_{pq,rs}$, the single and double replacement operators respectively are as introduced in [AJO95]

$$\hat{X}^{S}_{pq} = a^{\dagger}_{p}a_{q} + sa^{\dagger}_{\bar{q}}a_{\bar{p}} \quad \hat{X}^{S}_{p\bar{q}} = a^{\dagger}_{p}a_{\bar{q}} - sa^{\dagger}_{q}a_{\bar{p}} \quad \hat{X}^{S}_{\bar{p}q} = a^{\dagger}_{\bar{p}}a_{q} - sa^{\dagger}_{\bar{q}}a_{p}, \tag{4.28}$$

$$\hat{x}^{S_1,S_2}_{pq,rs} = \hat{X}^{S_1}_{pq}\hat{X}^{S_2}_{rs} - \delta_{rq}a^{\dagger}_{p}a_{s} - s_1\delta_{r\bar{p}}a^{\dagger}_{\bar{q}}a_{s} - s_2\delta_{\bar{s}q}a^{\dagger}_{p}a_{\bar{r}} - s_1s_2\delta_{\bar{p}\bar{s}}a^{\dagger}_{\bar{q}}a_{\bar{r}} \tag{4.29}$$

where s and $s_1, s_2 = \pm$ denote the symmetry character of the operators under time-reversal and hermitian conjugation respectively. The various terms of the Hamiltonian can be classified according to their ΔM_K value, which is the number of Kramers flips induced by applying a part of $\hat{\mathcal{H}}_{DC}$ on a given Slater determinant.

$$\hat{\mathcal{H}}_{DC} = \sum_{\Delta M_K=-2}^{2}\hat{H}_{\Delta M_K} \tag{4.30}$$

where

$$\begin{aligned}\hat{H}_{\Delta M_K=-2} &= \sum_{pqrs}\frac{1}{2}(\bar{p}q|\bar{r}s)\hat{x}^{++}_{\bar{p}q,\bar{r}s} \\ \hat{H}_{\Delta M_K=-1} &= \sum_{pq}h_{\bar{p}q}\hat{X}^{+}_{\bar{p}q} + \sum_{pqrs}\frac{1}{2}(\bar{p}q|rs)\hat{x}^{++}_{\bar{p}q,rs} \\ \hat{H}_{\Delta M_K=0} &= \sum_{pq}h_{pq}\hat{X}^{+}_{pq} + \sum_{pqrs}\left[\frac{1}{2}(pq|rs)\hat{x}^{++}_{pq,rs} + \frac{1}{4}(\bar{p}q|r\bar{s})\hat{x}^{++}_{\bar{p}q,r\bar{s}}\right] \\ \hat{H}_{\Delta M_K=+1} &= \sum_{pq}\frac{1}{2}h_{p\bar{q}}\hat{X}^{+}_{p\bar{q}} + \sum_{pqrs}\frac{1}{2}(p\bar{q}|rs)\hat{x}^{++}_{p\bar{q},rs} \\ \hat{H}_{\Delta M_K=+2} &= \sum_{pqrs}\frac{1}{8}(p\bar{q}|r\bar{s})\hat{x}^{++}_{p\bar{q},r\bar{s}}. \end{aligned} \tag{4.31}$$

The Kramers-restricted-correlation-interaction method takes advantage of this ΔM_K partition for its diagonalisation procedure. More details on the `LUCIAREL` algorithm implementation can be found in [KJF10].

Likewise, the operators that describe the $\mathcal{P},\mathcal{T}$-odd properties of interest in the search of new physics beyond the Standard Model can be expanded in second quantisation in the basis of Kramers-paired molecular spinors:

$$\hat{H}_{\mathcal{P},\mathcal{T}} = \sum_{p,q=1}^{P_u} h_{pq} a_p^\dagger a_q + \sum_{p=1}^{P_u}\sum_{q=P_u+1}^{P} h_{p\bar{q}} a_p^\dagger a_{\bar{q}} + \sum_{p=P_u+1}^{P}\sum_{q=1}^{P_u} h_{\bar{p}q} a_{\bar{p}}^\dagger a_q + \sum_{p,q=P_u+1}^{P} h_{\bar{p}\bar{q}} a_{\bar{p}}^\dagger a_{\bar{q}}. \tag{4.32}$$

where P is the total number of operators and P_u, the number of unbarred operators.

As shown in Section 2.4, those properties are evaluated as expectation value. Over relativistic Kramers-restricted-Configuration-Interaction wavefunctions, they take the form:

$$\langle \hat{H}_{\mathcal{P},\mathcal{T}} \rangle_{\psi_k} = \sum_{I,J=1}^{dim\mathcal{F}^t(M,N)} c_{kI}^* c_{kJ} \langle (\mathcal{S}\overline{\mathcal{T}})_I | \sum_{i=1}^{N} \hat{H}_{\mathcal{P},\mathcal{T}}(i) | (\mathcal{S}\overline{\mathcal{T}})_J \rangle. \tag{4.33}$$

One may further expand the expectation value by substituting both Hamiltonian operator and wavefunctions with their second-quantisation representation (Eqs. (4.26) and (4.32)). Thus, the contribution to the expectation value resulting from the first term of the Hamiltonian operator (Eq. (4.32)) reads as a contraction of CI densities, molecular integrals and coupling coefficients [FNK16]:

$$W(\psi_k)_1 = \sum_{I,J=1}^{dim\mathcal{F}^t(M,N)} c_{kI}^* c_{kJ} \sum_{m,n=1}^{P_u} h_{mn} \langle | \prod_{p=1}^{N_p\in\mathcal{S}_I} \prod_{\bar{p}=N_p+1}^{N_p\in\mathcal{S}_I+N_{\bar{p}}\in\overline{\mathcal{T}}_I} a_{\bar{p}} a_p a_m^\dagger a_n \prod_{q=1}^{N_p\in\mathcal{S}_J} \prod_{\bar{q}=N_p+1}^{N_p\in\mathcal{S}_J+N_{\bar{p}}\in\overline{\mathcal{T}}_J} a_q^\dagger a_{\bar{q}}^\dagger | \rangle. \tag{4.34}$$

4.2.4 Generalised Active Spaces.

An efficient treatement of heavy atoms and compounds by such a method is not trivial since they often exhibit complex electronic structure, namely, near degeneracies of atomic orbitals with different value of angular momentum and numerous unpaired electrons.

A way to deal with the complicated electronic structure is to apply the concept of *Generalised Active Spaces* (GAS) first introduced in non-relativistic quantum chemistry by Jeppe Olsen [Ols00]. It consists in defining an arbitrary number of active orbital spaces and ordering the orbitals into these spaces. Thus, some constraints are imposed on the electronic occupation, limiting the CI expansion to the terms judged of crucial importance to construct the wavefunction of the considered system. Typically, the orbital space is subdivided into a **Frozen Core** that includes the inner orbitals, an **External space** that comprises the virtual spinors and whose highest lying orbitals with energy greater than a defined cut-off are often deleted to reduce

Figure 4.2 – Generalised Active Space models for ThO CI wavefunctions [FN14] .

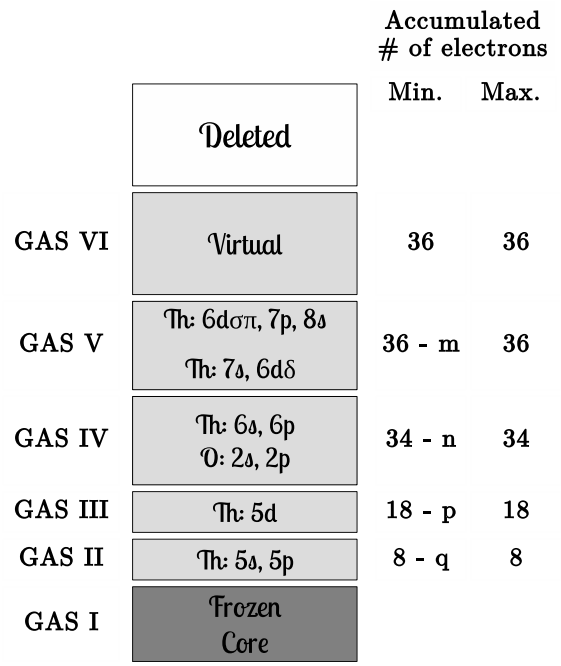

the computational cost. The remaining form a particle space since a certain number of electrons is allowed in this so-called **Virtual space**. Finally, the central part of the spinors space named **Active space**, itself divided into several subspaces.

Figure 4.2 displays an exemplifying choice of partitioning and parametrisation of the ThO molecule spinors space. In this scheme, min./max. indicate the minimum/maximum number of accumulated electrons after filling of the corresponding subspace and m, n, p, q specify the maximum number of holes allowed in the combined previous and considered GAS. In this way, n will point out the maximum number of excitations permitted in the combined hole spaces (GAS II-IV). Those excitations, included by non-zero n, p ans q, would account for both core-core correlations (among $5d$ electrons) and core-valence correlations (between $5d$ and higher-lying orbitals electrons). Lastly, the GAS V is a specific space since it is a mixed particle-hole space that comprises particles that are excited electrons from the lower-lying orbitals and holes due to excitations towards the virtual space limited by the m parameter.

Thus, though it requires an *a priori* qualitative knowledge of the electronic structure of the system, the sophisticated partitioning of the spinors space and parametrisation of electron occupation permit the construction of a large variety of wavefunction models to test in order to carry out an elaborate study of atomic or molecular properties such as the $\mathcal{P}, \mathcal{T}$-odd constants (*cf.* Chapters 5 and 6).

That concludes the last chapter of the theoretical part in which we presented the theory of the $\mathcal{P},\mathcal{T}$-odd interactions and derived the corresponding molecular parameters to be calculated. Furthermore, an introduction to the methodology employed for their calculation was proposed.

In the following application chapters, we will apply the GASCI method defined above to the calculation of the molecular parameters relevant to the search of $\mathcal{CP}$-violation in paramagnetic systems, starting with a promising candidate system for the detection of an electron electric dipole moment, the thorium fluoride molecular ion ThF^+ (Chapter 5). Then, a similar study will be conducted on another diatomic molecule already employed in an eEDM experiment, the thorium monoxide molecule (ThO) (Chapter 6). Finally, we will focus on the determination of the magnetic hyperfine interaction constant of the fluorine atom in diatomic molecules (Chapter 7).

5 Theoretical study on ThF^+.

Part of the work expounded below was published in: M. Denis, M. S. Norby, H. J. A. Jensen, A. S. P. Gomes, M. K. Nayak, S. Knecht, and T. Fleig, New J. Phys. 17, 043005 (2015), *Theoretical study on ThF^+, a prospective system in search of time-reversal violation.* [DNJ+15]

The low-lying electronic states of ThF^+, a possible candidate in the search for $\mathcal{P}$- and $\mathcal{T}$-violation, have been studied using high-level correlated relativistic *ab initio* multi-reference coupled-cluster and configuration interaction approaches. For the $^3\Delta$ state component with $\Omega = 1$ (electron electric dipole moment "science state") we obtain an effective electric field of $E_{\text{eff}} = 35.2 \left[\frac{\text{GV}}{\text{cm}}\right]$, a $\mathcal{P}$- and $\mathcal{T}$-odd electron-nucleon interaction constant of $W_S = 48.4$ [kHz], a magnetic hyperfine interaction constant of $A_{||} = 1833$ [MHz] for ^{229}Th ($I = 5/2$), and a very large molecular dipole moment of 4.03 [D]. The $\Omega = 1$ state is found to be more than 300 cm^{-1} lower in energy than $\Omega = 0^+$ ($^1\Sigma^+$), challenging the state assignment from an earlier theoretical study on this species [Barker et al, J. Chem. Phys **136**, 104305 (2012)].

5.1 Introduction.

The electron's EDM has, despite a vigorous search for over half a century, still not been detected. The most constraining upper bounds on the electron EDM have for some time been obtained from experimental and theoretical investigations on atoms [RM09, LK92], and such upper bounds are useful guiding constraints on beyond SM theories [BS91]. However, polar diatomic molecules have become the major players in this quest, since they offer an order of magnitude larger enhancement [SF78, RM09] of the ensuing energy shift than what could be achieved with an atom [San65, RCSD02](as exposed in Section 1.2.1). This means that, for a given measurement on a molecular system, the possible magnitude of the electron EDM is constrained to a smaller value, or conversely, that the effect of a smaller electron EDM can be detected through the measurement. The corresponding enhancement factor is not accessible by experimental means and has to be determined – preferrably

– *via* a molecular relativistic many-body calculation.

According to the most recent findings using the polar molecule ThO [CBC$^+$14, FN14, SPT13, DeM] the upper bound on the electron EDM is $|d_e| < 9.6 \times 10^{-29}\, e\,\mathrm{cm}$. This value is more than 16 times smaller than the most constraining upper bound from an atomic study [RCSD02]. Charged molecules offer an experimental advantage over neutral systems in that ion traps can be used which allow for long interrogation times. High-resolution spectroscopy employing rotating electric fields has been presented recently as a viable technique for symmetry violation searches in charged molecular ions [LBL$^+$11, CGS$^+$12]. The ionic systems used in these experiments are HfF^+ and, as a perspective molecular ion, ThF^+.

What the afore-mentioned molecules, and several others such as HfH^+, PtH^+ [MBD06] and WC [LCS$^+$13, WS11], have in common is an energetically low-lying $^3\Delta$ electronic state (in Λ-S coupling picture). In the fluorides and oxides this state is deeply bound which is an experimental advantage. The magnetic moment in the $\Omega = 1$ component of this term is approximately zero which helps reduce the vulnerability of the experiment to decoherence and systematic errors [LBL$^+$11].

HfF^+ and ThF^+ exhibit a considerably large EDM effective electric field in the relevant "science" state [PMIT07, FN13, MB08] and, at the same time, a small Λ (or Ω) doublet splitting. This latter property is an asset for efficient mixing of rotational parity eigenstates through the external electric laboratory field. While HfF^+, already employed in an eEDM experiment [LBL$^+$11], has been characterized in detail [AHT04, BABH11, PMIT07, PMT09, SMPT08, FN13] considerably less is known for ThF^+ [MB08, BAHP12, Iri12]. The joint experimental and theoretical work of Barker *et al.* [BAHP12] left some uncertainty as to whether the $\Omega = 1$ state is the ground-state or the first excited state, as there is an $\Omega = 0^+$ state ($^1\Sigma_0^+$) separated from it by only 315 cm^{-1}. The experimental resolution was not sufficient to unequivocally assign those states and, unlike HfF^+, the $\Omega = 1$ and 0^+ states of ThF^+ possess similar vibrational frequencies at around 658 cm^{-1}. Accompanying theoretical calculations were also inconclusive, but from the best estimate the $\Omega = 0^+$ state was proposed as ground state with the $\Omega = 1$ state higher by 65 cm^{-1} in Reference [BAHP12] and 202 cm^{-1} in Reference [HBA14a], respectively.

Turning to the EDM effective electric field in $\Omega = 1$ of ThF^+, the work of Meyer *et al.* [MB08] suggests an extremely large value of $E_{\mathrm{eff}} = 90\left[\frac{\mathrm{GV}}{\mathrm{cm}}\right]$. Recent and more rigorous relativistic many-body calculations on the isoelectronic ThO molecule have shown [FN14, SPT13] that the model calculation of Meyer *et al.* yields a significantly overestimated E_{eff} for the case of ThO (by more than 35%). It can therefore be expected that for this kind of molecules and electronic states the model of Meyer *et al.* contains a systematic error that is also present in the above prediction for E_{eff} in ThF^+.

We pursue two major goals in this work. Using spinor-based many-body methods which treat dynamic electron correlations and electronic spin-orbit interactions on the same footing, a rigorous determination of the electronic ground state of ThF^+ and some of its low-lying electronically excited states is carried out. Second, with the same uncompromising techniques we determine with high accuracy properties of the $^3\Delta_1$ ($\Omega = 1$) state which are of direct relevance for proposed measurements of the electron EDM. In particular, we present the first rigorous calculation of the eEDM $\mathcal{P},\mathcal{T}$-odd interaction constant and of the molecular static electric dipole moment. Furthermore, the magnetic hyperfine interaction constant is calculated for $\Omega = 1$ along with the scalar-pseudoscalar $\mathcal{P},\mathcal{T}$-odd interaction constant, both of which play an important role in the interpretation of corresponding and ongoing experimental measurements [CGS+12, CG14]. We also calculated static molecular electric dipole moments and electric transition moments, the latter of which are of interest regarding state preparation in an EDM experiment. Molecular dipole moments are directly related to the EDM effective electric field, since they are a measure of the mixing of parity eigenstates.

5.2 Application to ThF^+.

5.2.1 Technical details.

The determination of the spectroscopic characteristic and the calculation of all $\mathcal{P},\mathcal{T}$-odd and magnetic hyperfine expectation values were performed with the `DIRAC11` program package [DIRb].

We employed uncontracted atomic Gaussian basis sets for the description of both atoms' electronic shells. For thorium, Dyall's [Dya06, Dya12] double-ζ (DZ, dyall.cv2z, [26s23p17d13f1g]), triple-ζ (TZ', dyall.cv3z, [33s29p20d14f4g1h]) and quadruple-ζ (QZ', dyall.cv4z, [37s34p24d19f7g4h]) basis sets were used. For the latter basis set, QZ', all $5d, 6d, 7s$ correlating functions, except for the i function, have been added. For the fluorine atom, aug-cc-pVnZ (n=T, Q) and cc-pVnZ (n=D, T, Q) [Dun89] basis sets have been used.

Molecular spinors were optimized through all-electron four-component Dirac-Coulomb Hartree-Fock calculations. We based the open-shell calculations on an average-of-configuration Fock operator for two electrons in the three Kramers pairs of Th(7s, 6dδ), the other 96 electrons are restricted to closed shells.

We defined models of varying quality to perform GASCI calculations (see Section 4.2.4) of the effective electric field E_{eff}, the parallel magnetic hyperfine interaction constant $A_{||}$, the scalar-pseudoscalar electron-nucleon interaction constant W_S (respectively defined in Eqs. 2.83, 3.39 and 2.115) in the $\Omega = 1$ state and the vertical

excitation energy T_v of the $\Omega = 0$ state.

Table 5.1 – CI wavefunction models using refined active spinor spaces. The size of the P_m active space is given, in the name of the models, by an upper index X, which is the number of Kramers pairs (defined in Section 4.1.3.1) in the active space. The model $\mathcal{III}^{\mathcal{CI},3}$ thus comprises the minimal active space to describe the $\Omega = 0$ et $\Omega = 1$ states corresponding to $^1\Sigma_0$ and $^3\Delta_1$ in the Λ-S coupling picture. Models $\mathcal{III}^{\mathcal{CI},3}$ and $\mathcal{III}^{\mathcal{CI}+T,3}$ differ by the highest excitation rank allowed from the hole spaces to the particle space. In the latter, triple excitations are included.

Model	Th $6s$,$6p$ F $2s$,$2p$	Th $7s$,$6d\delta$	Th $6d\pi$	Th $6d\sigma$	Th $7p\pi$	Th $7p\sigma$,$8s$	< 10 a.u
$\mathcal{III}^{\mathcal{CI},3}$	$Q-SD$	P_m	$Q-SD$	$Q-SD$	$Q-SD$	$Q-SD$	$Q-SD$
$\mathcal{III}^{\mathcal{CI}+T,3}$	$Q-SD$	P_m	$Q-SDT$	$Q-SDT$	$Q-SDT$	$Q-SDT$	$Q-SDT$
$\mathcal{III}^{\mathcal{CI},5}$	$Q-SD$	P_m	P_m	$Q-SD$	$Q-SD$	$Q-SD$	$Q-SD$
$\mathcal{III}^{\mathcal{CI},6}$	$Q-SD$	P_m	P_m	P_m	$Q-SD$	$Q-SD$	$Q-SD$
$\mathcal{III}^{\mathcal{CI},8}$	$Q-SD$	P_m	P_m	P_m	P_m	$Q-SD$	$Q-SD$
$\mathcal{III}^{\mathcal{CI},10}$	$Q-SD$	P_m	P_m	P_m	P_m	P_m	$Q-SD$
$\mathcal{IV}^{\mathcal{CI}}$	frozen	P_m	P_m	P_m	P_m	P_m	$Q-SD$

We used two principal CI models, denoted as $\mathcal{III}^{CI}$ and $\mathcal{IV}^{CI}$, the former of which has been further refined to accomodate for varying size of the valence spinor space and for the inclusion of determinants with more than two particles in the virtual spinor space. This elaborate choice of models is motivated by earlier findings on the ThO system [FN14]. The models are defined in full detail in Table 5.1, using the nomenclature from Table 1 of [DNJ+15], for coherence.

For the calculation of the nuclear magnetic hyperfine coupling constant we use the thorium isotope ^{229}Th for which the nuclear magnetic moment has been determined to be $\mu = 0.45\mu_N$ [KLR+12]. Its nuclear spin quantum number is $I = 5/2$. In all calculations the speed of light was set to 137.0359998 a.u.

5.2.2 Results and discussion.

5.2.2.1 Spectroscopic study.

A preliminary study of the electronic structure of the ThF^+ molecular ion was performed with the minimal CI model $\mathcal{IV}^{CI}$. From the corresponding energy spectrum displayed in Fig. 5.1, it appears that the four lowest-lying states are the singlet $^1\Sigma_0$ and the three terms of the triplet $^3\Delta$.

We calculate the vertical transition energies of these four low-lying electronic states using triple-ζ basis set and the best CI model of this work $\mathcal{III}^{\mathcal{CI},10}$. They are presented in Table 5.2 where they are compared with the results obtained with the

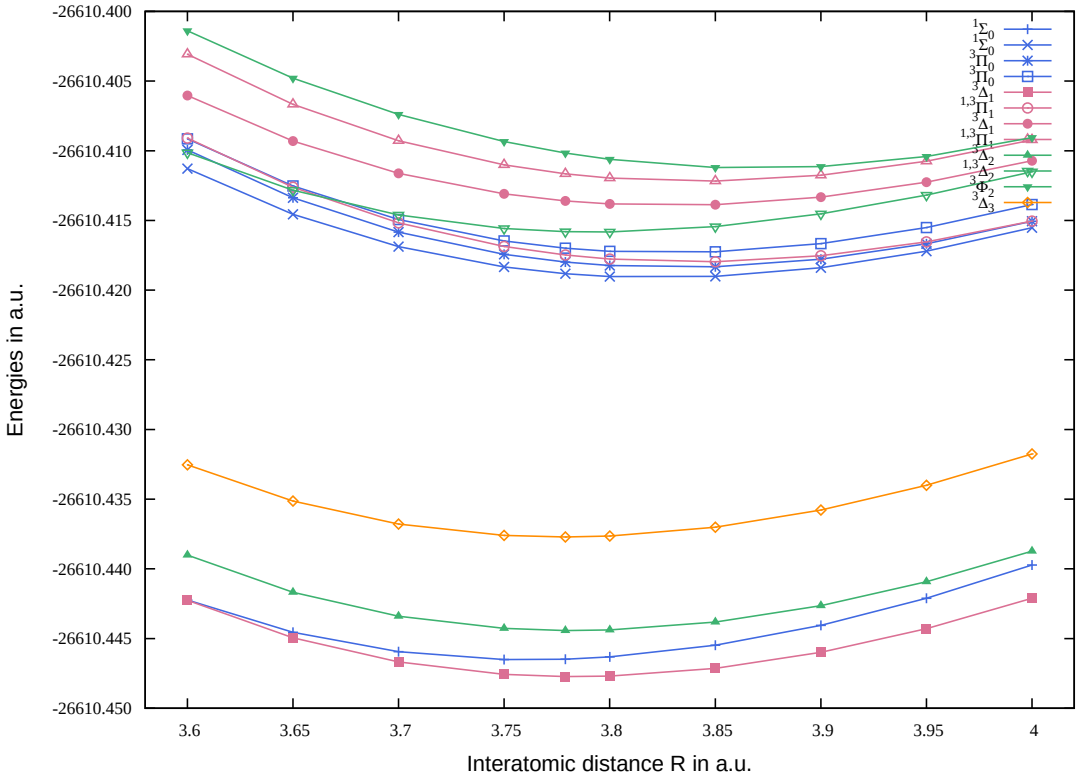

Figure 5.1 – Energy spectrum for low-lying electronic states using the TZ' basis set and the minimal CI model $\mathcal{IV}^{\mathcal{CI}}$.

$\mathcal{III}^{\mathcal{CC},f}$ deemed to be the best two-component model in [DNJ+15], a perturbative additive method MRCI+Q/SO and experimentally, respectively. It appears that all spinor-based methods presented in this table and in Table 3 of [DNJ+15] yield similar results that are in good agreement with the most recent experimental data [GCZ+16]. They all assign $^3\Delta_1$ state as the ground-state of the ThF^+ molecular ion and yield a good description of the excitation energies, in particular the $^3\Delta$ splittings which is widely underestimated by orbital-based methods such as the perturbative Coupled Cluster method that accounts for spin-orbit interaction in an additive way. A possible explanation for the underestimation of the $^3\Delta$ splittings and, particularly the $^3\Delta_2 -^3 \Delta_3$ energy difference is an insufficient treatment of the spin-orbit interaction that gives rise to an underestimation of the $\Delta\varepsilon_{\delta_{5/2}-\delta_{3/2}}$ energy shift that, in a Dirac-Coulomb approximation, exhibits a non-negligible value:

$$\Delta\varepsilon_{\delta_{5/2}-\delta_{3/2}} = 2166cm^{-1}. \tag{5.1}$$

So as to understand the greater error of perturbative additive methods for $^3\Delta_2 -^3 \Delta_3$ than for $^3\Delta_1 -^3 \Delta_2$, we lead an analysis of the $^3\Delta$ wavefunctions with the

Table 5.2 – Electronic spectra respectively established from vertical excitation energies with models four-component CI $\mathcal{III}^{\mathcal{CI},10}$ for internuclear distance $R = 3.779$ a.u., two-component $\mathcal{III}^{\mathcal{CC}}$ at $R = 3.743$ a.u. and excitation energies with the perturbative additive CI MRCI+Q/SO method. Experimental data have been added for comparison.

		Electronic state energy $[cm^{-1}]$			
Method	Model	$^1\Sigma^+_{0^+}$	$^3\Delta_1$	$^3\Delta_2$	$^3\Delta_3$
GASCI	$\mathcal{III}^{\mathcal{CI},10}$	538	0	1155	3012
IHFSCC	$\mathcal{III}^{\mathcal{CC},\mathrm{f}}$	318.99	0.00	1038.94	3161.99
MRCI+Q/SO[b]		0.0	202	1047	2163
Experiment[b]		0.00	315.0(5)	1052.5(5)	3150(15)
Experiment[c]		314.0(2)	0.00	1052.5(1.0)	3149(30)

[f] 2c-mmf approach and extrapolation to the basis set limit.
[b] Reference [BAHP12].
[c] Reference [GCZ+16].

same $\mathcal{III}^{\mathcal{CI},10}$ wavefunction model:

$$\begin{aligned} &^3\Delta_1 : 89\%\ \sigma^1_{-1/2}\delta^1_{3/2} \\ &^3\Delta_2 : 61\%\ \sigma^1_{1/2}\delta^1_{3/2} + 28\%\ \sigma^1_{-1/2}\delta^1_{5/2} \\ &^3\Delta_3 : 89\%\ \sigma^1_{1/2}\delta^1_{5/2}. \end{aligned} \tag{5.2}$$

It confirms that the $^3\Delta_2$ state is a mixing of two configurations, among which the occupation $\sigma^1_{1/2}\delta^1_{3/2}$ is the major contributor. Hence, a correct description of the spin-orbit splitting $\Delta\varepsilon_{\delta_{5/2}-\delta_{3/2}}$ is of crucial importance for the determination of the energy shift between the $^3\Delta_2$ and $^3\Delta_3$ that exhibit the occupation of the $\delta_{5/2}$ and $\delta_{3/2}$ spinors, respectively. As a consequence, an insufficient description of the spin-orbit splitting will lead to a greater error for $^3\Delta_2 -^3 \Delta_3$ than for $^3\Delta_1 -^3 \Delta_2$ in which the same δ spinor is occupied by an unpaired electron.

Furthermore, this lack of treatment of the spin-orbit interaction that leads to an underestimation of the term splittings is also a possible explanation for the differing predictions of the ground-state of ThF^+.

5.2.2.2 $\mathcal{P},\mathcal{T}$-odd and magnetic hyperfine interaction constants.

We now turn to the discussion of our results of direct relevance to the search for $\mathcal{P},\mathcal{T}$-odd effects in ThF^+. We have used a series of one-particle basis sets and CI models, all of which are defined in subsection 5.2.1 and Table 5.1.

First of all, it is well known that the $\mathcal{P},\mathcal{T}$-odd interaction constants are very sensitive to the electron spin density in the vicinity of the nucleus and one may

ponder the merits of the Gaussian basis sets employed in this work by pointing out the lack of description of the orbital functions in the core region. Hence, we address this issue by adding steep functions to the s space. The additional exponents (E) are obtained from two existing exponents a and b of the considered basis set through the following procedure,

$$\log E = \log a \pm \frac{\log a - \log b}{2} \tag{5.3}$$

and added to the list of exponents of the original Gaussian basis set. Table 5.3 displays the values of the effective electric field E_{eff} and the parallel magnetic hyperfine interaction constant using double-ζ and extended double-ζ basis sets with $E_1 = 1.103 \times 10^8$, $E_2 = 2.881 \times 10^7$, $E_3 = 8.434 \times 10^6$. It appears that extending the basis set in the core region is reflected by a tiny variation of the values of the order of 0.02%.

Table 5.3 – Calculated properties values for the $\Omega = 1$ ($^3\Delta_1$) science state of ThF^+ at an internuclear distance of $R = 3.779\ a_0$ using DCHF spinors with an average-of-occupation Fock operator for 2 electrons in 6 Kramers pairs, the wavefunction model $\mathcal{III}^{\mathcal{CI},6}$ and vDZ basis set with different added exponents.

Basis set	$E_{\text{eff}}\left[\frac{\text{GV}}{\text{cm}}\right]$	$A_{\parallel}$ [MHz]
vDZ	34.437	1821.3
vDZ+E_1	34.445	1819.7
vDZ+E_1+E_2	34.441	1820.6
vDZ+E_1+E_2+E_3	34.441	1820.7

In order to minimize error bars we test the influence of several criteria, starting with the choice of a spinor basis space. Three DCHF spinor spaces are tested, the first of them is the DCHF_2in3 model that yields average-of-occupation spinors for 2 electrons in 3 Kramers pairs, $7s_\sigma$ and $6d_\delta$ suitable for a well-balanced description of both $^1\Sigma^+$ and $^3\Delta$ states. The second model to be tested is DCHF_1in1_1in2, it corresponds to $^3\Delta$ state specific spinors with one electron occupying $7s_\sigma$ and 1 electron occupying $6d_\delta$. Finally, the closed-shell model DCHF_cs is included in our comparison. The results compiled in Table 5.4 confirm the strong sensitivity of vertical excitation energies to the spinor basis set. However, the variation of $\mathcal{P},\mathcal{T}$-odd properties between the two DCHF models relevant for a physically well motivated comparison, *i. e.* DCHF_2in3 and DCHF_1in1_1in2, is much smaller, of the order of 2%. Hence, in this work, the correlation models will be based on DCHF spinors with an average-of-occupation Fock operator for 2 electrons in 3 Kramers pairs.

Table 5.4 – Calculated properties and molecular static electric dipole moment $D = \left\langle {}^M\Lambda_\Omega | \hat{D}_z | {}^M\Lambda_\Omega \right\rangle$ for $\Omega = 1$ at $R = 3.779$ a_0, using the wavefunction model $\mathcal{III}^{\mathcal{CI},10}$, the vDZ basis set and a virtual cutoff value of 10 a.u.

Spinor basis	T_v [cm^{-1}]	$E_{\text{eff}}\left[\frac{\text{GV}}{\text{cm}}\right]$	$A_{\|\|}$ [MHz]	W_S [kHz]
DCHF_2in3	538	35.2	1833	48.3
DCHF_1in1_1in2	668	35.8	1789	49.3
DCHF_cs	425	33.0	1827	45.3

Then, we focus on the quality of the basis set. The results in Table 5.5 demonstrate that the effective electric field and the parallel magnetic hyperfine interaction constant (for ^{229}Th ($I = 5/2$)) are rather insensitive to the size of the basis set employed. Increasing the basis set cardinal number changes the value of the hyperfine interaction constant $A_{||}$ by less than 0.6% in magnitude. Likewise, the correction yielded by the TZ' basis set for the effective electric field E_{eff} is smaller than 2% and the use of the QZ' basis set leads to a further change of less than 0.1%. The latter very small correction is also found for the electron-nucleon interaction constant. The vertical excitation energy for $\Omega = 0$ (T_v) undergoes a slightly larger change. Replacing the DZ by the TZ' basis set doubles the value of T_v, an increase of 409 [cm^{-1}] on the absolute. Using the set of QZ' quality yields a correction of 11% in magnitude, less than 90 [cm^{-1}]. The sensitivity of this excitation energy to basis set extent was already observed in the results in Table 3 of [DNJ+15]. However, based on the results in Table 5.5 we conclude that the values of E_{eff}, $A_{||}$ and W_S for $\Omega = 1$ are sufficiently converged with the TZ' basis set, allowing us to use this basis set for further analysis.

Table 5.5 – Vertical excitation energy for $\Omega = 0^+$, electron EDM effective electric field, magnetic hyperfine interaction constant, and scalar-pseudoscalar electron-nucleon interaction constant for $\Omega = 1$ at an internuclear distance of $R = 3.779$ a_0 using basis sets with increasing cardinal number and the wavefunction model $\mathcal{III}^{\mathcal{CI},5}$.

Basis set	T_v[cm^{-1}]	$E_{\text{eff}}[\frac{\text{GV}}{\text{cm}}]$	$A_{\|\|}$[MHz]	W_S[kHz]
DZ	378	37.8	1824	51.90
TZ'	787	36.9	1836	50.73
QZ'	877	36.9	1830	50.77

The results in table 5.6 show that wavefunctions accounting only for correlation effects among the two outermost valence electrons ($\mathcal{IV}^{\mathcal{CI}}$) are too approximate for

determining E_{eff}, $A_{||}$ and W_S for $\Omega = 1$, although they do yield a correct qualitative description of the low-lying electronic valence states of the molecule and, in some cases, benefit from favorable error cancellations. It has been shown in reference [FN14] on the isoelectronic ThO molecule that these properties are essentially unaffected by accounting for electron correlations arising from Th core shells, and the reason for this has been explained *via* orbital (more precisely, spinor) perturbation theory. We have therefore carried out a study of the influence of the active spinor space, models of type $\mathcal{III}^{\mathcal{CI},X}$, and restricting the electron correlation treatment to the outermost electronic shells (Th $6s$,$6p$,$7s$,$6d$, F $2s$,$2p$).

Table 5.6 – Vertical excitation energy for $\Omega = 0^+$, electron EDM effective electric field, magnetic hyperfine interaction constant, and scalar-pseudoscalar electron-nucleon interaction constant for $\Omega = 1$ at an internuclear distance of $R = 3.779\ a_0$ using the TZ' basis set, varying number of correlated electrons and varying active spinor spaces.

CI model(TZ basis)	T_v[cm^{-1}]	$E_{\text{eff}}[\frac{\text{GV}}{\text{cm}}]$	$A_{\|\|}$[MHz]	W_S[kHz]
$\mathcal{IV}^{\mathcal{CI}}$	274	35.4	1749	49.44
$\mathcal{III}^{\mathcal{CI},3}$	1029	47.5	1842	65.78
$\mathcal{III}^{\mathcal{CI},5}$	787	36.9	1836	50.73
$\mathcal{III}^{\mathcal{CI},6}$	709	36.2	1836	49.90
$\mathcal{III}^{\mathcal{CI},8}$	598	35.6	1834	49.04
$\boldsymbol{\mathcal{III}^{\mathcal{CI},10}}$	538	**35.2**	**1833**	**48.35**
$\mathcal{III}^{\mathcal{CI},12}$		35.1	1832	

Our findings are very similar to those obtained for ThO in reference [FN14]. Increasing the size of the active space leads to significant corrections to the vertical excitation energy. The greatest change occurs when adding the energetically following π-type spinors to the minimal active space (step from $X = 3$ to $X = 5$). A similar drop of the values of the effective electric field and the hyperfine interaction constant is here observed. Including the energetically following spinors entails further decrease of all studied properties, but significantly less pronounced than the previous ones.

In view of the significant changes of the results when increasing the active spinor space, one could ponder the necessity to include excitation ranks higher than Doubles into the set of virtual spinors. We investigated this using the DZ basis (due to computational cost), and the results can be found in Table 5.7. The hyperfine interaction constant $A_{||}$ is insensitive to these higher excitations, allowing triple excitations to the virtual space changes the value by only 0.2%. However, the effective electric field as well as the S-PS interaction constant exhibit a strong dependence on higher

excitations. The inclusion of triple excitations yields a drop of 25% in magnitude, respectively. Interestingly, this dramatic decrease is also observed when excluding triple excitations and augmenting the active spinor space by seven additional σ- and π-type Kramers pairs. Such an augmentation introduces a subset of Triple and a subset of Quadruple excitations but avoids terms with three or more particles in the external spinor space, therefore leading to a much shorter CI expansion. The additional excitation classes can be written symbolically as $(\text{core})^h$,$(\text{active})^p$,$(\text{external})^q$, where "active" denotes the *additional* active-space spinors, h denotes the number of holes and p and q the number of particles in the respective spinor space. In case of the Triples, the additional sets of configurations then read as $(h = 1, p = 3, q = 0)$, $(h = 1, p = 2, q = 1)$ and $(h = 2, p = 1, q = 2)$. For the Quadruples one obtains only $(h = 2, p = 2, q = 2)$. Evidently, the augmentation of the active space largely covers the set of Triple excitations that are required for obtaining accurate values of E_{eff}, $A_{||}$, and W_S. In case of the excitation energies we observe that the additional Quadruple excitations, which are not present in the model $\mathcal{III}^{\mathcal{CI}+T,3}$, have a significant effect of stabilizing the Σ state relative to the Δ state, in accord with the discussion in the previous section.

Table 5.7 – Vertical excitation energy for $\Omega = 0^+$, electron EDM effective electric field, magnetic hyperfine interaction constant, and scalar-pseudoscalar electron-nucleon interaction constant for $\Omega = 1$ at an internuclear distance of $R = 3.779\ a_0$ using the DZ basis set and varying maximum excitation rank.

CI model(DZ basis)	$T_v[\text{cm}^{-1}]$	$E_{\text{eff}}[\frac{\text{GV}}{\text{cm}}]$	$A_{\|\|}$[MHz]	W_S[kHz]
$\mathcal{III}^{\mathcal{CI},3}$	654	47.0	1830	64.92
$\mathcal{III}^{\mathcal{CI},10}$	88	37.1	1832	51.06
$\mathcal{III}^{\mathcal{CI}+T,3}$	247	35.4	1834	48.64

In order to gain insight into the character of the excitations leading to important corrections, we carried out a detailed analysis of the wavefunction expansions referred to as $\mathcal{III}^{\mathcal{CI},3}$ and $\mathcal{III}^{\mathcal{CI},5}$. They turn out to be very similar, the expansion coefficients remaining almost unchanged with the exception of a determinant that is the next-to-leading contributor with a coefficient $c \approx 0.046$ in the expansion of $\mathcal{III}^{\mathcal{CI},5}$ whereas its coefficient is much smaller in the $\mathcal{III}^{\mathcal{CI},3}$ expansion ($c < 0.01$). This respective determinant can be written as a $\delta^1_{6d}(\pi\sigma)^1$ occupation which corresponds to a single excitation with respect to the leading determinant $\sigma^1_{7s}\delta^1_{6d}$ for this $\Omega = 1$ state. Since $\delta^1_{6d}(\pi\sigma)^1$ is already contained in the $\mathcal{III}^{\mathcal{CI},3}$ expansion, it is necessarily the additional higher excitations included in the $\mathcal{III}^{\mathcal{CI},5}$ expansion which lend amplitude to the $\delta^1_{6d}(\pi\sigma)^1$ determinant.

We carried out a Mulliken population analysis of the spinors occupied in this

Table 5.8 – Characterization of active-space Kramers pairs in the TZ' basis. Orbital angular momentum projection, spinor energy and principal atomic shell character.

Spinor(λ)	$\langle \hat{l}_z \rangle_{\varphi_i}$	$\varepsilon_{\varphi_i}[E_H]$	atomic character
σ	−0.001	−0.43	85% Th(s)
δ	1.966	−0.42	98% Th(d)
δ	−2.000	−0.41	99% Th(d)
$\pi\sigma$	−0.720	−0.14	50% Th(p), 45% Th(d)
π	1.025	−0.13	60% Th(d), 36% Th(p)
$\sigma\pi$	−0.290	−0.12	47% Th(d), 43% Th(p)
π	−0.980	−0.10	55% Th(p), 36% Th(d)
π	1.011	−0.09	64% Th(p), 29% Th(d)
σ	−0.005	−0.07	59% Th(p), 19% Th(f), 15% Th(d)
σ	−0.014	−0.06	90% Th(s)
$\pi\sigma$	−0.894	−0.03	89% Th(p)
π	1.006	−0.03	94% Th(p)
σ	−0.097	−0.02	65% Th(p), 29% Th(f)

decisive determinant. $\pi\sigma$ denotes a spinor of π-character with significant admixture of σ-character (see the fourth spinor in Table 5.8). In this case, the spinor is of Th(p) character with a 45% contribution of Th(d). Hence, the drop of the values of E_{eff}, $A_{||}$ and W_S is related to a shift of electron density from Th(7s) to Th(p) and Th(d), the two latter of which have an approximate angular node at the nucleus. It is, therefore, physically plausible that the mentioned higher excitations which lead to a shift of electron (spin) density from Th(s) to higher angular momentum entail a reduction of the EDM effective electric field and of the magnetic hyperfine interaction constant.

5.2.2.3 Electric dipole moments and transition dipole moments.

The electron EDM effective field stands in direct relationship with the static molecular electric dipole moment. We calculated this latter quantity as an expectation value over relativistic CI wavefunctions, and in addition, electric dipole transition moments between different electronic states in an energy window of up to roughly 8000 [cm^{-1}]. The results are compiled in Tables 5.9 and 5.10. Concerning the notation for electronic states we have here added information on dominant and minor contributors in Λ-S coupling to a given well-defined Ω state.

The absolute molecular dipole moment is very large for ThF^+, especially for the low-lying electronic states, and reaches into the range of the largest dipole moments for diatomic molecules. Concerning transition dipole moments we observe a generally good agreement with expected selection rules for transitions between different $^{2S+1}\Lambda_\Omega$

Table 5.9 – Molecular static electric dipole moments $\left\langle {}^M\Lambda_\Omega|\hat{D}_z|{}^M\Lambda_\Omega\right\rangle$, with $\hat{\vec{D}}$ the electric dipole moment operator, using the TZ basis set and the CI model $\mathcal{II}^{\mathcal{CI}}$. The origin is at the center of mass, and the internuclear distance is $R = 3.779$ $[a_0]$ (F nucleus at $z\vec{e}_z$ with $z < 0$). ${}^M\Lambda$ is an approximate notation and refers to the term derived from the leading Slater determinants and the information in Table 5.8.

${}^M\Lambda_\Omega$ State	T_v [cm^{-1}]	$\left\|\left\langle {}^M\Lambda_\Omega|\hat{D}_z|{}^M\Lambda_\Omega\right\rangle\right\|$ [D]
${}^1\Sigma_0^+$	630	3.941
${}^3\Delta_1$	0	4.029
${}^3\Delta_2$	1167	3.970
${}^3\Delta_3$	2986	4.034

states[1]. For example, the largest matrix element, $\left\|\left\langle {}^3\Phi_2({}^3\Pi_2)|\hat{\vec{D}}|{}^3\Delta_1\right\rangle\right\| = 1.34$ [D], is spin-allowed ($\Delta S = 0$) and also orbital angular momentum allowed (here $\Delta\Lambda = \pm 1$). In addition, $\Delta\Omega = \pm 1$ is also satisfied. On the other hand, very small transition moments are typically found for spin-forbidden transitions. Our study of transition moments covers a few more states than those reported in a recent study on actinide bonding by Heaven *et al.* [HBA14b], and the results agree quite well with the values obtained in that reference.

The comparison of Tables 5.9 and 5.10 shows that our larger set of results obtained with the smaller 2-electron CI expansion agrees quite well with the results from the more elaborate CI model, $\mathcal{IV}^{\mathcal{CI}}$. We therefore consider the values in Table 5.10 as a good approximation to the accurate values.

[1]The reader will find detailed informations on the selection rules in Appendix D.

Table 5.10 – Molecular static electric dipole moments $\left|\left|\left\langle {}^M\Lambda_\Omega|\hat{D}_z|{}^M\Lambda_\Omega\right\rangle\right|\right|$, transition dipole moments $\left|\left|\left\langle {}^M\Lambda'_\Omega|\hat{\vec{D}}|{}^M\Lambda_\Omega\right\rangle\right|\right|$, with $\hat{\vec{D}}$ the electric dipole moment operator (both in [D] units), and vertical transition energies for low-lying electronic states using the TZ' basis set and the CI model $\mathcal{DV}^{\mathcal{CI}}$. The origin is at the center of mass, and the internuclear distance is $R = 3.779$ $[a_0]$. $\left({}^M\Lambda_\Omega\right)$ denotes a term contributing at least 10% to the state. ^{1,3} denotes cases where Λ-S coupling breaks down significantly according to the analysis of our spinor-based ω-ω coupled wavefunctions.

${}^M\Lambda_\Omega$ state	T_v [cm^{-1}]	$^1\Sigma_0^+$	$^3\Delta_1$	$^3\Delta_2$	$^3\Delta_3$	$^1\Sigma_0(^3\Pi_0)$	$^3\Pi_0$	$^{1,3}\Pi_1(^3\Sigma_1)$	$^3\Pi_0(^1\Sigma_0)$	$^{1,3}\Delta_2(^3\Pi_2)$	$^3\Sigma_1$	$^{1,3}\Pi_1$	$^3\Phi_2(^3\Pi_2)$
$^1\Sigma_0^+$	274	4.004											
$^3\Delta_1$	0	0.012	4.075										
$^3\Delta_2$	724	0.000	0.070	4.022									
$^3\Delta_3$	2198	0.000	0.000	0.052	4.075								
$^1\Sigma_0(^3\Pi_0)$	6344	0.439	0.455	0.000	0.000	3.752							
$^3\Pi_0$	6528	0.000	0.571	0.000	0.000	0.000	2.116						
$^{1,3}\Pi_1(^3\Sigma_1)$	6639	0.868	0.142	0.218	0.000	0.197	0.000	2.375					
$^3\Pi_0(^1\Sigma_0)$	6747	0.003	0.391	0.000	0.000	0.929	0.000	0.094	2.717				
$^{1,3}\Delta_2(^3\Pi_2)$	7008	0.000	0.473	0.334	0.298	0.000	0.000	0.529	0.000	2.734			
$^3\Sigma_1$	7490	0.226	0.069	0.221	0.000	0.136	0.197	0.451	0.145	0.087	4.463		
$^{1,3}\Pi_1$	7918	0.667	0.052	0.801	0.000	0.011	0.064	0.107	0.043	0.444	0.209	2.708	
$^3\Phi_2(^3\Pi_2)$	8245	0.000	1.338	0.234	0.272	0.000	0.000	0.134	0.000	0.384	0.018	0.099	2.271

5.3 Conclusion.

In the earlier work of Barker *et al.* [BAHP12, HBA14b] $\Omega = 0^+$ had been proposed as the electronic ground state of ThF^+, supported by the measured intensities of the lowest band compared to those of other bands in a pulsed field ionization - zero kinetic energy (PFI-ZEKE) experiment. Accompanying many-body electronic structure calculations were judged to be inconclusive in this regard. From our discussion of relativistic many-body calculations, including those from reference [BAHP12] for excitation energies, we conclude that the assignment of the ground electronic state of ThF^+ remains an open issue. The models of Barker *et al.* suffer from the incomplete account of spin-orbit interaction and its intertwining with dynamic electron correlations, which becomes manifest in the poor description of the energetic splitting of the $^3\Delta$ state into its Ω components. Our present work and further spectroscopic study from [DNJ+15] take these effects into account rigorously which leads to a $^3\Delta_1$ ground state. Giving preference to assigning the ground state as $^1\Sigma_0^+$ is, therefore, no longer tenable from a theoretical point of view, based on our present findings. In any case, it is beyond reasonable doubt that the two respective states are the lowest-lying electronic states and that they are so close in energy that an eEDM experiment could be carried out irrespective of their ordering [CG14].

We conclude that our best model for the determination of $\mathcal{P},\mathcal{T}$-odd and magnetic hyperfine interaction constants is $\mathcal{III}^{\mathcal{CI},10}$ in the TZ' basis set (boldface in Table 5.6), which displays property values nearly converged with respect to the different degrees of freedom in the models we have tested. Our best prediction for the hyperfine constant in the $\Omega = 1$ "science state" is 1833 [MHz], which awaits confirmation from an experimental measurement. The obtained effective electric field of $E_{\text{eff}} = 35.2 \left[\frac{\text{GV}}{\text{cm}}\right]$ in this same state is more than 60% smaller than the value of $E_{\text{eff}} = 90 \left[\frac{\text{GV}}{\text{cm}}\right]$ obtained earlier by Meyer *et al.* [MB08]. The large deviation is very likely to be due to the limited set of electronic configurations and further model-inherent approximations used in the approach of Meyer *et al.* The smaller value of E_{eff} is a setback for potential electron EDM searches with this molecular ion, but given the body of other favorable properties (low-lying $^3\Delta_1$ state, large molecular dipole moment) of ThF^+ still large enough to retain the system as a promising candidate in search of $\mathcal{P},\mathcal{T}$ violation. In Table 5.11 we provide a summary of E_{eff} values in the respective science states of some diatomic molecules of current interest in this search. Our E_{eff} presently determined for ThF^+ is still larger than E_{eff} in the science state of the YbF molecule, in which a new upper bound to the electron EDM had been determined in 2011 [HKS+11]. The static electric transition dipole moments we have determined for a set of states below 9000 cm^{-1} in ThF^+ may also be helpful in devising a route for state preparation for an EDM measurement in this promising

molecular ion.

Table 5.11 – Effective electric field for the science states of selected diatomic candidate molecules in search of parity- and time-reversal violation.

Molecule	Electronic state	$E_{\text{eff}}[\frac{\text{GV}}{\text{cm}}]$
ThO	$^3\Delta_1$	75.2[1], 75.8[2]
YbF	$^2\Sigma^+_{1/2}$	26[3], 25[4], 24[5]
PbO	$^3\Sigma^+_1$	25[6]
ThF^+	$^3\Delta_1$	35.2[7], 90[8]
WC	$^3\Delta_1$	-36[9]

[1] Reference [FN14]
[2] Reference [ST14]
[3] Reference [Koz97]
[4] Reference [MKT98]
[5] Reference [Par98]
[6] Reference [KD02]
[7] this work
[8] Reference [MB08]
[9] Reference [LCS+13].

6 Thorium monoxide reloaded.

The following work was published in: M. Denis and T. Fleig, J. Chem. Phys. 145, 214307 (2016), *In search of discrete symmetry violations beyond the standard model: Thorium monoxide reloaded.*[DF16]

We present an updated electron electric dipole moment (EDM) effective electric field of $E_{\text{eff}} = 75.2 \left[\frac{\text{GV}}{\text{cm}}\right]$ and ^{229}Th magnetic hyperfine interaction constant $A_{||} = -1266$ [MHz], the nucleon-electron scalar-pseudoscalar interaction constant $W_S = 106.0$ [kHz], and the molecule-frame static electric dipole moment $D = -4.41$ [Debye] for the $^3\Delta_1$ science state of ThO. The criticisms of the results from reference [FN14] made in reference [ST15] are addressed and largely found to be unsubstantiated within the framework of the present approach. The present findings confirm the slightly relaxed constraints on relevant beyond-standard-model parameters, in particular the electron EDM, d_e, and the nucleon-electron scalar-pseudoscalar coupling constant, C_S.

6.1 Introduction

Recent experimental [CBC$^+$14] and theoretical [FN14, SPT13] studies on the ThO molecule have led to a new and improved upper bound on the electron EDM, d_e, if the upper bound to the $\mathcal{P},\mathcal{T}$-odd energy shift is interpreted in terms of the electron EDM alone. This upper bound is determined through $d_e = -\frac{\hbar\omega^{\mathcal{NE}}}{E_{\text{eff}}}$, where $\omega^{\mathcal{NE}}$ is an upper bound to a measured frequency shift and E_{eff} is the EDM effective electric field, *i.e.*, it is the combined result of a measurement and a molecular many-body calculation. Since the theoretical uncertainty for E_{eff} enters the upper bound on d_e directly, this uncertainty should be minimized.

The most accurate theoretical results for the required EDM effective electric field E_{eff} in the $^3\Delta_1$ science state of ThO from two different approaches (Skripnikov *et al.* [ST15] and Fleig *et al.* [FN14]) are at variance by $6.3 \left[\frac{\text{GV}}{\text{cm}}\right]$, or about 8%. In the present chapter, we present an additional elaborate study of higher-order electron correlation effects and relativistic effects beyond the Dirac-Coulomb Hamiltonian on

properties relevant to EDM studies in the ThO molecular system. These include an improved and more reliable value of E_{eff} for ThO ($^3\Delta_1$), the molecule-frame electric dipole moment, and the value of the ne-SPS interaction constant. The latter is determined as described in reference [DNJ+15] and represents the second leading $\mathcal{P},\mathcal{T}$-odd effect in ThO, allowing to constrain the electron-nucleon coupling C_S.

6.2 Technical details

To define the different models of the wavefunctions, we exploit a General Active Space concept presented in Section 4.2.4. The partitioning of the spinor space is shown in Fig. 4.2 and the parametrisation of the wavefunction models employed in this work is displayed in Table 6.1.

Table 6.1 – Parametrisation of the wavefunction models where K stands for the number of Kramers pairs in the active spinor space and m, n, p, q denote the accumulation constraints of the subspaces.

Parameter values	Correlation model
$m = 2, n = 2, p = 0, q = 0$	MR_K-CISD(18)
$m = 2, n = 3, p = 0, q = 0$	MR_K^{+T}-CISD(18)
$m = 2, n = 2, p = 2, q = 2$	MR_K-CISD(36)

We have studied the basis set completeness for the determination of EDM effective electric fields, sensitive to electron density around the nucleus, in ThO and other molecular systems. Since it is not the atomic core electrons creating spin density close to the nucleus but valence electrons (7s) in systems like ThO, the description of the core 'tail' of the 7s valence spinor by the atomic basis set is of importance. This is also the reason why it is not recommended to use effective core potentials for such properties but all-electron methods, as we do here and have done in the past. The uncontracted basis sets we use are specifically optimized for a good description of valence properties of systems where relativistic effects are large (Dyall basis sets [Dya06]). They are already dense in the core region, but we made systematic tests adding steep functions to the s and p spaces to assure that the applied basis sets describe the valence spinors accurately. Our tests revealed that the contribution of the added steep function exponents to the EDM effective electric field in the one-particle sector is on the order of 0.1%.

In order to account for the Gaunt interaction, we added the Gaunt term Eq. (4.4) to the Dirac-Coulomb Hamiltonian Eq. (4.5) that led to the all-electron molecular

Dirac-Coulomb-Gaunt Hamiltonian

$$\hat{H}^{DCG} = \sum_A \sum_i \left[c(\vec{\alpha} \cdot \vec{p})_i + \beta_i m_0 c^2 + V_{iA} \mathbb{1}_4 \right] + \sum_{i,j>i} \left(\frac{1}{r_{ij}} \mathbb{1}_4 - \frac{1}{2} \frac{\vec{\alpha}_i \vec{\alpha}_j}{r_{ij}} \right) + \sum_{A,B>A} V_{AB}, \tag{6.1}$$

where $\vec{\alpha}$ is a cartesian vector of Dirac matrices, V_{iA} is the potential-energy operator for electron i in the electric field of nucleus A, $\mathbb{1}_4$ is a unit 4×4 matrix and V_{AB} represents the potential energy due to the internuclear classical electrostatic repulsion of the clamped nuclei.

Accounting for the Gaunt interaction was possible at the Hartree-Fock level [SVSI09] in the `DIRAC` program package [DIRa]. Thus, the only $\mathcal{P},\mathcal{T}$-odd property implemented at this level, *i.e.*, the EDM effective electric field (E_{eff}), was evaluated as an expectation value of the operator over the Hartree-Fock spinors. Details on the implementation of the EDM operator can be found in reference [FN13]. The evaluation procedure for the magnetic hyperfine interaction constant $A_{||}$ and the ne-SPS interaction constant W_S have been presented in references [FN14] and [DNJ+15], respectively and in Sections 2.4 and 3.2 of this thesis.

In our work, the properties are evaluated as expectation values of the corresponding operators over the molecular wavefunction characterised by its Ω quantum number. In addition, we evaluate the molecular-frame electric dipole moment through both expectation value [Kne09] and derivative methods. It allows us to test the following relation $D = -\frac{\partial(\varepsilon(E))}{\partial E}\Big|_{E=0} \approx \left\langle {}^M\Lambda_\Omega | \hat{D}_z | {}^M\Lambda_\Omega \right\rangle$ obtained by applying the Hellmann-Feynman theorem[1] to the electrostatic interaction, $\frac{\partial(\varepsilon(E))}{\partial E} = e\langle \hat{z} \rangle_{\Psi_H}$ and Taylor expanding the field-dependent energy around the point $E = 0$. The deviation is comprised by the non-Hellmann-Feynman terms, which for molecule-frame dipole moments determined with restricted CI wavefunctions can be non-negligible. Due to the smallness of d_e and C_S [CRM15], non-Hellmann-Feynman terms are unimportant in the case of $\mathcal{P},\mathcal{T}$-odd properties.

6.3 Results and Discussion

In the present section we begin by addressing the particular issues raised by Skripnikov *et al.* in reference [ST15]. This is followed by the discussion of additional physical effects of relevance to EDM studies in ThO.

6.3.1 Spinor basis set

There are physically reasonable and unreasonable choices for the spinor basis in a correlation model which falls short of Full CI. Skripnikov *et al.* [ST15] include a less

[1] More details on the Hellmann-Feynman theorem can be found in Appendix E.

reasonable choice in their determination of the sensitivity of the MR-CI method with respect to spinor basis, namely ground-state ($^1\Sigma^+$) spinors (model Dirac-Coulomb-Hartree-Fock closed-shell, DCHF_cs). Naturally, the inclusion of such unmotivated choices will lead to arbitrarily large error bars, in the extreme case. For instance, any random excited state could also have been chosen for determining the spinor basis in the Hartree-Fock optimization.

Instead, we only use physically well motivated choices for spinor basis which in the present case are the following: i) DCHF spinors with an average-of-occupation Fock operator for 2 electrons in 3 Kramers pairs, $7s_\sigma$ and $6d_\delta$, model DCHF_2in3. Such a basis is not state specific but gives a balanced description of the ground $^1\Sigma^+$ and the excited $^{1,3}\Delta$ states which is an advantage in the determination of energetics. ii) DCHF spinors with 1 electron occupying $7s_\sigma$ and 1 electron occupying $6d_\delta$, model DCHF_1in1_1in2. This latter model is specific towards the excited $^{1,3}\Delta$ states and better suited for a property calculation in the $^3\Delta_1$ science state.

The comparative results are compiled in Table 6.2. Not surprisingly, the vertical excitation energy of $\Omega = 1$ depends strongly on whether the δ spinors are included in the DCHF averaging or not. With wavefunctions from the large active-space model MR_{12}-CISD(18) the hyperfine interaction constant undergoes changes of a few percent. However, $\mathcal{P},\mathcal{T}$-odd properties are almost totally insensitive to the choice of spinors. On the other hand, this is not the case, if the active space is chosen to resemble single-reference correlation methods more closely, which becomes evident from the second half of Table 6.2. Here, the spread of all calculated properties with respect to spinor basis is an impressive 10-20%. This is a further confirmation that the classes of higher excitations in the wavefunction in the analysis presented in reference [FN14] are essential for obtaining accurate properties in the $^3\Delta_1$ science state of ThO.

Our final results from reference [FN14] were based on DCHF_2in3 spinors, the properties for which are at variance from those using state-specific spinors by not more than 0.3% with a properly chosen active space. Similarly, the molecular static dipole moment obtained with model DCHF_1in1_1in2 differs from the DCHF_2in3 result by only 0.5%. Furthermore, the quite accurate 4c-MR_{12}-CISD(18) model shows that $\mathcal{P},\mathcal{T}$-odd constants are also insensitive to basis set enlargement, which had also been found earlier [FN14] using a less rigorous wavefunction model.

6.3.2 Active spinor space

We have carried out an additional study to confirm sufficient convergence of our results with respect to the size of the active spinor space. Results are compiled in Table 6.3. To this end, we have further increased the parameter K given in Fig. 1 of

Table 6.2 – Calculated properties and molecular static electric dipole moment $D = \left\langle {}^{M}\Lambda_\Omega | \hat{D}_z | {}^{M}\Lambda_\Omega \right\rangle$ for $\Omega = 1$ at $R = 3.477$ a_0, using the vDZ basis set and a virtual cutoff value of 50 a.u. Some results using the same correlation model and the vTZ basis set (see reference [FN14]) have been added for comparison.

Spinor basis	T_v [cm^{-1}]	$E_{\text{eff}}\left[\frac{\text{GV}}{\text{cm}}\right]$	$A_{\|\|}$ [MHz]	W_S [kHz]	D [Debye]
MR_{12}-CISD(18)					
DCHF_2in3 (vTZ)	5410	75.2	−1339	105.8	−4.165
DCHF_2in3	6069	75.1	−1333	105.3	−4.068
DCHF_1in1_1in2	6066	74.9	−1291	105.1	−4.089
DCHF_cs	7871	75.0	−1375	105.4	−4.125
MR_3-CISD(18)					
DCHF_2in3 (vTZ)	3832	81.0	−1292	114.1	−3.809
DCHF_2in3	4535	80.8	−1283	113.7	−3.722
DCHF_1in1_1in2	3851	84.3	−1174	118.8	−3.427
DCHF_cs	6495	73.4	−1389	104.3	−4.175

reference [FN14] to values which group types of spinors in accord with their principal atomic character. The active space corresponding to $K = 31$ includes spinors up to an energy of 0.527 a.u.

First, we note that the characteristic drop of E_{eff} (and also W_S) occurs largely independent of basis set extent, which is in accord with the analysis of this effect presented in reference [FN14]. Upon increasing the active space to $K = 31$, we observe a further slight decrease of the $\mathcal{P},\mathcal{T}$-odd constants. The corresponding configuration space adds a large number of triple and quadruple excitations to spaces with smaller value of K. These quadruples are of the type $occ^{16}val^2 \longrightarrow occ^{14}val*^2virt^2$ where the superindex is an occupation number, the occupied space (occ) comprises the Th 6s,6p and the O 2s,2p shells, the valence space is divided into Th 7s,6dδ (val) and spinors below an energy of 0.527 a.u. ($val*$), and the virtual space ($virt$) represents all spinors of higher energy.

6.3.3 Core correlations

The correction to the $\mathcal{P},\mathcal{T}$-odd properties by the inclusion of thorium inner-shell electrons in the correlation treatment was studied in a previous work [FN14] and estimated to be 0.25% by the comparison of the MR_3-CISD(18) and MR_3-CISD(36)* models. However, it was pointed out in reference [ST15] that the 36-electron calculation was performed with a smaller cut-off of virtual spinors of 5 Hartrees. Hence,

Table 6.3 – Calculated properties and molecular static electric dipole moment for $\Omega = 1$ at $R = 3.477$ a_0, using different active spinor spaces (X) with the wavefunction model MR_X-CISD(18) and vDZ basis set with a virtual cutoff of 50 a.u.

Model	$E_{\text{eff}}\left[\frac{\text{GV}}{\text{cm}}\right]$	$A_{\|\|}$ [MHz]	W_S [kHz]	$\left\langle {}^M\Lambda_\Omega \vert \hat{D}_z \vert {}^M\Lambda_\Omega \right\rangle$
MR_3-CISD(18)	80.8	−1283	113.7	−3.722
vTZ/MR_3-CISD(18)	81.0	−1292	114.1	−3.809
MR_9-CISD(18)	73.8	−1321	103.7	−4.060
MR_{12}-CISD(18)	74.7	−1341	105.0	−4.081
vTZ/MR_{12}-CISD(18)	75.2	−1339	106.0	−4.165
MR_{13}-CISD(18)	74.7	−1343	104.9	
vTZ/MR_{13}-CISD(18)	75.2	−1343	105.9	
MR_{17}-CISD(18)	74.8	−1334	105.2	
MR_{31}-CISD(18)	73.1	−1320	102.7	−4.189

by determining within their 2c-CCSD(T) framework that the truncation leads to a 3.3 GV/cm underestimation, Skripnikov *et al.* asserted that the uncertainty due to the number of explicitly correlated electrons amounts to 5%.

In order to check this figure, we carried out a study of the effect of the truncation of the virtual space for the MR_3-CISD(36) model. Results are shown graphically in Figure 6.1 where the values were rescaled to fit in the same plot. It appears that indeed convergence is not reached at the 5 Hartree cut-off level but values are accurate when we apply a 30 Hartree truncation. Hence, in [FN14] the values of the $\mathcal{P},\mathcal{T}$-odd properties in the MR_3-CISD(36)* model were underestimated by 1.7% at the most. The expansion of the virtual spinor space is accompanied by an increase of E_{eff}, W_S and $A_{||}$ on the absolute. The effect is strongest when adding p-type spinors to the virtual space. Besides, this study led us to perform the calculation of the properties for a 38 Hartrees cut-off, the same as for the 18-electron model in [FN14]. Therefore, the correction on the effective electric field, coming from the correlation of core electrons can be determined with greater confidence. It amounts to +1.2 GV/cm, *i.e.*, an increase of 1.5% in magnitude, which is significantly smaller than the +4.3 GV/cm alleged by Skripnikov *et al.* [ST15]. As to the molecular dipole moment D, it undergoes a non-negligible 0.241 D increase in magnitude.

Accounting for strict size-extensivity in our linear wavefunction expansions may lead to a further – albeit slight – increase of these corrections, on the absolute. The same is expected to hold true when further increasing the size of the atomic basis sets.

Figure 6.1 – Calculated properties (normalised to their maximal values) for $\Omega = 1$ at $R = 3.477$ a_0, using the wavefunction model MR_3-CISD(36), vTZ basis set and different cutoff values for the virtual spinor space.

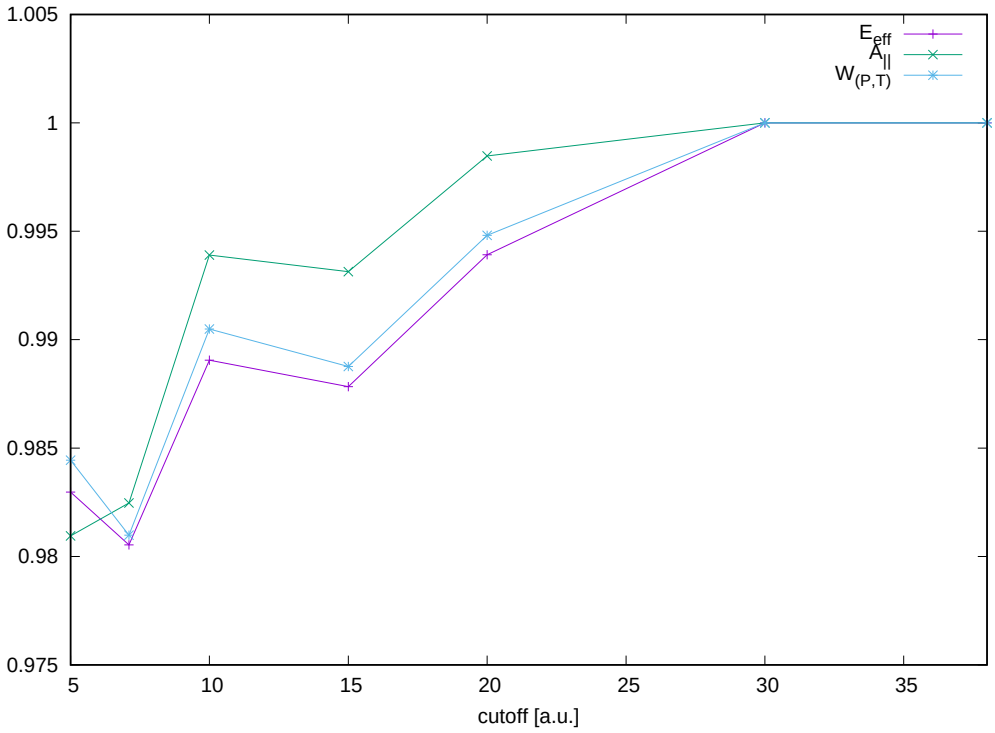

6.3.4 Subvalence and valence correlations

In order to start from more rigorous base values, the calculation of the $\mathcal{P},\mathcal{T}$-odd properties was performed within the vTZ/MR_{12}^{+T}-CISD(18) model that corresponds to the MR_K^{+T}-CISD(18) model defined in [FN14] with an active space of 12 Kramers pairs and the use of vTZ basis sets. This model differs from the previous reference model vTZ/MR_{12}-CISD(18) by allowing for three holes in the Th 6s, 6p and O 2s 2p subvalence spinors. It, therefore, covers the energetically most important set of "3o"-type excitations, identified as important in reference [ST15]. In particular, this model includes a subset of Quintuple excitations deriving from the following types of excited configurations: $occ^{16}val^2 \longrightarrow occ^{13}val*^3virt^2$, $occ^{16}val^2 \longrightarrow occ^{13}val*^4virt^1$, $occ^{16}val^2 \longrightarrow occ^{13}val*^5virt^0$ where the *occ*, *val* and *virt* spaces are the same as defined above and *val*∗ comprises the Th 7p, 8s, $8p_\pi$ spinors. The inclusion of these higher excitations from the subvalence spinors (*occ*) to the active space entails an increase of the values of 2.5% in magnitude for the $\mathcal{P},\mathcal{T}$-odd properties and 3.5% for the molecular dipole moment leading to the new base values to which will be added the various corrections discussed above.

6.3.5 Gaunt operator

For the evaluation, we employed the same state-specific model DCHF_1in1_1in2 as decribed above that is the most adequate for the calculation of the properties in the $^3\Delta_1$ molecular term. The comparison of the values of E_{eff} without and with the inclusion of the Gaunt operator shows a non-negligible decrease of 1.7% in magnitude. We expect a similar change for W_S that exhibits the same corrections as E_{eff}. Finally, the molecular-frame dipole moment undergoes a Gaunt correction of +0.9% in magnitude.

6.3.6 Molecule-frame electric dipole moment

We employed the MR_{12}-CISD(18) wavefunction to determine the molecule-frame electric dipole moment as an expectation value of the $\hat{D}_z$ operator. On the other hand, the electric field-dependent energies obtained at the same level of theory are used to calculate the electric dipole moment by a finite-field approach at five points that correspond to five field strengths, namely -0.005 a.u., -0.001 a.u, 0 a.u., +0.001 a.u., +0.005 a.u. Then the first derivative of the electric field-dependent energy around the point $E = 0$ yields the electronic part of the molecular dipole moment to which we need to add the nuclear part to obtain the permanent dipole moment (D). The

Table 6.4 – Calculated molecular dipole moment for $\Omega = 1$ at $R = 3.477$ a_0 using the wavefunction model MR_{12}-CISD(18) and vDZ basis set with a virtual cutoff of 50 a.u.

	D [Debye]
$\left\langle {}^M\Lambda_\Omega \middle\| \hat{D}_z \middle\| {}^M\Lambda_\Omega \right\rangle$	−4.069
$-\frac{\partial(\varepsilon(E))}{\partial E}\Big\|_{E=0}$	−4.128

results are compiled in Table 6.4. They show a difference of 1.5% in magnitude, which translates into a −0.06 Debye correction for the electric dipole moment evaluated as an expectation value. By adding this correction and the previous ones compiled in Table 6.5 to the base value, we obtain a value of the molecular-frame electric dipole moment $D = -4.41$ Debye to compare with the experimental data D=-4.098(3) Debye [Hes14], which means a relative error of 7.6%. We expect a further correction stemming from the inclusion of quadruple excitations from the subvalence space. Its magnitude should not be greater than the +0.145 Debye yielded by the triple excitations.

6.4 Conclusion

In this work, we reconsidered $\mathcal{P},\mathcal{T}$-odd and associated physical properties of the ThO molecule using rigorous four-component all-electron wavefunctions and obtained new (W_S, D) and updated (E_{eff}, $A_{||}$) results. Furthermore, some specific criticism made by Skripnikov et al. in Ref. [SPT13] was addressed. The main point is the alleged underestimated uncertainty on E_{eff} due to the choice of the spinor basis (7%); yet, our work reveals the insensitivity of $\mathcal{P},\mathcal{T}$-odd properties to proper choices of spinor space. Second, based on the analysis of their 18-electron MR(∞)-CISD model, Skripnikov et al. asserted that our previous final value obtained by an MR(12)-CISD calculation could undergo a significant increase of 5% in magnitude. Thus, even if the scalar-relativistic MR(∞)-CISD and our four-component MR(12)-CISD cannot be compared straightforwardly, we addressed this particular issue through two studies. A review of the effect of the size of the active space led to a correction of $-1.6\left[\frac{\text{GV}}{\text{cm}}\right]$. Second, in order to refine our understanding of the subvalence and valence correlations, we included higher excitations through the MR_{12}^{+T}-CISD(18) model. We came to perform a 7-billion determinant CI calculation that yielded new reference values. The latter model includes a subset of quadruple and even quintuple excitations with respect to the ground-state reference determinant besides the triple excitations from the subvalence to the active space. Furthermore, the influence of the inclusion of core electrons in the correlation space was analyzed by correlating up to 36 electrons and resulted in an increase of E_{eff} by $+1.2\left[\frac{\text{GV}}{\text{cm}}\right]$. The significant overshoot of the molecule-frame EDM upon including this correction and compared with the best experimental value suggests that the description of core-electron correlations is not significantly incomplete in the present study. A survey of the Gaunt interaction brought about an additional correction of $-1.3\left[\frac{\text{GV}}{\text{cm}}\right]$. All corrections are compiled in Table 6.5. Based on this study, we propose improved values of the EDM effective electric field $E_{\text{eff}} = 75.2\left[\frac{\text{GV}}{\text{cm}}\right]$, $A_{||} = -1266$ [MHz] and the electron-nucleon scalar-pseudoscalar interaction constant $W_S = 106.0$ [kHz] for the $^3\Delta_1$ science state of ThO.

The overshoot of the molecule-frame dipole moment could be partially explained by the lack of even higher excitations from the subvalence space than those already considered here. It is questionable, however, whether such corrections could significantly increase E_{eff} and W_S.

The discussion of possible errors in the present final values should not be based on the energy aspect since we now depart from a balanced description of ground and excited states and focus on the accurate description of properties in the science state alone. The error bars are here established by summing up the absolute value of the variations of the results observed between the most elaborate and second most

Table 6.5 – Final property values including corrections.

$E_{\text{eff}}\left[\frac{\text{GV}}{\text{cm}}\right]$	$A_{\|\|}$ [MHz]	W_S [kHz]	D [Debye]	
75.2[1]	−1339	106.0	−4.165	vTZ/MR$_{12}$-CISD(18)
77.1	−1309	108.5	−4.020	new base value from vTZ/MR$_{12}^{+T}$-CISD(18)
−0.2	+42	−0.2	−0.02	correction for Δ spinors
−1.6	+21	−2.3	−0.11	correction for active space size
+1.2	−20	+1.8	−0.24	core correlations
−1.3		−1.8	+0.04	Gaunt correction
			−0.06	Finite-field correction
75.2	−1266	106.0	−4.41	**Final value**

elaborate model for each studied effect, respectively. From the present results we thus obtain 6% for $A_{||}$, E_{eff} and W_S. As to E_{eff}, the present final value of $E_{\text{eff}} = 75.2\left[\frac{\text{GV}}{\text{cm}}\right]$ is within the uncertainty margins of the combined results from references [FN14] and [SPT13].

7 Hyperfine interaction constant of fluorine atom.

Polarized charged molecules in an ion trap [LCG+13] have been proposed as candidate systems in search of physics beyond the standard model. In particular, spatial parity, time-reversal $(\mathcal{P},\mathcal{T})$-odd effects such as the interaction due to an electric dipole moment of the electron (eEDM) may be investigated. The calculations of the hyperfine constants play a role of importance in those investigations since, as explained in Chapter 3, the comparison with the future experimental value of $A_{||}$ will be a probe for the accuracy of the decription of the electron spin density around the nucleus and thus, of the accuracy of the calculated value of the EDM effective electric field. Besides, a precise determination of the hyperfine levels is required for establishing the experimental protocol. Indeed, the value of $A_{||}$ is needed for the preparation of the molecular ion and also during the measurement of the $\mathcal{P},\mathcal{T}$-odd constants.

The parallel magnetic hyperfine interaction constant of heavy nuclei was investigated in previous works [FN14, DNJ+15]. We, hereby, focus on the hyperfine constant of the fluorine atom. We develop an accurate analytical framework to calculate the hyperfine interaction constant and perform a numerical study of $A_{||}$(F) in diatomic molecules by employing a spinor-based many-body correlation method.

7.1 Analytical study.

To gain more insight into the magnetic hyperfine interaction, we aim to evaluate the hyperfine interaction integrals in a π-state as in the case of CF, a system of interest in our study of $A_{||}$(F). We consider an hydrogen-like system for which we will need to apply an effective electric charge. The determination of an accurate 4-component wavefunction of the π-state represents a challenge. In this work, we consider two options: the exact solution of Dirac equation and the use of the restricted kinetic balance.

7.1.1 Hyperfine operator.

First, let us scrutinise the operator to evaluate as an expectation value over the 4-component wavefunction. The magnetic hyperfine interaction operator reads:

$$A_{hyp} = \frac{(\vec{\alpha} \times \vec{r})_z}{|\vec{r}|^3} \tag{7.1}$$

where $\vec{\alpha}$ are the 4×4 Dirac matrices built from the Pauli matrices

$$\alpha_i = \begin{pmatrix} \mathbf{0} & \sigma^i \\ \sigma^i & \mathbf{0} \end{pmatrix}$$

and the z-component of $\vec{\alpha} \times \vec{r}$ can be written as follows:

$$\frac{(\vec{\alpha} \times \vec{r})_z}{|\vec{r}|^3} = \frac{\alpha_x y - \alpha_y x}{r^3} = \frac{i \sin\theta}{r^2} \begin{pmatrix} 0 & 0 & 0 & e^{-i\varphi} \\ 0 & 0 & -e^{i\varphi} & 0 \\ 0 & e^{-i\varphi} & 0 & 0 \\ -e^{i\varphi} & 0 & 0 & 0 \end{pmatrix}. \tag{7.2}$$

If we write the wavefunction in the following form: $\psi = \begin{pmatrix} u_1 \\ u_2 \\ u_3 \\ u_4 \end{pmatrix}$, the integrand reads:

$$\psi^\dagger \frac{(\vec{\alpha} \times \vec{r})_z}{|\vec{r}|^3} \psi = \frac{i \sin\theta}{r^2} \left(u_1^\dagger u_4 e^{-i\varphi} - u_2^\dagger u_3 e^{i\varphi} + u_3^\dagger u_2 e^{-i\varphi} - u_4^\dagger u_1 e^{i\varphi} \right) . \tag{7.3}$$

The reader will note the coupling of small and large components.

7.1.2 Hyperfine integrals.

7.1.2.1 Exact Dirac wavefunction

In the first instance, we will employ the exact solutions of Dirac equation [BS12] as wavefunctions. For a state with $j = l + \frac{1}{2}$ or $j = l - \frac{1}{2}$ and particularly $j = \frac{3}{2}$ or $j = \frac{1}{2}$, the respective wavefunctions are given by:

$$\psi_{(j=l+\frac{1}{2})} = \begin{pmatrix} u_1 = g(r)\sqrt{\frac{l+m+\frac{1}{2}}{2l+1}} Y_{l,m-\frac{1}{2}} \\ u_2 = -g(r)\sqrt{\frac{l-m+\frac{1}{2}}{2l+1}} Y_{l,m+\frac{1}{2}} \\ u_3 = -if(r)\sqrt{\frac{l-m+\frac{3}{2}}{2l+3}} Y_{l+1,m-\frac{1}{2}} \\ u_4 = -if(r)\sqrt{\frac{l+m+\frac{3}{2}}{2l+3}} Y_{l+1,m+\frac{1}{2}} \end{pmatrix} \tag{7.4}$$

and

$$\psi_{(j=l-\frac{1}{2})} = \begin{pmatrix} \tilde{g}(r)\sqrt{\frac{l-m+\frac{1}{2}}{2l+1}}Y_{l,m-\frac{1}{2}} \\ \tilde{g}(r)\sqrt{\frac{l+m+\frac{1}{2}}{2l+1}}Y_{l,m+\frac{1}{2}} \\ -\imath\tilde{f}(r)\sqrt{\frac{l+m-\frac{1}{2}}{2l-1}}Y_{l-1,m-\frac{1}{2}} \\ \imath\tilde{f}(r)\sqrt{\frac{l-m-\frac{1}{2}}{2l-1}}Y_{l-1,m+\frac{1}{2}} \end{pmatrix} \tag{7.5}$$

with $m = m_j = l_z + s_z$.
They are formed of spherical harmonics and radial functions that depend on the considered orbitals. The radial functions for $2p_{\frac{3}{2}}$ and $2p_{\frac{1}{2}}$ are respectively:

$$\begin{aligned} g(r) &= \left(\frac{Z}{a_0}\right)^{\frac{3}{2}} \sqrt{\frac{1+\varepsilon_3}{2\Gamma(2\gamma_2+1)}} e^{\frac{-Zr}{N_3 a_0}} \left(\frac{2Z}{N_3 a_0}\right)^{\gamma_2-1} r^{\gamma_2-1} \\ f(r) &= -\sqrt{\frac{1-\varepsilon_3}{1+\varepsilon_3}} g(r), \end{aligned} \tag{7.6}$$

$$\begin{aligned} \tilde{g}(r) &= \left(\frac{2Z}{N_2 a_0}\right)^{\frac{3}{2}} \sqrt{\frac{2\gamma_1+1}{\Gamma(2\gamma_1+1)}} \sqrt{\frac{1+\varepsilon_2}{4N_2(N_2-1)}} e^{-\frac{\rho_2}{2}} \left[(N_2-2)\rho_2^{\gamma_1-1} - \frac{N_2-1}{2\gamma_1+1}\rho_2^{\gamma_1}\right] \\ \tilde{f}(r) &= -\sqrt{\frac{1-\varepsilon_2}{1+\varepsilon_2}} \frac{(2\gamma_1+1)N_2 - (N_2-1)\rho_2}{(2\gamma_1+1)(N_2-2) - (N_2-1)\rho_2} \tilde{g}(r). \end{aligned} \tag{7.7}$$

N_2, N_3, γ_1, γ_2, ε_2 and ε_3 that do not depend on r will be replaced at the end of the calculation and $\rho_2 = \frac{2Zr}{N_2 a_0}$.
The resultant wavefunctions for the three 2p orbitals read:

$$\psi_{2p_{\frac{3}{2},\frac{3}{2}}} = \frac{\sqrt{3}}{2\sqrt{2\pi}} \begin{pmatrix} u_1 = -\sin\theta e^{i\varphi} g(r) \\ u_2 = 0 \\ u_3 = \imath\cos\theta\sin\theta e^{i\varphi} f(r) \\ u_4 = -\imath\sin^2\theta e^{2i\varphi} f(r) \end{pmatrix} \tag{7.8}$$

$$\psi_{2p_{\frac{3}{2},\frac{1}{2}}} = \frac{1}{2\sqrt{2\pi}} \begin{pmatrix} 2\cos\theta g(r) \\ \sin\theta e^{\imath\varphi} g(r) \\ -\imath\left(3\cos^2\theta - 1\right) f(r) \\ 3\imath\cos\theta\sin\theta e^{\imath\varphi} f(r) \end{pmatrix} \tag{7.9}$$

$$\psi_{2p_{\frac{1}{2},\frac{1}{2}}} = \frac{1}{2\sqrt{\pi}} \begin{pmatrix} \cos\theta\tilde{g}(r) \\ -\sin\theta e^{\imath\varphi}\tilde{g}(r) \\ -\imath f(r) \\ 0 \end{pmatrix} \tag{7.10}$$

By determining their hermitian transpose, we get the integrands:

$$\psi^{\dagger}_{2p_{\frac{3}{2},\frac{3}{2}}} \frac{(\vec{\alpha}\times\vec{r})_z}{|\vec{r}|^3}\psi_{2p_{\frac{3}{2},\frac{3}{2}}} = -\frac{3}{4\pi}\frac{1}{r^2}f(r)g(r)\sin^4\theta \tag{7.11}$$

$$\psi^{\dagger}_{2p_{\frac{3}{2},\frac{1}{2}}} \frac{(\vec{\alpha}\times\vec{r})_z}{|\vec{r}|^3}\psi_{2p_{\frac{3}{2},\frac{1}{2}}} = -\frac{1}{4\pi r^2}f(r)g(r)\left(9\cos^2\theta\sin^2\theta-\sin^2\theta\right) \tag{7.12}$$

$$\psi^{\dagger}_{2p_{\frac{1}{2},\frac{1}{2}}} \frac{(\vec{\alpha}\times\vec{r})_z}{|\vec{r}|^3}\psi_{2p_{\frac{1}{2},\frac{1}{2}}} = -\frac{1}{2\pi r^2}\tilde{g}(r)\tilde{f}(r)\sin^2\theta\ . \tag{7.13}$$

Then, the spherical integrals are straightforward:

$$\left\langle \psi^{\dagger}_{2p_{\frac{3}{2},\frac{3}{2}}} \left| \frac{(\vec{\alpha}\times\vec{r})_z}{|\vec{r}|^3} \right| \psi_{2p_{\frac{3}{2},\frac{3}{2}}} \right\rangle = -\frac{16}{10}\cdot\int_0^{+\infty} f(r)g(r)dr \tag{7.14}$$

$$\left\langle \psi^{\dagger}_{2p_{\frac{3}{2},\frac{1}{2}}} \left| \frac{(\vec{\alpha}\times\vec{r})_z}{|\vec{r}|^3} \right| \psi_{2p_{\frac{3}{2},\frac{1}{2}}} \right\rangle = -\frac{8}{15}\int_0^{\infty} f(r)g(r)dr\ . \tag{7.15}$$

$$\left\langle \psi^{\dagger}_{2p_{\frac{1}{2},\frac{1}{2}}} \left| \frac{(\vec{\alpha}\times\vec{r})_z}{|\vec{r}|^3} \right| \psi_{2p_{\frac{1}{2},\frac{1}{2}}} \right\rangle = -\frac{4}{3}\int_0^{\infty} \tilde{g}(r)\tilde{f}(r)dr. \tag{7.16}$$

However, we are left with the non-trivial integrals over r : $I = \int_0^{\infty} f(r)g(r)dr$ and $\tilde{I} = \int_0^{\infty}\tilde{f}(r)\tilde{g}(r)dr$ that will be calculated aside. For that purpose, one needs to make use of the Γ special function that verifies *inter alia* $\Gamma(z) = \int_0^{\infty} t^{z-1}e^{-t}dt$ and $\Gamma(z+1) = z\Gamma(z)$. Thus, the first radial integral reads:

$$\begin{aligned} I &= -\frac{\sqrt{1-\varepsilon_3^2}}{2\Gamma(2\gamma_2+1)}\left(\frac{Z}{a_0}\right)^3\left(\frac{2Z}{N_3a_0}\right)^{2\gamma_2-2}\int_0^{\infty} r^{2\gamma_2-2}e^{\frac{-2Zr}{N_3a_0}}dr \\ &= -\sqrt{1-\varepsilon_3^2}\frac{Z^2N_3}{4a_0^2}\frac{\Gamma(2\gamma_2-1)}{\Gamma(2\gamma 2+1)} \end{aligned} \tag{7.17}$$

and, by substituting the constants with their following expression:

$$\begin{cases} N_3 = 2 \\ \gamma_2 = \sqrt{4-\alpha^2Z^2} \\ \varepsilon_3 = \frac{1}{\sqrt{1+\left(\frac{\alpha Z}{\gamma_2}\right)^2}} \Rightarrow \sqrt{1-\varepsilon_3^2} = \frac{\alpha Z}{2} \end{cases}\ . \tag{7.18}$$

the final expression of the integral is:

$$I = -\frac{\alpha Z^3}{4a_0^2}\frac{\Gamma(2\sqrt{4-\alpha^2Z^2}-1)}{\Gamma(2\sqrt{4-\alpha^2Z^2}+1)}. \tag{7.19}$$

The second radial integral $\tilde{I}$ is more complex and requires a few more steps of calculation.

$$\begin{aligned}\tilde{I} = &-\frac{\sqrt{1-\varepsilon_2^2}}{2\gamma_1+1}\frac{1}{4N_2(N_2-1)\Gamma(2\gamma_1+1)}\left(\frac{2Z}{N_2a_0}\right)^3\int_0^\infty dr e^{-\rho_2}\rho_2^{2\gamma_1-2}\\ &\cdot\left[N_2(N_2-2)(2\gamma_1+1)^2-2(2\gamma_1+1)(N_2-1)^2\rho_2+(N_2-1)^2\rho_2^2\right]\ .\end{aligned} \tag{7.20}$$

First, one needs to replace ρ_2 in the integral:

$$\begin{aligned}\tilde{I} = &-\frac{\sqrt{1-\varepsilon_2^2}}{2\gamma_1+1}\frac{(\Gamma(2\gamma_1+1))^{-1}}{4N_2(N_2-1)}\left(\frac{2Z}{N_2a_0}\right)^{2\gamma_1+1}\Big\{(N_2-1)^2\int_0^\infty e^{\frac{-2Zr}{N_2a_0}}r^{2\gamma_1}dr\\ &-2(2\gamma_1+1)(N_2-1)^2\int_0^\infty e^{\frac{-2Zr}{N_2a_0}}r^{2\gamma_1-1}dr+N_2(N_2-2)(2\gamma_1+1)^2\int_0^\infty e^{\frac{-2Zr}{N_2a_0}}r^{2\gamma_1-2}dr\Big\};\end{aligned} \tag{7.21}$$

then, by making use of the Γ function properties, the integral can be evaluated:

$$\begin{aligned}\tilde{I} = &-\frac{\sqrt{1-\varepsilon_2^2}}{N_2^3(N_2-1)}\frac{Z^2}{a_0^2}\frac{\Gamma(2\gamma_1-1)}{\Gamma(2\gamma_1+2)}\Big\{2(N_2-1)^2\gamma_1(2\gamma_1-1)-2(4\gamma_1^2-1)(N_2-1)^2\\ &+N_2(N_2-2)(2\gamma_1+1)^2\Big\}\ .\end{aligned} \tag{7.22}$$

So as to simplify the expression, the following identities can be shown:

$$\begin{aligned}&(1-\gamma_1)^2 = N_2^2-\alpha^2Z^2\\ &\sqrt{1-\varepsilon_2^2} = \frac{\alpha Z}{N^2}\\ &N_2(N_2-2) = (N_2-1)^2-1\end{aligned} \tag{7.23}$$

and by using them, one obtains the final result:

$$\tilde{I} = -\frac{\alpha Z^3}{a_0^2}\frac{\Gamma(2\gamma_1-1)}{\Gamma(2\gamma_1+2)}\frac{(N_2-1)^2(\gamma_1-1)-(2\gamma_1+1)^2}{N_2^4(N_2-1)}\ . \tag{7.24}$$

with

$$\begin{cases}\rho_2 = \frac{2Zr}{N_2a_0}\\ N_2 = \sqrt{2(\gamma_1+1)}\\ \varepsilon_2 = \left(1+\left(\frac{\alpha Z}{1+\gamma_1}\right)^2\right)^{-\frac{1}{2}}\\ \gamma_1 = \sqrt{1-\alpha^2Z^2}\end{cases}\ . \tag{7.25}$$

Then, the hyperfine integrals are given by:

$$\left\langle \psi^{\dagger}_{2p_{\frac{3}{2},\frac{3}{2}}} \left| \frac{(\vec{\alpha}\times\vec{r})_z}{|\vec{r}|^3} \right| \psi_{2p_{\frac{3}{2},\frac{3}{2}}} \right\rangle = \frac{48}{30}\cdot\frac{\alpha Z^3}{4a_0^2}\frac{\Gamma(2\sqrt{4-\alpha^2Z^2}-1)}{\Gamma(2\sqrt{4-\alpha^2Z^2}+1)} \tag{7.26}$$

$$\left\langle \psi^{\dagger}_{2p_{\frac{3}{2},\frac{1}{2}}} \left| \frac{(\vec{\alpha}\times\vec{r})_z}{|\vec{r}|^3} \right| \psi_{2p_{\frac{3}{2},\frac{1}{2}}} \right\rangle = \frac{2}{15}\frac{\alpha Z^3}{a_0^2}\frac{\Gamma(2\sqrt{4-\alpha^2Z^2}-1)}{\Gamma(2\sqrt{4-\alpha^2Z^2}+1)} \tag{7.27}$$

$$\left\langle \psi^{\dagger}_{2p_{\frac{1}{2},\frac{1}{2}}} \left| \frac{(\vec{\alpha}\times\vec{r})_z}{|\vec{r}|^3} \right| \psi_{2p_{\frac{1}{2},\frac{1}{2}}} \right\rangle = \frac{4}{3}\frac{\alpha Z^3}{a_0^2}\frac{\Gamma(2\gamma_1-1)}{\Gamma(2\gamma_1+2)}\frac{(N_2-1)^2(\gamma_1-1)-(2\gamma_1+1)^2}{N_2^4(N_2-1)}\,. \tag{7.28}$$

In order to verify our formalism, they are evaluated for the hydrogen atom where $(Z=1)$ and consequently $\gamma_1 \approx 1$, $N_2 \approx 2$:

$$\left\langle \psi^{\dagger}_{2p_{\frac{3}{2},\frac{3}{2}}} \left| \frac{(\vec{\alpha}\times\vec{r})_z}{|\vec{r}|^3} \right| \psi_{2p_{\frac{3}{2},\frac{3}{2}}} \right\rangle \approx \frac{\alpha}{30a_0^2}, \tag{7.29}$$

$$\left\langle \psi^{\dagger}_{2p_{\frac{3}{2},\frac{1}{2}}} \left| \frac{(\vec{\alpha}\times\vec{r})_z}{|\vec{r}|^3} \right| \psi_{2p_{\frac{3}{2},\frac{1}{2}}} \right\rangle \approx \frac{1}{90}\frac{\alpha}{a_0^2}, \tag{7.30}$$

$$\left\langle \psi^{\dagger}_{2p_{\frac{1}{2},\frac{1}{2}}} \left| \frac{(\vec{\alpha}\times\vec{r})_z}{|\vec{r}|^3} \right| \psi_{2p_{\frac{1}{2},\frac{1}{2}}} \right\rangle \approx \frac{1}{18}\frac{\alpha}{a_0^2}. \tag{7.31}$$

The formalism is complex and may be difficult to apply to more complex systems. Another strategy is to build the 4-component wavefunction thanks to the restricted kinetic balance, we implement this method in the following paragraph.

7.1.2.2 Restricted kinetic balance

The kinetic balance gives the small component from the large one through the following formula :

$$\psi^S = \frac{\vec{\sigma}\cdot\vec{p}}{2m_0c}\psi^L. \tag{7.32}$$

We will apply this method for the $(j, m_j) = (\frac{3}{2}, \frac{3}{2})$ state, (*i.e.* $m_l = 1, m_s = +\frac{1}{2}$). To this end, the hydrogen $2p_\pi$ wavefunction $(m_L = 1)$ multiplied by an α spin function is used to write the large component of our wavefunction:

$$\psi^L_{2p_{\frac{3}{2},\frac{3}{2}}} = \begin{pmatrix} \psi_{2p_\pi} \\ 0 \end{pmatrix} = \begin{pmatrix} \frac{x+iy}{\sqrt{64\pi a_0^5}} e^{\frac{-r}{2a_0}} \\ 0 \end{pmatrix} = \begin{pmatrix} \frac{1}{\sqrt{64\pi a_0^5}} \sin(\theta) e^{i\varphi} r e^{\frac{-r}{2a_0}} \\ 0 \end{pmatrix}. \tag{7.33}$$

In order to get the small component, one needs to apply the following operator on the large component:

$$\frac{\vec{\sigma}\cdot\vec{p}}{2m_0c} = -\frac{i\hbar}{2m_0c}\begin{pmatrix} \partial_z & \partial_x - i\partial_y \\ \partial_x + i\partial_y & -\partial_z \end{pmatrix} \tag{7.34}$$

$$\begin{aligned}\psi^S_{2p_{\frac{3}{2},\frac{3}{2}}} &= -\frac{i\hbar}{2m_0c}\begin{pmatrix} \partial_z & \partial_x - i\partial_y \\ \partial_x + i\partial_y & -\partial_z \end{pmatrix}\begin{pmatrix} \psi_{2p_\pi} \\ 0 \end{pmatrix} \\ &= -\frac{i\hbar}{2m_0c}\begin{pmatrix} \partial_z\psi_{2p_\pi} \\ (\partial_x + i\partial_y)\psi_{2p_\pi} \end{pmatrix}. \end{aligned} \tag{7.35}$$

Let us evaluate the derivatives by starting with

$$\partial_z\psi_{2p_\pi} = \partial_z\left(\frac{x+iy}{\sqrt{64\pi a_0^5}}e^{-\frac{r}{2a_0}}\right) = \frac{x+iy}{\sqrt{64\pi a_0^5}}\partial_z e^{-\frac{r}{2a_0}}, \tag{7.36}$$

if we expand r in terms of the cartesian coordinates, we get :

$$\partial_z e^{-\frac{r}{2a_0}} = \partial_z e^{-\frac{\sqrt{x^2+y^2+z^2}}{2a_0}} = -\frac{1}{2a_0}\frac{z}{r}e^{-\frac{r}{2a_0}}. \tag{7.37}$$

Similarly, one obtains:

$$\partial_x e^{-\frac{r}{2a_0}} = -\frac{1}{2a_0}\frac{x}{r}e^{-\frac{r}{2a_0}} \text{ and } \partial_y e^{-\frac{r}{2a_0}} = -\frac{1}{2a_0}\frac{y}{r}e^{-\frac{r}{2a_0}}. \tag{7.38}$$

Thus, the first component of $\psi^S_{2p_\pi}$ reads:

$$\partial_z\psi_{2p_\pi} = -\frac{1}{2a_0}\frac{x+iy}{\sqrt{64\pi a_0^5}}\frac{z}{r}e^{-\frac{r}{2a_0}}. \tag{7.39}$$

For the second component of $\psi^S_{2p_\pi}$, we need to evaluate the derivatives of ψ_{2p_π} with respect to x and y.

$$\partial_x\psi_{2p_\pi} = \frac{e^{-\frac{r}{2a_0}}}{\sqrt{64\pi a_0^5}}\left\{1 - \frac{1}{2a_0}\frac{x^2+ixy}{r}\right\} \tag{7.40}$$

Similarly,

$$\partial_y\psi_{2p_\pi} = i\frac{e^{-\frac{r}{2a_0}}}{\sqrt{64\pi a_0^5}}\left\{1 - \frac{1}{2a_0}\frac{y^2-ixy}{r}\right\}. \tag{7.41}$$

Hence,

$$\begin{aligned}(\partial_x + i\partial_y)\psi_{2p_\pi} &= \frac{e^{-\frac{r}{2a_0}}}{\sqrt{64\pi a_0^5}}\frac{1}{2a_0}\frac{y^2-x^2-2ixy}{r} \\ &= -\frac{e^{-\frac{r}{2a_0}}}{\sqrt{64\pi a_0^5}}\frac{1}{2a_0}\frac{(x+iy)^2}{r}. \end{aligned} \tag{7.42}$$

Then, by switching to spherical coordinates :

$$x + iy = r \sin\theta e^{i\varphi}, \tag{7.43}$$

we got the final expression for the $\psi^{4c}_{2p_{\frac{3}{2},\frac{3}{2}}}$ wavefunction:

$$\psi^{4c}_{2p_{\frac{3}{2},\frac{3}{2}}} = \frac{e^{-\frac{r}{2a_0}}}{\sqrt{64\pi a_0^5}} \begin{pmatrix} r\sin\theta e^{i\varphi} \\ 0 \\ \frac{i\hbar}{4\mathrm{m}_0 c a_0} r\cos\theta\sin\theta e^{i\varphi} \\ \frac{i\hbar}{4\mathrm{m}_0 c a_0} r\sin^2\theta e^{2i\varphi} \end{pmatrix}. \tag{7.44}$$

Now, one can write the integrand of the hyperfine interaction integrals:

$$\begin{aligned} \psi^{4c\,\dagger}_{2p_{\frac{3}{2},\frac{3}{2}}} \frac{(\vec{\alpha}\times\vec{r})_z}{|\vec{r}|^3} \psi^{4c}_{2p_{\frac{3}{2},\frac{3}{2}}} &= \frac{e^{-\frac{r}{a_0}}}{64\pi a_0^5} \frac{i\sin\theta}{r^2} \left(u_1^\dagger u_4 e^{-i\varphi} - u_4^\dagger u_1 e^{i\varphi} \right) \\ &= -\frac{2\hbar}{4\mathrm{m}_0 c a_0} \frac{1}{64\pi a_0^5} \sin^4\theta e^{-\frac{r}{a_0}} \end{aligned} \tag{7.45}$$

Finally, the integral is calculated

$$\begin{aligned} \int \psi^{4c\,\dagger}_{2p_{\frac{3}{2},\frac{3}{2}}} \frac{(\vec{\alpha}\times\vec{r})_z}{|\vec{r}|^3} \psi^{4c}_{2p_{\frac{3}{2},\frac{3}{2}}} dV &= \frac{-\hbar}{128\pi \mathrm{m}_0 c a_0^6} \int_0^\infty r^2 e^{-\frac{r}{a_0}} dr \int_0^\pi \sin^5\theta d\theta \int_0^{2\pi} d\varphi \\ &= \frac{-\hbar}{128\pi \mathrm{m}_0 c a_0^6} \cdot 2a_0^3 \cdot \frac{16}{15} \cdot 2\pi \\ &= \frac{-\hbar}{30 a_0^3 m_0 c}\ . \end{aligned} \tag{7.46}$$

If we make use of the definition of a_0 in the atomic units:

$$a_0 = \frac{\hbar}{m_0 c\alpha}, \tag{7.47}$$

the result is:

$$\left\langle \psi^\dagger_{2p_{\frac{3}{2},\frac{3}{2}}} \left| \frac{(\vec{\alpha}\times\vec{r})_z}{|\vec{r}|^3} \right| \psi_{2p_{\frac{3}{2},\frac{3}{2}}} \right\rangle = \frac{-\alpha}{30 a_0^2}\ . \tag{7.48}$$

This hyperfine integral is identical with the value obtained with the exact Dirac wavefunction for a $Z = 1$ system (7.29) with the exception of the sign that remains to be elucidated.

7.1.3 Numerical tests.

Let us test our results by comparing them with numerical values given by `DIRAC` program for a GASCI calculation.

7.1.3.1 Hydrogen-like systems.

First, we aim to evaluate the integrals in an excited state of the hydrogen atom. For that purpose, we need to find a basis set that reproduces well the energy and the wavefunction of the 2p orbital, that occurs to be a non-trivial issue. Even such a large basis set as the Dunning aug-cc-pV6Z fails, the energy of the 2p-orbital obtained with this basis is $E(2p) = -3.1$ eV . Adding p-optimized exponents is required. To that end, we calculate the expectation value of r over the $2p_\sigma$ wavefunction:

$$|2p_\sigma\rangle = |n = 2, l = 1, m_l = 0\rangle = a_0^{-\frac{3}{2}} \frac{1}{2\sqrt{6}} \frac{r}{a_0} e^{-\frac{r}{a_0}} \frac{1}{2} \sqrt{\frac{3}{\pi}} cos\theta, \tag{7.49}$$

and we get:

$$\langle 2p_\sigma | r | 2p_\sigma \rangle = 5a_0. \tag{7.50}$$

Then, we seek a gaussian $g(r) = \frac{r}{a_0} e^{-\alpha(\frac{r}{a_0})^2}$ with an α-exponent such as the gaussian is maximal for $r = 5a_0$. If we set to zero the derivative of $g(r)$ with respect to r:

$$\frac{\partial g(r)}{\partial r} = \left(\frac{1}{a_0} - \frac{2r^2\alpha}{a_0^3} \right) := 0, \tag{7.51}$$

$\alpha = \frac{a_0^2}{2r^2}$ and in particular for $r = 5a_0$, $\alpha = \frac{1}{50}$. This p-optimized exponent and three multiples are added to the Dunning aug-cc-pV6Z basis set, yielding the proper energy for the 2p orbital $E(2p) = -3.4$ eV . Thus, one can compare our analytical values of the hyperfine integrals with the numerical results where the hyperfine operator is evaluated over GASCI wavefunctions. For the three 2p-states of the hydrogen atom, our calculations are in very good agreement with the numeric as one can see in Table 7.1.

Table 7.1 – Values of hyperfine integral for 2p orbitals of hydrogen atom

	$2p_{\frac{1}{2},\frac{1}{2}}$	$2p_{\frac{3}{2},\frac{3}{2}}$	$2p_{\frac{3}{2},\frac{1}{2}}$
Analytical	$4.054.10^{-4}$	$2.432.10^{-4}$	$8.11.10^{-5}$
Numerical	$4.048.10^{-4}$	$2.429.10^{-4}$	$8.10.10^{-5}$

7.1.3.2 Many-electron systems.

Our method proved to be efficient and accurate for the hydrogen atom, though, we aim to use it on many-electron systems. In this purpose, the effective electric charge in the π-state must be determined. Our strategy is the following, Z_{eff} will be deduced from the energy difference between the two spin-orbit levels ($J = \frac{1}{2}$ and

$J = \frac{3}{2}$) of the 2p orbital that is known to scale as Z_{eff}^4 and whose expression can be analytically obtained for the hydrogen atom in Pauli formalism $\Delta E^H_{p_{\frac{1}{2}-\frac{3}{2}}} = \frac{1}{32}\frac{\alpha^2 e^2}{a_0}$. Then, Z_{eff} reads:

$$Z_{eff} = \sqrt[4]{\frac{\Delta E_{p_{\frac{1}{2}-\frac{3}{2}}}}{\Delta E^H_{p_{\frac{1}{2}-\frac{3}{2}}}}} \tag{7.52}$$

where the spin-orbit splitting of the 2p will be either determined with the Hartree-Fock energy of the two levels or evaluated through experimental data.
We apply this strategy to the fluorine atom by deducing the effective electric charge from the experimental $^2P_{\frac{1}{2}} -^2 P_{\frac{3}{2}}$ energy shift: $\Delta E_{^2P_{\frac{1}{2}-\frac{3}{2}}} = 404.10\ \text{cm}^{-1}$[Moo71], $Z_{eff}^{Exp} = 5.76$. Using this value in Eqs. (7.29) to (7.31) leads to analytically calculated hyperfine integrals at a variance with numerical results of 7% at the most (see Table 7.2), which is satisfying since we only aim to get a qualitative overview.

$2p_{(J,m_J)}$	$(\frac{1}{2},\frac{1}{2})$	$(\frac{3}{2},\frac{3}{2})$	$(\frac{3}{2},\frac{1}{2})$
Analytical	7.774×10^{-2}	1.550×10^{-2}	4.651×10^{-2}
Numerical	7.459×10^{-2}	1.432×10^{-2}	4.297×10^{-2}

Table 7.2 – Hyperfine integrals values.

Obviously, the following step will be to apply this method to molecules, starting with a diatomic molecule like CF. To do so, one will have to tackle the issue of determining the respective effective charge of each atom with accuracy. We have not found a satisfying method so far.

7.2 Numerical study.

In addition to the development of a theoretical analytical framework to calculate with accuracy the hyperfine interaction constant of the fluorine, we employ a rigorous spinor-based many-body correlation method for a further study of $A_{||}(F)$ in diatomic molecules.

For the determination of the parallel magnetic hyperfine interaction constant $A_{||}$ for the ^{19}F isotope, the values of the nuclear magnetic moment and the nuclear quantum number were required; the first one is determined to be $\mu = 2.62727\mu_N$ [Kay][Ful76] and $I = \frac{1}{2}$. Wavefunctions are obtained from 4−component Configuration Interaction theory based on molecular spinors optimized through all-electron four-component Hartree-Fock calculations using the Dirac-Coulomb Hamiltonian. These calculations are carried out using a modified local version of the `DIRAC11`

program package [DIRb] and Gaussian basis sets, Dyall's triple-ζ for thorium and Hafnium, Dunning's cc-pVnZ for smaller atoms (carbon, fluorine, hydrogen).

7.2.1 Lighter F diatomics (HF^+, CF, MgF)

In an effort to understand phenomena at stake in hyperfine interaction in diatomic molecules, we evaluate $A_{||}$ in light molecules containing a fluorine atom. We consider the ion HF^+, the fluoromethylidyne (CF) and the magnesium monofluoride (MgF). The fluoromethylidyne is a molecule of interest since it is a system very similar to ThF^+ for which a reliable determination of the hyperfine constant is of the utmost importance for the development of upcoming experiments of eEDM. As a matter of fact, its configuration is mainly C^+F^- when ThF^+ is $Th^{2+}F^-$, this means that in both systems the fluorine atom is almost closed shell and thus, the single electrons are localized on the other nucleus, respectively Carbon and Thorium. Besides, the atoms display identical ionization potential, Carbon first ionization potential is equal to Thorium second ionization potential. However, there is a major difference between CF and ThF^+, it comes to the equilibrium distance, which is significantly smaller in the Fluoromethylidyne.

In addition to this intermediate system, we turn our interest to the hydrogen fluoride ion HF^+ that presents a radically different configuration, *i. e.* an occupation by the unpaired electron of a spinor with a dominant Fluorine atomic character. Finally, we include in our study the available value of $A_{||}$ in an other Fluoride diatomic compound, MgF. The wide diversity of electronic configurations and the equally wide range of internuclear distances, allows for the comparison and enables us to correlate the electronic spin density of the unpaired electron(s) around the nucleus and the value of its hyperfine constant. In that purpose, the atomic spinor character of the molecular orbital occupied by the single electron obtained by a Mulliken analysis and the equilibrium internuclear distance for the various diatomic molecules are displayed in Table 7.3 along with the parallel magnetic hyperfine interaction constant. The wavefunction analysis is not available for MgF, nevertheless, the molecular orbital occupied by the single electron is expected to be mainly of Mg s-character [KJEWJW71].

As one could expect by looking at the expression of the magnetic hyperfine interaction constant (Eq. (3.39)), the latter proves to depend strongly on the electron spin density in the vicinity of the Fluorine nucleus. This is reflected by the smallness of the $A_{||}$ value when the weights of F atomic orbitals in the wavefunction of the unpaired electron are minor as exhibited in CF and even smaller if the equilibrium distance is larger, the spin density of the electron of interest around the F nucleus being weakened by the distance, as it is the case for the magnesium monofluoride mo-

Table 7.3 – Hyperfine interaction constant, fluorine spinor character in the molecular orbital occupied by the unpaired electron and equilibrium distance in fluoride compounds.

System	State	F spinor character	R_e [a.u.]	$A_{\|\|}$[MHz]
HF+	$^2\Pi_{1/2}$	0.4924(F(p_x)+F(p_y))	1.892[a]	9210
CF	$^2\Pi_{1/2}$	0.0239(F(p_x)+F(p_y))	2.403[b]	1348
MgF	$^2\Sigma_{1/2}$		3.307[c]	321[d]

[a] Reference [GLF75] [c] Reference [KJEWJW71]
[b] Reference [CH70] [d] Reference [SPN+15].

lecule. Conversely, when the single electron occupies an orbital mainly of F character with a rather small equilibrium distance, like in HF^+, the value of $A_{||}$ is significantly greater. Hence, the strong connection between electron spin density near the nucleus and magnitude of $A_{||}$ is confirmed.

7.2.2 HfF^+ and ThF^+

The parallel magnetic hyperfine interaction constant $A_{||}$ for ^{19}F is calculated in diatomic molecules of interest for the search of the electric dipole moment of the electron. Dyall's thorium and hafnium triple-ζ basis sets [Dya06] and Dunning's fluorine cc-pVTZ [Dun89] are employed for molecular calculations.

In line with our expectations, both systems exhibit weak values of $A_{||}(F)$ in the science state, the state in which is made the eEDM experiment [CGS+12]. Actually, the molecular orbitals occupied by the single electrons are essentially atomic ones respectively localized on hafnium (6s, $5d_\delta$) and thorium (7s, $6d_\delta$). Indeed the contributions of fluorine orbitals to occupied spinors prove to be minor. By examining the outcomes, given by a Mulliken population analysis, in Table 7.4, one can observe that the preponderant F orbital exhibits a minor weight of only 0.001 . Hence, the electron spin density in the vicinity of the fluorine nucleus is pretty weak and the hyperfine interaction between those electrons and the fluorine nucleus is similarly small.

For further understanding, $A_{||}$(F) is scrutinized in the $^3\Delta_1$ state of the ThF^+ system. First, we look at the effect of a small modification of the wavefunction by increasing the active space of the configuration of interaction model. Using the same process employed in [DNJ+15], we gradually add spinors to a minimal active space including the 7s and $6d_\delta$ orbitals of the thorium atom; these models are named MR_X-CISD(18) where X is the number of kramers pairs included in the active space. Results compiled in Table 7.5 show a decrease of $A_{||}$(F) whilst increasing the size of the active space, notably two major drops occur at the steps $X = 3 \rightarrow X = 5$ and

Table 7.4 – Hyperfine interaction constant, fluorine spinor character in the molecular orbitals occupied by the unpaired electrons, σ and δ respectively, and equilibrium distance in fluoride diatomic molecules candidate for EDM experiments.

System	Model	F spinor weight in occupied MOs σ	F spinor weight in occupied MOs δ	R_e [a.u.]	$A_{\|\|}$[MHz]
ThF^+	MR_{10}-CISD(18)	0.001 p_z(F)	0.0003 (p_x(F)+p_y(F))	3.75	**4.3**
HfF^+	MR_6-CISD(20)	0.0004 p_z(F)	0.0002(p_x(F)+p_y(F))	3.41	**45.2**

$X = 8 \rightarrow X = 10$. They correspond to the adding of σ-type orbitals which gives rise to a shift of the spin density towards the thorium nucleus. Then, the reduced spin density around the fluorine nucleus leads to a significant decrease of its parallel magnetic hyperfine interaction constant. To confirm this latter assumption, we define a new model MR_{10}-CISD(20) in which the fluorine 1s spinors are included. It arises that the value of $A_{||}$(F) is doubled, an outcome consistent with a shift of the spin density towards the fluorine nucleus.

Table 7.5 – Hyperfine constant for fluorine in $\Omega = 1$ state of ThF^+ at an internuclear distance of $R = 3.779\ a_0$ using the vTZ basis set and varying active spinor spaces.

CI model	$A_{\|\|}(F)[MHz]$
MR_3-CISD(18)	6.48
MR_5-CISD(18)	6.12
MR_6-CISD(18)	5.68
MR_8-CISD(18)	5.79
MR_{10}-CISD(18)	4.28
MR_{12}-CISD(18)	4.12
MR_{13}-CISD(18)	4.14
MR_{10}-CISD(20)	8.89

HfF^+ exhibits sharply greater $A_{||}$ even though the weights of the Fluorine orbitals in the wavefunction expansion are similar to those observed in ThF^+. However, their equilibrium distance differs (see Table 7.4). Then, even if the electron spin density is, in both cases, localised on the heavy nucleus, the fluorine nucleus is nearer from this density in HfF^+ and, as a consequence, gives rise to a stronger hyperfine interaction than in ThF^+. Thus, while we assumed that the equilibrium distance of the molecules played a role in the magnitude of $A_{||}$, it turns out to be of crucial importance in $A_{||}$.

Finally, the calculation of the hyperfine interaction constant for both nuclei in the EDM systems allows for the determination of the corresponding energy splitting between hyperfine levels. The results obtained for I(Th)= 5/2, $\mu(^{229}\text{Th}) = 0.45\ \mu_N$ [KLR+12], I(Hf)= 7/2 and $\mu(^{177}\text{Hf}) = 0.7936\ \mu_N$[Sto05] are displayed in Table 7.6.

Table 7.6 – Hyperfine energy shift in cm^{-1} for both atoms in the $\Omega = 1$ state of ThF^+ and HfF^+.

System	ΔE_{hyp}(Th/Hf)	ΔE_{hyp}(F)
ThF^+	0.0612	1.428×10^{-4}
HfF^+	0.0444	1.509×10^{-3}

In order to test the effectiveness and the accuracy of the numerical method for the determination of the parallel magnetic hyperfine interaction constant and thus for the $\mathcal{P}, \mathcal{T}$-odd constants, experimental data would be required. Nevertheless, no experimental values are available for $A_{||}$, to the best of our knowledge, in the relevant sytems.

8 Summary.

In this thesis, we searched for evidence of phenomena that would violate the combined parity and charge conjugation symmetries, proposed as an explanation for the baryon asymmetry of the Universe, one of the main shortcomings of the Standard Model of particles.

Our work outlined a large range of interaction constants violating both parity and time-reversal symmetries of interest in the search of New Physics beyond the Standard Model, namely, the electron Electric Dipole Moment (eEDM), the electron-nucleon scalar-pseudoscalar (enSPS) and the nuclear magnetic quadrupole moment (nMQM) interactions. The calculation of the corresponding parameters was implemented for diatomic molecules such as ThO that was employed in cutting-edge eEDM experiments and allowed for the assignment of the most constraining upper-bound on the eEDM or ThF^+, a promising candidate for upcoming experiments in the search of $\mathcal{CP}$-violation due to its $^3\Delta_1$ ground-state and its ionic character. We used an elaborate four-component relativistic configuration interaction approach. Through detailed analysis, the properties were determined with accuracy and their error bars minimised.

Those results will be of crucial importance in the interpretation of the measurements since, as previously expounded, an upper bound or a value of the fundamental constants can only be assigned if one combines both experimental and theoretical results. Hence, coupling the theoretical molecular parameter values and their error bars, calculated in this work, with experimental energy shift measurements allows the evaluation of the range of the possible values of the fundamental constants (d_e and C_S for instance) and, above all, of their error bars, as plotted in Figures 2.1 and 8.1.

Furthermore, another useful parameter was calculated, that is the parallel magnetic hyperfine interaction constant. This latter allows for testing the accuracy of the description of the electron spin density around the nucleus upon which the eEDM is very sensitive and, a precise knowledge of the hyperfine structure is essential to prepare the molecules in the wanted state and design the experimental process.

Figure 8.1 – Fit in the $d_e - C_S$ plane of the recent experimental and theoretical results in both paramagnetic and diamagnetic systems [Jun15].

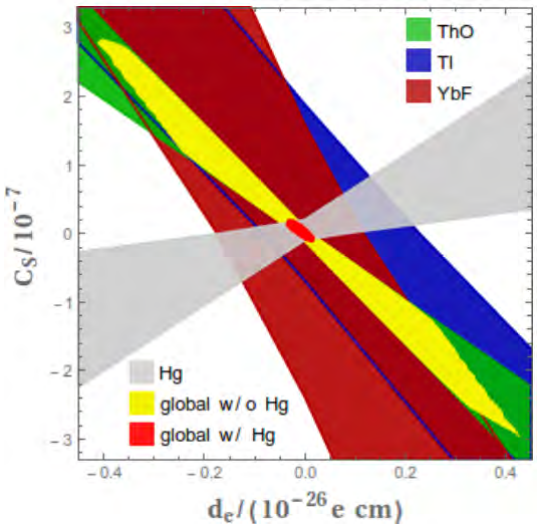

These studies revealed among other facts the insensitivity of the $\mathcal{P},\mathcal{T}$-odd parameters to the choice of the spinor basis set as well as the adequacy of the use of the triple-ζ gaussian basis sets for their calculation. Besides, the size of the active spinor space turns out to be the crucial parameter in the correlation treatment of the wavefunctions employed for the calculation of the constants. Those features may be instructive for future studies of the $\mathcal{P},\mathcal{T}$-odd constants in polar paramagnetic diatomic molecules.

Several eEDM experiments are planned with the paramagnetic diatomic molecules in the following years. They consist in either using new promising molecules such as ThF^+ or upgrading already existing experiments (YbF, ThO ...) in order to lower the systematic errors and thus, the upper bound on eEDM.

Besides improving uncertainty of the current and incoming experiments in paramagnetic systems, a way to further constrain the models beyond the Standard Model is to investigate diamagnetic systems such as Hg or Xe atoms and take advantage of the linear combination of d_e and C_S expected to be orthogonal to that in paramagnetic sytems that all exhibit similar combination. In this way, crossing the results from both types of systems will lead to more stringent limit on constants than would an improvement of uncertainty, even of one order of magnitude, for a single parameter in one kind of system. Fig. 8.1 illustrates how including the results of diamagnetic systems reduces the error ellipses of the values of d_e and C_S (yellow (only paramagnetic) and red (diamagnetic Hg included) ellipses to be compared) and thus further constrains the range of their possible values. As a consequence, the following theoretical studies and experiments should address P,T-violating interac-

tions in diamagnetic systems in addition to paramagnetic systems and the results be combined to efficiently constrain new physics.

Hund's coupling cases.

Hund's coupling cases account for the way the various angular momenta can be coupled in diatomic molecules. The angular momenta at stake in such systems are:

- L: electronic orbital angular momentum,
- S: electronic spin angular momentum,
- J_e: electronic total angular momentum ($\mathbf{J}_e$=$\mathbf{L}$+$\mathbf{S}$),
- J: total angular momentum ($\mathbf{J}$=$\mathbf{J}_e$+$\mathbf{R}$),
- R: nuclei rotational angular momentum

The choice of good quantum numbers among these momenta depends on the relative magnitude of the different possible coupling. As a matter of fact, the Hund's cases are defined by the ranking of electrostatic, spin-orbit and spin-rotation interactions whose strength is governed by ΔE, the spin-orbit constant A and the rotational constant B respectively [BJ03]. The two cases of interest in our study will be presented above. Their coupling schemes are displayed in Figures A.1 and A.2 [BC03].

Hund's case (a) The case (a) is a well description of configurations that exhibit $|\Delta E| \gg |A| \gg B$. The electronic orbital $\mathbf{L}$ and spin angular momenta are strongly coupled to the internuclear axis (z) through the electrostatic interaction which has axial symmetry. Hence, these angular momenta precess about this axis and their z-component: Λ and Σ are well defined and good quantum numbers. Their sum Ω couples to the rotational angular momentum $\mathbf{R}$ to form $\mathbf{J}$. The case (a) is said to be a decoupled basis set since $\mathbf{L}$ and $\mathbf{S}$ are decoupled along the z-axis. Finally, the appropriate set of quantum numbers to describe this case is $|S, \Sigma, \Lambda, \Omega, J\rangle$.

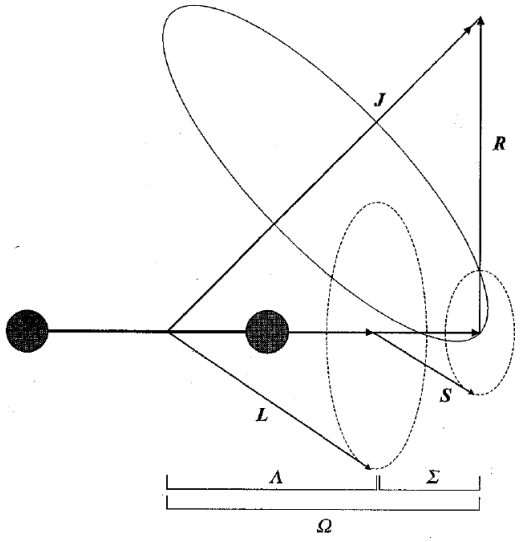

Figure A.1 – Vector coupling diagram for Hund's case (a)

Hund's case (c) In case (c), the ranking is $|A| \gg |\Delta E| \gg B$, the strongest interaction is the spin-orbit interaction that leads to a strong coupling of **L** and **S**. This coupling results in the total electronic angular momentum $\mathbf{J}_e$ whose z-component is Ω. Therefore, the projection Λ and Σ are no longer defined since the electrostatic interaction is weaker than spin-orbit. The resulting $\mathbf{J}_e$ couples with the rotational momentum **R** to form the total angular momentum **J**. Hence, the relevant manifold of quantum numbers to define that kind of system is $|J_e, \Omega, J; M_J\rangle$, in particular, Ω characterizes the different electronic states. Hund's case (c) can be observed in diatomic molecules that contain heavy atoms.

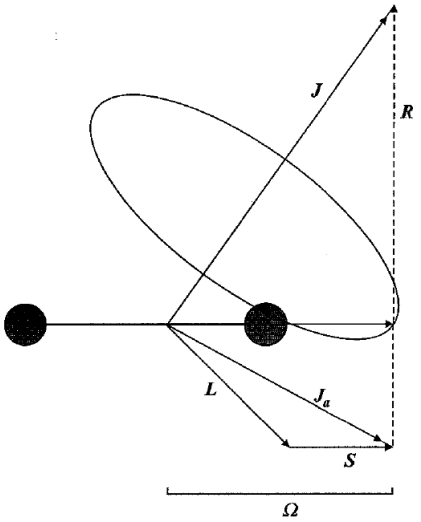

Figure A.2 – Vector coupling diagram for Hund's case (c)

One has to keep in mind that the Hund's cases are idealised situations and molecules may exhibit intermediate coupling scheme as it is the case in the $^3\Delta_1$ state of ThO and ThF^+ where, despite a dominant spin-orbit interaction, the projection of $\mathbf{L}$ and $\mathbf{S}$, Λ and Σ respectively, are pretty well defined.

B Minimal coupling.

The purpose of this chapter is to motivate the use of the so-called *minimal substitution rule* or *minimal coupling* to account for the effect of an external magnetic field, namely in Dirac equation (Eq. (2.3)). In this chapter, we will derive it within the Gaussian unit system which entails the presence of c in the following expression,

$$\mathbf{p} \to \boldsymbol{\pi} = \mathbf{p} + \frac{e}{c}\mathbf{A}. \tag{B.1}$$

The starting point is the interaction Lagrangian of a charged particle in external electromagnetic fields in the non-relativistic limit:

$$\mathcal{L}_{int}^{n.r.} = e\phi. \tag{B.2}$$

Then, we seek a relativistic form for the interaction Lagrangian $\mathcal{L}_{int}$ that respects the Lorentz and translationally invariant nature of $\gamma\mathcal{L}$ [1] [Jac99] and tends towards Eq. (B.2) in the non-relativistic limit. A hint is the presence of ϕ in Eq. (B.2). Since ϕ is the zero-component of the four-vector potential, we expect the vector potential $\mathbf{A}$ to appear in $\mathcal{L}_{int}$ through a scalar product of A^α and another four-vector. The only appropriate four-vector is the four-velocity of the particle U^α:

$$U^\alpha = (\gamma c, \gamma \mathbf{u}). \tag{B.3}$$

Hence, the interaction Lagrangian necessarily reads:

$$\mathcal{L}_{int} = \frac{e}{\gamma c} U_\alpha A^\alpha \tag{B.4}$$

or, more explicitly,

$$\mathcal{L}_{int} = e\phi - \frac{e}{c}\mathbf{u}\cdot\mathbf{A}. \tag{B.5}$$

[1] Here γ is the Lorentz factor defined as $\gamma^{-1} = \sqrt{1-\beta^2} = \sqrt{1-\frac{u^2}{c^2}}$.

By summing up the free particle Lagrangian and the interaction Lagrangian, one obtains the total relativistic Lagrangian:

$$\mathcal{L} = -\frac{mc^2}{\gamma} - \frac{e}{c}\mathbf{u} \cdot \mathbf{A} + e\phi. \tag{B.6}$$

One gets the canonical momentum $\boldsymbol{\pi}$, conjugate coordinate of the position coordinate $\mathbf{x}$ by making use of the definition:

$$\pi_i \equiv \frac{\partial \mathcal{L}}{\partial u_i}. \tag{B.7}$$

It yields:

$$\pi_i = \gamma m u_i + \frac{e}{c} A_i \tag{B.8}$$

or, in a vectorial notation, and subsituting $\mathbf{p}$ to its definition:

$$\boldsymbol{\pi} = \mathbf{p} + \frac{e}{c}\mathbf{A}. \tag{B.9}$$

C Non-stationary Foldy-Wouthuysen Transformation.

Here we adress the Foldy-Wolthuysen Transformation of the non stationary Dirac equation. The transformed hamiltonian shall be derived from the Schrödinger equation. The wavefunction ψ that undergoes the same unitary transformation as in the stationary case:

$$\psi' = e^{i\bar{S}}\psi \tag{C.1}$$

has to be substituted in the Schrödinger equation

$$i\hbar\frac{\partial\psi}{\partial t} = \mathcal{H}\psi, \tag{C.2}$$

leading to

$$i\hbar\frac{\partial\psi'}{\partial t} = i\hbar\frac{\partial e^{i\bar{S}}}{\partial t}\psi + i\hbar e^{i\bar{S}}\frac{\partial\psi}{\partial t}. \tag{C.3}$$

Then by using (C.2) and (C.1), we get a Schrödinger equation for the transformed wavefunction:

$$i\hbar\frac{\partial\psi'}{\partial t} = i\hbar\frac{\partial e^{i\bar{S}}}{\partial t}e^{-i\bar{S}}\psi' + e^{i\bar{S}}\mathcal{H}e^{-i\bar{S}}\psi' \tag{C.4}$$

where the transformed hamiltonian reads:

$$\mathcal{H}' = i\hbar\frac{\partial e^{i\bar{S}}}{\partial t}e^{-i\bar{S}} + e^{i\bar{S}}\mathcal{H}e^{-i\bar{S}}. \tag{C.5}$$

We derive the expansion of $e^{i\bar{S}}$ (3.4)

$$\begin{aligned}\frac{\partial e^{i\bar{S}}}{\partial t} = {} & i\frac{\partial\bar{S}}{\partial t} + \frac{i^2}{2!}\left(\bar{S}\frac{\partial\bar{S}}{\partial t} + \frac{\partial\bar{S}}{\partial t}\bar{S}\right) + \frac{i^3}{3!}\left(\bar{S}\bar{S}\frac{\partial\bar{S}}{\partial t} + \bar{S}\frac{\partial\bar{S}}{\partial t}\bar{S} + \frac{\partial\bar{S}}{\partial t}\bar{S}\bar{S}\right) \\ & + \frac{i^4}{4!}\left(\bar{S}\bar{S}\bar{S}\frac{\partial\bar{S}}{\partial t} + \bar{S}\bar{S}\frac{\partial\bar{S}}{\partial t}\bar{S} + \bar{S}\frac{\partial\bar{S}}{\partial t}\bar{S}\bar{S} + \frac{\partial\bar{S}}{\partial t}\bar{S}\bar{S}\bar{S}\right)\end{aligned} \tag{C.6}$$

and replace it in (C.5). Then, the additional term gives:

$$\begin{aligned} i\hbar\frac{\partial e^{i\bar{S}}}{\partial t}e^{-i\bar{S}} =& -\hbar\frac{\partial\bar{S}}{\partial t} - \frac{i\hbar}{2}\left(\bar{S}\frac{\partial\bar{S}}{\partial t} - \frac{\partial\bar{S}}{\partial t}\bar{S}\right) - \frac{i^2\hbar}{2\times 3}\left(\bar{S}\bar{S}\frac{\partial\bar{S}}{\partial t} - 2\bar{S}\frac{\partial\bar{S}}{\partial t}\bar{S} + \frac{\partial\bar{S}}{\partial t}\bar{S}\bar{S}\right) \\ & -\frac{i^3\hbar}{3!\times 4}\left(\bar{S}\bar{S}\bar{S}\frac{\partial\bar{S}}{\partial t} - 3\bar{S}\bar{S}\frac{\partial\bar{S}}{\partial t}\bar{S} + 3\bar{S}\frac{\partial\bar{S}}{\partial t}\bar{S}\bar{S} - \frac{\partial\bar{S}}{\partial t}\bar{S}\bar{S}\bar{S}\right) + \dots \\ =& -\hbar\frac{\partial\bar{S}}{\partial t} - \frac{i\hbar}{2}\left[\bar{S},\frac{\partial\bar{S}}{\partial t}\right] + \frac{\hbar}{6}\left[\bar{S},\left[\bar{S},\frac{\partial\bar{S}}{\partial t}\right]\right] + \frac{i\hbar}{24}\left[\bar{S},\left[\bar{S},\left[\bar{S},\frac{\partial\bar{S}}{\partial t}\right]\right]\right] + \dots \end{aligned} \tag{C.7}$$

We keep the terms that will contribute to the new Hamiltonian up to order $\frac{1}{c^2}$ for the first transformation:

$$i\hbar\frac{\partial e^{i\bar{S}}}{\partial t}e^{-i\bar{S}} = -\hbar\frac{\partial\bar{S}}{\partial t} - \frac{i\hbar}{2}\left[\bar{S},\frac{\partial\bar{S}}{\partial t}\right] + O(c^{-3}) \tag{C.8}$$

and evaluate them:

$$\frac{\partial\bar{S}}{\partial t} = -\frac{i\beta}{2m_0c^2}\frac{\partial\mathcal{O}}{\partial t}, \tag{C.9}$$

$$\left[\bar{S},\frac{\partial\bar{S}}{\partial t}\right] = -\frac{1}{4m_0^2c^4}\left[\beta\mathcal{O},\beta\frac{\partial\mathcal{O}}{\partial t}\right] = \frac{1}{4m_0^2c^4}\left[\mathcal{O},\frac{\partial\mathcal{O}}{\partial t}\right]. \tag{C.10}$$

In the latter, we made use of $\left[\beta,\frac{\partial\mathcal{O}}{\partial t}\right] = \frac{\partial}{\partial t}[\beta,\mathcal{O}]$. These two terms are added to the stationary transformed hamiltonian found in (3.12) where $\mathcal{E}'$ and $\mathcal{O}'$ write now:

$$\mathcal{E}' = \mathcal{E} + \frac{\beta\mathcal{O}^2}{2m_0c^2} - \frac{1}{8m_0^2c^4}\left[\mathcal{O},\left\{[\mathcal{O},\mathcal{E}] + i\hbar\frac{\partial\mathcal{O}}{\partial t}\right\}\right] - \frac{\beta\mathcal{O}^4}{8m_0^3c^6} \tag{C.11}$$

$$\mathcal{O}' = \frac{\beta}{2m_0c^2}\left\{[\mathcal{O},\mathcal{E}] + i\hbar\frac{\partial\mathcal{O}}{\partial t}\right\} - \frac{\mathcal{O}^3}{3m_0^2c^4}\ . \tag{C.12}$$

As shown above the second transformation yields the following transformed hamiltonian: $\mathcal{H}'' = \beta m_0c^2 + \mathcal{E}'$ that gives:

$$\mathcal{H}'' = \beta m_0c^2 + \mathcal{E} + \frac{\beta\mathcal{O}^2}{2m_0c^2} - \frac{1}{8m_0^2c^4}\left[\mathcal{O},\left\{[\mathcal{O},\mathcal{E}] + i\hbar\frac{\partial\mathcal{O}}{\partial t}\right\}\right] - \frac{\beta\mathcal{O}^4}{8m_0^3c^6} \tag{C.13}$$

One can note that the same terms as in the stationary case appear with the exception of the commutator $\left[\mathcal{O},\left\{[\mathcal{O},\mathcal{E}] + i\hbar\frac{\partial\mathcal{O}}{\partial t}\right\}\right]$ that displays an extra term. Yet, this term only brings the non stationary contribution of the electric field: $\frac{\partial\boldsymbol{A}}{\partial t}$;

$$[\mathcal{O},\mathcal{E}] + i\hbar\frac{\partial\mathcal{O}}{\partial t} = i\hbar ec\boldsymbol{\alpha}\cdot\left(\nabla\phi + \frac{\partial\boldsymbol{A}}{\partial t}\right) \equiv i\hbar ec\boldsymbol{\alpha}\cdot\boldsymbol{E}\ . \tag{C.14}$$

Then, the same final even hamiltonian as the stationary one (Eq. (3.30)) emerged:

$$\begin{aligned}\mathcal{H}_{even} =& \beta m_0 c^2 - e\phi + \frac{\beta \boldsymbol{\pi}^2}{2m} + \beta g_S \mu_B \boldsymbol{S}\cdot\boldsymbol{B} + \frac{e\hbar^2}{8m_0^2c^2}\nabla\cdot\boldsymbol{E} \\ & - \frac{e\hbar}{4m_0^2c^2}\boldsymbol{S}\cdot(\boldsymbol{\pi}\times\boldsymbol{E} - \boldsymbol{E}\times\boldsymbol{\pi}) - \frac{\beta\boldsymbol{\pi}^4}{8m_0^3c^2}. \end{aligned} \tag{C.15}$$

The physical interpretation of the various terms is the same as in the stationary case (Section 3.1).

Selection rules.

In the dipole approximation, the transition probability from a state $|\psi_a\rangle$ to a state $|\psi_b\rangle$ is given by $|\mathbf{M}_{ba}|^2$ where $\mathbf{M}_{ba}$ is proportional to the matrix element of the electric transition dipole moment $\hat{\mathbf{d}}$ between the two states

$$\left\langle \psi_b | \hat{\mathbf{d}} | \psi_a \right\rangle \tag{D.1}$$

with $\hat{\mathbf{d}} = -e\hat{\mathbf{r}}$. Herewith, the selection rules for electronic transitions can be deduced from the study of the matrix elements of the position operator

$$\langle \psi_b | \hat{\mathbf{r}} | \psi_a \rangle \, . \tag{D.2}$$

In this way, we aim to identify the non-vanishing integrals that correspond to the allowed transitions by employing the powerful theorem of the group theory:

Be a symmetry group $\mathcal{G}$ and a function $f(x)$ that can be classified in one of its irreducible representations, *i.e.*, $f(x) \in \Gamma(\mathcal{G})$, an integral of this function over a symmetric range will vanish if the irreducible representation of the integrand is not the totally symmetric representation of $\mathcal{G}$:

$$f(x) \notin \left\{\Gamma^{(tot)}\right\} \Rightarrow \int_{-a}^{+a} f(x)dx = 0, \text{ with } a, x \in \mathbb{R} \text{ and } a \neq 0. \tag{D.3}$$

Let us consider the exemplifying case of the atomic $1s \rightarrow 2s$ transition. A possible atomic symmetry group is the $\mathcal{O}(3)$ group whose irreducible representations are closely connected to the atomic orbitals, $\left\{\Gamma^{(s)}, \Gamma^{(p)}, \Gamma^{(d)}, ..\right\}$. The $\hat{\mathbf{r}}$ operator that we aim to evaluate as an overlap transforms as a p-orbital: $\Gamma^{(\hat{\mathbf{r}})} = \Gamma^{(p)}$ and thus, the irrep of the integrand of the transition matrix element $\langle \psi_{2s} | \hat{\mathbf{r}} | \psi_{1s} \rangle$ is:

$$\Gamma^{(s)} \otimes \Gamma^{(p)} \otimes \Gamma^{(s)} = \Gamma^{(s)} \otimes \Gamma^{(p)} = \Gamma^{(p)}. \tag{D.4}$$

Since the integrand transforms as the $\Gamma^{(p)}$ symmetry group which is not the totally symmetric irrep, $\Gamma^{(s)}$ in that case, the integral vanishes and thus, the transition $1s \to 2s$ is forbidden. This rule will be written as $1s \nrightarrow 2s$.

Likewise, one can deduce the selection rules for molecular electronic transitions. In the molecular framework, the electronic-state configurations are described by term symbols of the form:

$$^{2S+1}\Lambda_{\Omega} \tag{D.5}$$

where S is the total spin quantum number, Λ the total orbital quantum number. Σ and Ω are the projection onto the molecular axis of S and J_e, the total electronic angular momentum quantum number, respectively. Ω can also be defined as

$$\Omega = \Lambda + \Sigma. \tag{D.6}$$

The rules summarised in [AF11] can be classified into three categories.
First ones are conditions on the total spin:

$$\Delta S = 0,\ \Delta\Sigma = 0 \tag{D.7}$$

that translate into the invariance of the spin multiplicity during a transition. Thus, transitions between states that exhibit different spin multiplicity are forbidden.
The other rule applies to the orbital angular momentum:

$$\Delta\Lambda = 0, \pm 1; \tag{D.8}$$

hence a $\Sigma^+ \to \Pi$ transition may be allowed while $\Sigma^- \to \Phi$ is forbidden. Furthermore, the latter rule entails the same restriction on Ω,

$$\Delta\Omega = 0, \pm 1 \tag{D.9}$$

in vertue of Eqs. (D.6) and (D.7).
Finally, the last rules stem from parity considerations. For homonuclear molecules, only transitions of different parity, denoted u and g, with respect to inversion operation are allowed $g \leftrightarrow u$. As to heteronuclear molecules, the conditions $+ \leftrightarrow +$ and $- \leftrightarrow -$ apply.

E Hellmann-Feynman theorem.

In this chapter, we will derive the *Hellmann-Feynman* theorem [Güt32, Hel37, Fey39] that relates the derivative of the total energy with respect to a perturbation parameter, to the expectation value of the derivative of the Hamiltonian with respect to the same parameter.

Be a total Hamiltonian operator composed of an unperturbed and a perturbation Hamiltonian that accounts for the effects of a perturbation λ:

$$\hat{\mathcal{H}} = \hat{\mathcal{H}}^{(0)} + \hat{\mathcal{H}}_\lambda, \tag{E.1}$$

if we assume

$$\hat{\mathcal{H}} \left|\psi_H\right\rangle = \varepsilon(\lambda) \left|\psi_H\right\rangle, \tag{E.2}$$

the total energy of the system that depends on the perturbation reads:

$$\varepsilon(\lambda) = \left\langle \psi_H | \hat{\mathcal{H}} | \psi_H \right\rangle = \left\langle \psi_H | \hat{\mathcal{H}}^{(0)} + \hat{\mathcal{H}}_\lambda | \psi_H \right\rangle \tag{E.3}$$

where ψ_H is the exact wavefunction of the system.

The derivation of the Hellmann-Feynman theorem starts with the differentiation of the expectation value of the Hamiltonian Eq. (E.3) with respect to the λ parameter:

$$\frac{\partial \varepsilon(\lambda)}{\partial \lambda} = \left\langle \frac{\partial \psi_H}{\partial \lambda} \left| \hat{\mathcal{H}} \right| \psi_H \right\rangle + \left\langle \psi_H \left| \frac{\partial \hat{\mathcal{H}}}{\partial \lambda} \right| \psi_H \right\rangle + \left\langle \psi_H \left| \hat{\mathcal{H}} \right| \frac{\partial \psi_H}{\partial \lambda} \right\rangle \tag{E.4}$$

where the derivative product rule is applied. Then, if we make use of Eq. (E.2)

$$\begin{aligned} \frac{\partial \varepsilon(\lambda)}{\partial \lambda} &= \varepsilon(\lambda) \left\langle \frac{\partial \psi_H}{\partial \lambda} \middle| \psi_H \right\rangle + \varepsilon(\lambda) \left\langle \psi_H \middle| \frac{\partial \psi_H}{\partial \lambda} \right\rangle + \left\langle \psi_H \left| \frac{\partial \hat{\mathcal{H}}}{\partial \lambda} \right| \psi_H \right\rangle \\ &= \varepsilon(\lambda) \frac{\partial}{\partial \lambda} \left\langle \psi_H | \psi_H \right\rangle + \left\langle \psi_H \left| \frac{\partial \hat{\mathcal{H}}}{\partial \lambda} \right| \psi_H \right\rangle \end{aligned} \tag{E.5}$$

the derivative of the product $\langle\psi_H|\psi_H\rangle$ springs out. Yet, this product is a constant scalar and thus the derivative gives zero and the term vanishes, yielding the Hellmann-Feynman theorem:

$$\frac{\partial\varepsilon(\lambda)}{\partial\lambda} = \left\langle \psi_H \left| \frac{\partial\hat{\mathcal{H}}}{\partial\lambda} \right| \psi_H \right\rangle . \tag{E.6}$$

One has to keep in mind that the theorem only holds for exact wavefunctions and energies. Otherwise, the relation between the derivative of the energy and the derivative of the expectation value of the Hamiltonian operator with respect to a perturbation parameter is only an approximation and the deviation is comprised by the so-called *non-Hellmann-Feynman* terms.

French Summary.

De nos jours, l'incomplétude du modèle standard des particules est largement reconnue. L'une de ses failles les plus évidentes est le manque d'explication de l'énorme excédent de matière par rapport à l'antimatière dans l'univers, que l'on appelle l'asymétrie baryonique de l'univers. De nouvelles violations de $\mathcal{CP}$ (conjugaison de charge et parité spatiale) absentes dans le modèle standard sont supposées être responsables de cette asymétrie. Une telle violation pourrait être observée dans la matière ordinaire à travers un ensemble d'interactions violant les symétries de parité et de renversement du temps (impaires pour $\mathcal{P}, \mathcal{T}$) dont les prépondérantes sont les interactions du moment dipolaire électrique de l'électron (eEDM), électron-nucléon scalaire-pseudoscalaire (enSPS) et du moment quadripolaire magnétique nucléaire (nMQM). Ainsi, une preuve expérimentale d'une constante d'interaction impaire pour $\mathcal{P}, \mathcal{T}$ serait une preuve de cette nouvelle physique au-delà du modèle standard.

Le calcul des paramètres moléculaires correspondants est réalisé en utilisant une approche d'interaction de configurations relativiste à quatre composantes dans des molécules diatomiques polaires contenant un actinide, qui sont des systèmes particulièrement appropriés pour les expériences eEDM, tels que ThO qui a permis d'assigner à l'eEDM la borne supérieure la plus contraignante et ThF^+ qui sera utilisé dans une expérience à venir. Ces résultats sont d'une importance cruciale dans l'interprétation des mesures puisque les constantes fondamentales ne peuvent être évaluées que si l'on associe les mesures de décalages énergétiques et les paramètres moléculaires théoriques.

Contexte général.

L'EDM comme test de nouvelle physique.

L'électron est-il une sphère ?

On parle souvent de la recherche du moment dipolaire électrique(EDM) de l'électron comme de l'étude de la forme de l'électron. En effet, dans un souci de simplification, le sujet compliqué et assez abstrait de l'existence probable d'un mo-

ment dipolaire électrique de l'électron est réduite à la plus simple question de la sphéricité de l'électron. Ainsi, les médias grand public ont relayé les récents résultats des expériences EDM comme la mesure de la sphéricité de l'électron. Cependant, cette description doit être clarifiée puisque l'électron est supposé être un objet ponctuel, même si cette affirmation n'est valide que dans une certaine mesure. En réalité, une valeur limite du rayon de l'électron a été établie en se basant sur la différence entre un moment magnétique électronique mesuré et la valeur théorique donnée par l'électrodynamique quantique(QED) dans le cadre d'un électron ponctuel. La borne supérieure ainsi obtenue est de $R_e < 10^{-18}$ m [HFG08].

En fait, l'enjeu des expériences EDM n'est pas la forme de l'électron lui-même mais l'asphéricité de sa distribution de charge. La détection d'une distortion, d'un écart par rapport à une distribution sphérique est une tâche ardue pour les expérimentateurs car ce qu'ils s'attendant à mesurer est remarquablement petit. Comme image, si la distribution était de la taille du système solaire, la déviation serait de la largeur d'un cheveu [Hin14]. La déviation donne à la distribution de charge une forme ovoïde ou en goutte d'eau qui engendre une différence de charge entre les deux pôles qui implique l'existence d'un moment dipolaire électrique allant d'un côté de la distribution déformée à l'autre.

Violation de symétrie $\mathcal{CP}$ et BAU.

Alors, il n'est pas déraisonalble de se demander pourquoi l'on voudrait s'escrimer à mesurer une quantité si petite. Malgré sa modeste taille, l'asymétrie de la distribution de charge est loin d'être insignifiante pour la compréhension de la physique des particules et la nature de l'univers. Un moment dipolaire électrique d'un électron, et plus généralement d'une particule élémentaire, doit s'aligner parallèlement ou anti-parallèlement avec le spin, selon le théorème de projection pour un opérateur vectoriel $\hat{\mathbf{V}}$:

$$\langle \alpha', JM_J|\hat{V}_q|\alpha', JM_J\rangle = \frac{\langle \alpha', JM_J|\hat{\mathbf{J}}\cdot\hat{\mathbf{V}}|\alpha', JM_J\rangle}{\hbar^2 J^2(J+1)}\langle JM_J|\hat{J}_q|JM_J\rangle^1 \tag{F.7}$$

où α et α' désignent les nombres quantiques invariant par rotation, $\hat{\mathbf{J}}$ est l'opérateur vectoriel du moment angulaire, J le nombre quantique du moment angulaire et M_J sa projection selon l'axe z.

Or, lors d'une transformation de renversement du temps, la direction du spin est renversée tandis que le moment dipolaire électrique permanent, qui est une propriété statique, reste inchangé (voir Fig. F.1), ainsi la particule qui en résulte a une direction d'EDM opposée par rapport au spin. La conservation de la symétrie $\mathcal{T}$ impliquerait la double dégénérescence des particules qui possède à la fois un spin et un EDM,

[1] Ici et dans le reste du manuscrit, les symboles en gras indiquent les quantités vectorielles.

selon leur direction relative, ce qui n'est pas cohérent avec les observations, par conséquent, la symétrie de renversement du temps est nécessairement violée. Le théorème $\mathcal{CPT}$ qui affirme la conservation des symétries de conjugaison de charge, inversion de parité et renversement du temps combinées est supposé valide et mène à la conclusion suivante; l'existence d'un EDM non-nul d'une particule élémentaire violerait conjointement les symétries de conjugaison de charge ($\mathcal{C}$) qui transforme une particule en son anti-particule et d'inversion de parité ($\mathcal{P}$) qui change le signe des coordonnées spatiales. Ceci contredit la déclaration de Landau [Lan57] qui affirmait que la symétrie $\mathcal{CP}$ ne pouvait être violée parce qu'une telle violation "semblerait extrêmement étrange" [Hin97].

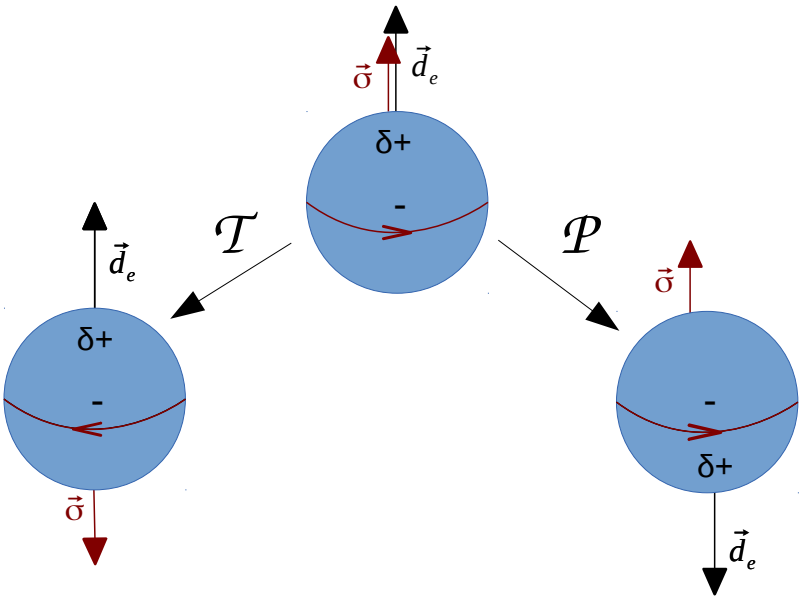

Figure F.1 – Violation des symétries $\mathcal{P}$ et $\mathcal{T}$.

Or, Sakharov [Sak67] a avancé la violation $\mathcal{CP}$ comme une explication de la prédominance de matière par rapport à l'antimatière, également appelée asymétrie baryonique de l'univers (BAU). Il s'agit d'un des plus grands mystères de la physique puisqu'il n'existe toujours aucune théorie qui explique pourquoi l'antimatière est présente en si petite quantité alors que matière et antimatière sont supposées avoir été créées juste après le Big Bang en quantités égales et être régies par les mêmes lois.

Le modèle standard (SM), la théorie la plus concluante de la physique des particules, inclut des phénomènes violant la symétrie $\mathcal{CP}$ qui peuvent être observés tels que les désintégrations des mésons K neutres [Ala99, eaNC99] et B [eaBC01a, eaBC01b]. C'est la conséquence du mélange de saveur dans le secteur des quarks inclu dans la matrice Cabibbo–Kobayashi–Maskawa (CKM) [KM73] Cependant, dans le modèle standard, l'interaction de l'électron avec les quarks engendre un moment dipolaire

électrique permanent extrêmement faible ($10^{-38} e.cm$), qui ne devrait pas être observable dans les expériences et qui ne fournit pas un niveau suffisant de violation $\mathcal{CP}$ pour expliquer l'asymétrie baryonique de l'univers. Alors, des théories allant au-delà du modèle standard ont été développées, les échecs du modèle standard et ces théories seront présentées plus en détails dans la section suivante. Les théories introduisent de nouvelles sources de violation $\mathcal{CP}$ et de nouvelles particules dont les interactions avec l'électron pourraient induire une plus grande asymétrie de la distribution de charge et par conséquence, un EDM plus grand que celui prévu par le modèle standard. Il y aurait un gain de dix ordres de grandeur et l'interaction atteindrait la gamme de valeurs que les expériences actuelles sont capables de mesurer. De surcroît, chaque extension au modèle standard prédit des gammes de valeurs différents pour les EDMs. Ainsi, la détection d'un EDM permanent d'une particule fondamentale permettrait de tester ces théories. Aucun EDM n'a encore été mesuré mais en améliorant la sensibilité de la mesure, les experimentateurs ont pu disqualifier quelques modèles qui prédisaient de trop grandes valeurs pour le moment dipolaire électrique de l'électron, *i. e.* supérieures à la précision actuelle $9.6 \times 10^{-29} e.cm$ [CBC+14]. Les expériences d'EDM sont remarquables parce qu'elles permettent de sonder la nouvelle physique, comme cela est fait dans les super collisionneurs tels que le LHC où les physiciens essaient de créer les nouvelles particules prédites en faisant entrer en collision des protons, mais à très faible énergie dans un laboratoire ordinaire.

Beyond the standard model.

Malgré ses nombreux succès dans la prédiction de phénomènes et de particules, tels que l'existence des bosons W et Z ou la désintégration du bozon Z, tous les deux confirmés expérimentalement au CERN [Rub85, CKS+12], la très élégante description du monde donnée par le modèle standard n'est pas exhaustive. En plus de l'asymétrie baryonique de l'univers, le manquement le plus frappant du modèle standard est l'impossibilité d'y inclure la gravité et son cadre théorique, la *relativité générale*, empêchant ainsi les physiciens de réaliser ce qu'on appelle la *grande unification*. Il y a eu des tentatives d'expliquer la gravité dans le cadre du modèle standard, notamment en ajoutant une particule, le *graviton*; Cependant, aucune ne réussit à recréer les observations expérimentales et expliquer la faiblesse de l'intensité de la force gravitationnelle comparée aux trois autres forces (forces électromagnétique, faible et forte). Cela constitue le *problème de hiérarchie* avec le large spectre de masses parmi les particules élémentaires qui soulève aussi la question de la masse du boson de Higgs plus petite qu'attendue. Un autre échec du modèle standard est qu'il ne rend compte que de la matière visible, que l'on estime ne constituer que 5% de l'univers. Donc, les constituants majeurs ne sont pas décrits par le modèle standard qui ne fournit pas de particules appropriées pour constituer la matière et l'énergie sombres

que l'on estime former respectivement 26% et 69% de l'univers. Même si la matière sombre ne peut être observer, des signes de son existence peuvent être trouvés dans ses effets gravitationnels sur la matière ordinaire. Afin de répondre aux problèmes du modèle standard, un grand nombre d'extensions ont été développées, parmi lesquels se trouvent les modèles symétriques gauche-droite [PS73], les modèles multi-Higgs [Wei76] ou les fameux modèles supersymétriques [HK85]. Les valeurs proposées pour le moment dipolaire électrique de l'électron par ces modèles [Liu86, BZ90, BHS95] et le modèle standard sont rassemblées dans le Tableau F.1, de même que l'actuelle borne supérieure apportée par l'expérience [CBC$^+$14] alliée à la théorie [SPT13] qui a atteint la gamme de valeurs décisive qui permet de contraindre la nouvelle physique et de disqualifier certaines de ces nouvelles théories des particules comme explications probables de l'univers.

Table F.1 – Valeurs prédites du moment dipolaire électrique de l'électron [Com99].

Model	$d_e[e.cm]$
Modèle standard	$< 10^{-38}$
Symétrie gauche-droite	$10^{-28} - 10^{-26}$
Multi-Higgs	$10^{-28} - 10^{-27}$
Supersymétrie	$\leq 10^{-25}$
Borne supérieure expérimentale	9.6×10^{-29}

Les extensions au modèle standard les plus populaires et prometteuses sont ceux qui incluent la supersymétrie. Elles ne cherchent pas à invalider ou remplacer le modèle standard mais à la compléter en comblant ses lacunes. L'idée de base est la prédiction d'un ou plusieurs superpartenaires pour chaque particule ordinaire (*i.e.* inclue dans le modèle standard) qui partageraient des propriétés identiques, à l'exception majeur du spin ; si la particle est un boson (spin entier) alors la super-particule associée sera un fermion (spin demi-entier) et inversement, une particule fermionique aura un superpartenaire bosonique. Les nouvelles particules résoudraient le problème de la masse du boson de Higgs en annulant les contributions venant du modèle standard qui rendent le boson de Higgs lourd.

Toutefois, cette très harmonieuse image du monde est de toute évidence erronée, puisque les superpartenaires sont censés partager la même masse que leur particule associée de même que leurs interactions avec les autres particules connues et non connues et de ce fait, elles devraient déjà avoir été détectées. Alors, les théoriciens ont pensé à des processus qui pourraient avoir brisé la supersymétrie ; c'est en fait ce

qui distingue les nombreux modèles supersymétriques les uns des autres [2]. Quelque soit le méchanisme, il aurait rendu les superpartenaires très massique à tel point qu'aucune expérience n'ait jusqu'à présent atteint un niveau d'énergie suffisant pour les détecter. Il reste de l'espoir de les voir au LHC grâce à la conservation de la parité $\mathcal{R}^3$ qui pose qu'une superparticule ne peut se désintégrer qu'en une autre particule supersymétrique, de sorte que la particule supersymétrique la plus légère (LSP) est extrêmement stable and donc assez facile à trouver, à condition de chercher dans la bonne gamme de masses. De plus, le LSP correspond totalement au profil de la matière sombre - stable, électriquement neutre, intéragissant faiblement avec la matière ordinaire - ce qui résoudrait un autre problème du modèle standard.

Measurer un EDM.

Choix d'un système.

Comme exposé précédemment, les moments dipolaires électriques sont des quantités extrêmement petites, ce qui pose quelques problèmes quand il s'agit de construire une expérience pour les mesurer. L'un est ce qu'on appelle le problème du moment magnétique. Effectivement, les expérimentateurs mesurent un décalage en énergie qui est dû aux effets Stark et Zeeman qui s'écrit : $hw = 2(\mu B + d_e E)$, où μ est le moment dipolaire magnétique. Afin de réduire l'incertitude, ils aspirent à obtenir des interactions de même intensité. Par exemple, considérons l'EDM d'un électron et une valeur cohérente avec la plupart des théories au-delà du modèle standard : $d_e = 5 \times 10^{-28}$ e.cm et un champ électrique de 10 kV/cm, la grandeur typique de fonctionnement dans les expériences atomiques [KSH+12]. Alors, l'interaction EDM est de l'ordre de $d_e \boldsymbol{\sigma} \times \mathbf{E} \approx 1$ nHz et l'interaction magnétique serait de la même grandeur pour un champ magnétique de 10^{-19} T, ce qui est bien trop faible pour être gardé sous contrôle. Ceci devient encore plus évident quand on compare ce nombre au champ magnétique de la Terre qui est de $\approx 5.10^{-5}$ T. De plus, s'il était appliqué sur un électron nu, un champ électrique aussi puissant provoquerait l'accéleration de la particule chargée, rendant la mesure impossible. Par conséquent, les premières expériences EDM ont été réalisées sur des neutrons [SPR57].

En 1965, Sandars [San65] a indiqué la pertinence d'utiliser des atomes dans la recherche de l'EDM de l'électron en remarquant que le théorème de Schiff Sandars [San65] - qui pose qu'un atome n'a pas de moment dipolaire électrique permanent même si l'électron en possède un - devenait caduc quand on prenait en compte la

[2] Le lecteur trouvera des détails sur les différents modèles supersymétriques dans [Lyk10].

[3] La parité $\mathcal{R}$ est une symétrie introduite dans les modèles supersymétriques qui empêche les couplages indésirables qui ne conservent pas les nombres leptonique et baryonique. Il attribue une parité $\mathcal{R}$ $+1$ aux particules et -1 aux superparticules.

relativité. Il a démontré que, non seulement un atome avec un électron célibataire pouvait avoir un moment dipole mais l'EDM d'un électron non apparié serait amplifié et de plusieurs ordres de grandeur plus grand que dans le cas de l'électron libre. Le facteur d'amplification défini comme le rapport de l'EDM atomique sur l'EDM de l'électron [PR05] :

$$R \propto \frac{Z^3\alpha^2}{J(J+\frac{1}{2})(J+1)} \tag{F.8}$$

avec J, le moment angulaire et Z, le nombre atomique. Il en résulte une amplification de quelques centaines pour un électron dans un atome lourd électriquement paramagnétique tel que le Césium, Thallium dont les facteurs respectifs sont +114 [HLMP] and −585 [LK92]. Le résultat le plus précis obtenu par un expérience atomique a été donné par l'expérience de Berkeley sur l'atome de Thallium qui a réussi à produire un champ électrique de 100 kV/cm. L'interprétation de leur mesure associée au facteur d'amplification calculé par [LK92] a mené à une borne supérieure pour l'EDM de l'électron de $|d_e| \leq 1.6 \times 10^{-27}$e.cm [RCSD02]. Cependant, les expériences atomiques font face à des difficultés qui empêchent les physiciens d'améliorer plus avant la sensibilité. Entre autres problèmes, comme expliqué précédemment, il y a le contrôle des champs magnétiques parasites qui imitent l'effet d'un EDM. Un des plus importants est le champ magnétique engendré par le mouvement de l'électron dans le champ électrique appliqué :

$$\mathbf{B}_m = \frac{\mathbf{v}}{c^2} \times \mathbf{E} \tag{F.9}$$

et qui est beaucoup plus grand que le femtoTesla (fT) nécessaire pour avoir des interactions magnétique et électrique de même intensité. Même si les expérimentateurs ont développé des stratégies pour répondre à ces enjeux, il est apparu qu'une nouvelle génération d'expériences était requise, c'est là que les molécules diatomiques entrent en jeu. De telles molécules sont plus sensibles à l'effet de l'existence d'un EDM de l'électron, le facteur d'amplification peut atteindre 10^6, plusieurs ordres de grandeur plus grand que dans les atomes. Remarquons que dans le cadre moléculaire, le facteur d'amplification R n'est plus pertinant, il faut définir le champ électrique effectif $\mathcal{E}_{\text{eff}}$ lié au champ électrique interne des molécules $\mathcal{E}_{int}$ via $\langle \mathbf{d_e} \cdot \boldsymbol{\mathcal{E}}_{int} \rangle = d_e \mathcal{E}_{\text{eff}}$ et à R par $R = \frac{\mathcal{E}_{\text{eff}}}{\mathcal{E}_{\text{lab}}}$ car le champ électrique dépend de la polarisation et n'est plus proportionnel au champ électrique apliqué $\mathcal{E}_{\text{lab}}$. Sur la Figure F.2, the champ électrique effectif $\mathcal{E}_{\text{eff}}$ est tracé en fonction du champ électrique appliqué $\mathcal{E}_{\text{lab}}$. La forme non linéaire due au facteur de polarisation est celle d'un rotateur rigide et la valeur asymptotique du champ électrique $\mathcal{E}_{\text{eff,max}}$ doit être déterminé théoriquement, ce qui est un des buts de cette thèse.

Dans les molécules diatomiques, la grandeur de l'intéraction à détecter est de l'ordre du mHz et le champ magnétique ne doit être controlé qu'au niveau du pT ce

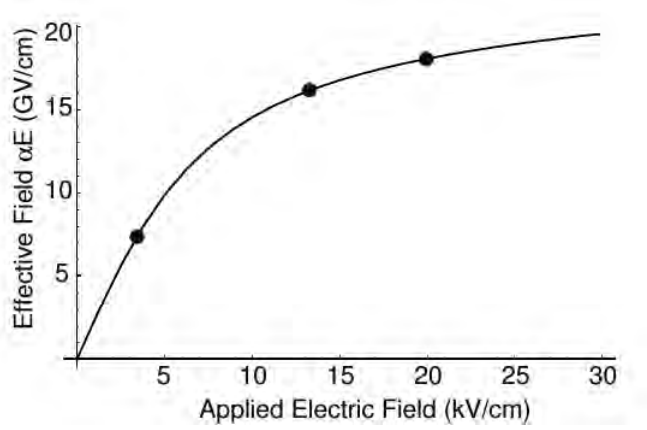

Figure F.2 – Facteur d'amplification pour YbF [SAHH06].

qui reste faible mais raisonnable. D'autant plus que de nombreuses caractéristiques des molécules choisies tendent à supprimer ou au moins à fortement réduire les effets des champs magnétiques. Tout d'abord, ce genre de molécules posséde une large polarisabilité électrique qui ne garantit pas seulement un grand facteur d'amplification et une complète polarisation dans un modeste champ électrique de laboratoire $\mathcal{E}_{\text{lab}}$ (de l'ordre de 1′0 V/cm pour ThO [VSG$^+$11]), minimisant la puissance du champ magnétique dû à la fuite de courant et rendant l'écart à mesurer indépendant du champ électrique de laboratoire, mais cela assure aussi un large écart de Stark qui annule l'effet du champ magnétique de mouvement (F.9).

La large polarisabilité est garantie par la structure de doublet Ω qui apporte d'autres avantages pour la détection d'un EDM de l'électron. L'un est la possibilité pour les experimentateurs de réaliser le renversement spectroscopique. Chacun des deux état du doublet Ω possède un dipole et donc un champ électrique effectif respectivement aligné parallèlement ou anti-parallèlement avec le champ électrique de laboratoire. Ainsi, cela donne accès à l'interaction inverse sans avoir à renversé le champ électrique appliqué. Dans une section à venir, il sera expliqué en quoi cela constitue un avantage pour l'expérience.

Enfin, de nombreuses expériences sont menées sur des molécules qui présentent un état $^3\Delta_1$ de basse énergie, comme ThO, HfF^+ ou ThF^+, qui dérive d'une occupation $s^1 d_\delta^1$. Cette configuration est vraiment appropriée puisqu'elle garantit les caractéristiques principales requises pour avoir un EDM non nul et une molécule diatomique très polaire, ces avantages ont été mis en avant pour la première fois par [MBD06]. En effet, l'électron "de science" qui occupe l'orbital s subit l'amplification relativiste de l'EDM de l'électron grâce au bon recouvrement avec le noyau tandis que l'electron d_δ "de spectroscopie" permet la grande polarisabilité de la molécule. De plus, le moment magnétique total qui s'écrit $m_\Omega = -g_s \mu_B (\Sigma + \frac{\Lambda}{2})$ avec g_s le facteur g de spin, μ_B le magnéton de Bohr, Σ le nombre quantique de spin total et

Λ le nombre quantique orbital total, s'annule puisque dans l'état qui nous intéresse, on a $\Sigma = -1$ et $\Lambda = 2$ ou $\Sigma = 1$ et $\Lambda = -2$ [4]. Cette propriété réduit encore plus les effets des champs $\mathcal{B}$ résiduels.

Les expériences EDM actuelles, de même que les précédentes, ne mesurent pas mais plutôt améliorent la sensibilité pour pouvoir assigner une borne supérieure limite à l'EDM. Toutefois, l'objectif ultime est bien entendu de réellement mesurer un EDM de l'électron. Le facteur de qualité pour l'incertitude expérimentalement qui rend compte du bruit statistique, c'est-à-dire la meilleure sensibilité atteignable, est :

$$\delta d_e = \frac{\hbar}{2\mathcal{E}_{\text{eff}}\tau\sqrt{N}} \tag{F.10}$$

où τ est le temps de cohérence, N le nombre de mesures soit N=$\dot{\text{N}}$T avec $\dot{\text{N}}$ le taux de détection et T la période d'intégration de l'expérience. Dans le tableau F.2, nous avons rassemblé la valeur de ces paramètres dans les expériences eEDM les plus récentes pour comparaison.

Table F.2 – Comparaison des paramètres du facteur de qualité dans les expériences eEDM les plus récentes[LBL+11, Stu10].

Groupe	Molécule	$\mathcal{E}_{\text{lab}}$(V/cm)	$\mathcal{E}_{\text{eff}}$(V/cm)	τ(s)	$\dot{\text{N}}$(s^{-1})
Imperial College	YbF	8.3×10^3	1.3×10^{10}	10^{-3}	
ACME	ThO	10^2	10^{11}	2×10^{-3}	10^5
JILA	HfF^+	5	2×10^{10}	0.3	10

Processus expérimental.

La figure F.3 montre le schéma de mesure de l'expérience ThO mené par la collaboration ACME qui a fourni la limite la plus restrictive de l'EDM de l'électron. La détermination du moment dipolaire électrique moléculaire qui permet l'évaluation du moment dipolaire électrique de l'électron est réalisé par l'intermédiaire d'une série de mesures du décalage d'énergie entre les différents sous-niveaux $^3\Delta_1$.

Décrivons la structure de l'ensemble d'états. Dans de tels états, les nombres quantiques appropriés sont J, M_J, Ω où Ω est la valeur absolue de la projection du moment angulaire électronique total J_e selon l'axe moléculaire, J est le moment angulaire total, somme de J_e et de la rotation nucléaire R, et M_J est sa projection selon l'axe moléculaire.

[4] Cette affirmation est valide parce que dans cet état spécifique, le cas de Hund (a) reste approprié. Pour plus de détails sur les cas de Hund, voir Appendix A.

Figure F.3 – Structure de niveaux d'énergie de ThO dans l'état $^3\Delta_1(J=1)$ dans des champs électrique et magnétique appliqués [VCG+].

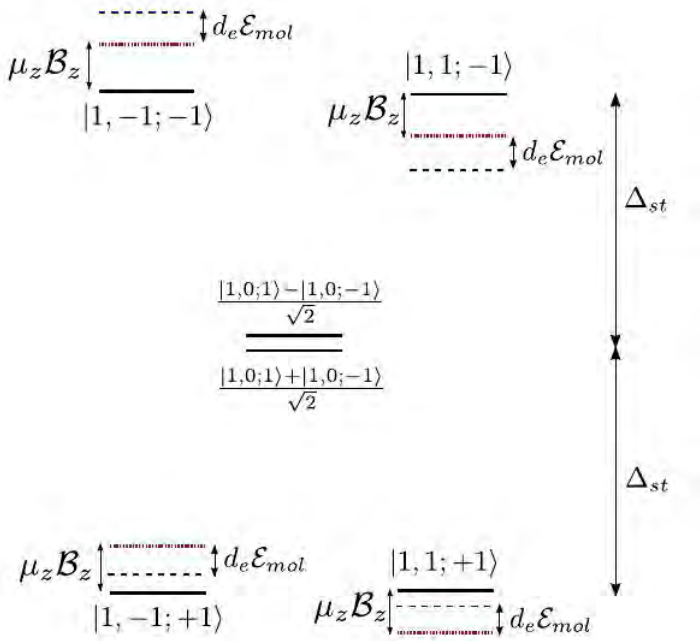

En l'absence du champ électrique externe, les états propres du sytème sont les états de parité $|\pm\rangle = (|\Omega=+1\rangle \pm |\Omega=-1\rangle)$ selon la superposition symétrique ou anti-symétrique des deux états $|\Omega|=1$ séparés par l'énergie de doublement de Ω.
Quand un champ électrique externe, suffisamment grand pour polariser la molécule, est appliqué, les états propres sont mélangés, ce qui donne des états $M_J = \pm 1$ bien décrits par le cas (c) de Hund pour lesquels le bon nombre quantique est Ω. Ils sont séparés en pairs de niveaux qui correspondent à $\mathcal{N} = \pm 1$ où $\mathcal{N}$ reflète l'alignement ou l'anti-alignement du dipole moléculaire (et donc de $\mathcal{E}_{eff}$) avec le champ électrique externe $\mathcal{E}_{lab}$. (Le lecteur notera que les états $M_J = 0$ ne sont pas perturbés par le champ électrique.)
Pour finir, l'application d'un champ magnétique externe ($\mathcal{B}$) et l'existence d'un EDM permanent de l'électron (d_e) alliés à un champ électrique interne induisent des décalages Zeeman et EDM qui s'ajoutent à l'effet Starck pour arriver à l'écart d'énergie suivant:

$$\Delta E_H = -\tilde{\mathcal{N}} d(J)|\mathcal{E}| - M_J g(J)\mu_B \tilde{\mathcal{B}}|\mathcal{B}| - M_J \tilde{\mathcal{N}}\eta\mu_B|\mathcal{E}|\tilde{\mathcal{B}}|\mathcal{B}| - M_J\tilde{\mathcal{N}}\tilde{\mathcal{E}} d_e \mathcal{E}_{eff} \quad \text{(F.11)}$$

où $d(J)$ et $g(J)$ sont respectivement le moment dipolaire électrique et les facteurs g de l'état J, η reflète la diffèrence de $g(J)$ entre les paires $\mathcal{N}$ et une quantité marquée avec un "~" indique le signe de cette quantité qui sera renversé pendant l'expérience, $\tilde{\mathcal{N}} = sign(\mathcal{N})$, $\tilde{\mathcal{B}} = sign(\mathbf{B}\cdot\mathbf{e_z})$ et $\tilde{\mathcal{E}} = sign(\mathbf{E}\cdot\mathbf{e_z})$ où $\mathbf{e_z}$ est le vecteur unitaire

Figure F.4 – Structure des niveaux d'énergie de HfF^+ dans l'état $^3\Delta_1(J = 1)$ incluant l'écart hyperfin respectivement en l'absence de champ électrique (a), en présence d'un champ électrique externe (b) et sous l'effet d'un champ magnétique appliqué en sus d'un champ éléctrique et de l'existence d'un eEDM permanent (c) [LBL+11].

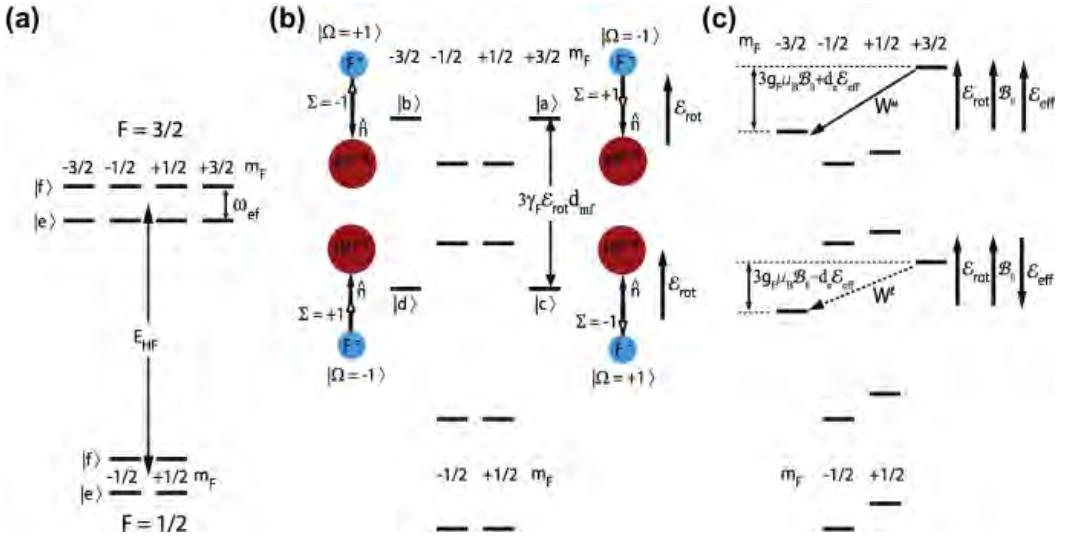

le long de l'axe moléculaire. Notons que les différents niveaux $\mathcal{N}$ présentent des décalages Stark opposés quand l'effet Zeeman a un signe opposé pour deux niveaux M_J et la direction de l'EDM de l'électron est déterminée par M_J. Ces propriétés permettent d'isoler un effet des autres en jouant avec le jeu de paramètres $\{\tilde{\mathcal{B}}, \tilde{\mathcal{E}}, \tilde{\mathcal{N}}\}$. Ainsi, en mesurant la différence d'énergie entre les états $M_J = \pm 1$ à travers un mesure de précession de spin :

$$\Delta E(\mathcal{N}) = 2(\mathcal{N} d_e \mathcal{E}_{eff} + g_{\mathcal{N}} \mu_B \mathcal{B}), \tag{F.12}$$

et en commutant entre les paires $\mathcal{N} = \pm 1$, on peut déterminer l'interaction eEDM indépendamment du champ magnétique :

$$\Delta E(1) - \Delta E(-1) = 4 d_e \mathcal{E}_{eff}. \tag{F.13}$$

Toutefois, la mesaure n'est pas totalement à l'abri de l'effet de champs magnétiques à cause de la différence non nulle de $g(J)$ entre les deux niveaux $\mathcal{N}$.

Le schéma de l'expérience JILA (Figure F.4) est très similaire à celui employé par ACME. La spécificité des expériences menées à JILA est l'emploi de cette méthode sur des ions moléculaires qui fournissent des atouts supplémentaires pour la mesure, en particulier de longues périodes de cohérence dues à la facilité de les piéger.

Interactions impaires pour $\mathcal{P}, \mathcal{T}$.

Afin de compléter et affiner les assertions de la section précédente, il convient de souligner que le moment dipolaire électrique d'un système donné inclut plusieurs contributions possibles, ne provenant pas seulement du supposé EDM de l'électron. Ainsi, l'EDM d'un système peut s'écrire comme une somme sur les différentes sources,

$$d_i = \sum_j \alpha_{ij} C_j \tag{F.14}$$

où les C_j sont les paramètres fondamentaux qui violent les symétries $\mathcal{P}$ et $\mathcal{T}$ et qui rendent compte de la force des interactions correspondantes qui ne conservent pas $\mathcal{CP}$ et α_{ij}, les facteurs d'amplification dépendants du sytème pour lesquels des calculs théoriques sont nécessaires. En prenant en compte les sept contributeurs majeurs, Eq. (F.14) peut être développé [CRM15]:

$$d = \alpha_{d_e} d_e + \alpha_{C_S} C_S + \alpha_{C_T} C_T + \alpha_{\bar{d}_n} \bar{d}_n + \alpha_{\bar{d}_p} \bar{d}_p + \alpha_{g_\pi^0} \bar{g}_\pi^0 + \alpha_{g_\pi^1} \bar{g}_\pi^1 \tag{F.15}$$

où d_e est l'EDM de l'électron, C_S, C_T et C_P sont respectivement les constantes scalaire-pseudoscalaire, tenseur-pseudotenseur et pseudoscalaire-scalaire de l'interaction électron-nucléon, $\bar{d}_n$ et $\bar{d}_p$ sont les contributions à faible distance aux EDMs du proton et du neutron et $\bar{g}_\pi^0$ et $\bar{g}_\pi^1$ sont les constantes des couplages isoscalaire et isovecteur pion-nucleon.

Dans le secteur paramagnétique dans le champ d'application de cette thèse, les paramètres contributeurs dominants sont d_e et C_S. Des contraintes limites plus robustes et indépendantes des modèles peuvent être assignées sur ces constantes d'interaction [Jun13]. Premièrement, il faudrait prendre en compte le paramètre scalaire-pseudoscalaire électron-nucleon que l'on pourrait naïvement fixer à zéro. De même, pour affiner les limites supérieures, l'on doit considérer les incertitudes expérimentales et l'incertitude numérique sur le rapport théorique $\frac{\alpha_{C_S}}{\alpha_{d_e}}$. Enfin, de meilleurs contraintes sur d_e et C_S sont établis à travers une correspondance des résultats obtenus par les récentes mesures sur les systèmes paramagnétiques Tl, YbF et ThO qui présentent une combinaison similaire des deux termes. De cette façon, comme montré sur la Fig. F.5, des ellipses d'erreur sont obtenues et permettent d'attribuer aux paramètres des limites plus robustes.

Afin d'extraire des expériences les constantes fondamentales d_e, $k_{\mathcal{P},\mathcal{T}}$ et M, respectivement le moment dipolaire électrique de l'électron, la constante scalaire-pseudoscalaire sans dimension et le moment quadrupolaire magnétique nucléaire, la détermination de paramètres moléculaires est requise. Ces paramètres sont évalués comme valeurs moyennes sur la fonction d'onde de l'état considéré caractérisé par le nombre quantique Ω, projection du moment électronique total sur l'axe moléculaire.

Figure F.5 – Correspondance dans le plan $d_e - C_S$ des résultats expérimentaux récents dans les systèmes paramagnétiques [Jun15].

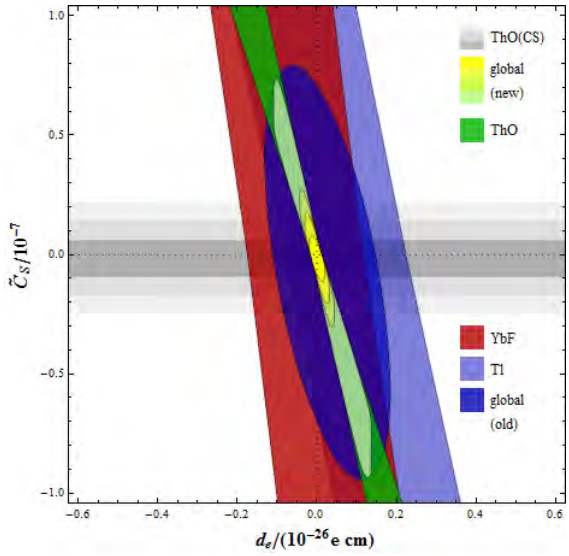

Le facteur de l'interaction de l'EDM de l'électron est donné par

$$W_d := \frac{2\imath c}{\Omega e\hbar}\left\langle \sum_{j=1}^{n} \gamma_j^0\gamma_j^5\mathbf{p}^2 \right\rangle_{\psi_\Omega}, \tag{F.16}$$

l'interaction scalaire-pseudoscalaire électron-nucléon impaire pour $\mathcal{P},\mathcal{T}$ est caractérisée par

$$W_{\mathcal{S}} := \frac{\imath G_F}{\Omega\sqrt{2}} Z \left\langle \sum_{j=1}^{n} \gamma_j^0\gamma_j^5\rho_N(\mathbf{r}) \right\rangle_{\psi_\Omega} \tag{F.17}$$

et l'interaction du MQM nucléaire avec les électrons est décrite par

$$W_M := \frac{3}{2\Omega}\left\langle \sum_{j=1}^{n} \left(\frac{\boldsymbol{\alpha}_j \times \mathbf{r}_{jA}}{r_{jA}^5}\right)_k (r_{jA})_k \right\rangle_{\psi_\Omega}. \tag{F.18}$$

Les valeurs des paramètres d'interaction ne peuvent être obtenues que par calcul théorique qui nécessite une détermination précise de la stucture électronique du système. Une manière d'en tester la précision est de calculer un paramètre avec des caractéristiques similaires à celles des constantes d'interaction impaires pour les symétries $\mathcal{P},\mathcal{T}$, *inter alia*, la sensibilité à la densité de spin électronique au voisinage du noyau. Cependant, contrairement aux constantes, le paramètre test de la qualité de la fonction d'onde doit être mesurable. La constante d'interaction hyperfine magnétique parallèle $A_{||}$ satisfait ces conditions. Dans la suite, la théorie hyperfine sera développée et la constante d'interaction hyperfine magnétique parallèle dérivée.

Interaction hyperfine.

Dans le conteste de la recherche de nouvelle physique au-delà du modèle standard à travers la détermination de la valeur ou d'une borne supérieure des constantes impaires sous les transformations $\mathcal{P}, \mathcal{T}$, il est instructif et nécessaire, à plus d'un titre d'examiner l'interaction hyperfine. Entre autres, comme exposé plus haut, la constante d'interaction hyperfine magnétique présente des caractéristiques analogues à celles des constantes impaires pour $\mathcal{P}, \mathcal{T}$ que nous recherchons. L'une d'elles est la forte dépendance en la densité électronique près du noyau. Cette qualité permet d'obtenir des informations précieuses concernant la fonction d'onde et en particulier, la densité de spin au voisinage du noyau. De surcroît, d'un point de vue expérimental, il est crucial de connaître avec une grande précision l'énergie des différents états électroniques. Ce dernier impose d'identifier les niveaux hyperfins. La bonne connaissance des états est utile pour élaborer un procédé de préparation des états et identifier et limiter les incertitudes des mesures.

Foldy-Wouthuysen Transformation.

Pour avoir un aperçu du sens physique de l'équation de Dirac à quatre composantes, il est utile de cherche un hamiltonien à deux composantes qui contiendrait les champs électromagnétiques et resterait relativiste. Une telle méthode a été développée par Foldy et Wouthuysen [FW50] et sera employé dans la suite.

L'hamiltonien de Dirac $\mathcal{H} = c\boldsymbol{\alpha} \cdot \boldsymbol{p} + \beta m_0 c^2$ pour une particule libre ou $\mathcal{H} = c\boldsymbol{\alpha} \cdot (\boldsymbol{p} + e\boldsymbol{A}) + \beta m_0 c^2 - e\phi$ dans un champ électromagnétique connecte les états d'énergies négative et positive. L'objectif de ce travail est de dériver un hamiltonien relativistiquement correct dans une forme de Pauli à deux composantes qui n'agit que sur les états d'énergie positive. Nous pouvons séparer les termes qui couplent les fonctions d'onde électronique et positronique des termes non couplant dans l'hamiltonien. Ils seront respectivement appelés opérateurs impairs ($\mathcal{O}$) et pairs ($\mathcal{E}$) Alors, nous écrivons :

$$\mathcal{H} = \beta m_0 c^2 + \mathcal{E} + \mathcal{O} \tag{F.19}$$

où $\mathcal{E} = -e\phi$ et $\mathcal{O} = c\,\boldsymbol{\alpha}\cdot\,[\boldsymbol{p} + e\boldsymbol{A}]$. Même si $\beta m_0 c^2$ a des éléments de matrice nuls entre les fonctions d'onde électroniques et positroniques, nous ne l'incluons pas dans l'opérateur $\mathcal{E}$ car son ordre de grandeur est beaucoup plus grand. Nous nous efforcerons par le moyen de transformations unitaires successives, de diminuer l'ordre de grandeur de l'opérateur impair jusqu'à ce qu'il s'annule dans un hamiltonien correct à l'ordre $\frac{1}{c^2}$[BC03, Str98]. Définissons la transformation de Foldy-Wouthuysen [FW50]. Dans le cas stationnaire, le nouvel hamiltonien $\mathcal{H}'$ après une transformation

de Foldy-Wouthuysen sera donné par :

$$\mathcal{H}' = e^{i\bar{S}}\mathcal{H}e^{-i\bar{S}}. \tag{F.20}$$

avec l'opérateur $\bar{S}$ défini tel que :

$$\bar{S} = -\frac{i\beta\mathcal{O}}{2m_0c^2} \tag{F.21}$$

où $\mathcal{H}$ est l'hamiltonien actuel et $\mathcal{O}$ sa partie impaire.

En développant les exponentielles,

$$e^{i\bar{S}} = 1 + i\bar{S} + \frac{i^2}{2!}\bar{S}^2 + \frac{i^3}{3!}\bar{S}^3 + \frac{i^4}{4!}\bar{S}^4 + \dots \text{ et } e^{-i\bar{S}} = 1 - i\bar{S} + \frac{i^2}{2!}\bar{S}^2 - \frac{i^3}{3!}\bar{S}^3 + \frac{i^4}{4!}\bar{S}^4 + \dots \tag{F.22}$$

et les remplaçant dans (F.20) jusqu'à l'ordre $\bar{S}^4$, nous obtenons :

$$\begin{aligned}
&e^{i\bar{S}_i}\mathcal{H}e^{-i\bar{S}_i} \\
=&\mathcal{H} - \mathcal{H}i\bar{S} + \mathcal{H}\frac{i^2}{2!}\bar{S}^2 - \mathcal{H}\frac{i^3}{3!}\bar{S}^3 + \mathcal{H}\frac{i^4}{4!}\bar{S}^4 + i\bar{S}\mathcal{H} - i\bar{S}\mathcal{H}i\bar{S} + i\bar{S}\mathcal{H}\frac{i^2}{2!}\bar{S}^2 + i\bar{S}\mathcal{H}\frac{i^3}{3!}\bar{S}^3 \\
&+ \frac{i^2}{2!}\bar{S}^2\mathcal{H} - \frac{i^2}{2!}\bar{S}^2\mathcal{H}i\bar{S} + \frac{i^2}{2!}\bar{S}^2\mathcal{H}\frac{i^2}{2!}\bar{S}^2 + \frac{i^3}{3!}\bar{S}^3\mathcal{H} - \frac{i^3}{3!}\bar{S}^3\mathcal{H}i\bar{S} + \frac{i^4}{4!}\bar{S}^4\mathcal{H} + O(\bar{S}^5) \\
=&\mathcal{H} + i[\bar{S},\mathcal{H}] + \frac{i^2}{2!}[\bar{S},[\bar{S},\mathcal{H}]] + \frac{i^3}{3!}[\bar{S}[\bar{S},[\bar{S},\mathcal{H}]]] + \frac{i^4}{4!}[\bar{S}[\bar{S}[\bar{S},[\bar{S},\mathcal{H}]]]] + O(\bar{S}^5)
\end{aligned} \tag{F.23}$$

Ainsi, l'hamiltonien après la transformation sera donnée par :

$$\mathcal{H}' = \mathcal{H}[\bar{S},\mathcal{H}] + \frac{i^2}{2!}[\bar{S},[\bar{S},\mathcal{H}]] + \frac{i^3}{3!}[\bar{S}[\bar{S},[\bar{S},\mathcal{H}]]] + \frac{i^4}{4!}[\bar{S}[\bar{S}[\bar{S},[\bar{S},\mathcal{H}]]]] \tag{F.24}$$

Après deux transformations et quelques substitutions pour faire apparaitre les champs électrique et magnétique, on obtient l'hamiltonien suivant:

$$\begin{aligned}
\mathcal{H}'' =&\beta m_0c^2 - e\phi + \frac{\beta\boldsymbol{\pi}^2}{2m_0} + \beta g_S\mu_B\boldsymbol{S}\cdot\boldsymbol{B} + \frac{e\hbar^2}{8m_0^2c^2}\nabla\cdot\boldsymbol{E} \\
&- \frac{e\hbar}{4m_0^2c^2}\boldsymbol{S}\cdot(\boldsymbol{\pi}\times\boldsymbol{E} - \boldsymbol{E}\times\boldsymbol{\pi}) - \frac{\beta\boldsymbol{\pi}^4}{8m_0^3c^2}.
\end{aligned} \tag{F.25}$$

Dans un effort d'analyse de l'hamiltonien qui agit seulement sur les états d'énergie positive, nous posons $\beta = 1$ et remplaceons les matrices σ 4×4 par les matrices 2×2 σ puisque l'hamiltonien est maintenant exclusivement pair. Il nous reste alors sept termes auxquels nous donnons un sens physique. Les trois premiers terms sont facilement interprétés, il s'agit de l'énergie de masse au repos, de l'énergie potentielle électrique et de l'énergie cinétique de l'électron. De plus, le septième terme $-\frac{\beta\boldsymbol{\pi}^4}{8m_0^3c^2}$ est une correction relativiste à l'énergie cinétique. Le quatrième terme $g_S\mu_B\boldsymbol{S}\cdot\boldsymbol{B}$ est l'interaction du moment magnétique de spin avec le champ magnétique qui mène au couplage spin-orbit. Enfin, le cinquième term qui n'a aucun équivalent en mécanique quantique non-relativiste est appelé terme de Darwin et le sixième montre l'interaction d'un moment électrique perpendiculaire créé par un moment magnétique en mouvement avec le champ électrique.

Constante d'interaction hyperfine magnétique.

Le paramètre qui caractérise l'interaction hyperfin et qui peut être un test de la précision de la détermination des constantes impaires pour $\mathcal{P},\mathcal{T}$ est la constante d'interaction hyperfine magnétique parallèle $A_{||}$. Il rend compte de l'interaction de deux moments dipolaires magnétiques, respectivement ceux du noyau et de l'électron, qui mène au couplage du spin nucléaire $\mathbf{I}$ et du moment électronique total $\mathbf{J} = \mathbf{S} + \mathbf{L}$ where $\mathbf{S}$ est le spin de l'électron et $\mathbf{L}$ est son moment angulaire. Dans les travaux qui seront présentés dans cette thèse, la constante hyperfine est évaluée dans des molécules diatomiques qui constituent des systèmes à plusieurs électrons. Alors, l'expression adéquat pour un noyau A est

$$A_{||} = \frac{\mu_z(A)}{I\Omega} \left\langle \sum_{i=1}^{n} \left(\frac{\vec{\alpha}_i \times \vec{r_{iA}}}{r_{iA}^3} \right)_z \right\rangle_\psi . \tag{F.26}$$

où l'opérateur est sommé sur les n électrons i de la molécule.

Cette constante est calculée numériquement sur un pied d'égalite avec les paramètres impaires pour $\mathcal{P},\mathcal{T}$ comme une valeur moyenne sur la fonction d'onde moléculaire de l'état électronique d'intérêt.

Etude théorique de ThF^+.

Le travail présenté ci-dessous a été publié en partie dans : M. Denis, M. S. Norby, H. J. A. Jensen, A. S. P. Gomes, M. K. Nayak, S. Knecht, and T. Fleig, New J. Phys. 17, 043005 (2015), *Theoretical study on ThF^+, a prospective system in search of time-reversal violation.* [DNJ$^+$15]

Les états électroniques de basse énergie de ThF^+, un candidat possible pour la recherche de violation des symétries $\mathcal{P}$ et $\mathcal{T}$, ont été étudiés en utilisant les approches *ab initio* multiréférencielles relativistes hautement corrélées de cluster couplé et d'interaction de configurations. Pour la composante avec $\Omega = 1$ de l'état $^3\Delta$ ("état de science" du moment dipolaire électrique de l'électron) nous obtenons un champ électrique effectif de $E_{\text{eff}} = 35.2 \left[\frac{\text{GV}}{\text{cm}}\right]$, une constante d'interaction impaire pour $\mathcal{P}$ et $\mathcal{T}$ électron-nucléon de $W_{P,T} = 48.4$ [kHz], une constante d'interaction hyperfine magnétique de $A_{||} = 1833$ [MHz] pour ^{229}Th ($I = 5/2$), et un très grand moment dipolaire moléculaire de 4.03 [D]. L'état $\Omega = 1$ est identifié comme étant plus de 300 cm^{-1} plus bas en énergie que $\Omega = 0^+$ ($^1\Sigma^+$), remettant en cause l'assignation des états d'une étude théorique précédente sur ces espèces [Barker et al, J. Chem. Phys **136**, 104305 (2012)].

L'énorme surplus de matière sur l'anti matière dans notre univers est un fait qui reste inexpliqué par le modèle standard (SM) des particules élémentaires [DK04]. Une violation microscopique des symétries de conjugaison de charge ($\mathcal{C}$) et de parité

spatiale ($\mathcal{P}$) a été identifiée comme une des différentes conditions [Sak67] qui peut donner naissance à un nombre baryonique notable et expliquer cette asymétrie. Il est attendu que la violation de $\mathcal{CP}$ diagonale en saveur, absente dans le modèle standard, doit être recherchée [PR05] et que les moments dipolaires électriques (EDMs) [FSB03] constituent un test sensible d'une telle nouvelle physique au-delà du modèle standard. Etant donnée la validité du théorème $\mathcal{CPT}$ [SW64],la mesure d'un EDM serait la première signature de violation d'invariance par renversement du temps ($\mathcal{T}$) [Sac87].

L'EDM de l'électron, malgré une recherche vigoureuse depuis un demi-siècle, n'a toujours pas été détecté. les bornes supérieurs les plus contraignantes pour l'EDM de l'électron ont, pendant un temps, été obtenues à partir des recherches expérimentales et théoriques sur des atomes [RM09, LK92], et de telles bornes supérieures sont des contraintes directrices utiles sur les théories au-delà du modèle standard [BS91]. Cependant, les molecules diatomiques polaires sont devenues des acteurs majeurs dans cette quête, puisqu'ils offrent une amplification de plusieurs ordres de grandeur plus grande [SF78, RM09] des décalages d'énergie subséquents que ce qui pourrait être réalisé avec un atome [San65, RCSD02]. Cela signifie que, pour une mesure donnée dans un système moléculaire, l'intensité possible de l'EDM de l'électron est contrainte à une plus petite valeur, ou inversement, que l'effet d'un plus petit EDM de l'électron peut être détecté à travers la mesure. Le facteur d'amplification correspondant n'est pas accessible par des moyens expérimentaux et doit être déterminé – préférablement – *via* un calcul relativiste moléculaire à plusieurs corps.

Selon les découvertes les plus récentes utilisant la molécule polaire ThO [CBC$^+$14, FN14, SPT13, DeM] la borne supérieure sur l'EDM de l'électron est $|d_e| < 9.6 \times 10^{-29}\, e\,\mathrm{cm}$. Cette valeur est plus que 16 fois plus petite que la borne supérieure la plus contraignante venant d'une étude atomique [RCSD02]. Les molécules chargées offrent un avantage expérimental sur les sytèmes neutres, en ce que les pièges à ions peuvent être utilisés, ce qui permet de longues périodes d'interrogation. La spectroscopie à haute résolution qui emploie des champs électriques en rotation a été présentée récemment comme une technique viable pour les recherches de violation de symétries dans des ions moléculaires chargés [LBL$^+$11, CGS$^+$12]. Les systèmes ioniques employés dans ces expériences sont HfF^+ et, comme perspective l'ion moleculaire, ThF^+.

Ce que les molécules susmentionnées, et quelques autres telles que HfH^+, PtH^+ [MBD06] et WC [LCS$^+$13, WS11], ont en commun est un état électronique $^3\Delta$ de basse énergie (dans la représentation du couplage Λ-S). Dans les fluorures et oxides cet état est profondément lié, ce qui est un avantage expérimental. Le moment magnétique dans la composante $\Omega = 1$ de ce terme est approximativement zéro, ce qui aide à réduire la vulnérabilité de l'expérience à la décohérence et aux erreurs systématiques [LBL$^+$11].

HfF^+ et ThF^+ présentent un champ électrique effectif EDM considérablement

grand dans l'état "de science" pertinent [PMIT07, FN13, MB08] et, en même temps, un petit écart de doublet Λ (ou Ω). Cette dernière propriété est un atout pour un mélange efficace des états propres rotationnels de parité à travers le champ électrique externe de laboratoire. Tandis que HfF^+ a été caractérisé en détail [AHT04, BABH11, PMIT07, PMT09, SMPT08, FN13], on en connait considérablement moins pour ThF^+ [MB08, BAHP12, Iri12]. Le travail expérimental et théorique de Barker *et al.* [BAHP12] a laissé quelques incertitudes quant à savoir si l'état $\Omega = 1$ est l'état fondamental ou le premier état excité, comme il y a un état $\Omega = 0^+$ ($^1\Sigma_0^+$) séparé de seulement 315 cm^{-1}. La résolution expérimentale n'était pas suffisante pour assigner ces états sans équivoque and, contrairement à HfF^+, les états $\Omega = 1$ et 0^+ possèdent des fréquences vibrationnelles similaires autour de 658 cm^{-1}. Les calculs théoriques accompagnants étaient aussi non concluant, mais à partir de la meilleure estimation l'état $\Omega = 0^+$ a été proposé comme état fondamental avec l'état $\Omega = 1$ plus haut de respectivement 65 cm^{-1} dans la référence [BAHP12] et 202 cm^{-1} dans la référence [HBA14a].

Quant au champ électrique effectif EDM dans $\Omega = 1$ de ThF^+, le travail de Meyer *et al.* [MB08] suggère une valeur extrêmement grande de $E_{\text{eff}} = 90 \left[\frac{\text{GV}}{\text{cm}}\right]$. Des calculs relativistes récents et plus rigoureux à plusieurs corps sur la molécule isoélectronique ThO a montré [FN14, SPT13] que le modèle de calcul de *et al.* apportait un E_{eff} significamment surestimé pour le cas de ThO (de plus de 35%). On peut alors s'attendre pour ce genre de molécules et états électroniques à ce que le modèle de Meyer *et al.* contienne une erreur systématique qui est aussi présente dans la prédiction ci-dessus pour E_{eff} dans ThF^+.

Nous poursuivons deux objectifs majeurs dans ce travail. En utilisant des méthodes à plusieurs corps basées sur les spineurs qui traitent les correlations électroniques dynamiques et les interactions spin-orbit sur le même pied, un détermination rigoureuse de l'état fondamental électronique de ThF^+ et quelques uns de ses états électroniquement excités de basse énergie est mise en œuvre. Deuxièmement, avec les mêmes techniques intransigeantes, nous déterminons avec une grande précision des propriétés de l'état $^3\Delta_1$ ($\Omega = 1$) qui sont directement pertinents pour les mesures proposées de l'EDM de l'électron.

En particulier, nous présentons le premier calcul rigoureux de la constante d'interaction eEDM impaire pour les symétries $\mathcal{P}, \mathcal{T}$ et du moment dipolaire électrique moléculaire statique. De plus, la constante d'interaction hyperfine magnétique est calculée pour $\Omega = 1$ de même que la constante d'interaction scalaire-pseudoscalaire impaire pour $\mathcal{P}, \mathcal{T}$, les deux jouent un rôle important dans l'interprétation des mesures expérimentales correspondantes et à venir [CGS+12, CG14]. Nous avons aussi calculé les moments dipolaires électriques moléculaires et les moments de transition électrique, les derniers sont utiles concernant la préparation de l'état dans une expérience

EDM. Les moments dipolaires moléculaires sont directement liés au champ électrique effectif EDM, pusiqu'ils sont une mesure du mélange des états propres de parité.

Dans le travail antérieur de Barker *et al.* [BAHP12, HBA14b] $\Omega = 0^+$ a été proposé comme l'état fondamental de ThF^+, supporté par les intensités mesurées de la bande la plus basse comparées à cellles des autres bandes dans une ionisation de champ pulsé -énergie cinétique zéro, expérience (PFI-ZEKE) Les calculs à plusieurs corps de structure électronique qui accompagnaient ont été jugés non concluant à ce sujet. De notre discussion des calculs relativistes à plusieurs corps, incluant ceux de la référence [BAHP12] pour les énergies d'excitation, nous concluons que l'assignation de l'état fondamental électronique de ThF^+ reste une question ouverte. Les modèles de Barker *et al.* souffre d'un traitement incomplet de l'interaction spin-orbit et de son entrelacement avec les corrélations électroniques dynamiques, ce qui devient manifeste dans la pauvre description de la division de l'état $^3\Delta$ entre ses composantes Ω. Notre travail actuel et une plus ample étude dans [DNJ+15] prennent en compte ces effets rigoureusement qui mènent à un état fondamental $^3\Delta_1$. Assigner préférentiellement l'état fondamental comme étant $^1\Sigma_0^+$ est, donc, plus tenable d'un point de vue théorique, basé sur nos récentes découvertes. Dans tous les cas, il est certain, au-delà du doute raisonnable, que les deux états respectifs sont les deux états électroniques de plus basse énergie et qu'ils sont si près en énergie qu'une expérience eEDM pourrait être mené peu importe leur ordre [CG14].

Nous concluons que notre meilleur modèle pour la détermination des constantes d'interaction impaires pour $\mathcal{P}, \mathcal{T}$ et hyperfine magnétique est $\mathcal{III}^{\mathcal{CI},10}$ dans la base TZ' (en gras dans 7.5), qui affiche des valeurs de propriétés presque convergées par rapport aux différents degrés de liberté dans les modèles testés. Notre meilleure prédiction pour la constante hyperfine dans l'état "de science" est 1833 [MHz], ce qui demande confirmation d'une mesure expérimentale. Le champ électrique effectif de $E_{\text{eff}} = 35.2 \left[\frac{\text{GV}}{\text{cm}}\right]$ dans ce même état est plus que 60% plus petit que la valeur de $E_{\text{eff}} = 90 \left[\frac{\text{GV}}{\text{cm}}\right]$ obtenue précédemment par Meyer *et al.* [MB08].

La large différence est très probablement due à l'ensemble limité de configurations électroniques et d'autres approximations inhérentes au modèle utilisé dans l'approche de Meyer *et al.* La plus valeur de E_{eff} est un revers pour de potentielles recherches de l'EDM de l'électron avec cet ion moléculaire, mais le nombre d'autres propriétés favorables (état $^3\Delta_1$ de basse énergie, grand moment dipolaire moléculaire) de ThF^+ est suffisamment grand pour retenir le système comme un candidat prometteur dans la recherche de violation $\mathcal{P}, \mathcal{T}$. Dans le tableau F.3, nous fournissons un résumé des valeurs de E_{eff} dans les états "de science" de quelques molécules diatomiques d'intérêt dans cette recherche. Notre E_{eff} déterminé ici pour ThF^+ reste plus grand que E_{eff} dans l'état de "science" de la molécule YbF, pour laquelle un nouvelle

borne supérieure avait été déterminée en 2011 [HKS$^+$11]. Les moments dipolaires électriques statiques de transition que nous avons déterminés pour un ensemble d'états en dessous de 9000 cm^{-1} dans ThF$^+$ peut aussi être utile pour choisir un chemin de préparation de l'état pour une mesure d'EDM dans cet ion moléculaire prometteur.

Table F.3 – Champ électrique effectif pour les états de sciences dans une sélection de molécules diatomiques candidates dans la recherche de violation de parité et de renversement du temps.

Molecule	Etat électronique	$E_{\text{eff}}[\frac{\text{GV}}{\text{cm}}]$
ThO	$^3\Delta_1$	75.2[1]; 75.8[2]
YbF	$^2\Sigma^+_{1/2}$	26[3] 25[4] 24[5]
PbO	$^3\Sigma^+_1$	25[6]
ThF$^+$	$^3\Delta_1$	35.2[7]; 90[8]
WC	$^3\Delta_1$	-36[9]

[1] Référence [FN14] [6] Référence [KD02]
[2] Référence [ST14] [7] Ce travail
[3] Référence [Koz97] [8] Référence [MB08]
[4] Référence [MKT98] [9] Référence [LCS$^+$13].
[5] Référence [Par98]

ThO revisité.

Le travail suivant a été publié dans : M. Denis and T. Fleig, J. Chem. Phys. 145, 214307 (2016), *In search of discrete symmetry violations beyond the standard model: Thorium monoxide reloaded.*[DF16]

Nous présentons une valeur réactualisée du champ électrique effectif du moment dipolaire électrique de l'électron (EDM) de $E_{\text{eff}} = 75.2\left[\frac{\text{GV}}{\text{cm}}\right]$ et de la constante d'intéraction hyperfine magnétique pour ^{229}Th de $A_{||} = -1266$ [MHz], la constante d'interaction scalaire-pseudoscalaire nucléon-électron $W_S = 106.0$ [kHz], et le moment dipolaire électrique moléculaire $D = -4.41$ [Debye] dans l'état de science $^3\Delta_1$ de ThO. Les critiques des résultats de la référence [J. Mol. Spectrosc. **300**, 16 (2014)] adressées dans la référence [J. Chem. Phys. **142**, 024301 (2015)] sont traitées et il s'avèrent être largement infondées dans le cadre de la présente apporche. Les découvertes présentes confirment les contraintes légèrement assouplies sur les paramètres au-delà du modèle standard concernés, en particulier l'EDM de l'électron, d_e et la constante de couplage scalaire-pseudoscalaire nucléon-électron, C_S.

La violation de symétrie ($\mathcal{CP}$) diagonale en saveur, absente dans le modèle standard des particules élémentaires [RvdSB$^+$08], pourrait expliquer l'asymétrie baryonique de l'univers [Sak67, DK04] et *via* le théorème $\mathcal{CPT}$ [SW64], se manifester dans la matière ordinaire à travers des interactions de leptons violant la parité spatiale ($\mathcal{P}$) et le renversement du temps ($\mathcal{T}$). Dans la recherche de détection de telles violations de symétries physiques discrètes au-delà de celles déjà connues et intégrées dans le modèle standard [ERMvK13], les études sur les molécules diatomiques sont devenues des sondes hautement sensibles dans le régime des basses énergies [HKS$^+$11, CBC$^+$14, LCG$^+$13]. Dans les systèmes électroniquement paramagnétiques, le moment dipolaire de l'électron (EDM) et l'interaction scalaire-pseudoscalaire nucléon-électron (ne-SPS) sont les sources dominantes de violation $\mathcal{P},\mathcal{T}$ à l'échelle atomique.

Des études expérimentales [CBC$^+$14] et théoriques [FN14, SPT13] récentes sur la molécule ThO ont mené à une nouvelle borne supérieure améliorée sur l'EDM de l'électron, d_e, si la borne supérieure à l'écart d'énergie impair pour $\mathcal{P},\mathcal{T}$ est interprété en terme de l'EDM de l'électron seul. Cette borne supérieure est déterminée à travers $d_e = -\frac{\hbar\omega^{\mathcal{NE}}}{E_{\text{eff}}}$, où $\omega^{\mathcal{NE}}$ est une borne supérieure d'un écart de fréquences mesuré et E_{eff} est le champ électrique effectif EDM, *i.e.*, il s'agit du résultat conjoint d'une mesure et d'un calcul moléculaire à plusieurs corps. Puisque l'incertitude théorique pour E_{eff} entre directement dans la borne supérieure de d_e, cette incertitude devrait être minimisée.

Les résultats théoriques les plus précis pour le champ électrique effectif EDM requis E_{eff} dans l'état de science $^3\Delta_1$ de ThO à partir de deux approches différentes (Skripnikov *et al.* [ST15] et Fleig *et al.* [FN14]) divergent de 6.3 $\left[\frac{\text{GV}}{\text{cm}}\right]$, soit environ 8%. Dans le présent article, nous présentons une étude élaborée additionnelle des effets de corrélations électroniques d'ordre élevé et des effets relativistes au-delà de l'hamiltonien Dirac-Coulomb sur les propriétés pertinentes pour les études EDM dans le système moléculaire ThO. Cela inclut une valeur améliorée et plus fiable de E_{eff} pour ThO ($^3\Delta_1$), le moment dipolaire électrique moléculaire, et la valeur de la constante d'interaction ne-SPS. Ce dernier est déterminé comme décrit dans la référence [DNJ$^+$15] et représente le deuxième effet impair pour $\mathcal{P},\mathcal{T}$ le plus important dans ThO, permettant de contraindre le couplage électron-nucléon C_S.

Dans ce travail, nous avons reconsidéré les propriétés impaires pour $\mathcal{P},\mathcal{T}$ et associées de la molécule ThO en utilisant des fonctions d'onde rigoureuses tout électrons à quatre composantes et obtenu des résultats nouveaux (W_S, D) et actualisés (E_{eff}, $A_{||}$). De plus, nous avons répondu à des critiques spécifiques adressées par Skripnikov *et al.* dans Ref. [SPT13]. Le point principal est l'incertitude supposément sous-estimée de E_{eff} due au choix de la base de spineurs (7%); pourtant, notre travail

révèle l'insensibilité des propriétés impaires pour $\mathcal{P}, \mathcal{T}$ aux choix adéquats de l'espace des spineurs. Deuxièmement, se basant sur l'analyse du modèle MR(∞)-CISD à 18 électron, Skripnikov et al. ont affirmé que notre valeur finale précédente obtenue par un calcul MR(12)-CISD pourrait subir une baisse significative de 5%. Alors, même si le MR(∞)-CISD scalaire-relativiste et notre MR(12)-CISD à quatre composantes ne peuvent être comparés directement, nous considérons cette question particulière à travers deux études. Une revue de l'effet de taille de l'espace actif a apporté une correction de $-1.6\left[\frac{\mathrm{GV}}{\mathrm{cm}}\right]$. Et, afin d'affiner notre compréhension des corrélations de sousvalence et valence, nous avons inclu de plus hautes excitations à travers le modèle MR_{12}^{+T}-CISD(18). Nous avons été amenés à réaliser un calcul CI à 7 milliards de déterminants qui a donné les nouvelles valeurs de référence. Le dernier modèle inclut un sous-ensemble de quadruples et quintuples excitations par rapport au déterminant de référence de l'état fondamental en sus des triples excitations de la sous-valence vers l'espace actif. De surcroît, l'influence de l'inclusion des électrons de cœur dans l'espace de corrélation a été analysé en corrélant jusqu'à 36 électrons et aboutit à une baisse de E_{eff} de $+1.2\left[\frac{\mathrm{GV}}{\mathrm{cm}}\right]$. La variation significative de l'EDM moléculaire sous l'inclusion de cette correction et comparé à la meilleure valeur expérimentale suggère que la description des corrélations cœur-électrons est significativement incomplète dans la présente étude. Une inspection de l'interaction de Gaunt a apporté une correction additionnelle de $-1.3\left[\frac{\mathrm{GV}}{\mathrm{cm}}\right]$. Toutes les corrections sont rassemblées dans le tableau F.4. Basé sur cette étude, nous proposons des valeurs amélioriées du champ

Table F.4 – Valeurs finales des propriétés incluant les corrections.

$E_{\mathrm{eff}}\left[\frac{\mathrm{GV}}{\mathrm{cm}}\right]$	$A_{\|\|}$ [MHz]	W_S [kHz]	D [Debye]	
75.2[1]	−1339	106.0	−4.165	vTZ/MR_{12}-CISD(18)
77.1	−1309	108.5	−4.020	nouvelle valeur de base vTZ/MR_{12}^{+T}-CISD(18)
−0.2	+42	−0.2	−0.02	correction pour les spineurs Δ
−1.6	+21	−2.3	−0.11	correction pour la taille de l'espace actif
+1.2	−20	+1.8	−0.24	corrélations de cœur
−1.3		−1.8	+0.04	correction Gaunt
			−0.06	Correction champ fini
75.2	−1266	106.0	−4.41	**Valeur finale**

électrique effectif $E_{\mathrm{eff}} = 75.2\left[\frac{\mathrm{GV}}{\mathrm{cm}}\right]$, $A_{||} = -1266$ [MHz] et la constante d'interaction scalaire-pseudoscalaire électron-nucléon $W_S = 106.0$ [kHz] pour l'état de science $^3\Delta_1$ de ThO.

La sous-estimation significative du moment dipolaire moléculaire pourrait s'expliquer par le manque d'excitations de l'espace de sous-valence plus hautes que celles con-

sidérés ici. Cependant, savoir si de telles corrections pourraient significativement diminuer E_{eff} et W_S est discutable.

La discussion des erreurs possibles des présentes valeurs ne devraient pas se baser sur l'aspect énergétique puisque nous partons maintenant d'un description équilibrée des états fondamental et excités et se concentre sur la description précise des propriétés dans l'état de science uniquement. Les barres d'erreur sont ici établies en sommant les valeurs absolues des variations des résultats observées entre le modèle le plus élaboré et le deuxième plus élaboré pour chaque effet étudié. A partir des résultats présents, nous obtenons alors 6% pour $A_{||}$, E_{eff} et W_S. Quant à E_{eff}, la présente valeur finale de $E_{\text{eff}} = 75.2 \left[\frac{\text{GV}}{\text{cm}}\right]$, elle est dans les marges d'incertitude des résultats conjoints des références [FN14] et [SPT13].

Constante d'interaction hyperfine de l'atome de fluor.

Les molécules chargées polarisées dans un piège à ions [LCG$^+$13] ont été proposées comme des systèmes candidats dans la recherche de physique au-delà du modèle standard. En particulier, les effets impairs pour la parité spatiale et le renversement du temps $(\mathcal{P}, \mathcal{T})$ tels que l'interaction due à un moment dipolaire électrique de l'électron (eEDM) peuvent être examinée. Les calculs des constantes hyperfines jouent un rôle important dans ces investigations puisque, comme expliqué plus haut, la comparaison avec de futures valeurs expérimentales de $\text{A}_{||}$ serait un test de la précision de la description de densité de spin électronique autour du noyau et donc, de la précision de la valeur calculée de champ électrique effectif EDM. De plus, une détermination précise des niveaux hyperfins est requis pour établir le protocole expérimental. En effet, la valeur de $\text{A}_{||}$ est nécessaire pour la préparation de l'ion moléculaire et aussi pendant la mesure des constantes impaires pour $\mathcal{P}, \mathcal{T}$.

Nous avons examiné la constante d'interaction hyperfine magnétique parallèle du noyau lourd dans des travaux précédents [FN14, DNJ$^+$15]. Nous nous concentrons ici sur la constante hyperfine de l'atome de fluor. Nous développons un cadre analytique précis pour calculer la constante d'interaction hyperfine.

Analytical study.

Pour avoir une meilleure compréhension de l'interaction hyperfine magnétique, nous aspirons à évaluer les intégrales d'interaction hyperfine dans un état π comme dans le cas de CF, un système d'intérêt dans notre étude de $\text{A}_{||}$(F). Nous considérons an système hydrogénoïde pour lequel nous aurons besoin d'une charge électrique

effective. La détermination d'une fonction d'onde à quatre composante rigoureuse de l'état π représente un challenge.

Hyperfine integrals.

Nous emploierons les solutions exactes de l'équation de Dirac [BS12] en tant que fonctions d'onde. Pour un état avec $j = l + \frac{1}{2}$ ou $j = l - \frac{1}{2}$ et particulièrement $j = \frac{3}{2}$ ou $j = \frac{1}{2}$, les fonctions d'onde respectives sont données par

$$\psi_{(j=l+\frac{1}{2})} = \begin{pmatrix} u_1 = g(r)\sqrt{\frac{l+m+\frac{1}{2}}{2l+1}}Y_{l,m-\frac{1}{2}} \\ u_2 = -g(r)\sqrt{\frac{l-m+\frac{1}{2}}{2l+1}}Y_{l,m+\frac{1}{2}} \\ u_3 = -if(r)\sqrt{\frac{l-m+\frac{3}{2}}{2l+3}}Y_{l+1,m-\frac{1}{2}} \\ u_4 = -if(r)\sqrt{\frac{l+m+\frac{3}{2}}{2l+3}}Y_{l+1,m+\frac{1}{2}} \end{pmatrix} \tag{F.27}$$

et

$$\psi_{(j=l-\frac{1}{2})} = \begin{pmatrix} \tilde{g}(r)\sqrt{\frac{l-m+\frac{1}{2}}{2l+1}}Y_{l,m-\frac{1}{2}} \\ \tilde{g}(r)\sqrt{\frac{l+m+\frac{1}{2}}{2l+1}}Y_{l,m+\frac{1}{2}} \\ -\imath\tilde{f}(r)\sqrt{\frac{l+m-\frac{1}{2}}{2l-1}}Y_{l-1,m-\frac{1}{2}} \\ \imath\tilde{f}(r)\sqrt{\frac{l-m-\frac{1}{2}}{2l-1}}Y_{l-1,m+\frac{1}{2}} \end{pmatrix} \tag{F.28}$$

avec $m = m_j = l_z + s_z$.
Elles sont formées d'harmoniques sphériques et de fonctions radiales qui dépendent des orbitales considérées. Les fonctions radiales de $2p_{\frac{3}{2}}$ et $2p_{\frac{1}{2}}$ sont respectivement :

$$\begin{aligned} g(r) &= \left(\frac{Z}{a_0}\right)^{\frac{3}{2}}\sqrt{\frac{1+\varepsilon_3}{2\Gamma(2\gamma_2+1)}}e^{\frac{-Zr}{N_3a_0}}\left(\frac{2Z}{N_3a_0}\right)^{\gamma_2-1}r^{\gamma_2-1} \\ f(r) &= -\sqrt{\frac{1-\varepsilon_3}{1+\varepsilon_3}}g(r), \end{aligned} \tag{F.29}$$

$$\begin{aligned} \tilde{g}(r) &= \left(\frac{2Z}{N_2a_0}\right)^{\frac{3}{2}}\sqrt{\frac{2\gamma_1+1}{\Gamma(2\gamma_1+1)}}\sqrt{\frac{1+\varepsilon_2}{4N_2(N_2-1)}}e^{-\frac{\rho_2}{2}}\left[(N_2-2)\rho_2^{\gamma_1-1} - \frac{N_2-1}{2\gamma_1+1}\rho_2^{\gamma_1}\right] \\ \tilde{f}(r) &= -\sqrt{\frac{1-\varepsilon_2}{1+\varepsilon_2}}\frac{(2\gamma_1+1)N_2-(N_2-1)\rho_2}{(2\gamma_1+1)(N_2-2)-(N_2-1)\rho_2}\tilde{g}(r). \end{aligned} \tag{F.30}$$

N_2, N_3, γ_1, γ_2, ε_2 and ε_3 that do not depend on r will be replaced at the end of the calculation and $\rho_2 = \frac{2Zr}{N_2a_0}$.
Les fonctions d'ondes résultants pour les trois orbitales 2p s'écrivent :

$$\psi_{2p_{\frac{3}{2},\frac{3}{2}}} = \frac{\sqrt{3}}{2\sqrt{2\pi}}\begin{pmatrix} u_1 = -\sin\theta e^{i\varphi}g(r) \\ u_2 = 0 \\ u_3 = \imath\cos\theta\sin\theta e^{i\varphi}f(r) \\ u_4 = -\imath\sin^2\theta e^{2i\varphi}f(r) \end{pmatrix} \tag{F.31}$$

$$\psi_{2p_{\frac{3}{2},\frac{1}{2}}} = \frac{1}{2\sqrt{2\pi}} \begin{pmatrix} 2\cos\theta g(r) \\ \sin\theta e^{\imath\varphi} g(r) \\ -\imath\left(3\cos^2\theta - 1\right) f(r) \\ 3\imath\cos\theta\sin\theta e^{\imath\varphi} f(r) \end{pmatrix} \tag{F.32}$$

$$\psi_{2p_{\frac{1}{2},\frac{1}{2}}} = \frac{1}{2\sqrt{\pi}} \begin{pmatrix} \cos\theta\tilde{g}(r) \\ -\sin\theta e^{\imath\varphi}\tilde{g}(r) \\ -\imath f(r) \\ 0 \end{pmatrix} \tag{F.33}$$

Après calcul, les intégrales hyperfines sont données par :

$$\left\langle \psi^{\dagger}_{2p_{\frac{3}{2},\frac{3}{2}}} \left| \frac{(\vec{\alpha}\times\vec{r})_z}{|\vec{r}|^3} \right| \psi_{2p_{\frac{3}{2},\frac{3}{2}}} \right\rangle = \frac{48}{30}\cdot\frac{\alpha Z^3}{4a_0^2}\frac{\Gamma(2\sqrt{4-\alpha^2Z^2}-1)}{\Gamma(2\sqrt{4-\alpha^2Z^2}+1)} \tag{F.34}$$

$$\left\langle \psi^{\dagger}_{2p_{\frac{3}{2},\frac{1}{2}}} \left| \frac{(\vec{\alpha}\times\vec{r})_z}{|\vec{r}|^3} \right| \psi_{2p_{\frac{3}{2},\frac{1}{2}}} \right\rangle = \frac{2}{15}\frac{\alpha Z^3}{a_0^2}\frac{\Gamma(2\sqrt{4-\alpha^2Z^2}-1)}{\Gamma(2\sqrt{4-\alpha^2Z^2}+1)} \tag{F.35}$$

$$\left\langle \psi^{\dagger}_{2p_{\frac{1}{2},\frac{1}{2}}} \left| \frac{(\vec{\alpha}\times\vec{r})_z}{|\vec{r}|^3} \right| \psi_{2p_{\frac{1}{2},\frac{1}{2}}} \right\rangle = \frac{4}{3}\frac{\alpha Z^3}{a_0^2}\frac{\Gamma(2\gamma_1-1)}{\Gamma(2\gamma_1+2)}\frac{(N_2-1)^2(\gamma_1-1)-(2\gamma_1+1)^2}{N_2^4(N_2-1)}\,. \tag{F.36}$$

Afin de vérifier notre formalisme, les intégrales sont évaluées pour l'atome d'hydrogène où $(Z=1)$ et par conséquence, $\gamma_1 \approx 1$, $N_2 \approx 2$:

$$\left\langle \psi^{\dagger}_{2p_{\frac{3}{2},\frac{3}{2}}} \left| \frac{(\vec{\alpha}\times\vec{r})_z}{|\vec{r}|^3} \right| \psi_{2p_{\frac{3}{2},\frac{3}{2}}} \right\rangle \approx \frac{\alpha}{30a_0^2}, \tag{F.37}$$

$$\left\langle \psi^{\dagger}_{2p_{\frac{3}{2},\frac{1}{2}}} \left| \frac{(\vec{\alpha}\times\vec{r})_z}{|\vec{r}|^3} \right| \psi_{2p_{\frac{3}{2},\frac{1}{2}}} \right\rangle \approx \frac{1}{90}\frac{\alpha}{a_0^2}, \tag{F.38}$$

$$\left\langle \psi^{\dagger}_{2p_{\frac{1}{2},\frac{1}{2}}} \left| \frac{(\vec{\alpha}\times\vec{r})_z}{|\vec{r}|^3} \right| \psi_{2p_{\frac{1}{2},\frac{1}{2}}} \right\rangle \approx \frac{1}{18}\frac{\alpha}{a_0^2}. \tag{F.39}$$

Test numérique.

Testons nos résultats en les comparant avec les résultats numériques donnés par le programme `DIRAC` pour un calcul GASCI. Dans un premier lieu, nous cherchons à évaluer les intégrales dans un état excité de l'atome d'hydrogène. Ansi, comparons les valeurs analytiques des intégrales hyperfines avec les résultats numérique où l'opérateur est évalué sur les fonctions d'onde GASCI. Pour les trois états 2p de

Table F.5 – Valeurs de l'intégrale hyperfine pour les orbitales 2p de l'atome d'hydrogène.

	$2p_{\frac{1}{2},\frac{1}{2}}$	$2p_{\frac{3}{2},\frac{3}{2}}$	$2p_{\frac{3}{2},\frac{1}{2}}$
Analytique	$4.054.10^{-4}$	$2.432.10^{-4}$	$8.11.10^{-5}$
Numerique	$4.048.10^{-4}$	$2.429.10^{-4}$	$8.10.10^{-5}$

l'atome d'hydrogène, nos calculs sont en très bon accord avec le numérique comme l'on peut le voir dans le tableau F.5.

Notre méthode s'est avérée efficace et rigoureuse pour l'atome d'hydrogène, cependant, nous aspirons à l'utiliser sur des systèmes polyélectroniques. Pour cela, la charge électrique effective dans l'état π doit être déterminée. Notre stratégie est la suivant, Z_{eff} sera déduite de la différence d'énergie entre les deux niveaux spin-orbit ($J = \frac{1}{2}$ and $J = \frac{3}{2}$) de l'orbital 2p que l'on sait varier comme Z_{eff}^4 et dont l'expression peut être obtenue analytiquement pour l'atome d'hydrogène dans le formalisme de Pauli $\Delta E^H_{p_{\frac{1}{2}-\frac{3}{2}}} = \frac{1}{32}\frac{\alpha^2 e^2}{a_0}$. Alors, Z_{eff} s'écrit :

$$Z_{eff} = \sqrt[4]{\frac{\Delta E_{p_{\frac{1}{2}-\frac{3}{2}}}}{\Delta E^H_{p_{\frac{1}{2}-\frac{3}{2}}}}} \tag{F.40}$$

où l'écart spin-orbit de 2p sera soit déterminé avec l'énergie Hartree-Fock des deux niveaux, soit évalué grâce aux données expérimentales. Nous appliquons cette stratégie à l'atome de fluor en déduisant la charge électrique effective de l'écart d'énergie expérimentale ${}^2P_{\frac{1}{2}} - {}^2P_{\frac{3}{2}}$: $\Delta E_{{}^2P_{\frac{1}{2}-\frac{3}{2}}} = 404.10\ \mathrm{cm}^{-1}$[Moo71], $Z_{eff}^{Exp} = 5.76$. Utiliser cette valeur dans Eqs. (F.37) to (F.39) donne des intégrales hyperfines calculées analytiquement qui diffèrent des résultats numériques au plus de 7% (voir Table F.6), ce qui est satisfaisant puisque nous cherchons à obtenir une vision qualitative.

$2p_{(J,m_J)}$	$(\frac{1}{2},\frac{1}{2})$	$(\frac{3}{2},\frac{3}{2})$	$(\frac{3}{2},\frac{1}{2})$
Analytique	7.774×10^{-2}	1.550×10^{-2}	4.651×10^{-2}
Numerique	7.459×10^{-2}	1.432×10^{-2}	4.297×10^{-2}

Table F.6 – Valeurs des intégrales hyperfines.

Evidemment, l'étape suivant sera d'appliquer cette méthode à des molécules, en commençant par une molécule diatomique comme CF. Pour ce faire, il faut s'attaquer à la question de la détermination de la charge électrique effective respective de chaque atome avec précision. Nous n'avons pas, jusque là, trouver de méthode satisfaisante.

Résumé.

Dans cette thèse, nous avons cherché les preuves de l'existence de phénomènes qui violeraient les symétries conjointes de parité et conjugaison de charge, proposés comme explication de l'asymétrie baryonique de l'univers, l'un des principaux défauts du modèle standard des particules.

Notre travail a présenté un ensemble de constantes d'interaction violant les symétries de parité et de renversement du temps d'intérêt dans la recherche de nouvelle physique au-delà du modèle standard, notamment, les interactions du moment dipolaire de l'électron (eEDM), scalaire-pseudoscalaire électron-nucléon (enSPS) et du moment quadrupolaire magnétique nucléaire (nMQM). Le calcul des paramètres correspondants a été réalisé pour des molécules diatomiques telles que ThO qui a été utilisée dans des expériences eEDM de pointe et permis d'assigner la borne supérieure la plus contraignante de l'eEDM ou ThF^+ un candidat prometteur pour les expériences de recherche de violation $\mathcal{CP}$ à venir pour son état fondamental $^3\Delta_1$ et son caractère ionique. Nous avons employé une approche élaborée d'interaction de configurations relativiste à quatre composantes. A travers une analyse détaillée les propriétés ont été déterminées avec précision et leurs barres d'erreur minimisées.

Ces résultats seront d'une importance cruciale dans l'interprétation des mesures puisque, comme exposé précédemment, une borne supérieure ou une valeur des constantes fondamentales ne peut être assignée que si l'on combine les mesures de différence d'énergie expérimentales et les paramètres moléculaires théoriques.

En outre, un autre paramètre utile a été calculé, il s'agit de la constante d'interaction hyperfine magnétique parallèle. Elle permet de tester la précision de la description de la densité de spin électronique autour du noyau à laquelle l'eEDM est très sensible et, une connaissance précise de la structure hyperfine est essentiel pour préparer les molécules dans l'état désiré et concevoir le procédé expérimental.

Les études ont révélé, entre autres faits, l'insensibilité des paramètres impairs pour $\mathcal{P},\mathcal{T}$ au choix de la base de spineurs ainsi que la pertinence de l'utilisation des bases gaussiennes triple-ζ pour leur calcul. Aussi, la taille de l'espace actif des spineurs s'avère être le paramètre crucial dans le traitement de la correlation des fonctions d'ondes utilisées pour le calcul des constantes. Ces caractéristiques pourraient être instructives pour les futures études des constantes impaires pour $\mathcal{P},\mathcal{T}$ dans des molécules diatomiques polaires paramagnétiques.

Quelques expériences eEDM sont prévues avec des molécules diatomiques paramagnétiques dans les années à venir. Elles consistent soit à utiliser de nouvelles molécules prometteuses telles que ThF^+ soit à améliorer les expériences préexistantes (YbF, ThO ...) afin de diminuer les erreurs systématiques et donc, la borne supérieure de l'eEDM.

Figure F.6 – Superposition dans le plan $d_e - C_S$ des résultats expérimentaux récents dans des systèmes paramagnétiques et diamagnétiques [Jun15].

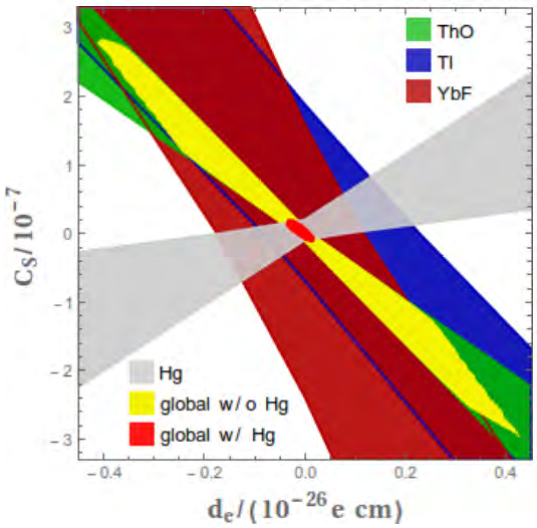

Outre l'amélioration de l'incertitude des expériences en cours ou à venir sur des systèmes paramagnétiques, une manière de contraindre plus les modèles au-delà du modèle standard est d'étudier les systèmes diamagnétiques telles que les atomes Hg ou Xe et de tirer avantage de la combinaison linéaire de d_e et C_S que l'on attend orthogonale à celle des systèmes paramagnétiques qui présentent tous une combinaison similaire. De cette façon, croiser les résultats des deux types de systèmes méneront à des limites plus contraignantes sur les constantes que ce que ferait une améliorant d'incertitude, même d'un ordre de grandeur, pour un seul paramètre dans un unique système (Fig. F.6). Par conséquent, les études théoriques et expériences à venir devraient s'intéresser aux interactions violant P, T dans les systèmes diamagnétiques en complément des systèmes paramagnétiques et les résultats conjugués pour efficacement contraindre la nouvelle physique.

Bibliography

[Aer84] P. J. C. Aerts. Use of molecular symmetry in hartree-fock-dirac scf calculations. *Chem. Phys. Lett.*, 104(1):28, 1984.

[AF11] P. W. Atkins and R. S. Friedman. *Molecular quantum mechanics*. Oxford university press, 2011.

[AHT04] A. G. Adam, W. S. Hopkins, and D. W. Tokaryk. High-resolution visible laser spectroscopy of HfF. *J. Mol. Spectrosc.*, 225(1):1, 2004.

[AJO95] G. A. Aucar, H. J. Aa. Jensen, and J. Oddershede. Operator representations in Kramers bases. *Chem. Phys. Lett.*, 232(1):47, 1995.

[Ala99] Alavi-Harati et al. (KTeV Collaboration). Observation of direct *CP* violation in $k_{s,l} \to \pi\pi$ decays. *Phys. Rev. Lett.*, 83:22, 1999.

[BABH11] B. J. Barker, I. O. Antonov, V. E. Bondybey, and M. C. Heaven. Communication: Spectroscopic measurements for HfF^+ of relevance to the investigation of fundamental constants. *J. Chem. Phys.*, 134:201102, 2011.

[BAHP12] B. J. Barker, I. O. Antonov, M. C. Heaven, and K. A. Peterson. Spectroscopic investigations of ThF and ThF^+. *J. Chem. Phys.*, 136:104305, 2012.

[Bal97] K. Balasubramanian. *Relativistic Effects in Chemistry Part A: Theory and Techniques*. Wiley-Interscience, 1997.

[BC03] J. M. Brown and A. Carrington. *Rotational Spectroscopy of Diatomic Molecules*. Cambridge Molecular Science. Cambridge University Press, 2003.

[Bet29] H. Bethe. Termaufspaltung in kristallen. *Ann. Phys. (Berlin)*, 395(2):133, 1929.

[BHS95] R. Barbieri, L. Hall, and A. Strumia. Violations of lepton flavour and CP in supersymmetric unified theories. *Nuc. Phys. B*, 445(2–3):219, 1995.

[BJ03] B. H. Bransden and C. J. Joachain. *Physics of Atoms and Molecules; 2nd ed.* Prentice-Hall, Harlow, 2003.

[BR51] G. E. Brown and D. G. Ravenhall. On the interaction of two electrons. *Proc. Roy. Soc. London A*, 208(1095):552, 1951.

[Bre29] G. Breit. The effect of retardation on the interaction of two electrons. *Phys. Rev.*, 34:553, 1929.

[BS91] W. Bernreuther and M. Suzuki. The electric dipole moment of the electron. *Rev. Mod. Phys.*, 63(2):313, 1991.

[BS12] H. A. Bethe and E. E. Salpeter. *Quantum mechanics of one-and two-electron atoms*. Springer Science & Business Media, 2012.

[BZ90] S. M. Barr and A. Zee. Electric Dipole Moment of the Electron and of the Neutron. *Phys. Rev. Lett.*, 65(23):2920, 1990.

[CBC+14] The ACME Collaboration, J. Baron, W. C. Campbell, D. DeMille, J. M. Doyle, G. Gabrielse, Y. V. Gurevich, P. W. Hess, N. R. Hutzler, E. Kirilov, I. Kozyryev, B. R. O'Leary, C. D. Panda, M. F. Parsons, E. S. Petrik, B. Spaun, A. C. Vutha, and A. D. West. Order of Magnitude Smaller Limit on the Electric Dipole Moment of the Electron. *Science*, 343:269, 2014.

[CG14] E. A. Cornell and D. N. Gresh, 2014. Private communication.

[CGS+12] K. C. Cossel, D. N. Gresh, L. C. Sinclair, T. Coffrey, L. V. Skripnikov, A. N. Petrov, N. S. Mosyagin, A. V. Titov, R. W. Field, , E. R. Meyer, E. A. Cornell, and J. Ye. Broadband velocity modulation spectroscopy of HfF^+: Towards a measurement of the electron electric dipole moment. 546:1, 2012.

[CH70] A. Carrington and B. J. Howard. Gas-phase electron resonance spectrum and dipole moment of CF. *Mol. Phys.*, 18:225, 1970.

[CJD07] E. D. Commins, J. D. Jackson, and D. P. DeMille. The electric dipole moment of the electron: An intuitive explanation for the evasion of schiff's theorem. *Am. J. Phys.*, 75(6):532, 2007.

[CKS+12] S. Chatrchyan, V. Khachatryan, A. M. Sirunyan, A. Tumasyan, W. Adam, E. Aguilo, T. Bergauer, M. Dragicevic, J. Eroe, C. Fabjan, M. Friedl, R. Fruehwirth, V. M. Ghete, J. Hammer, N. Hoermann, J. Hrubec, M. Jeitler, W. Kiesenhofer, V. Knuenz, M. Krammer, D. Liko, I. Mikulec, M. Pernicka, B. Rahbaran, C. Rohringer, H. Rohringer, R. Schoefbeck, J. Strauss, A. Taurok, P. Wagner, W. Waltenberger, G. Walzel, E. Widl, C-E. Wulz, V. Mossolov, N. Shumeiko, J. S. Gonzalez, S. Bansal, T. Cornelis, E. A. De Wolf, X. Janssen, S. Luyckx, L. Mucibello, S. Ochesanu, B. Roland, R. Rougny, M. Selvaggi, Z. Staykova, H. Van Haevermaet, P. Van Mechelen, N. Van Remortel, A. Van Spilbeeck, F. Blekman, S. Blyweert, J. D'Hondt, R. G. Suarez, A. Kalogeropoulos, M. Maes, A. Olbrechts, Doninck W. Van, Mulders P. Van, Onsem GP. Van, and Villella. Observation of Z decays to four leptons with the CMS detector at the LHC. *J. High Energy Phys.*, 2012(12), 2012.

[Com99] E. D. Commins. Electric Dipole Moments of Leptons. volume 40 of *Advances In Atomic, Molecular, and Optical Physics*. 1999.

[CRM15] T. Chupp and M. Ramsey-Musolf. Electric dipole moments: A global analysis. *Phys. Rev. C*, 91(3):035502, 2015.

[DeM] D. DeMille and On behalf of the ACME collaboration 2014 ASME: search for the electron's electric dipole moment 24th Int. Conf. on Atomic Physics (ICAP 2014), (Washington, DC, 3-8 August 2014) (http://icap2014.org/book-abstracts-download).

[DF90] K. G. Dyall and K. Fægri. Kinetic balance and variational bounds failure in the solution of the dirac equation in a finite gaussian basis set. *Chem. Phys. Lett.*, 174(1):25, 1990.

[DF07] K. G. Dyall and K. Faegri. *Introduction to Relativistic Quantum Chemistry*. Oxford University Press, 2007.

[DF16] M. Denis and T. Fleig. In search of discrete symmetry violations beyond the standard model: Thorium monoxide reloaded. *J. Chem. Phys.*, 145(21):214307, 2016.

[DIRa] DIRAC, a relativistic ab initio electronic structure program, Release DIRAC15 (2015), written by R. Bast, T. Saue, L. Visscher, and H. J. Aa. Jensen, with contributions from V. Bakken, K. G. Dyall, S. Dubillard, U. Ekstroem, E. Eliav, T. Enevoldsen, E. Fasshauer, T. Fleig,

O. Fossgaard, A. S. P. Gomes, T. Helgaker, J. Henriksson, M. Ilias, Ch. R. Jacob, S. Knecht, S. Komorovsky, O. Kullie, J. K. Laerdahl, C. V. Larsen, Y. S. Lee, H. S. Nataraj, M. K. Nayak, P. Norman, G. Olejniczak, J. Olsen, Y. C. Park, J. K. Pedersen, M. Pernpointner, R. Di Remigio, K. Ruud, P. Salek, B. Schimmelpfennig, J. Sikkema, A. J. Thorvaldsen, J. Thyssen, J. van Stralen, S. Villaume, O. Visser, T. Winther, and S. Yamamoto (see http://www.diracprogram.org).

[DIRb] DIRAC, a relativistic ab initio electronic structure program, Release DIRAC11 (2011), written by R. Bast, H. J. Aa. Jensen, T. Saue, and L. Visscher, with contributions from V. Bakken, K. G. Dyall, S. Dubillard, U. Ekström, E. Eliav, T. Enevoldsen, T. Fleig, O. Fossgaard, A. S. P. Gomes, T. Helgaker, J. K. Lærdahl, J. Henriksson, M. Iliaš, Ch. R. Jacob, S. Knecht, C. V. Larsen, H. S. Nataraj, P. Norman, G. Olejniczak, J. Olsen, J. K. Pedersen, M. Pernpointner, K. Ruud, P. Sałek, B. Schimmelpfennig, J. Sikkema, A. J. Thorvaldsen, J. Thyssen, J. van Stralen, S. Villaume, O. Visser, T. Winther, and S. Yamamoto (see http://dirac.chem.vu.nl).

[Dir58] P. A. M. Dirac. *The Principles of Quantum Mechanics, IV.* Oxford University Press, Oxford, 1958.

[DK04] M. Dine and A. Kusenko. The origin of the matter-antimatter asymmetry. *Rev. Mod. Phys.*, 76:1, 2004.

[DNJ+15] M. Denis, M. S. Nørby, H. J. Aa. Jensen, A. S. Pereira Gomes, M. K. Nayak, S. Knecht, and T. Fleig. Theoretical study on thf + , a prospective system in search of time-reversal violation. *New J. Phys.*, 17(4):043005, 2015.

[Dun89] T. H. Jr. Dunning. Gaussian Basis Sets for Use in Correlated Molecular Calculations. I. The Atoms Boron Through Neon and Hydrogen. *J. Chem. Phys.*, 90:1007, 1989.

[Dya] Dyall basis sets. `http://dirac.chem.sdu.dk/basisarchives/dyall/index.html`.

[Dya06] K. G. Dyall. Relativistic double-zeta, triple-zeta, and quadruple-zeta basis sets for the actinides Ac-Lr. *Theoret. Chim. Acta*, 90:491, 2006.

[Dya12] K. G. Dyall. Core correlating basis functions for elements 31-118. *Theoret. Chim. Acta*, 131:1217, 2012.

[eaBC01a] B. Aubert et al. (BABAR Collaboration). Measurement of *CP*-violating asymmetries in b^0 decays to *CP* eigenstates. *Phys. Rev. Lett.*, 86:2515, 2001.

[eaBC01b] K. Abe et al. (Belle Collaboration). Observation of large CP violation in the neutral B meson system. *Physical Review Letters*, 87(9):091802, 2001.

[eaNC99] V. Fanti et al. (NA48 Collaboration). A new measurement of direct CP violation in two pion decays of the neutral kaon. *Physics Letters B*, 465:335, 1999.

[ERMvK13] J. Engel, M. J. Ramsey-Musolf, and U. van Kolck. Electric dipole moments of nucleons, nuclei, and atoms: The Standard Model and beyond. *Prog. Part. Nuc. Phys.*, 71:21, 2013.

[FDK14] V. V. Flambaum, D. DeMille, and M. G. Kozlov. Time-reversal symmetry violation in molecules induced by nuclear magnetic quadrupole moments. *Phys. Rev. Lett.*, 113(10):103003, 2014.

[Fey39] R. P. Feynman. Forces in molecules. *Phys. Rev.*, 56:340, 1939.

[FJOV06] T. Fleig, H. J. Aa. Jensen, J. Olsen, and L. Visscher. The generalized active space concept for the relativistic treatment of electron correlation. III. Large-scale configuration interaction and multiconfiguration self-consistent-field four-component methods with application to UO2. *J. Chem. Phys.*, 124(10), 2006.

[Fle10] T. Fleig. Relativistic string-based electron correlation methods. In Ishikawa Y. Barysz, M., editor, *Relativistic Methods for Chemists*, volume 10 of *Challenges and Advances in Computational Chemistry and Physics*, page 407. 2010.

[FN13] T. Fleig and M. K. Nayak. Electron electric-dipole-moment interaction constant for HfF^+ from relativistic correlated all-electron theory. *Phys. Rev. A*, 88:032514, 2013.

[FN14] T. Fleig and M. K. Nayak. Electron electric dipole moment and hyperfine interaction constants for ThO. *J. Mol. Spectrosc.*, 300:16, 2014.

[FNK16] T. Fleig, Malaya K. Nayak, and Mikhail G. Kozlov. Tan, a molecular system for probing $\mathcal{P},\mathcal{T}$-violating hadron physics. *Phys. Rev. A*, 93:012505, 2016.

[FOM01] T. Fleig, J. Olsen, and C. M. Marian. The generalized active space concept for the relativistic treatment of electron correlation. i. kramers-restricted two-component configuration interaction. *J. Chem. Phys.*, 114(11):4775, 2001.

[FOV03] T. Fleig, J. Olsen, and L. Visscher. The generalized active space concept for the relativistic treatment of electron correlation. II: Large-scale configuration interaction implementation based on relativistic 2- and 4-spinors and its application. *J. Chem. Phys.*, 119:2963, 2003.

[FSB03] N. Fortson, P. Sandars, and S. Barr. The search for a permanent electric dipole moment. *Phys. Today*, 56(6):33, 2003.

[Ful76] G. H. Fuller. Nuclear spins and moments. *Journal of Physical and Chemical Reference Data*, 5(4):835, 1976.

[FW50] L. L. Foldy and S. A. Wouthuysen. On the Dirac Theory of Spin 1/2 Particles and Its Non-Relativistic Limit. *Phys. Rev.*, 78:29, 1950.

[Gau29] J. A. Gaunt. The triplets of helium. *Proc. Roy. Soc. London A*, 122(790):513, 1929.

[GCZ+16] D. N. Gresh, K. C. Cossel, Y. Zhou, J. Ye, and E. A. Cornell. Broadband velocity modulation spectroscopy of ThF^+ for use in a measurement of the electron electric dipole moment. *J. Mol. Spectr.*, 319:1, 2016.

[GLF75] S. Gewurtz, H. Lew, and P. Flainek. The Electronic Spectrum of HF+. *Can. J. Phys.*, 53(11):1097, 1975.

[Güt32] P. Güttinger. Das verhalten von atomen im magnetischen drehfeld. *Zeitschrift für Physik*, 73(3):169, 1932.

[HBA14a] M. C. Heaven, B. J. Barker, and I. O. Antonov. Spectroscopy and structure of the simplest actinide bonds. *J. Phys. Chem. A*, 118(46):10867, 2014.

[HBA14b] M. C. Heaven, B. J. Barker, and I. O. Antonov. Spectroscopy and Structure of the Simplest Actinide Bonds. *J. Phys. Chem. A*, 118:10867, 2014.

[Hel37] H. Hellmann. *Einführung in die Quantenchemie*. Franz Deuticke, 1937.

[Hes14] P. W. Hess. *Improving the Limit on the Electron EDM: Data Acquisition and Systematics Studies in the ACME Experiment.* Dissertation, The Department of Physics, Harvard University, Cambridge, Massachusetts, 2014.

[HFG08] D. Hanneke, S. Fogwell, and G. Gabrielse. New measurement of the electron magnetic moment and the fine structure constant. *Phys. Rev. Lett.*, 100:120801, 2008.

[Hin97] E. A. Hinds. Testing time reversal symmetry using molecules. *Phys. Scr.*, 1997(T70):34, 1997.

[Hin14] E. A. Hinds. Is the electron round? Searching for the electron's EDM. Ecole des Houches 2014.

[HK85] H. E. Haber and G. L. Kane. The search for supersymmetry: Probing physics beyond the standard model. *Phys. Rep.*, 117(2–4):75, 1985.

[HKS+11] J. J. Hudson, D. M. Kara, I. J. Smallman, B. E. Sauer, M. R. Tarbutt, and E. A. Hinds. Improved measurement of the shape of the electron. *Nature*, 473:493, 2011.

[HLMP] A. C. Hartley, E. Lindroth, and Ann-M. Martensson-Pendrill. Parity non-conservation and electric dipole moments in caesium and thallium. *J. Phys. B*, 23(19):3417.

[Iri12] K. K. Irikura. Gas-phase energetics of thorium fluorides and their ions. *J. Phys. Chem. A*, 117(6):1276, 2012.

[Jac99] J. D. Jackson. *Classical electrodynamics.* Wiley, New York, 3rd edition, 1999.

[JDSF96] H. J. Aa. Jensen, K. G. Dyall, T. Saue, and K. Fægri. Relativistic four-component multiconfigurational self-consistent field theory for molecules: Formalism. *J. Chem. Phys.*, 104:4083, 1996.

[Jun13] M. Jung. A robust limit for the electric dipole moment of the electron. *Journal of High Energy Physics*, (5):168, 2013.

[Jun15] M. Jung. Bounds on new physics from electric dipole moments. arXiv:1509.05013, 2015.

[Kay] Kaye & Laby, Tables of Physical & Chemical Constants. `http://www.kayelaby.npl.co.uk/chemistry/3_8/3_8_1.html`.

[KD02] M. G. Kozlov and D. DeMille. Enhancement of the Electric Dipole Moment of the Electron in PbO. *Phys. Rev. Lett.*, 89:133001, 2002.

[KJEWJW71] L. B. Knight Jr, W. C. Easley, W. Weltner Jr, and M. Wilson. Hyperfine interaction and chemical bonding in MgF, CaF, SrF, and BaF molecules. *J. Chem. Phys.*, 54(1):322, 1971.

[KJF10] S. Knecht, H. J. Aa. Jensen, and T. Fleig. Large-Scale Parallel Configuration Interaction. II. Two- and four-component double-group general active space implementation with application to BiH. *J. Chem. Phys.*, 132:014108, 2010.

[KL95] M. G. Kozlov and L. N. Labzowsky. Parity violation effects in diatomics. *J. Phys. B*, 28(10):1933, 1995.

[KL12] I. B. Khriplovich and S. Lamoreaux. *CP Violation Without Strangeness: Electric Dipole Moments of Particles, Atoms, and Molecules*. Theoretical and Mathematical Physics. Springer Berlin Heidelberg, 2012.

[KLR+12] G. A. Kazakov, A. N. Litvinov, I. Romanenko, L. P. Yatsenko, A. V. Romanenko, M. Schreitl, G. Winkler, and T. Schumm. Performance of a ^{229}Thorium solid-state nuclear clock. arXiv:1204.3268v3 [physics.atom-ph], 2012.

[KM73] M. Kobayashi and T. Maskawa. CP violation in the renormalizable theory of weak interaction. *Prog. Theor. Phys.*, 49:652, 1973.

[Kne09] S. Knecht. *Parallel Relativistic Multiconfiguration Methods: New Powerful Tools for Heavy-Element Electronic-Structure Studies*. Dissertation, Heinrich-Heine-Universität Düsseldorf, Düsseldorf, Germany, 2009.

[Kos63] G. F. Koster. *Properties of the thirty-two point groups*. Massachusetts institute of technology press research monograph. M.I.T. Press, 1963.

[Koz97] M. G. Kozlov. Enhancement of the electric dipole moment of the electron in the YbF molecule. *J. Phys. B*, 30:L607, 1997.

[Kra30] H. A. Kramers. Théorie générale de la rotation paramagnétique dans les cristaux. *Proc. Amsterdam*, XXXIII:959, 1930.

[KSH+12] D. M. Kara, I. J. Smallman, J. J. Hudson, B. E. Sauer, M. R. Tarbutt, and E. A. Hinds. Measurement of the electron's electric dipole

moment using YbF molecules: methods and data analysis. *New J. Phys.*, 14(10):103051, 2012.

[Lan57] L. D. Landau. On the conservation laws for weak interactions. *Nucl. Phys.*, 3:127, 1957.

[LBL+11] A. E. Leanhardt, J. L. Bohn, H. Loh, P. Maletinsky, E. R. Meyer, L. C. Sinclair, R. P. Stutz, and E. A. Cornell. High-resolution spectroscopy on trapped molecular ions in rotating electric fields: A new approach for measuring the electron electric dipole moment. *J. Mol. Spectrosc.*, 270(1):1, 2011.

[LCG+13] H. Loh, K. C. Cossel, M. C. Grau, K-K. Ni, E. R. Meyer, J. L. Bohn, J. Ye, and E. A. Cornell. Precision spectroscopy of polarized molecules in an ion trap. *Science*, 342(6163):1220, 2013.

[LCS+13] J. Lee, J. Chen, L. V. Skripnikov, A. N. Petrov, A. V. Titov, N. S. Mosyagin, and A. E. Leanhardt. Optical spectroscopy of tungsten carbide for uncertainty analysis in electron electric dipole moment search. *Phys. Rev. A*, 87:2013, 2013.

[Liu86] J. Liu. Electric dipole moment of the electron in left-right models. *Nuc. Phys. B*, 271:531, 1986.

[LK92] Z. W. Liu and H. P. Kelly. Analysis of atomic electric dipole moment in thallium by all-order calculations in many-body perturbation theory. *Phys. Rev. A*, 45(7):R4210, 1992.

[LL81] L. D. Landau and L. M. Lifshitz. *Course of Theoretical Physics. Volume 3: Quantum Mechanics.* Butterworth-Heinemann, 3rd ed., 1981.

[LLS89] E. Lindroth, B. W. Lynn, and P. G. H. Sandars. Order α^2 theory of the atomic electric dipole moment due to an electric dipole moment on the electron. *J. Phys. B*, 22:559, 1989.

[Lyk10] J. D. Lykken. Beyond the Standard Model. CERN Yellow Report CERN-2010-002, pp. 101-109, arXiv:1005.1676, 2010.

[MB08] E. R. Meyer and J. L. Bohn. Prospects for an electron electric-dipole moment search in metastable ThO and ThF^+. *Phys. Rev. A*, 78:010502, 2008.

[MBD06] E. R. Meyer, J. L. Bohn, and M. P. Deskevich. Candidate molecular ions for an electron electric dipole moment experiment. *Phys. Rev. A*, 73(6):062108, 2006.

[MKT98] N. S. Mosyagin, M. G. Kozlov, and A. V. Titov. Electric dipole moment of the electron in the ybf molecule. *J. Phys. B*, 31:L763, 1998.

[Moo71] C. E. Moore. Atomic energy levels as derived from the analysis of optical spectra – hydrogen through vanadium. In *Nat. Stand. Ref. Data Ser., NSRDS-NBS 35 Vol. I.* 1971.

[MPL91] A.-M. Mårtensson-Pendrill and E. Lindroth. Limit on a P - and T -Violating Electron-Nucleon Interaction. *EPL*, 15(2):155, 1991.

[Ols00] J. Olsen. The initial implementation and applications of a general active space coupled cluster method. *J. Chem. Phys.*, 113:7140, 2000.

[ORJJ88] J. Olsen, B. O. Roos, P. Jørgensen, and H. J. Aa. Jensen. Determinant based configuration interaction algorithms for complete and restricted configuration interaction spaces. *J. Chem. Phys.*, 89:2185, 1988.

[Par98] F. Parpia. *Ab initio* calculation of the enhancement of the electric dipole moment of an electron in the YbF molecule. *J. Phys. B*, 31:1409, 1998.

[PMIT07] A. N. Petrov, N. S. Mosyagin, T. A. Isaev, and A. V. Titov. Theoretical study of HfF^+ in search for the electron electric dipole moment. *Phys. Rev. A*, 76:030501(R), 2007.

[PMT09] A. N. Petrov, N. S. Mosyagin, and A. V. Titov. Theoretical study of low-lying electronic terms and transition moments for HfF^+ for the electron electric dipole moment search. *Phys. Rev. A*, 79:012505, 2009.

[PR05] M. Pospelov and A. Ritz. Electric dipole moments as probes of new physics. *Ann. Phys.*, 318(1):119, 2005. Special Issue.

[PS73] J. C. Pati and A. Salam. Is Baryon Number Conserved? *Phys. Rev. Lett.*, 31(10):661, 1973.

[RCSD02] B. C. Regan, E. D. Commins, C. J. Schmidt, and D. DeMille. New Limit on the Electron Electric Dipole Moment. *Phys. Rev. Lett.*, 88(7):071805, 2002.

[RM09] B. L. Roberts and W. J. Marciano, editors. *Lepton Dipole Moments*, volume 20, chapter 14, page 519. Advances Series on Directions in High Energy Physics, World Scientific, New Jersey, 2009. E. D. Commins and D. DeMille, The Electric Dipole Moment of the Electron.

[Rub85] C. Rubbia. Experimental observation of the intermediate vector bosons W^+, W^-, and Z^0. *Rev. Mod. Phys.*, 57:699, 1985.

[RvdSB+08] M. Raidal, A. van der Schaaf, I. Bigi, M. L. Mangano, Y. Semertzidis, S. Abel, S. Albino, S. Antusch, E. Arganda, B. Bajc, S. Banerjee, C. Biggio, M. Blanke, W. Bonivento, G. C. Branco, D. Bryman, A. J. Buras, L. Calibbi, A. Ceccucci, P. H. Chankowski, S. Davidson, A. Deandrea, D. P. DeMille, F. Deppisch, M. A. Diaz, B. Duling, M. Felcini, W. Fetscher, F. Forti, D. K. Ghosh, M. Giffels, M. A. Giorgi, G. Giudice, E. Goudzovskij, T. Han, P. G. Harris, M. J. Herrero, J. Hisano, R. J. Holt, K. Huitu, A. Ibarra, O. Igonkina, A. Ilakovac, J. Imazato, G. Isidori, F. R. Joaquim, M. Kadastik, Y. Kajiyama, S. F. King, K. Kirch, M. G. Kozlov, M. Krawczyk, T. Kress, O. Lebedev, A. Lusiani, E. Ma, G. Marchiori, A. Masiero, L. Masina, G. Moreau, T. Mori, M. Muntel, N. Neri, F. Nesti, C. G. J. Onderwater, P. Paradisi, S. T. Petcov, M. Picariello, V. Porretti, A. Poschenrieder, M. Pospelov, L. Rebane, M. N. Rebelo, A. Ritz, L. Roberts, A. Romanino, J. M. Roney, A. Rossi, R. Rückl, G. Senjanovic, N. Serra, T. Shindou, Y. Takanishi, C. Tarantino, A. M. Teixeira, E. Torrente-Lujan, K. J. Turzynski, T. E. J. Underwood, S. K. Vempati, and O. Vives. Flavor physics of leptons and dipole moments. *Eur. Phys. J. C*, 57:13, 2008.

[RW07] M. Reiher and A. Wolf. *Relativistic Quantum Chemistry*. Wiley-VCH, 2007.

[Sac87] R. G. Sachs. *The physics of time reversal*. University of Chicago Press, 1987.

[SAHH06] B. E. Sauer, H. T. Ashworth, J.J.and Tarbutt M. R. Hudson, and E. A. Hinds. Probing the electron EDM with cold molecules. *At. Phys.*, 20(physics/0611155):44, 2006.

[Sak67] A. D. Sakharov. Violation of CP invariance, C asymmetry, and baryon asymmetry of the universe. *JETP Lett.*, 5:24, 1967.

[Sal58] E. E. Salpeter. Some Atomic Effects of an Electronic Electric Dipole Moment. *Phys. Rev.*, 112:1642, 1958.

[San65] P. G. H. Sandars. The electric dipole moment of an atom. *Phys. Lett.*, 14(3):194, 1965.

[Sch63] L. I. Schiff. Measurability of Nuclear Electric Dipole Moments. *Phys. Rev.*, 132(5):2194, 1963.

[SF78] O. P. Sushkov and V. V. Flambaum. Parity breaking effects in diatomic molecules. *JETP*, 48:608, 1978.

[SH84] R. E. Stanton and S. Havriliak. Kinetic balance: A partial solution to the problem of variational safety in Dirac calculations. *J. Chem. Phys.*, 81(4):1910, 1984.

[SJ99] T. Saue and H. J. Aa. Jensen. Quaternion symmetry in relativistic molecular calculations: The Dirac–Hartree–Fock method. *J. Chem. Phys.*, 111(14):6211, 1999.

[SMPT08] L. V. Skripnikov, N. S. Mosyagin, A. N. Petrov, and A. V. Titov. On the search for time variation in the fine-structure constant: Ab initio calculation of HfF+. *JETP lett.*, 88(9):578, 2008.

[SPN+15] S. Sasmal, H. Pathak, M. K. Nayak, N. Vaval, and S. Pal. Relativistic extended-coupled-cluster method for the magnetic hyperfine structure constant. *Phys. Rev. A*, 91(2):022512, 2015.

[SPR57] J. H. Smith, E. M. Purcell, and N. F. Ramsey. Experimental Limit to the Electric Dipole Moment of the Neutron. *Phys. Rev.*, 108(1):120, 1957.

[SPT13] L. V. Skripnikov, A. N. Petrov, and A. V. Titov. Communication: Theoretical study of ThO for the electron electric dipole moment search. *J. Chem. Phys.*, 139:221103, 2013.

[ST14] L. V. Skripnikov and A. V. Titov. Theoretical study of thorium monoxide for the electron electric dipole moment search, II: Electronic properties of $H^3\Delta_1$ in ThO. arXiv:1410.2485v1 [physics.atom-ph], 2014.

[ST15] L. V. Skripnikov and A. V. Titov. Theoretical study of ThO for the electron electric dipole moment search: Electronic properties of $H^3\Delta_1$ in ThO. *J. Chem. Phys.*, 142:024301, 2015.

[Sto05] N.J. Stone. Table of nuclear magnetic dipole and electric quadrupole moments. *At. Data Nucl. Data Tables*, 90(1):75, 2005.

[Str98] P. Strange. *Relativistic Quantum Mechanics: With Applications in Condensed Matter and Atomic Physics*. Religious Studies; 47. Cambridge University Press, 1998.

[Stu10] R. P. Stutz. *Towards measuring the electron electric dipole moment using trapped molecular ions*. PhD thesis, University of Colorado, 2010.

[Suc80] J. Sucher. Foundations of the relativistic theory of many-electron atoms. *Phys. Rev. A*, 22(2):348, 1980.

[SVSI09] J. Sikkema, L. Visscher, T. Saue, and M. Iliaš. The molecular mean-field approach for correlated relativistic calculations. *J. Chem. Phys.*, 131:124116, 2009.

[SW64] R. F. Streater and A. S. Wightman. *PCT, Spin Statistics, And All That*. W. A. Benjamin Inc., New York, Amsterdam, 1964.

[Tal86] J. D. Talman. Minimax Principle for the Dirac Equation. *Phys. Rev. Lett.*, 57:1091, 1986.

[TFJ08] J. Thyssen, T. Fleig, and H. J. Aa. Jensen. A Direct Relativistic Four-Component Multi-Configuration Self-Consistent-Field Method for Molecules. *J. Chem. Phys.*, 129:034109, 2008.

[VCG+] A. C. Vutha, W. C. Campbell, Y. V. Gurevich, N. R. Hutzler, M. Parsons, D. Patterson, E. Petrik, B. Spaun, J. M. Doyle, G. Gabrielse, and D. DeMille. Search for the electric dipole moment of the electron with thorium monoxide. *J. Phys. B*, 43(7):074007.

[Vis96] L. Visscher. On the construction of double group molecular symmetry functions. *Chem. Phys. Lett.*, 253(1):20, 1996.

[Vis02] L. Visscher. The Dirac equation in quantum chemistry: Strategies to overcome the current computational problems. *J. Comp. Chem.*, 23(8):759, 2002.

[VSG+11] A. C. Vutha, B. Spaun, Y. V. Gurevich, N. R. Hutzler, E. Kirilov, J. M. Doyle, G. Gabrielse, and D. DeMille. Magnetic and electric dipole moments of the $H\ ^3\Delta_1$ state in ThO. *Phys. Rev. A*, 84(3):034502, 2011.

[Wei76] S. Weinberg. Gauge Theory of CP Nonconservation. *Phys. Rev. Lett.*, 37(11):657, 1976.

[Wig32] E. Wigner. Ueber die Operation der Zeitumkehr in der Quantenmechanik. *Göttingen Nachr.*, page 546, 1932.

[WS11] F. Wang and T. C. Steimle. Communication: Electric dipole moment and hyperfine interaction of tungsten monocarbide, WC. *J. Chem. Phys.*, 134:201106, 2011.

[YHN+07] T. Yanai, R. J. Harrison, T. Nakajima, Y. Ishikawa, and K. Hirao. New implementation of molecular double point-group symmetry in four-component relativistic gaussian-type spinors. *Int. J. Quantum Chem.*, 107(6):1382, 2007.